

**The behavior of Tapered High Strength Concrete Filled
Steel Tube (CFST) Column connected to Encased Steel
Reinforced Concrete Composite (SRC) Column**

سلوك العمود الفولاذي ذو القطاع المخروطي المملوء بالخرسانة عالية المقاومة
(CFST) المتصل بعمود مركب الخرسانة المسلحة المغلف بالفولاذ (SRC)

by

YASSER MOHAMED ABDELHAMID AZZAZY

**Dissertation submitted in fulfilment
of the requirements for the degree of
MSc STRUCTURAL ENGINEERING
at
The British University in Dubai**

April 2020

DECLARATION

I warrant that the content of this research is the direct result of my own work and that any use made in it of published or unpublished copyright material falls within the limits permitted by international copyright conventions.

I understand that a copy of my research will be deposited in the University Library for permanent retention.

I hereby agree that the material mentioned above for which I am author and copyright holder may be copied and distributed by The British University in Dubai for the purposes of research, private study or education and that The British University in Dubai may recover from purchasers the costs incurred in such copying and distribution, where appropriate.

I understand that The British University in Dubai may make a digital copy available in the institutional repository.

I understand that I may apply to the University to retain the right to withhold or to restrict access to my thesis for a period which shall not normally exceed four calendar years from the congregation at which the degree is conferred, the length of the period to be specified in the application, together with the precise reasons for making that application.



Signature of the student

COPYRIGHT AND INFORMATION TO USERS

The author whose copyright is declared on the title page of the work has granted to the British University in Dubai the right to lend his/her research work to users of its library and to make partial or single copies for educational and research use.

The author has also granted permission to the University to keep or make a digital copy for similar use and for the purpose of preservation of the work digitally.

Multiple copying of this work for scholarly purposes may be granted by either the author, the Registrar or the Dean only.

Copying for financial gain shall only be allowed with the author's express permission.

Any use of this work in whole or in part shall respect the moral rights of the author to be acknowledged and to reflect in good faith and without detriment the meaning of the content, and the original authorship.

ABSTRACT

The use of Convectional Concrete Column is often limited in high-rise Buildings due to the constraint from the architects on increasing size of the columns, so the composite columns provide appropriate solution to satisfy the architect and the Client with smaller column size. Nowadays, Composite Columns have been widely developed in the construction of the high-rise buildings, long span structures, and bridges. Composite columns have two main types, encased composite columns (SRC) and concrete filled steel tube columns (CFST).

This research is focusing on the behavior of a tapered concrete filled steel tube column (CFST) connected to encased composite column (SRC). The purpose of having two different sections along the column height is to enhance the flexure resistance of the column at the top edge by introducing CFST element, while the lower part is modeled as SRC element and it is mainly subjected to axial compression with significant reduction in bending moments compared to the top part of the column. The behavior of the tapered CFST column connected to SRC column has been studied using two main different parameters. The first parameter is the type of loading, such as pure axial compression, axial compression and uni-axial bending, and axial compression and bi-axial bending. The second parameter is the concrete strength, with different concrete strengths ranging from C40MPa to C70MPa. Both parameters have been carefully considered in the analysis of the composite column. The steel section used in the research design model has a yield strength of 355MPa. The steel reinforcement used in the model has a yield strength of 500MPa.

The column has been modeled using 3D-Fiber (Solid) Finite Element Method. The cross sectional of the columns has been divided into tiny fiber (solid) elements. The advantage of using a fiber (solid) element is easy to assign the tiny element as concrete or steel, even stiffeners plates have been modeled by adopting the fiber element methodology. The maximum size of the fiber (solid) element is (10mm x 10mm) which warrant more accurate results in terms of stress and strain. The vertical rebar was ignored from the 3D Fiber Model. The stresses and strains extracted from the 3D-FE models have been compared to the simplified formulas adopted by EUROCODE-4 and American Standards AISC / ANCI .

The research illustrates the load path and stress / strain distribution through different structural elements connected to each other under deferent type of loading. The results demonstrate that the 3D-FEM displays some differences in the composite section capacity under different type of loading compared to the simplified formula adopted by Eurocode and AISC/ANCI. The stress and strain distribution demonstrate a smooth transition between CFST element and SRC element with local stress concertation on the concrete and steel at the interface between CFST element and SRC element. The concentration in the stresses is not considered in the simplified formula by the standards codes, so it should be carefully considered in the section capacity.

الملخص

في المباني الشاهقة الارتفاع يفرض المصمم المعماري بعض القيود على زيادة أبعاد الأعمدة التقليدية، لذلك توفر الأعمدة المركبة يعتبر الحل المناسب للمهندس المعماري وكذلك للمالك لتقليل أبعاد الأعمدة الإنشائية. في الوقت الحاضر، تم تطوير الأعمدة المركبة على نطاق واسع في تشييد المباني الشاهقة الارتفاع والهياكل ذات البحور الطويلة وكذلك الجسور. الأعمدة المركبة لها نوعان رئيسيان عمود مركب مغلف وعمود أنبوب فولاذي مملوء بالخرسانة.

يركز البحث على سلوك عمود الأنبوب الفولاذي المملوء بالخرسانة والمتغير الأبعاد والمتصل بالعمود المركب المغلف. الغرض من وجود نوعين مختلفين ومتصلين ببعضهما بطول العمود هو تعزيز مقاومة الانحناء للعمود في الحافة العلوية من خلال إدخال عنصر الأنبوب الفولاذي المملوء بالخرسانة في حين أن الجزء السفلي يكون عمود مركب مغلف ويخضع بشكل أساسي للضغط المحوري مع تقليل كبير لعزوم الانحناء مقارنة بالجزء العلوي من العمود الفولاذي المملوء بالخرسانة. سلوك العمود الفولاذي المملوء بالخرسانة المتصل بالعمود المركب المغلف تم دراسته باستخدام عاملين مختلفين رئيسيين، العامل الأول هو نوع حالات التحميل مثل الضغط المحوري والضغط المحوري مصحوباً بانحناء أحادي المحور والضغط المحوري مصحوباً بانحناء ثنائي المحور. العامل الثاني هو قوة إجهاد الخرسانة والتي تتغير من 40 نيوتن/مم² إلى 70 نيوتن/مم². كلا العاملين تم دراستهما بعناية من خلال التحليل الإنشائي للعمود المركب. قوة إجهاد الفولاذ المستخدم في البحث هي 355 نيوتن/مم² و 275 نيوتن/مم². إجهاد حديد التسليح المستخدم في العمود المركب المغلف هو 500 نيوتن/مم².

تم نمذجة العمود باستخدام طريقة العناصر المحددة للألياف ثلاثية الأبعاد وتم تقسيم المقطع العرضي للأعمدة إلى عناصر ألياف دقيقة. تتمثل ميزة استخدام عناصر الألياف في تعيين العناصر بسهولة كالخرسانة أو الفولاذ حتى أن لوحات التقوية يتم نمذجتها أيضاً. الحجم الأقصى لعنصر الألياف هو (10 مم * 10 مم) مما يضمن نتائج أكثر دقة من حيث الإجهاد والاستطالة. تم إهمال حديد التسليح الرأسي من نموذج الألياف ثلاثية الأبعاد. تمت مقارنة الإجهادات والاستطالة المستخرجة من النموذج الإنشائي ثلاثي الأبعاد مع الطرق الأخرى المبسطة المعتمدة من الأكواد الأمريكية والكود الأوروبي.

يوضح البحث مسار الحمل وتوزيع الضغط / الإجهاد من خلال عناصر هيكلية مختلفة متصلة ببعضها البعض تحت نوع تحميل مختلف. أظهرت النتائج أن النموذج الإنشائي ثلاثي الأبعاد يعطي نتائج مختلفة مقارنة بالطرق المبسطة المعتمدة من الأكواد الأمريكية والكود الأوروبي. يوضح توزيع الضغط والاستطالة انتقالاً سلساً للأحمال بين العمود الفولاذي المملوء بالخرسانة والعمود المركب المغلف مع وجود زيادة ملحوظة في الإجهادات في بعض الأماكن نتيجة اتصال عناصر إنشائية مختلفة الخصائص مما يتطلب النظر بعناية في مقاومة العمود المركب للأحمال المختلفة مع الأخذ بعين الاعتبار تركيز الإجهادات الموضح بالنموذج الإنشائي ثلاثي الأبعاد.

DEDICATION

I dedicated this work to my parents who raised me to believe first in Allah and then in myself to pursue my goals in this life and to have the confidence and faith to achieve them.

I dedicated also this work to my wife who supported me to accomplish this work and for her encouragement to achieve my goals.

Thank you for all your support, and encouragements

All credits go back to you.

ACKNOWLEDGEMENTS

It was a significant challenge to prepare this dissertation. I would like to express my sincere gratitude to all people supporting and encourage me to complete high graduate study.

Grateful acknowledgement is deeply expressed to Prof. Abid Abu Tair who guided and advised me a lot through the entire journey to complete the work.

Sincere acknowledgement id expressed to my tutors and all staff at the British university in Dubai for their support.

TABLE OF CONTENTS:

1. INTRODUCTION	1
1.1 COMPOSITE ELEMENTS DESIGN AND CONSTRUCTION.....	2
1.2 ENCASED STEEL REINFORCED COMPOSITE COLUMN (SRC).....	2
1.3 CONCRETE FILLED STEEL TUBE COLUMN (CFST).....	5
1.4 RESEARCH SIGNIFICANCE.....	7
1.5 RESEARCH CHALLENGE.....	7
1.6 RESEARCH OBJECTIVE.....	8
1.7 CASE STUDY.....	8
1.8 SCOPE.....	9
2. LITERATURE REVIEW	10
2.1 INTRODUCTION.....	11
2.2 ADVANCE TECHNOLOGY OF CONSTRUCTION MATERIAL.....	11
2.3 HIGH STRENGTH AND HIGH-PERFORMANCE CONCRETE.....	11
2.4 CONCRETE MODULUS OF ELASTICITY (YOUNG’S MODULUS).....	15
2.5 HIGH STRENGTH AND HIGH-PERFORMANCE STEEL.....	15
2.6 BEHAVIOR OF CONFINED CONCRETE IN THE COMPOSITE COLUMN.....	18
2.7 BOND BETWEEN STEEL AND CONCRETE.....	20
2.8 COMPOSITE DESIGN PROVISION IN ACCORDANCE WITH AMERICAN SPECIFICATIONS.....	21
2.8.1 ACI PROVISION FOR COMPRESSIVE STRENGTH OF COMPOSITE COLUMN.....	23
2.8.2 ANCI / AISC PROVISION FOR COMPRESSIVE STRENGTH OF ENCASED COMPOSITE COLUMN.....	23
2.8.3 ANCI / AISC PROVISION FOR COMPRESSIVE STRENGTH OF CONCRETE FILLED STEEL TUBE COLUMN.....	25
2.8.4 ACI PROVISION FOR COMBINED FLEXURE AND AXIAL FORCES.....	27
2.8.5 ANCI / AISC PROVISION FOR ENCASED COMPOSITE AND FOR FILLED COMPOSITE WITH COMPACT SECTIONS SUBJECT TO COMBINED FLEXURE AND AXIAL FORCES.....	28
2.8.6 ANCI / AISC PROVISION FOR FILLED COMPOSITE WITH NONCOMPACT OR SLENDER SECTIONS SUBJECT TO COMBINED FLEXURE AND AXIAL FORCES.....	28
2.8.7 LOAD TRANSFER.....	29
2.8.8 MECHANISM OF FORCE TRANSFER.....	31
2.8.8.1 Direct Bearing Force Mechanism.....	31
2.8.8.2 Direct Bond Interaction Mechanism.....	31
2.8.8.3 Shear Connection Force Mechanism.....	32
2.8.8.4 Tensile Strength of Steel Headed Stud Anchor in Composite Members.....	35

2.8.8.5	<i>Strength of Steel Headed Stud anchors for Interaction of shear and Tension in Composite Members.....</i>	36
2.8.8.6	<i>Shear Strength of Steel Channel Anchors in Composite Members.....</i>	37
2.8.8.7	<i>Detailing Requirements for Steel Studs and Anchors in Composite Elements.....</i>	37
2.9	COMPOSITE DESIGN PROVISION IN ACCORDANCE WITH EUROCODE 4 SPECIFICATIONS.....	38
2.9.1	EUROCODE 4 DESIGN PROVISION FOR COMPOSITE COLUMN SUBJECT TO AXIAL COMPRESSION LOADS.....	40
2.9.2	EUROCODE 4 DESIGN PROVISION FOR COMPOSITE COLUMN SUBJECT TO AXIAL COMPRESSION AND UNIAXIAL FLEXURE BENDING.....	42
2.9.3	EUROCODE 4 DESIGN PROVISION FOR COMPOSITE COLUMN SUBJECT TO AXIAL COMPRESSION AND BIAXIAL FLEXURE BENDING.....	44
2.9.4	TRANSFER SHEAR FORCES EFFECT ON THE COMPOSITE COLUMN DESIGN RESISTANCE.....	45
2.9.5	EUROCODE PROVISION FOR THE P-M INTERACTION DIAGRAM.....	46
2.9.6	EFFECTIVE FLEXURE STIFFNESS OF THE COMPOSITE COLUMNS.....	47
2.9.7	SECOND ORDER INFLUENCE, GEOMETRICAL, AND MEMBER IMPERFECTIONS.....	50
2.9.8	CRITICAL BUCKLING LOAD ON THE COMPOSITE COLUMN.....	53
2.9.9	EUROCODE 4 PROVISION FOR SHEAR FORCES TRANSFER.....	53
2.10	ISOLATED STEEL REINFORCED CONCRETE COLUMN (ISRC).....	60
2.11	PRECEDING AND CURRENT RESEARCHES ON THE CONCRETE FILLED TUBE COLUMNS.....	63
3.	RESEARCH METHODOLOGY.....	114
3.1	INTRODUCTION.....	115
3.2	RESEARCH APPROACH.....	115
3.3	RESEARCH STRATEGY.....	115
3.4	DATA COLLECTION.....	116
4.	RESEARCH RESULTS.....	117
4.1	INTRODUCTION.....	118
4.2	CASE STUDY.....	118
4.3	SIMPLIFIED METHOD FOR THE CFST COLUMN CAPACITY OF THE CASE STUDY.....	125
4.3.1	ANCI / AISC PROVISION.....	125
4.3.2	EUROCODE 4 PROVISION.....	125
4.4	RESEARCH DESIGN MODEL.....	126
4.4.1	3D-FIBER (SOLID) FINITE ELEMENT MODEL.....	128
4.4.2	BOUNDARY CONDITIONS.....	129
4.4.3	COLUMN RESISTANCE TO AXIAL COMPRESSION LOADS.....	130

4.4.3.1	Stresses on the Encased Composite Column subject to Axial Compression Loads.....	130
4.4.3.1.1	Encased Column Analysis under Axial compression Load, C40MPa, S355MPa.....	131
4.4.3.1.2	Encased Column Analysis under Axial compression Load, C50MPa, S355MP.....	133
4.4.3.1.3	Encased Column Analysis under Axial compression Load, C60MPa, S355MPa.....	135
4.4.3.1.4	Encased Column Analysis under Axial compression Load, C70MPa, S355MPa.....	137
4.4.3.1.5	Encased Column Analysis under Axial compression Load, C40MPa, S275MPa.....	139
4.4.3.1.6	Encased Column Analysis under Axial compression Load, C50MPa, S275MPa.....	141
4.4.3.1.7	Encased Column Analysis under Axial compression Load, C60MPa, S275MPa.....	143
4.4.3.1.8	Encased Column Analysis under Axial compression Load, C70MPa, S275MPa.....	145
4.4.3.2	Stresses on the CFST Composite Column subject to Axial Compression Loads.....	147
4.4.3.2.1	CFST Column Analysis under Axial Compression Load, C40MPa, S355MPa.....	147
4.4.3.2.2	CFST Column Analysis under Axial Compression Load, C50MPa, S355MPa.....	149
4.4.3.2.3	CFST Column Analysis under Axial Compression Load, C60MPa, S355MPa.....	151
4.4.3.2.4	CFST Column Analysis under Axial Compression Load, C70MPa, S355MPa.....	153
4.4.3.2.5	CFST Column Analysis under Axial Compression Load, C40MPa, S275MPa.....	155
4.4.3.2.6	CFST Column Analysis under Axial Compression Load, C50MPa, S275MPa.....	157
4.4.3.2.7	CFST Column Analysis under Axial Compression Load, C60MPa, S275MPa.....	159
4.4.3.2.8	CFST Column Analysis under Axial Compression Load, C70MPa, S275MPa.....	161
4.4.3.3	Stresses on the Stiffener Plates Welded to CFST & Encased under Axial Compression Load.....	163
4.4.4	COLUMN RESISTANCE TO AXIAL COMPRESSION AND UNI-DIRECTION MOMENTS.....	165
4.4.4.1	Stresses on the Encased Column subject to Axial Compression and Uni-Direction Moments....	165
4.4.4.1.1	Encased Column Analysis under Axial Compression and Uni-Direction Moments, C40MPa, S355MPa.....	166
4.4.4.1.2	Encased Column Analysis under Axial Compression and Uni-Direction Moments, C50MPa, S355MPa.....	168
4.4.4.1.3	Encased Column Analysis under Axial Compression and Uni-Direction Moments, C60MPa, S355MPa.....	170
4.4.4.1.4	Encased Column Analysis under Axial Compression and Uni-Direction Moments, C70MPa, S355MPa.....	172
4.4.4.1.5	Encased Column Analysis under Axial Compression and Uni-Direction Moments, C40MPa, S275MPa.....	174
4.4.4.1.6	Encased Column Analysis under Axial Compression and Uni-Direction Moments, C50MPa, S275MPa.....	176
4.4.4.1.7	Encased Column Analysis under Axial Compression and Uni-Direction Moments, C60MPa, S275MPa.....	178

4.4.4.1.8	Encased Column Analysis under Axial Compression and Uni-Direction Moments, C70MPa, S275MPa.....	180
4.4.4.2	Stresses on the CFST Composite Column subject to Axial Compression and Uni-Direction Moments.....	182
4.4.2.1	CFST Column Analysis under Axial Compression and Uni-Direction Moments, C40MPa, S355MPa.....	183
4.4.2.2	CFST Column Analysis under Axial Compression and Uni-Direction Moments, C50MPa, S355MPa.....	185
4.4.2.3	CFST Column Analysis under Axial Compression and Uni-Direction Moments, C60MPa, S355MPa.....	187
4.4.2.4	CFST Column Analysis under Axial Compression and Uni-Direction Moments, C70MPa, S355MPa.....	189
4.4.2.5	CFST Column Analysis under Axial Compression and Uni-Direction Moments, C40MPa, S275MPa.....	191
4.4.2.6	CFST Column Analysis under Axial Compression and Uni-Direction Moments, C50MPa, S275MPa.....	193
4.4.2.7	CFST Column Analysis under Axial Compression and Uni-Direction Moments, C60MPa, S275MPa.....	195
4.4.2.8	CFST Column Analysis under Axial Compression and Uni-Direction Moments, C70MPa, S275MPa.....	197
4.4.4.3	Stresses on the Stiffener Plates welded to the CFST and Encased Element, under Axial Compression and Uni-Direction Bending Moments.....	199
4.4.5	COLUMN RESISTANCE TO AXIAL COMPRESSION AND BI-AXIAL BENDING MOMENTS.....	202
4.4.5.1	Stresses on Encased Composite Column subject to Axial Compression & Bi-Axial Bending.....	202
4.4.5.1.1	Encased Column Analysis under Axial Compression and Bi-Axial Moments, C40MPa, S355MPa.....	203
4.4.5.1.2	Encased Column Analysis under Axial Compression and Bi-Axial Moments, C50MPa, S355MPa.....	205
4.4.5.1.3	Encased Column Analysis under Axial Compression and Bi-Axial Moments, C60MPa, S355MPa.....	207
4.4.5.1.4	Encased Column Analysis under Axial Compression and Bi-Axial Moments, C70MPa, S355MPa.....	209
4.4.5.1.5	Encased Column Analysis under Axial Compression and Bi-Axial Moments, C40MPa, S275MPa.....	211
4.4.5.1.6	Encased Column Analysis under Axial Compression and Bi-Axial Moments, C50MPa, S275MPa.....	213

4.4.5.1.7	Encased Column Analysis under Axial Compression and Bi-Axial Moments, C60MPa, S275MPa.....	215
4.4.5.1.8	Encased Column Analysis under Axial Compression and Bi-Axial Moments, C70MPa, S275MPa.....	217
4.4.5.2	Stresses on the CFST Composite Column subject to Axial Compression and Bi-Axial Bending.....	219
4.4.5.2.1	CFST Column Analysis under Axial Compression & Bi-Axial Moments, C40MPa, S355MPa.....	220
4.4.5.2.2	CFST Column Analysis under Axial Compression & Bi-Axial Moments, C50MPa, S355MPa.....	222
4.4.5.2.3	CFST Column Analysis under Axial Compression & Bi-Axial Moments, C60MPa, S355MPa.....	224
4.4.5.2.4	CFST Column Analysis under Axial Compression & Bi-Axial Moments, C70MPa, S355MPa.....	226
4.4.5.2.5	CFST Column Analysis under Axial Compression & Bi-Axial Moments, C40MPa, S275MPa.....	228
4.4.5.2.6	CFST Column Analysis under Axial Compression & Bi-Axial Moments, C50MPa, S275MPa.....	230
4.4.5.2.7	CFST Column Analysis under Axial Compression & Bi-Axial Moments, C60MPa, S275MPa.....	232
4.4.5.2.8	CFST Column Analysis under Axial Compression & Bi-Axial Moments, C70MPa, S275MPa.....	234
4.4.5.3	Stresses on the Stiffener Plates welded to the CFST and Encased Element, under Axial Compression and Bi-Axial Moments.....	236
5.	DISCUSSION OF RESULTS.....	238
5.1	INTRODUCTION.....	239
5.2	COMPOSITE COLUMN BEHAVIOR SUBJECT TO CONCENTRIC AXIAL COMPRESSION LOAD.....	239
5.2.1	<i>Encased Composite Column Subject to Concentric Axial Compression Load.....</i>	<i>239</i>
5.2.2	<i>CFST Composite Column Subject to Concentric Axial Compression Load.....</i>	<i>246</i>
5.2.3	<i>Steel Stiffener Plates Behavior connected to CFST and Encased Column under Concentric Axial Compression Loads.....</i>	<i>251</i>
5.3	COMPOSITE COLUMN BEHAVIOR UNDER AXIAL COMPRESSION AND UNI-DIRECTION BENDING.....	252
5.3.1	Encased Composite Column Subject to Axial Compression and Uni-direction Bending.....	252
5.3.2	CFST Composite Column Subject to Axial Compression and Uni-direction Bending.....	256

5.3.3	Steel Stiffener Plates Behavior connected to CFST and Encased Column under Axial Compression Load and Uni-direction Bending.....	259
5.4	COMPOSITE COLUMN BEHAVIOR UNDER AXIAL COMPRESSION AND BI-AXIAL BENDING.....	260
5.4.1	Encased Column Subject to Axial Compression and Bi-Axially Bending Moments.....	260
5.4.2	CFST Composite Column Subject to Axial Compression and Bi-Axially Bending Moments.....	264
5.4.3	Steel Stiffener Plates Behavior connected to CFST and Encased Column under Axial Compression and Bi-Axial Bending Moments.....	268
6.	SUMMARY AND CONCLUSION.....	269
6.1	COMPOSITE COLUMN SUBJECT TO UNI-AXIAL COMPRESSION LOAD.....	271
6.2	COMPOSITE COLUMN SUBJECT TO COMBINED AXIAL COMPRESSION AND UNI-DIRECTION BENDING.....	273
6.3	COMPOSITE COLUMN SUBJECT TO COMBINED AXIAL COMPRESSION AND BI-DIRECTION BENDING.....	275
6.4	RECOMMENDATION FOR DESIGN AND FUTURE RESEARCHES.....	277
6.4.1	Design Recommendations.....	277
6.4.2	Research Recommendations.....	278
7.	REFERENCES.....	279
8.	APPENDICES.....	284
	Appendix (A) <u>Unit Conversions (Imperial Units to SI Units)</u>	285

LIST OF FIGURES:

Figure 1.1:	Typical SRC Column Arrangements.....	4
Figure 1.2:	Strain Distribution, (a) Fully Connected SRC Column; (b) Partially Connected SRC Column.....	4
Figure 1.3:	Shear Studs Constitutive Curves.....	5
Figure 1.4:	Local Buckling Mode for the Cross Sectional of the Concrete Filled Tube.....	6
Figure 1.5:	Elastic Local Buckling Change along Length of the Concrete Filled Tube.....	6
Figure 2.1:	Stress-Strain Relationship Curve of Concrete, Collins at al. (1993) model.....	12
Figure 2.2:	Stress-Strain Relationship Curve of Confined Concrete, Collins at al. (1991).....	13
Figure 2.3:	Stress-Strain Relationship Curve for High Performance Steel and Conventional Steel [Salmon and Johnson, 1996].....	16
Figure 2.4:	Effect of b/t Ratio on High Strength Steel Box Column Axial Load Capacity from (Ricles et al., 1996).....	17
Figure 2.5:	Three Different Confinement Zones in Encased Composite Column,[Chen& Lin, 2006]..	18
Figure 2.6A:	Confinement Factor for Partially Confined Concrete, [Chen and Lin, 2006].....	19
Figure 2.6B:	Confinement Factor for Highly Confined Concrete, [Chen and Lin, 2006].....	19
Figure 2.7:	Unfactored Axial Forces – Flexure Moment Interaction Diagram based on LRFD and ACI Code.....	27
Figure 2.8:	Angle between Shear Friction Reinforcement and Crack Plane.....	35
Figure 2.9:	Typical cross sections of different types of composite columns.....	38
Figure 2.10:	P-M Interaction Diagram for Combined Compression and Uniaxial Flexure Bending.....	43
Figure 2.11:	Simplified P-M Interaction Diagram and corresponding stress distribution.....	43
Figure 2.12:	Determination of Design Factor (μ_d) related to Compression and Flexure.....	44
Figure 2.13:	Creep Coefficient $\phi(t_0)$ for Concrete in inside condition, Relative Humidity (RH=50%)...48	
Figure 2.14:	Creep Coefficient $\phi(t_0)$ for Concrete in outside condition, Relative Humidity(RH=80%)..49	
Figure 2.15:	Methodology of calculating the creep coefficient $\phi(t_0)$ in normal environment situation.....	49
Figure 2.16:	Buckling Modes with relevant effective length for different boundary conditions.....	53
Figure 2.17:	Additional Frictional Forces introduced in the composite columns due to the use of headed studs.....	55
Figure 2.18:	Concrete Filled Circular Tube Section Partially Loaded.....	57
Figure 2.19:	Stirrups Arrangements for Partially Encased Steel Sections.....	57

Figure 2.20:	Direct and in-direct connected to concrete areas for the transverse design reinforcement.....	58
Figure 2.21:	Isolated Steel Reinforced Concrete Column (Layout & 3D View).....	62
Figure 2.22:	Tomii and Skino's Model of Confined Concrete utilized by Zhang & Shahrooz [1997].....	72
Figure 2.23:	Chart of Iterating Forces Characteristics, Kawaguchi et. al. [1998].....	76
Figure 2.24:	Scale Effect on Compressive Strength of Circular Plain Concrete Column, McNamara [1935].....	80
Figure 2.25:	Cross Sectional Details of CFST Column Specimens with Plain Concrete and Steel Fiber, Serkan Tokgoz & Cengiz Dundar [2010].....	81
Figure 2.26:	CFST Test Setup, Tokgoz & Cengiz Dundar [2010].....	81
Figure 2.27:	CFST Column Cross Section and Stress Distribution, Tokgoz & Cengiz Dundar [2010].....	82
Figure 2.28:	Typical Deformation Geometry of CFST Column, Tokgoz & Cengiz Dundar [2010].....	83
Figure 2.29:	Four Failure Mechanism, Jang-Woon Beak and Hyeon-Jong Hwang [2012].....	84
Figure 2.30:	Fiber Strain Distribution in CFST Column subject to Uniaxial and Biaxial Loading, Liang, et. al. [2014].....	86
Figure 2.31:	Section Geometry and its Connection Details, Jin-Won Kim et. al. [2014].....	88
Figure 2.32:	Cross Section of SRSCFSHS Column, Jing-ming Cai et. al. [2016].....	90
Figure 2.33:	Axial Load Strain Curve for Theoretical and Experimental, Jing-ming Cai et. al. [2016].....	91
Figure 2.34:	Cross Sections of Tested Columns, Ziang Zhu et. al. [2017].....	92
Figure 2.35:	Stress Strain Curve of Hollow Steel Columns, T. Kibryia [2017].....	95
Figure 2.36:	Stress Strain Curve of Filled Columns, T. Kibryia [2017].....	95
Figure 2.37:	Stress Strain Curve of Braced Columns, T. Kibryia [2017].....	96
Figure 2.38:	Tested Column Arrangements, T. Kibryia [2017].....	97
Figure 2.39:	Strain Gauge Arrangements, T. Kibryia [2017].....	98
Figure (2.40):	Column Test Setup, Morino, et. al. [1984].....	100
Figure (2.41):	Load -Deflection Curve, Morino, et. al. [1984].....	102
Figure (2.42):	Fiber Model of Encase Composite Column.....	104
Figure (2.43):	Encased Composite Column Section utilized in the study by El-Tawil, et. al. [1999].....	104
Figure (2.44):	Encased Composite Column with Seismic Tie Requirements (S-08).....	105
Figure (2.45):	Cross Sectional Tested by Dundar, et. al. [2007].....	107
Figure (2.46):	Experimental Testing Setup, Dundar, et. al. [2007].....	108
Figure (2.47):	Failure Modes of the Tested Column, Z. Huang, et. al. [2018].....	111

Figure (2.48):	Load-Displacement Relationship for Tested Columns under Compression.....	112
Figure (2.49):	Load-Midspan Displacement Relationship for Tested Columns under Flexure.....	112
Figure (4.1):	Case Study of Tapered CFST Column connected to Encased Composite Column.....	119
Figure (4.1a):	Detail-A Case Study, Enlarged Column Elevation.....	120
Figure (4.1b):	Case Study, Encased Composite Column.....	121
Figure (4.1c):	Case Study, Connection between CFST Column and Encased Composite Column.....	121
Figure (4.1d):	Case Study, Concrete Filled Steel Tube (CFST) Column.....	121
Figure (4.2):	Case Study, 3D geometry of the case study (Design vs Construction).....	122
Figure (4.3):	Research Design Model Geometry.....	127
Figure (4.4):	3D Fiber (Solid) Finite Element Model.....	128
Figure (4.5):	Design Model Boundary Conditions and Straining Action Diagram.....	129
Figure (4.6):	Stresses of the Encased Column under Axial Compression Load, $P_u = 2,500$ kN, Concrete Cylinder, Strength C40MPa, Steel Grade, S355MPa.....	132
Figure (4.7):	Stresses of the Encased Column under Axial Compression Load, $P_u = 3,125$ kN, Concrete Cylinder, Strength C50MPa, Steel Grade, S355MPa.....	134
Figure (4.8):	Stresses of the Encased Column under Axial Compression Load, $P_u = 3,500$ kN, Concrete Cylinder Strength C60MPa, Steel Grade, S355MPa.....	136
Figure (4.9):	Stresses of the Encased Column under Axial Compression Load, $P_u = 4,000$ kN, Concrete Cylinder, Strength C70MPa, Steel Grade, S355MPa.....	138
Figure (4.10):	Stresses of the Encased Column under Axial Compression Load, $P_u = 2,500$ kN, Concrete Cylinder, Strength C40MPa, Steel Grade, S275MPa.....	140
Figure (4.11):	Stresses of the Encased Column under Axial Compression Load, $P_u = 3,125$ kN, Concrete Cylinder Strength C50MPa, Steel Grade, S275MPa.....	142
Figure (4.12):	Stresses of the Encased Column under Axial Compression Load, $P_u = 3,500$ kN, Concrete Cylinder Strength, C60MPa, Steel Grade, S275MPa.....	144
Figure (4.13):	Stresses of the Encased Column under Axial Compression Load, $P_u = 4,000$ kN, Concrete Cylinder Strength, C70MPa, Steel Grade, S275MPa.....	146
Figure (4.14):	Stresses along CFST Column, C40MPa, S335MPa.....	148
Figure (4.15):	Stresses along CFST Column, C50MPa, S355MPa.....	150
Figure (4.16):	Stresses along CFST Column, C60MPa, S355MPa.....	152
Figure (4.17):	Stresses along CFST Column, C70MPa, S355MPa.....	154
Figure (4.18):	Stresses along CFST Column, C40MPa, S275MPa.....	156
Figure (4.19):	Stresses along CFST Column, C50MPa, S275MPa.....	158
Figure (4.20):	Stresses along CFST Column, C60MPa, S275MPa.....	160

Figure (4.21):	Stresses along CFST Column, C70MPa, S275MPa.....	162
Figure (4.22):	Stresses' Contours Along Stiffener Plates under Axial Compression Loads.....	164
Figure (4.23):	Stresses' Contours Along Encased Composite Column, C40MPa, S355MPa.....	167
Figure (4.24):	Stresses' Contours Along Encased Composite Column, C50MPa, S355MPa.....	169
Figure (4.25):	Stresses' Contours Along Encased Composite Column, C60MPa, S355MPa.....	171
Figure (4.26):	Stresses' Contours Along Encased Composite Column, C70MPa, S355MPa.....	173
Figure (4.27):	Stresses' Contours Along Encased Composite Column, C40MPa, S275MPa.....	175
Figure (4.28):	Stresses' Contours Along Encased Composite Column, C50MPa, S275MPa.....	177
Figure (4.29):	Stresses' Contours Along Encased Composite Column, C60MPa, S275MPa.....	179
Figure (4.30):	Stresses' Contours Along Encased Composite Column, C70MPa, S275MPa.....	181
Figure (4.31):	Stresses' Contours Along CFST Composite Column, C40MPa, S355MPa.....	184
Figure (4.32):	Stresses' Contours Along CFST Composite Column, C50MPa, S355MPa.....	186
Figure (4.33):	Stresses' Contours Along CFST Composite Column, C60MPa, S355MPa.....	188
Figure (4.34):	Stresses' Contours Along CFST Composite Column, C70MPa, S355MPa.....	190
Figure (4.35):	Stresses' Contours Along CFST Composite Column, C40MPa, S275MPa.....	192
Figure (4.36):	Stresses' Contours Along CFST Composite Column, C50MPa, S275MPa.....	194
Figure (4.37):	Stresses' Contours Along CFST Composite Column, C60MPa, S275MPa.....	196
Figure (4.38):	Stresses' Contours Along CFST Composite Column, C70MPa, S275MPa.....	198
Figure (4.39):	Stresses' Contours Along Stiffener Plates, under Axial Compression and Uni-Direction Bending S355MPa.....	200
Figure (4.40):	Stresses' Contours Along Stiffener Plates, under Axial Compression and Uni-Direction Bending S275MPa.....	201
Figure (4.41):	Stresses' Contours Along Encased Composite Column, C40MPa, S355MPa.....	204
Figure (4.42):	Stresses' Contours Along Encased Composite Column, C50MPa, S355MPa.....	206
Figure (4.43):	Stresses' Contours Along Encased Composite Column, C60MPa, S355MPa.....	208
Figure (4.44):	Stresses' Contours Along Encased Composite Column, C70MPa, S355MPa.....	210
Figure (4.45):	Stresses' Contours Along Encased Composite Column, C40MPa, S275MPa.....	212
Figure (4.46):	Stresses' Contours Along Encased Composite Column, C50MPa, S275MPa.....	214
Figure (4.47):	Stresses' Contours Along Encased Composite Column, C60MPa, S275MPa.....	216
Figure (4.48):	Stresses' Contours Along Encased Composite Column, C70MPa, S275MPa.....	218
Figure (4.49):	Stresses' Contours Along CFST Composite Column, C40MPa, S355MPa.....	221
Figure (4.50):	Stresses' Contours Along CFST Composite Column, C50MPa, S355MPa.....	223

Figure (4.51):	Stresses' Contours Along CFST Composite Column, C60MPa, S355MPa.....	225
Figure (4.52):	Stresses' Contours Along CFST Composite Column, C70MPa, S355MPa.....	227
Figure (4.53):	Stresses' Contours Along CFST Composite Column, C40MPa, S275MPa.....	229
Figure (4.54):	Stresses' Contours Along CFST Composite Column, C50MPa, S275MPa.....	231
Figure (4.55):	Stresses' Contours Along CFST Composite Column, C60MPa, S275MPa.....	233
Figure (4.56):	Stresses' Contours Along CFST Composite Column, C60MPa, S275MPa.....	235
Figure (4.57):	Stresses' Contours Along Stiffener Plates, under Axial Compression and Bi-Axial Bending.....	237
Figure (5.1):	Nominal Compressive Strength for Encased Column with Steel Grade, S355 MPa.....	240
Figure (5.2):	Concrete Compressive Stress of Encased Column under Nominal Compressive Loads specified in the 3D-Fiber (Solid) Model, S355 MPa.....	241
Figure (5.3):	Steel Compressive Stress of Encased Column under Nominal Compressive Loads specified in the 3D-Fiber (Solid) Model, S355 MPa.....	241
Figure (5.4):	Nominal Compressive Strength of Encased Column Adopted by Codes and 3D-Fiber Model for Both Steel Grades, S275MPa and S355MPa.....	242
Figure (5.5):	Nominal Compressive Strength for Encased Column with Steel Grade, S275 MPa.....	243
Figure (5.6):	Concrete Compressive Stress of Encased Column under Nominal Compressive Loads specified in the 3D-Fiber (Solid) Model, S275 MPa.....	244
Figure (5.7):	Steel Compressive Stress of Encased Column under Nominal Compressive Loads specified in the 3D-Fiber (Solid) Model, S275 MPa.....	245
Figure (5.8):	Nominal Compressive Strength for CFST Column with Steel Grade, S355 MPa.....	247
Figure (5.9):	Concrete Compressive Stress of CFST Column under Nominal Compressive Loads specified in the 3D-Fiber (Solid) Model, Steel Grade S355 MPa.....	248
Figure (5.10):	Steel Compressive Stress of CFST Column under Nominal Compressive Loads specified in the 3D-Fiber (Solid) Model, Steel Grade 355 MPa.....	248
Figure (5.11):	Nominal Compressive Strength for CFST Column with Steel Grade, S275 MPa.....	249
Figure (5.12):	Nominal Compressive Strength of CFST Column Adopted by Codes and 3D-Fiber Model for Both Steel Grades, S275MPa and S355MPa.....	250
Figure (5.13):	Compression Steel Stresses in the Stiffener Plates under Axial Compression Loads.....	251
Figure (5.14):	Nominal Compressive Strength of Encased Column under Axial Compression and Uni-direction Bending Moments.....	253
Figure (5.15):	Concrete Compressive Stress of Encased Column under Axial Compression Load and Uni-direction Bending as extracted from 3D-Fiber (Solid) Model, S275MPa, and S355 MPa.....	255
Figure (5.16):	Steel Compressive Stress of Encased Column under Axial Compression Load and Uni-direction Bending as extracted from 3D-Fiber (Solid) Model, S275MPa, and S355 MPa.....	255
Figure (5.17):	Maximum Eccentric Compression Load on CFST Column, $e_x=85.75\text{mm}$, S355MPa.....	256

Figure (5.18):	Maximum Eccentric Compression Load on CFST Column, $e_x=85.75\text{mm}$, S275MPa.....	257
Figure (5.19):	Concrete Compressive Stress of CFST Column under Nominal Compressive Loads specified in the 3D-Fiber (Solid) Model, Steel Grade S275MPa, and S355 MPa.....	258
Figure (5.20):	Steel Compressive Stress of CFST Column under Nominal Compressive Loads specified in the 3D-Fiber (Solid) Model, Steel Grade S275MPa, and S355 MPa.....	258
Figure (5.21):	Compression Steel Stresses on the Stiffener Plates under Axial Compression Loads and Uni-Direction Bending Moments.....	259
Figure (5.22):	Nominal Compressive Strength of the Encased Section under Biaxial loading, Steel Grade S355MPa, $e_x=85.75\text{mm}$, and $e_y=104.50\text{mm}$	261
Figure (5.23):	Nominal Compressive Strength of the Encased Section under Biaxial loading, Steel Grade S275MPa, $e_x=85.75\text{mm}$, and $e_y=104.50\text{mm}$	261
Figure (5.24):	Stress Distributions along Concrete of the Encased Composite Column.....	263
Figure (5.25):	Stress Distributions along Steel I Section Embedded in the Encased Composite Column.....	263
Figure (5.26):	Maximum Eccentric Compression Load on the CFST Column, $e_x=85.75\text{mm}$, $e_y=104.50\text{mm}$, S355MPa.....	265
Figure (5.27):	Maximum Eccentric Compression Load on the CFST Column, $e_x=85.75\text{mm}$, $e_y=104.50\text{mm}$, S275MPa.....	265
Figure (5.28):	Concrete Compressive Stress of CFST Column under Bi-Axially Loading specified in the 3D-Fiber (Solid) Model, Steel Grade S275MPa, and S355 MPa.....	266
Figure (5.29):	Steel Compressive Stress of CFST Column under Bi-Axially Loading specified in the 3D-Fiber (Solid) Model, Steel Grade S275MPa, and S355 MPa.....	267
Figure (5.30):	Steel Stresses in the Stiffener Plates under Axial Compression Loads and Bi-Axial Bending Moments, Steel Grade S275MPa, and S355MPa.....	268

LIST OF TABLES:

Table [2.1]:	Limitation of Width to Thickness Ratios for Compression Steel Elements in Composite Members subject to Axial Compression Load, (ANCI / AISC 360-16).....	26
Table [2.2]:	Coefficient C_p and C_m as per ANCI / AISC 360-16.....	29
Table [2.3]:	Local Buckling requirements, Maximum values (d/t) & (h/t) with f_y in N/mm ² as extracted from Eurocode 4 Part 1.1.....	39
Table [2.4]:	Determination of Factor β related to the second order analysis theory.....	51
Table [2.5]:	Imperfection Factor for Buckling Modes.....	51
Table [2.6]:	Buckling Modes and Imperfections for Different types of Composite Columns.....	52
Table [2.7]:	Design Shear Strength (t_{Rd}) as per Eurocode 4.....	54
Table [2.8]:	Different Methods to Design Shear Studs.....	61
Table [2.9];	Main Factors utilized by Zhang and Shahrooz.....	71
Table [2.10]:	Tested Columns' Stiffnesses, Hull [1998].....	73
Table [2.11]:	Ratio between Experimental Capacities and Theoretical Capacities, Hull [1998].....	74
Table [2.12]:	Summary of Design Parameters for test specimens extracted from Jin-Won Kim et. al. [2014].....	87
Table [2.13]:	Properties and Sizing of SRSCFSHS Column Jing-ming Cai et. al. [2016].....	91
Table [2.14]:	Geometry of the Steel Tubes used in the Experimental Work, T. Kibryia [2017].....	94
Table [2.15]:	Ultimate Strength of Encased Composite Columns Specimens, El-Tawil, et. al. [1999]..	106
Table [2.16]:	Curvature Ductilities.....	106
Table [2.17]:	Details of Columns Specimens, Dundar, et. al. [2007].....	108
Table [2.18]:	Experimental and Theoretical Results of RC Columns, Dundar, et. al. [2007].....	109
Table [2.19]:	Failure Loads for each Specimen and its Failure Mechanism, Z. Huang, et. al. [2018]...	113
Table [4.1]:	Straining Actions Along Column Height.....	124
Table [4.2]:	Nominal Compressive Strength of the Encased Composite Column, C40MPa, S355.....	131
Table [4.3]:	Nominal Compressive Strength of the Encased Composite Column, C50MPa, S355.....	133
Table [4.4]:	Nominal Compressive Strength of the Encased Composite Column, C60MPa, S355.....	135
Table [4.5]:	Nominal Compressive Strength of the Encased Composite Column, C70MPa, S355.....	137
Table [4.6]:	Nominal Compressive Strength of the Encased Composite Column, C40MPa, S275.....	139
Table [4.7]:	Nominal Compressive Strength of the Encased Composite Column, C50MPa, S275.....	141
Table [4.8]:	Nominal Compressive Strength of the Encased Composite Column, C60MPa, S275.....	143
Table [4.9]:	Nominal Compressive Strength of the Encased Composite Column, C70MPa, S275.....	145

Table [4.10]:	Nominal Compressive Strength of the CFST Composite Column, C40MPa, S355.....	147
Table [4.11]:	Nominal Compressive Strength of the CFST Composite Column, C50MPa, S355.....	149
Table [4.12]:	Nominal Compressive Strength of the CFST Composite Column, C60MPa, S355.....	151
Table [4.13]:	Nominal Compressive Strength of the CFST Composite Column, C70MPa, S355.....	153
Table [4.14]:	Nominal Compressive Strength of the CFST Composite Column, C40MPa, S275.....	155
Table [4.15]:	Nominal Compressive Strength of the CFST Composite Column, C50MPa, S275.....	157
Table [4.16]:	Nominal Compressive Strength of the CFST Composite Column, C60MPa, S275.....	159
Table [4.17]:	Nominal Compressive Strength of the CFST Composite Column, C70MPa, S275.....	161
Table [4.18]:	Stresses on the Steel Stiffener Plates.....	163
Table [4.19]:	Encased Column Section Capacity under Axial Compression and Uni-Direction Bending, C40MPa, S355.....	166
Table [4.20]:	Encased Column Section Capacity under Axial Compression and Uni-Direction Bending, C50MPa, S355.....	168
Table [4.21]:	Encased Column Section Capacity under Axial Compression and Uni-Direction Bending, C60MPa, S355.....	170
Table [4.22]:	Encased Column Section Capacity under Axial Compression and Uni-Direction Bending, C70MPa, S355.....	172
Table [4.23]:	Encased Column Section Capacity under Axial Compression and Uni-Direction Bending, C40MPa, S275.....	174
Table [4.24]:	Encased Column Section Capacity under Axial Compression and Uni-Direction Bending, C50MPa, S275.....	176
Table [4.25]:	Encased Column Section Capacity under Axial Compression and Uni-Direction Bending, C60MPa, S275.....	178
Table [4.26]:	Encased Column Section Capacity under Axial Compression and Uni-Direction Bending, C70MPa, S275.....	180
Table [4.27]:	CFST Column Section Capacity under Axial Compression and Uni-Direction Bending, C40MPa, S355.....	183
Table [4.28]:	CFST Column Section Capacity under Axial Compression and Uni-Direction Bending, C50MPa, S355.....	185
Table [4.29]:	CFST Column Section Capacity under Axial Compression and Uni-Direction Bending, C60MPa, S355.....	187
Table [4.30]:	CFST Column Section Capacity under Axial Compression and Uni-Direction Bending, C70MPa, S355.....	189
Table [4.31]:	CFST Column Section Capacity under Axial Compression and Uni-Direction Bending, C40MPa, S275.....	191
Table [4.32]:	CFST Column Section Capacity under Axial Compression and Uni-Direction Bending, C50MPa, S275.....	193

Table [4.33]:	CFST Column Section Capacity under Axial Compression and Uni-Direction Bending, C60MPa, S275.....	195
Table [4.34]:	CFST Column Section Capacity under Axial Compression and Uni-Direction Bending, C70MPa, S275.....	197
Table [4.35]:	Stresses on the Steel Stiffener Plates due to Axial Compression and Uni-Direction Bending.....	199
Table [4.36]:	Encased Column Section Capacity under Axial Compression and Bi-Axial Bending, C40MPa, S355.....	203
Table [4.37]:	Encased Column Section Capacity under Axial Compression and Bi-Axial Bending, C50MPa, S355.....	205
Table [4.38]:	Encased Column Section Capacity under Axial Compression and Bi-Axial Bending, C60MPa, S355.....	207
Table [4.39]:	Encased Column Section Capacity under Axial Compression and Bi-Axial Bending, C70MPa, S355.....	209
Table [4.40]:	Encased Column Section Capacity under Axial Compression and Bi-Axial Bending, C40MPa, S275.....	211
Table [4.41]:	Encased Column Section Capacity under Axial Compression and Bi-Axial Bending, C50MPa, S275.....	213
Table [4.42]:	Encased Column Section Capacity under Axial Compression and Bi-Axial Bending, C60MPa, S275.....	215
Table [4.43]:	Encased Column Section Capacity under Axial Compression and Bi-Axial Bending, C70MPa, S275.....	217
Table [4.44]:	CFST Column Section Capacity under Axial Compression and Bi-Axial Bending, C40MPa, S355.....	220
Table [4.45]:	CFST Column Section Capacity under Axial Compression and Bi-Axial Bending, C50MPa, S355.....	222
Table [4.46]:	CFST Column Section Capacity under Axial Compression and Bi-Axial Bending, C60MPa, S355.....	224
Table [4.47]:	CFST Column Section Capacity under Axial Compression and Bi-Axial Bending, C70MPa, S355.....	226
Table [4.48]:	CFST Column Section Capacity under Axial Compression and Bi-Axial Bending, C40MPa, S275.....	228
Table [4.49]:	CFST Column Section Capacity under Axial Compression and Bi-Axial Bending, C50MPa, S275.....	230
Table [4.50]:	CFST Column Section Capacity under Axial Compression and Bi-Axial Bending, C60MPa, S275.....	232
Table [4.51]:	CFST Column Section Capacity under Axial Compression and Bi-Axial Bending, C70MPa, S275.....	234

Table [4.52]:	Stresses on the Steel Stiffener Plates due to Axial Compression and Uni-Direction Bending.....	236
---------------	--	-----

CHAPTER I

INTRODUCTION

1.1 COMPOSITE ELEMENTS DESIGN AND CONSTRUCTION

Composite structures comprise mainly two different materials, steel and concrete.

The use of composite structures has been widely developed in the construction of high-rise buildings, bridges and long span structures.

The use Convectional Concrete Column is limited in the high-rise buildings due to the constraint from the architects on increasing size of the columns, so the composite columns provide appropriate solution to the architect and the Client with less column sizing.

Composite columns have two main types described as follow:

- Encased Steel Reinforce Composite Column (Wide Flange section encased in RC columns (SRC)
- Concrete Filled Steel Tube Column (CFST)

The composite column provides the following benefits;

- a. Utilize the full advantages of both materials, high strength steel section with appropriate ductility contributes to the bearing capacity and ductility of the concrete.
- b. Increase the bearing capacity of the columns without significant increase in the sizing of the columns.
- c. Provide less dimensions of the columns compared to conventional reinforced concrete columns which is a vital requirement by the architect.
- d. Improve axial and bending stiffnesses of the columns.
- e. Protect steel sections from buckling
- f. Protect steel sections from fire in case of using encase composite columns
- g. Reducing weight of the columns
- h. Eliminate formwork in case of using concrete filled steel tube column.

1.2 ENCASED STEEL REINFORCED COMPOSITE COLUMN (SRC)

The SRC Column comprises steel section encased by reinforced concrete. **Fig. (1.1)** is showing standard arrangements for the SRC Column. The interaction between steel and concrete is a significant design issue, since the column resistance is affected by the bond between steel and concrete, in case of having full connection between steel and

concrete, then no relative slip is anticipated at the interface between steel and concrete and the strain of two different materials at the interface would be consistent. The load transfer between steel and concrete is recognized by the shearing forces at the interface between concrete and steel. In case both sections concrete, and steel are partially connected or there is no connection between steel and concrete, then it might be possible to have relative slip on the interface level, and consequently the strain distribution of the concrete and steel will not be compatible. **Fig. (1.2)** showing strain distribution of the SRC column.

The shear resistance on the encased (SRC) column at the interface between steel and concrete is achieved through bond stress and shear connectors. The shear connectors can be flexible connectors such as studs, or deformed rebar, and can be rigid connectors such steel plates or channels.

Japanese researchers illustrated that the bond stress between concrete and steel is lower than the bond between concrete and smooth rebar by 45% (AIJ-SRC-2002).

Accordingly; the bond stresses between concrete and steel to be ignored in case of using shear connectors. It is stated also that the bond stress can be significantly enhanced by providing steel section with rough surface or ribs.

The main objective of the shear connectors installed in the composite column is to transfer axial load between concrete and steel element.

The shear studs are commonly used in the composite elements due to the ease of fabrication and installation, in addition; it can reduce the stress concentration at the interface with the concrete. Ollgaard (1977) suggested the following formulas for the shear stud curvature.

$$V = V_u (1 - e^{-ns})^m \quad \text{Eqn. (1.1)}$$

Where:

V_u Ultimate strength of the shear Stud

S Relative Slip (mm)

m, n Parameter Calibrated by experiments, $m=0.558$, $n=1$

R.P. Johnson recommended that $m=0.989$, $n=1.535$; while Aribert suggested $m=0.80$, and $n=0.70$.

Fig. (1.3) showing constitutive curves for the shear studs

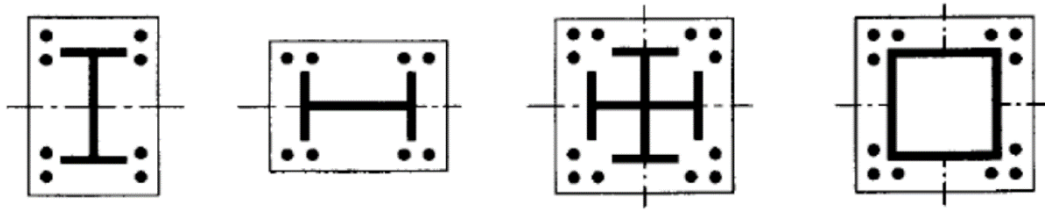


Fig. (1.1) Typical SRC Column Arrangements

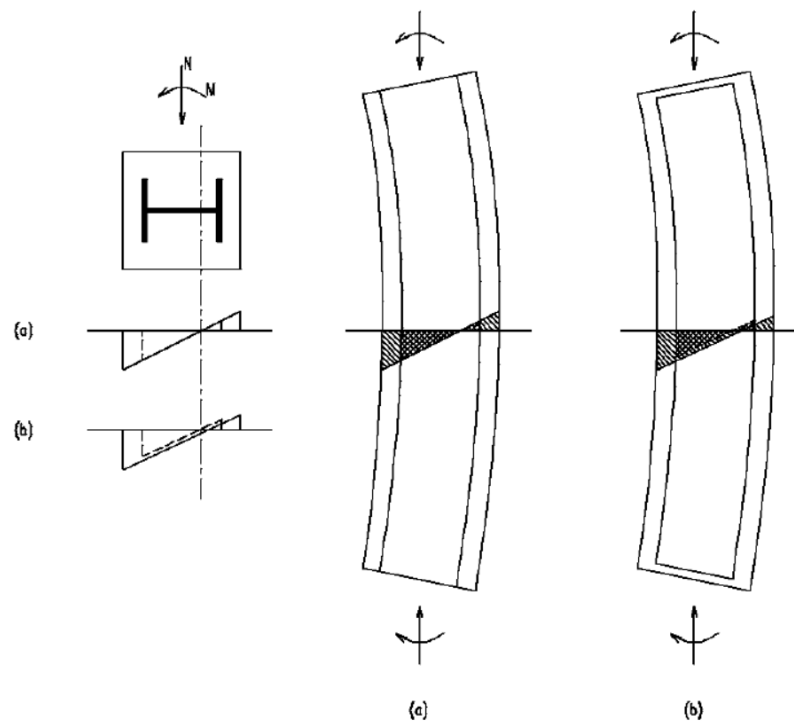


Fig. (1.2) Strain Distribution, (a) Fully Connected SRC Column; (b) Partially Connected SRC Column

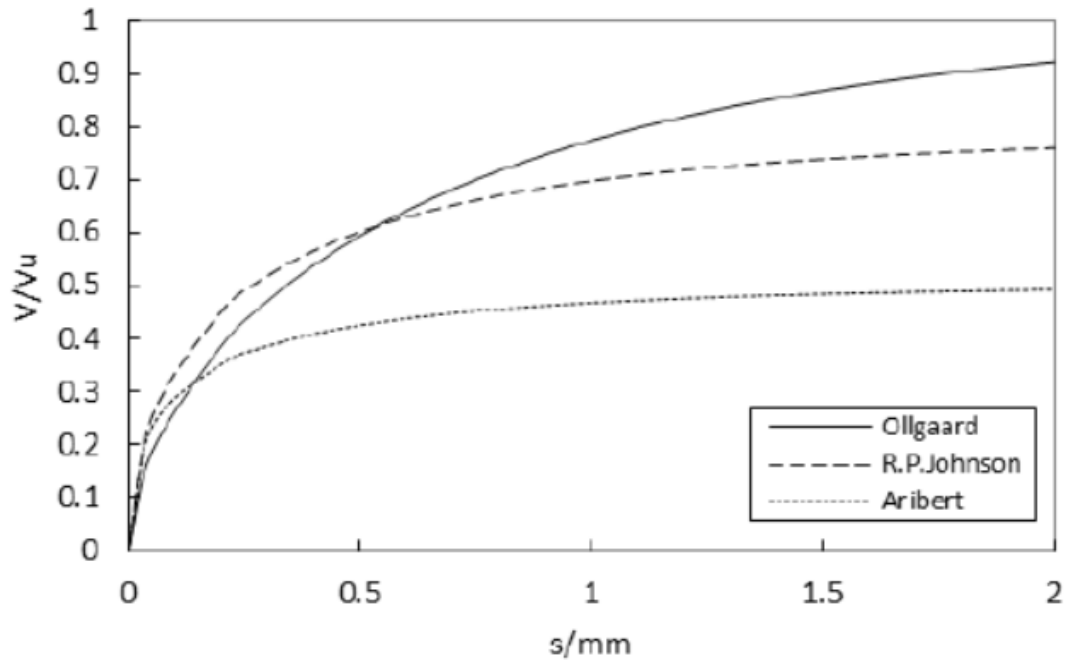


Fig. (1.3) Shear Studs Constitutive Curves

1.3 CONCRETE FILLED STEEL TUBE COLUMN (CFST)

The behavior of the concrete filled tube column is basically different from the behavior of the hollow steel tube column. The filling of the steel tube by concrete has a major impact on the composite section stiffness, strength, and its ductility.

The increase in the stiffness, strength and ductility is a result of the contribution of the concrete, in addition; the concrete change elastic local buckling mode by holding the steel tube to deform inwards as presented in **Fig. (1.4)** and **Fig. (1.5)**.

The elastic local buckling has been studied by Bradford et al. [1998] and it was shown that the buckling factor for the rectangular hollow steel tube increased from 4.0 to 10.60 with concrete filled tube section. Based on this finding; the buckling stresses of the rectangular filled section is 2.65 times the hollow steel tube section. For the circular filled tube, the local buckling stresses is 1.73 times the circular hollow steel tube.

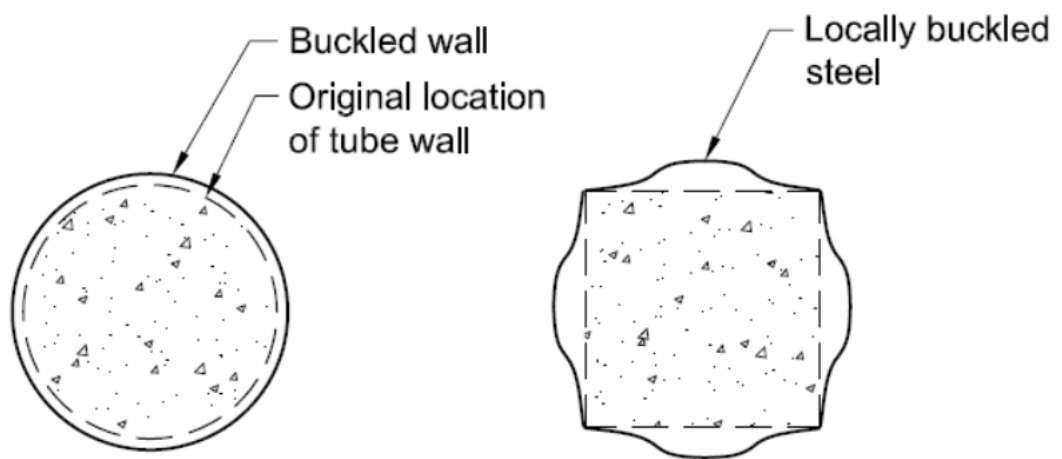


Fig. (1.4) Local Buckling Mode for the Cross-Sectional of the Concrete Filled Tube

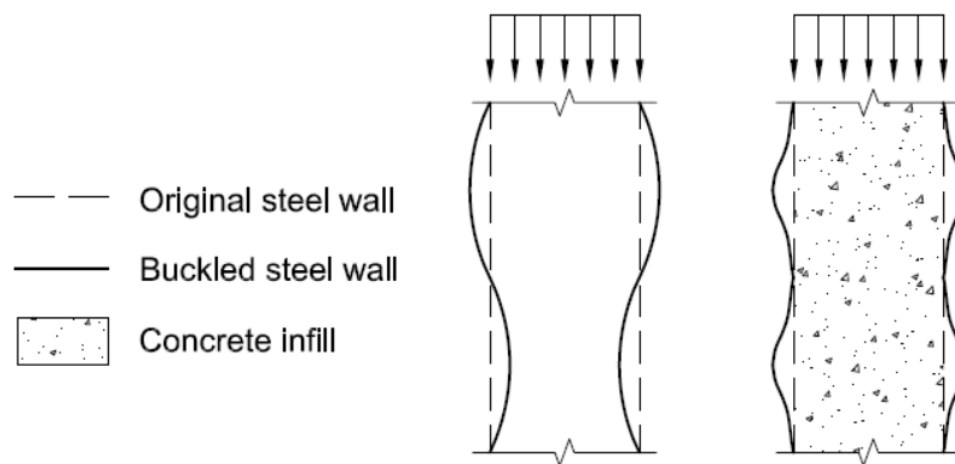


Fig. (1.5) Elastic Local Buckling Change along Length of the Concrete Filled Tube

1.4 RESEARCH SIGNIFICANCE

The composite column is commonly used in the high-rise buildings in order to reduce the sizing of the columns and to enhance the ductility and concrete. The use of Encased column is easier than CFST column in terms fabrication and installation, however the CFST column provides more resistance to combined axial compression and bi-axial bending and could be more efficient in some cases as per the design requirements.

The research is quite essential to understand the behavior of the two different composite elements connected to each other under different parameters and different type of loading.

Furthermore; it provides a detailed comparison between simplified analysis method and the detailed finite element approach, consequently; it allows the Engineer to understand the load path / stress distribution along both composite members, and to be considered in the design of similar cases.

The research as well provides insight for future researches might be conducted for similar cases

1.5 RESEARCH CHALLENGE

The challenge in this research is to create a 3D model with boundary conditions inline with the actual case study and to ensure that the load path is correct and transferred from the CFST element to the Encased element as predicted by the simplified methods adopted by the international codes.

The 3D Fiber (Solid) Model has been developed in order to study the behavior of each single element including stiffener plates and overlapping between CFST member and Encased member.

With this sophisticated element, it was essential to examine the intended column under different cases of loading and to compare the results with the formulas adopted by AISc316-16, ACI318-11, and Eurocode-4.

The behavior of the CFST element or Encased element has been widely studied individually in the past with massive number of experimental work, but connecting both

element to each other under large axial compression load with bi-axial flexure is a major challenge for the Engineer and required more investigation and testing to ensure the load transferred inline with the design assumptions.

1.6 RESEARCH OBJECTIVES

The research objective to illustrate the following:

1. Study the behavior of a tapered concrete filled steel tube column connected to encased composite column under three different loading as follow:
 - a. Axial compression load.
 - b. Combined Axial Compression and Uni-Direction Bending.
 - c. Combined Axial Compression and Bi-Direction Bending.
2. Provide Comparison between the simplified approach adopted by different codes such AISC316-16, ACI 318-11, and urocode-4.
3. Provide a comparison between simplified methods by codes and the 3D Fiber (Solid) Model.
4. Study the effect on the column strength using different parameters such as changing concrete strength and/or steel grade as well.
5. Study the load transfer from the CFST element to the encased element.
6. Study the stress distribution along the column height and provide insight about the local stress concertation.
7. Study the stress distribution and load path through the overlapping zone between CFST Element and Encased element.

1.7 CASE STUDY

The case study utilized in this research was an existing high rise building of 250m height (3B+G+60) with a major transfer floor at level 11. There were two encased composite columns from the foundation up to level 10, then those two columns have been changed to tapered CFST columns from level 10 to 11 in order to withstand a significant increase in the bi-axial bending moments at the interface with the transfer slab. Level 10 was MEP floor, so it was accepted by the architect to have tapered column geometry. The encased composite column was (1400 x 1400) mm with embedded heavy I steel Section of (1000 x 1000 x 100) mm. The concrete of the encased column was confined by a closed stirrup of T16 @ every 200mm. the vertical rebar used in the encased column was 40T40. The tapered steel tube of the CFST column was varying from

(1400 x 1400 x 100) mm at the interface with the encased column to (2250 x 2250 x 100) mm at the top part embedded into the transfer slab.

The size of the CFST column is (2000x2000x100) at the interface with the Transfer slab which has been considered in the design of the column under gravity and bi-axially bending.

The concrete cylinder strength used in the composite columns was 70MPa. The depth of the transfer slab was 2.50m and it is supporting about 50 floors above the transfer level. The steel grade used in this element was S355, and the rebar has been provided with grade 500MPa.

Fig. (4.1) and **(4.2)** in Chapter (4) provide full detailed information about the case study adopted in this research.

1.8 SCOPE

The subsequent chapters display a comprehensive summary of the previous researches conducted for the CFST Column and Encased Column and the results of the case study analyzed using a detailed finite element approach.

Chapter (2) demonstrates Literature review including international code provisions for the design of the composite columns and the previous researches conducted for the Composite Columns.

Chapter (3) describe the research methodology and data collected for the research.

Chapter (4) shows the results of the case study adopted in the research. Chapter (5) presents a technical discussion for the results. Chapter (6) provides a summary, conclusion and recommendation.

CHAPTER 2

LITERATURE REVIEW

2.1 INTRODUCTION

Literature Review is focusing on the various parameters affecting the behavior of the composite columns.

Those various parameters including concrete strength, steel section strength, steel reinforcement grade, shear studs, stiffness, bond strength, friction strength, and steel section characteristics.

This Chapter illustrates the design approach of the encased composite column and concrete filled tube column in-line with the provision of Eurocode 4 and American Standard, Load and Resistance Factor Design (AISC -LRFD).

A narrative for the Composite Mega Columns has been presented in this chapter in order to illustrate the current research and testing adopted for this type of composite columns with 4 isolated steel sections (ISRC).

The Literature review reports on previous researches and experimental works conducted for the Composite Columns and the parameters affecting their behaviors under different type of loadings.

2.2 ADVANCE TECHNOLOGY OF CONSTRUCTION MATERIAL

The use of advance material is widely used in the construction of the high-rise buildings, bridges, long span structures, and other complex and irregular structures.

The advance materials such as high strength concrete, and high-performance steel have an influence impact on the strength, stiffness and durability of the composite elements compare to conventional material which is making their use in the construction of the complicated structures more privilege than conventional materials.

2.3 HIGH STRENGTH AND HIGH-PERFORMANCE CONCRETE

[Popovics, 1973] has developed the stress strain relationship for the normal strength concrete by adopting the following formula:

$$f_c / f'_c = \epsilon_c / \epsilon'_c \left[n / \{n-1-(\epsilon_c / \epsilon'_c)\} \right] \quad \text{Eqn. (2.1)}$$

Where:

f_c Concrete Compressive Stress

f'_c Concrete Compressive Strength

ϵ_c Compressive Strain of Concrete

ϵ'_c Ultimate crushing strain of Concrete

n Concrete curve fitting factor

[Nilson, 1987] stated that the high strength concrete has higher modulus of elasticity, consequently creep development on the long term is significantly reduced by increasing the concrete strength.

The stress-strain relationship formula for the high strength concrete has been developed by [Collins & Mitchell, 1991] as follow:

$$f_c / f'_c = \epsilon_c / \epsilon'_c \left[n / \{n-1-(\epsilon_c / \epsilon'_c)^{nk}\} \right]$$

Eqn. (2.2)

Where:

$$n = 0.80 + f'_c / 2500$$

$$k = 0.67 + f'_c / 9000$$

The stress-strain relationship curve presented in **Fig. (2.1)** is describing the difference between high strength concrete and normal strength concrete as developed by Collins et. al. [1993].

Concrete crushing compressive strain has been identified between 0.002 to 0.003 for normal strength concrete and high strength concrete.

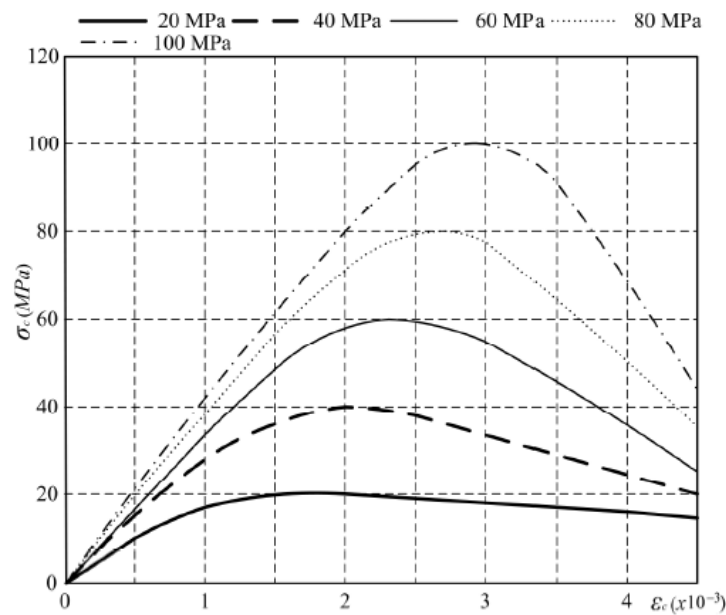


Fig. 2.1 Stress-Strain Relationship Curve of Concrete, Collins et al. (1993) model

The stress-strain relationship in **Fig. (2.1)** illustrates that the high strength concrete has a rapid post-peak unloading response compared to that of normal strength concrete.

The stress-strain relationship behavior of the confined concrete has been described by Collins and Mitchell, [1991] using the following formula:

$$f_c / f'_{cc} = \epsilon_c / \epsilon'_{cc} \left[n / \{n-1 + (\epsilon_c / \epsilon'_{cc})^{nk} \} \right] \quad \text{Eqn. (2.3)}$$

$$k = [0.67 + \{f'_c / 62\}] * f'_c / \epsilon'_{cc} \geq 1.0 \text{ (MPa)}$$

$$n = E_c / [E_c - \{f'_{cc} / \epsilon'_{cc}\}]$$

Where:

f'_{cc} Ultimate Compressive Strength of Confined Concrete (MPa)

ϵ'_{cc} Strain at Ultimate Compressive Strength of Confined Concrete

The failure mode of the high strength concrete is more brittle than conventional concrete which has large ductility. The confinement of concrete has an influence on the concrete characteristics.

Fig. (2.2) describes the predicted stress-strain relationship curves of the normal strength concrete and high strength concrete with lateral confinement developed by Collins et. al. [1991]. The stress-strain curve of the confined concrete demonstrating the increase in the concrete strength, ductility, and crushing strain for the confined high strength concrete compare to the un-confined high strength concrete.

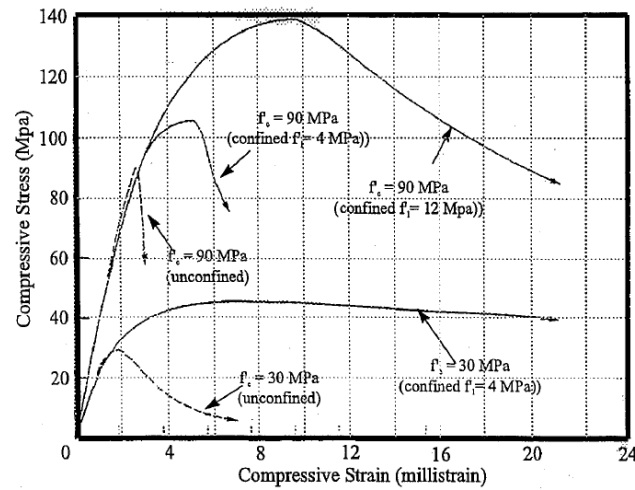


Fig. 2.2 Stress-Strain Relationship Curve of Confined Concrete, Collins et al. (1991)

The ACI Committee defined the high strength concrete as concrete with compressive cylinder strength $\geq 55\text{MPa}$. The reason of selecting concrete strength of 55MPa as high strength concrete is the additional requirements in terms of mixtures, testing, and operation.

The concrete performance is affected by the type of the aggregate and curing methodology of the concrete.

Russel H.G. [1993] summarized the following performance requirements based on ACI definition of the High-Performance Concrete:

- High Workability concrete
- Self-Consolidated Concrete (SCC)
- Foamed Concrete
- High Strength Concrete
- Lightweight Concrete
- No-fines Concrete
- Pumped Concrete
- Sprayed Concrete
- Waterproofed Concrete
- Autoclaved aerated Concrete
- Roller Compacted Concrete

High Performance Concrete is engineered to enhance durability, and strength of the concrete compare to Conventional Concrete.

High Performance Concrete Mixes can be similar to the Conventional Concrete Mixes, but the proportions are considerably different since it is designed to improve the strength and durability and provide a good resistance to the surrounding environment.

The mixture proportions of the high strength and high-performance concrete can be identified as follow:

- Cement
- Supplementary cementitious material (GGBS, Fly Ash, Silica Fume, Natural Pozzolan, etc.).
- Aggregate, size and grading

- Chemical Admixtures (Water reducing Admixture, Retarding Admixtures, Accelerating Admixtures, Aire Entrainment Agents, Shrinkage Reducing Agents, Steel Corrosion Inhibitors, Anti-Washout Admixtures, Alkali-Aggregate Reaction Inhibitors, etc.
- Water

2.4 CONCRETE MODULUS OF ELASTICITY (YOUNG'S MODULUS)

[Thomas and Raeder, 1934] identify the Young's modulus as the slope of tangent to the stress-strain curve for uniaxial compression at 25% of the maximum compressive stress. The calculated values were ranging between 29 and 36 GPa for concrete cylinder strength ranging from 69 to 76MPa.

There are a lot of researches done afterwards to calculate the elastic modulus of elasticity of the concrete, [Ahmad and Shah, 1985] introduced the following formula for the modulus of elasticity of high strength concrete which already published in ACI 363-10

$$E_c = 3.385 \times 10^{-5} \times w_c^{2.5} \times (f'_c)^{0.5} \text{ (MPa)} \quad \text{for } f'_c < 84\text{MPa} \quad \text{Eqn. (2.4)}$$

The ACI 363-10 specify the concrete with axial compressive strength of 55MPa or higher as high strength concrete.

ACI 318-11, specify two equations to calculate the elastic modulus of elasticity of the concrete as follow:

$$E_c = 4700 (f'_c)^{0.5} \text{ (MPa)} \quad \text{Eqn. (2.5)}$$

$$E_c = W_c^{1.5} * 0.043 * (f'_c)^{0.5} \text{ (MPa)} \quad \text{Eqn. (2.6)}$$

2.5 HIGH STRENGTH AND HIGH-PERFORMANCE STEEL

Nowadays, the advance steel technology produces high strength steel plates with low carbon, good weldability, ductility, corrosion resistance, and fracture toughness.

Fig. (2.3) illustrates the stress-strain relationship curves of the high-performance steel and conventional steel.

It is noted in **Fig. (2.3)** that the high-performance steel establishes strain harden directly after yielding similar to the conventional steel but the strain hardening modulus is lower in the conventional steel.

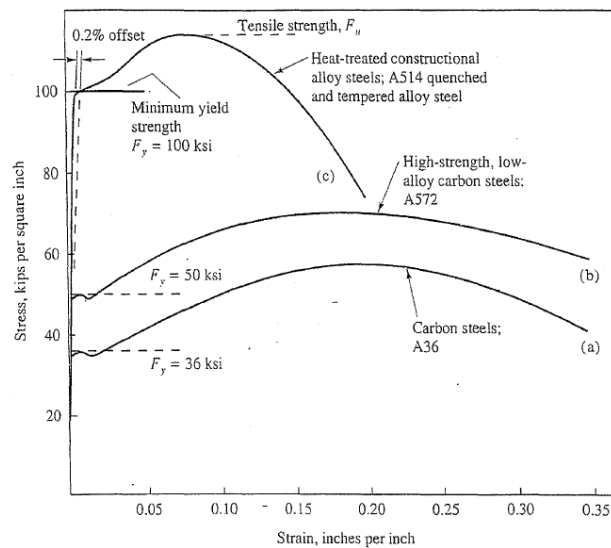


Fig. 2.3 Stress-Strain Relationship Curve for High Performance Steel and Conventional Steel
[Salmon and Johnson, 1996]

The two main differences between high performance steel and conventional steel is the higher ratio of the yield steel to the ultimate stress (Yield Stress Ratio), and the lower value of the strain ductility of high-performance steel compared to the conventional steel.

The above mentioned two factors, Strain Ductility and Yield Stress Ratio have a significant impact on the plasticity behavior of the tension members [Sooi et al., 1995].

High performance steel demonstrates less reserved capacity after yielding compared to the conventional steel for the member subject to uniaxial tension load as a result of its high yield stress ratio [Sooi et al., 1995].

High performance steel illustrates less inelastic elongation than that of conventional steel as a result of the its lower strain ductility.

Flexure members of high-performance steel has a small ratio of the maximum moment to the plastic moment in comparison of conventional steel members [Ricles et al., 1996].

An analytical study with experimental program [Ricles et al., 1996] on hollow steel tubes made from high performance steel in order to examine the behavior of the high-performance steel subject to axial compression load.

The outcome of the above study and experimental program demonstrated that the local buckling of the hollow steel tube controls its compression capacity to less than its yield load.

Fig. (2.4) shows that the capacity of the hollow steel tube under compression load is reduced by the increase in the width to thickness ratio (b/t), so the use of high-performance steel has no influence on the local buckling.

Filling the steel tube with concrete would allow the member to buckle under higher load, therefore the capacity of the section under compression load will be significantly increased.

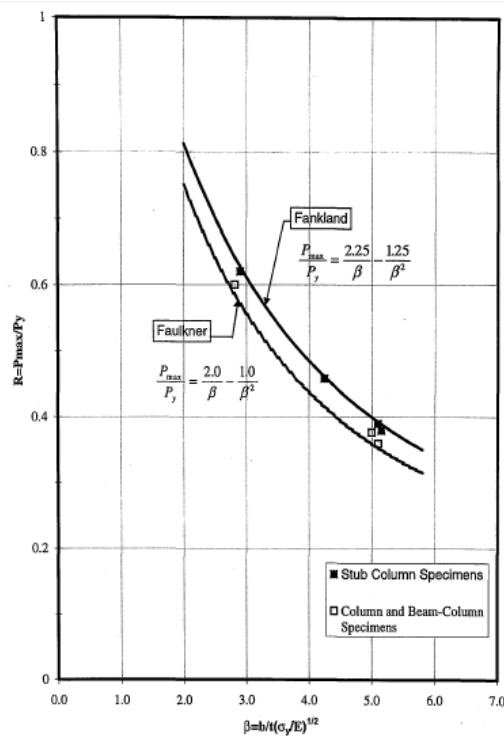


Fig. 2.4 Effect of b/t Ratio on High Strength Steel Box Column Axial Load Capacity from (Ricles et al., 1996)

2.6 BEHAVIOR OF CONFINED CONCRETE IN THE COMPOSITE COLUMNS

The concrete filled steel tube column provides full confinement to the concrete and the concrete behavior is consistent along the entire concrete cross section. Much experimental works and testing illustrated that the confinement effect in the concrete filled tube column enhance the ductility but does not increase the section capacities.

Mander et al. [1988] and Sheikh et al. [1988] have studied the behavior of conventional concrete column due to confinement and it was concluded that the confinement is different along concrete cross section. Chen and Lin [2006] proposed three different zones for the confinement. Those three zones are categorized into highly confined concrete, partially confined concrete, and unconfined concrete. **Fig. (2.5)** presenting the three different confined zones for the encased composite columns.

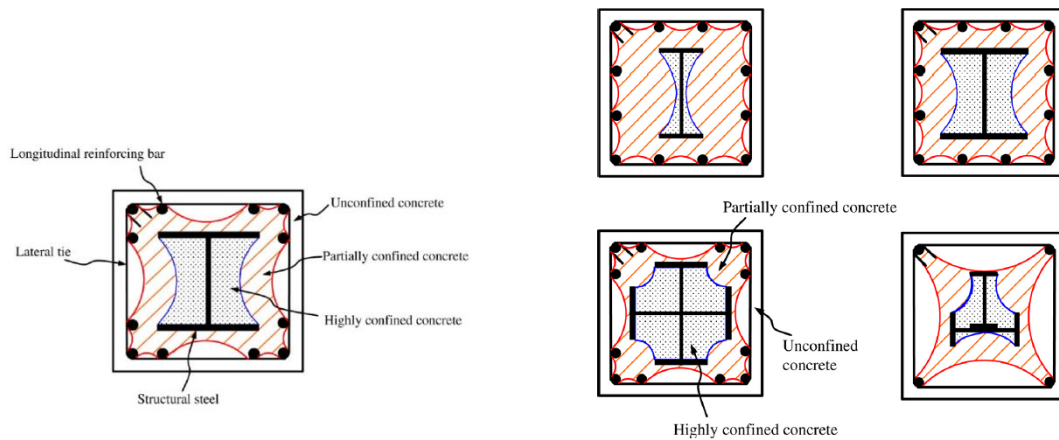


Fig. 2.5 Three Different Confinement zones in the Encased Composite Column, [Chen and Lin, 2006]

The following formula illustrated the relation between confined compressive concrete strength (f_c) and unconfined compressive strength (f_{cc}).

$$f_{cc} = f_c \cdot K_i \quad \text{Eqn. (2.7)}$$

Where:

K_i Confinement Factor, K_p for partially confined, and K_h for highly confined.

f_c Unconfined concrete cylinder compressive strength

f_{cc} Confined compressive strength

Fig. (2.6A) & (2.6B) showing the methodology to calculate the confinement factors as proposed by Chen and Lin [2006].

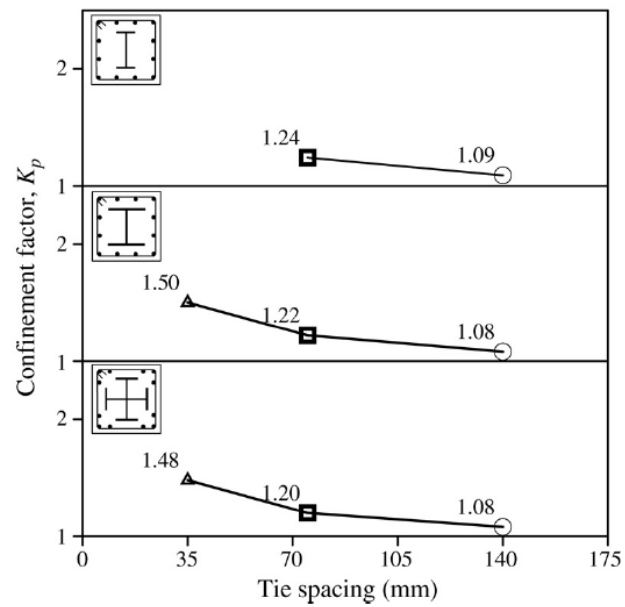


Fig. 2.6A Confinement Factor for Partially Confined Concrete, [Chen and Lin, 2006]

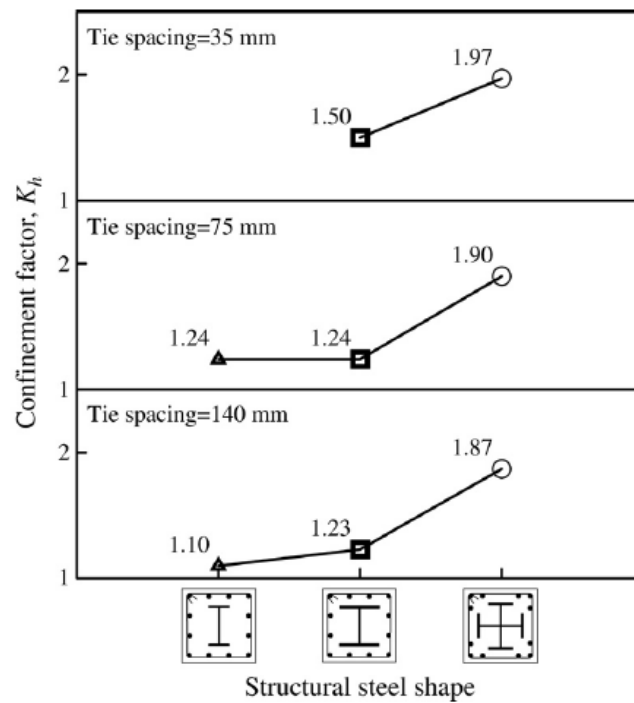


Fig. 2.6B Confinement Factor for Highly Confined Concrete, [Chen and Lin, 2006]

2.7 BOND BETWEEN STEEL AND CONCRETE

The bond stresses mechanism between concrete and steel in the circular CFST column has been studied by Roeder et. al. [1999] by conducting 153 experimental load testing, 49 square CFST and 104 Circular CFST. The diameter of the steel tube was ranging between 250mm and 650mm with d/t ratios ranging from 20 to 110. The column specimens have been experimented under axial compression loads on the top of the column. The CFST column was fixed at the base. Strain gauges have been fixed along the column height to measure the strain on the outside of the steel tube. The results of this research highlighted that the bond stress has no relation to the concrete strength, and it has inverse relation with the slenderness ratio (b/t), so the bond stress is reduced significantly by increasing the ratio (b/t). The width of the composite CFST column has an impact on the concrete shrinkage which derive the bond strength mechanism, so the concrete shrinkage was leading to retrogradation of bond resistance. Roeder et. al. [1999] extracted from a linear regression analysis the following parameters:

$$\tau_{\text{bond}} = 2.314 - 0.0195 (b/t) \quad \text{Eqn. (2.8)}$$

$$\tau_{\text{bond-}2\sigma} = 2.109 - 0.0260 (b/t) \quad \text{Eqn. (2.9)}$$

Where:

τ_{bond} Average bond strength (MPa)

$\tau_{\text{bond-}2\sigma}$ Bond Strength (MPa)

Sangeetha, et. al. [2017] investigated the bond stress between concrete and steel tube by conducting experimental testing of 20 specimens for RC columns, Hollow Steel Tube Columns, and CFST columns with different concrete admixtures. The conclusion of their research based on performing Push out test for the CFST specimens that the maximum bond strength between steel tube and concrete is 1.50MPa and the average bond stress is 1.10MPa. in addition; the bond strength can be enhanced by introducing flexible shear connectors (Shear Studs) or rigid shear connectors (Internal Plates) welded to the steel tubes.

2.8 COMPOSITE DESIGN PROVISION IN ACCORDANCE WITH AMERICAN SPECIFICATIONS

This section is focusing on the design provision for the concrete filled steel tube columns and encased composite column subject to axial load and biaxial load in-line with the American National Standard Institute and American Institute of Steel Construction (ANSI / AISC 360-16).

As per ANCI / AISC 360-16, the following criteria shall be adopted for the qualification of Composite Columns;

- Longitudinal reinforcement and Lateral Ties to be provided for Encased Steel Reinforce Composite Column (SRC). The minimum ratio of the longitudinal reinforcement shall be 0.004 of the total gross area of the concrete encasement column based upon the stress transfer under service load from the concrete to the reinforcement rebar as a result of the creep and shrinkage. The longitudinal reinforcement is essential to resist episodic flexure not considered in the analysis. The ties and transverse reinforcement shall follow the provision of ACI 318, with a minimum spacing of 300mm for 10mm bar diameter or 400mm for bar diameter ≥ 12 mm.
- Longitudinal bars are not required for Filled Composite Steel Tube Member (CFST)
- A minimum of 1% of the total composite cross section must be compromised of steel shape, tubing, or pipes.
- The compressive strength of the concrete (f'_c) shall be not less than 21MPa and shall not exceed 70MPa for the normal weight of the concrete. the concrete compressive strength of light weight concrete to be in-between (21MPa) to (42MPa). A higher concrete strength can be permitted subject to conducting appropriate testing and analysis.
- The reinforcement rebar shall have a minimum yield strength of 550MPa in-line with ACI 318
- The slenderness of the filled composite section is categorized as compact, noncompact or slender depend on the slenderness ratio b/t or D/t specified in [Table \[2.1\]](#) extracted from ANCI / AISC 360-16.
- To control the local deformation of the rectangular filled composite section during concrete pouring as a result of high hydrostatic pressure, the following serviceability limits are suggested by (Leon et al., 2011) or it is recommended to provide additional external supports to the filled section during concrete pouring.

$$\sigma_{max} = \max \left[\left(\frac{2h_c}{b_c + 4h_c} \right) \frac{ph_c^2}{t^2} \right. \\ \left. \frac{1}{3} \left(\frac{3b_c + 4h_c}{b_c + 4h_c} \right) \frac{ph_c^2}{t^2} \right] \leq 0.5F_y \quad \text{Eqn. (2.10)}$$

$$\delta_{max} = \frac{1}{32} \left(\frac{5b_c + 4h_c}{b_c + 4h_c} \right) \frac{ph_c^4}{E_s t^3} \leq \frac{L}{2,000} \quad \text{Eqn. (2.11)}$$

Where:

hc Longer inner width = (h-2t)

bc Shorter inner width = (b-2t)

t Wall thickness

h Longer overall width

b Shorter overall width

L Pressure Length

p Hydrostatic Pressure

ACI 318-11 highlighting that the yield stress (fy) of the steel sections used in the composite columns

shall not exceed 350MPa.

ACI 318-11 allows to provide composite columns with or without longitudinal bars.

In addition; ACI Code has a limitation to the thickness of the steel encasement for the Composite Columns with a concrete core encased by structural steel which is the minimum of the following two formulas:

$$b * (f_y/3E_s)^{0.5} \quad \text{for each face of width } b \quad \text{Eqn. (2.12)}$$

$$h * (f_y/8E_s)^{0.5} \quad \text{for circular sections of diameter } h \quad \text{Eqn. (2.13)}$$

2.8.1 ACI PROVISION FOR COMPRESSIVE STRENGTH OF COMPOSITE COLUMN

The compression capacity of the CFST Column has been addressed in the ACI code considering the

concrete compressive stress is $0.85f'_c$ and the steel stress is at yield stress level.

The ACI code introduced reduction factors as a result of any eccentricity might be occurred on the columns.

The following formula addressing the ultimate compression load on the columns subject to pure compression load without bending moments.

This formula presented based on the plastic stress distribution method which allows the steel to the yield stress $[F_y]$ and concrete to compressive strength $[0.85f'_c]$

$$\phi P_{n,max} = 0.85\phi [0.85f'_c (A_g - A_s) + F_y A_s] \quad \text{Eqn. (2.14)}$$

Where:

ϕ Strength Reduction Factor = 0.75

A_g cross sectional gross area (mm²)

A_s area of steel (mm²)

f'_c concrete compressive strength (MPa)

F_y yield strength of the steel (MPa)

2.8.2 ANCI / AISC PROVISION FOR COMPRESSIVE STRENGTH OF ENCASED COMPOSITE COLUMN

The ANCI / AISC 360-16 design basis of the Composite Columns has the same fundamental of the design of the steel columns, but it has been modified to accommodate the concrete effect on the steel yield stress, and Young's Modulus of the steel element. The following formulas identify the design compressive strength of the double symmetric axially loaded encased composite column based on the ANCI / AISC 360-16 taking into consideration the buckling effect on the member slenderness.

If $P_{no} / P_e \leq 2.25$

$$\phi_c P_n = \phi_c * P_{no} [0.658^{P_{no}/P_e}] \quad \text{Eqn. (2.15)}$$

If $P_{no} / P_e > 2.25$

$$\phi_c P_n = \phi_c * 0.877 P_e \quad \text{Eqn. (2.16)}$$

Where:

$$P_{no} = F_y A_s + F_{ysr} A_{sr} + 0.85 f'_c A_c = \text{Nominal Axial Compressive Strength} \quad \text{Eqn. (2.17)}$$

$$P_e = \text{Elastic Critical Buckling Loads} = \pi^2 (E_{eff}) / L_c^2 \quad \text{Eqn. (2.18)}$$

A_c Area of concrete (mm²)

A_s Area of steel section (mm²)

A_{sr} Area of steel reinforcement (mm²)

E_c Concrete Modulus of Elasticity [$0.043 W_c^{1.5} (f'_c)^{0.5}$] (MPa)

E_s Steel Modulus of Elasticity = 200,000 MPa

ϕ_c Strength Reduction Factor = 0.75 (LRFD)

E_{eff} effective elastic stiffness of the composite member (N.mm²) = $E_s I_s + E_s I_{sr} + C_1 E_c I_c$

C_1 Rigidity Coefficient = $0.25 + 3 [(A_s + A_{sr}) / A_g] \leq 0.70$

F_y Yield Stress of Steel Section

F_{ysr} Yield Stress of Reinforcement Rebar

I_c Elastic Moment of Inertia of Concrete Section (mm⁴)

I_s Elastic Moment of Inertia of Steel Section (mm⁴)

I_{sr} Elastic Moment of Inertia of Reinforcement Bars (mm⁴)

K Effective Length Factor

L	overall unbraced length of the member
L _c	Effective Length of the Member = K * L
f' _c	Concrete compressive strength (MPa)
W _c	Concrete Density (2,500 kg/m ³)

2.8.3 ANCI / AISC PROVISION FOR COMPRESSIVE STRENGTH OF CONCRETE FILLED STEEL TUBE COLUMN

The following formulas identify the design compressive strength of the double symmetric axially loaded filled composite column based on the ANCI / AISC 360-16 taking into consideration the buckling effect on the member slenderness.

a) Compact Sections

$$P_{no} = P_p \quad \text{Eqn. (2.19)}$$

Where:

$$P_p = F_y A_s + C_2 f'_c [A_c + A_{sr} \{E_s / E_c\}] \quad \text{Eqn. (2.20)}$$

C₂ = 0.95 for Circular section and 0.85 for rectangular section

b) Non-Compact Sections

$$P_{no} = P_p - \left[(P_p - P_y) * (\lambda - \lambda_p)^2 / (\lambda_r - \lambda_p)^2 \right] \quad \text{Eqn. (2.21)}$$

Where:

λ, λ_p , and λ_r Slenderness Ratio as identified in [Table \[2.1\]](#)

P_p = As per Equation (2.18)

$$P_y = F_y A_s + 0.70 f'_c [A_c + A_{sr} \{E_s / E_c\}] = \text{Axial Yield Strength} \quad \text{Eqn. (2.22)}$$

c) **Slender Sections**

$$P_{no} = F_{cr} A_s + 0.70 f'_c [A_c + A_{sr} \{E_s / E_c\}] \quad \text{Eqn. (2.23)}$$

Where:

F_{cr} Buckling Stresses

$$F_{cr} = 9E_s / (b/t)^2 \quad \text{for Rectangular Sections} \quad \text{Eqn. (2.24)}$$

$$F_{cr} = 0.72F_y / [(D/t) * (F_y/E_s)]^{0.2} \quad \text{for Circular Sections} \quad \text{Eqn. (2.25)}$$

d) **Effective Filled Composite Column Stiffness**

$$EI_{eff} = E_s I_s + E_s I_{sr} + C_3 E_c I_c \quad \text{Eqn. (2.26)}$$

Where; C_3 is the Rigidity Coefficient of Filled Composite Member under Compression

$$C_3 = 0.45 + 3 * [(A_s + A_{sr}) / A_g] \leq 0.90 \quad \text{Eqn. (2.27)}$$

Description of Element	Width-to-Thickness Ratio	λ_p Compact/ Noncompact	λ_r Noncompact/ Slender	Maximum Permitted
Walls of Rectangular HSS and Box Sections of Uniform Thickness	b/t	$2.26 \sqrt{\frac{E}{F_y}}$	$3.00 \sqrt{\frac{E}{F_y}}$	$5.00 \sqrt{\frac{E}{F_y}}$
Round HSS	D/t	$\frac{0.15E}{F_y}$	$\frac{0.19E}{F_y}$	$\frac{0.31E}{F_y}$

Table [2.1] Limitation of Width to Thickness Ratios for Compression Steel Elements in Composite Members subject to Axial Compression Load, (ANCI / AISC 360-16)

2.8.4 ACI PROVISION FOR COMBINED FLEXURE AND AXIAL FORCES

The capacity of the composite columns carrying out axial load and bending moment can be presented using the interaction between axial forces and flexure bending moments.

The fundamental of the P-M interaction relationship in the ACI code assuming that the maximum compression strain at the extreme concrete compression fiber is equal to 0.003 using the basis of uniform stress distribution modeled as a rectangular compressive stress block of $0.85f'_c$.

Fig. (2.7) represent the Interaction diagram between Axial Forces and Bending Moments.

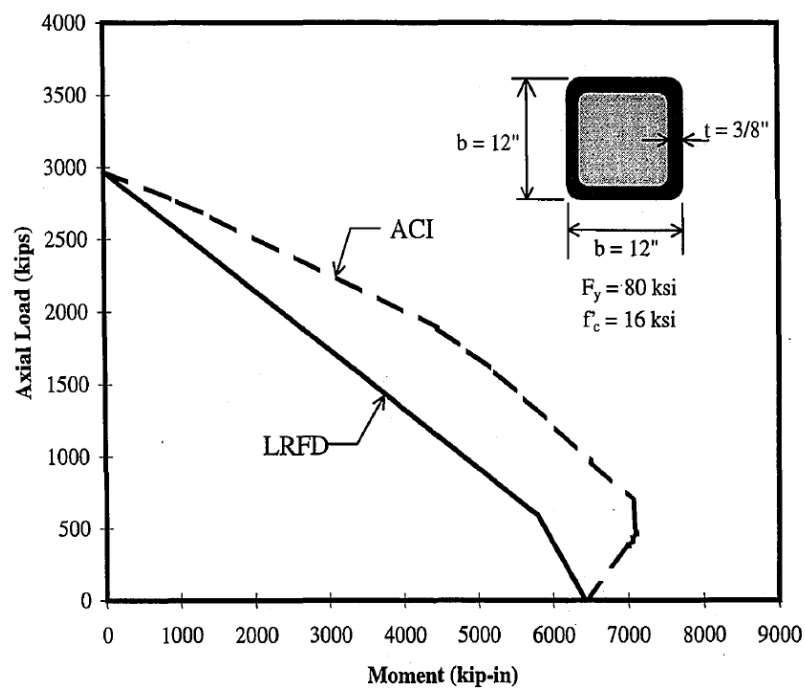


Fig. 2.7 Unfactored Axial Forces – Flexure Moment Interaction Diagram based on LRFD and ACI Code.

2.8.5 ANCI / AISC PROVISION FOR ENCASED COMPOSITE AND FOR FILLED COMPOSITE WITH COMPACT SECTIONS SUBJECT TO COMBINED FLEXURE AND AXIAL FORCES

ANCI / AISC identify the capacity of the encased composite columns (SRC) subject to Axial Forces and Flexure Bending using the following empirical formulas for LRFD Load of Combinations.

a) If $P_r / P_c \geq 0.20$

$$\left[P_r / P_c \right] + \left[8/9 \left\{ (M_{rx}/M_{cx}) + (M_{ry}/M_{cy}) \right\} \right] \leq 1.0 \quad \text{Eqn. (2.28)}$$

b) If $P_r / P_c < 0.20$

$$\left[P_r / 2P_c \right] + \left[8/9 \left\{ (M_{rx}/M_{cx}) + (M_{ry}/M_{cy}) \right\} \right] \leq 1.0 \quad \text{Eqn. (2.29)}$$

Where:

P_r Required (Ultimate) Axial Strength

P_c Design Axial Strength = $\phi_c P_n$

M_r Required (Ultimate) Flexure Strength

M_c Design Flexure Strength = $\phi_b M_n$

ϕ_c Compression Resistance Factor = 0.90

ϕ_b Flexure Resistance Factor = 0.90

2.8.6 ANCI / AISC PROVISION FOR FILLED COMPOSITE WITH NONCOMPACT OR SLENDER SECTIONS SUBJECT TO COMBINED FLEXURE AND AXIAL FORCES

ANCI / AISC identify the capacity of the concrete filled steel tube composite columns (CFST) subject to Axial Forces and Flexure Bending using the following methods:

- a) Using the interaction formulas adopted for the filled composite with compact section
- b) Using the Effective Stress-Strain Method which allow to calculate the nominal strength considering the strain compatibility and effective stress-strain relationship curve for both materials steel and concrete including the influence of the local buckling, yielding, interaction, and concrete confinement condition.
- c) Using the following empirical formulas:

- If $P_r / P_c \geq C_p$

$$\left[P_r / P_c \right] + \left[\{ (1-C_p) / c_m \} * (M_r / M_c) \right] \leq 1.0 \quad \text{Eqn. (2.30)}$$

- If $P_r / P_c < C_p$

$$\left[(1-C_m) / c_p \right] \left[P_r / P_c \right] + \left[M_r / M_c \right] \leq 1.0 \quad \text{Eqn. (2.31)}$$

Where C_p and C_m can be calculated from [Table \[2.2\]](#)

$$C_{sr} = (A_s F_y + A_{sr} F_{yr}) / A_c f'_c \quad \text{Eqn. (2.32)}$$

Filled Composite Member Type	C_p	C_m	
		when $C_{sr} \geq 0.5$	when $C_{sr} < 0.5$
Rectangular	$C_p = \frac{0.17}{C_{sr}^{0.4}}$	$C_m = \frac{1.06}{C_{sr}^{0.11}} \geq 1.0$	$C_m = \frac{0.90}{C_{sr}^{0.36}} \leq 1.67$
Round HSS	$C_p = \frac{0.27}{C_{sr}^{0.4}}$	$C_m = \frac{1.10}{C_{sr}^{0.08}} \geq 1.0$	$C_m = \frac{0.95}{C_{sr}^{0.32}} \leq 1.67$

Table [2.2] Coefficient C_p and C_m as per ANCI / AISC 360-16

2.8.7 LOAD TRANSFER

The distribution of the external forces applied on the composite column subject to the following:

1. External Forces Applied Directly to the Steel Section

In case of having the external forces applied directly to the steel section, then the required forces to be transferred to the concrete (V'_r) shall be calculated from the following formula:

$$V'_r = P_r (1 - F_y A_s / P_{no}) \quad \text{Eqn. (2.33)}$$

Where:

P_{no}	Nominal compressive strength, to be determined from equation (2.17) for encase composite without the length effect and to be determined from equation (2.19) and (2.21) for Compact and non-compact filled composite column respectively.
P_r	Total external forces applied to the composite section

The above formula is not applicable to slender filled composite column, because the external forces for slender filled composite column is applied directly to concrete or concurrently to the steel and concrete.

2. External Forces Applied Directly to the Concrete Element

In case the external forces applied directly to the concrete of encasement composite or filled composite, then the required force to be transferred to the steel can be calculated from the following formula:

- The forces to be transferred to compact or non-compact encased or filled composite

$$V'_r = P_r (F_y A_s / P_{no}) \quad \text{Eqn. (2.34)}$$

- The forces to be transferred to slender filled composite

$$V'_r = P_r (F_{cr} A_s / P_{no}) \quad \text{Eqn. (2.35)}$$

Where:

F_{cr} (MPa) Critical buckling stress derived from equation (2.24) and (2.25).

P_{no} (N) Nominal compressive Strength derived from equation (2.17).

3. External Forces Applied Concurrently to Concrete and Steel

In case the external forces applied concurrently to the steel and concrete for both types encased composite or filled composite, the transferred forces to be determined based on the equilibrium of the cross section. The external forces are not allowed to be transferred directly to a slender steel section due the stress concentration which is leading to local buckling.

2.8.8 MECHANISM OF FORCE TRANSFER

The mechanism of force transfer can be classified to direct bearing, shear connection, and direct bond interface.

The mechanism of force transfer of direct bond interface is applicable only to encased composite columns.

2.8.8.1 Direct Bearing Force Mechanism

In case the forces are transferred by direct bearing mechanism for encased composite or filled composite, the ultimate bearing strength of the concrete can be calculated from the following formula:

$$\phi_B R_n = 1.70 f_c A_1 \quad \text{Eqn. (2.36)}$$

$$\phi_B R_n = \phi_B 0.85 f_c A_1 (A_2/A_1)^{0.5} \quad \text{Eqn. (2.37)}$$

Where:

ϕ_B	Bearing Strength Reduction Factor = 0.65
A_1	Concrete Loaded Area (mm ²)
A_2	Bearing Area of lower base of tapered wedge with slope of 1 vertical to 2 horizontal (mm ²)
f_c	Concrete Compressive Strength (MPa)

2.8.8.2 Direct Bond Interaction Mechanism

Direct bond is basically introduced due to the friction mechanism between concrete and steel. The filled concrete steel tube column with bigger cross section, thinner plate thicknesses, rectangular flat geometry, smooth surface interface, and high shrinkage concrete has minimal contribution to bond strength between steel and concrete.

The filled concrete steel tube with smaller cross section, thicker steel plates, circular tube geometry, rough surface at the interface, low shrinkage concrete has a great contribution a valuable bond strength.

The effect of the bending moment is leading to higher bond strength as well.

$$\phi R_n = P_b L_{in} F_{in} \quad \text{Eqn. (2.38)}$$

Where:

ϕ Shear Strength Reduction Factor = 0.50

F_{in} Nominal Bond Stress (MPa) = $2100 t/H^2 \leq 0.70 \text{ MPa}$ for Rectangular Section
= $5300 t/D^2 \leq 1.40 \text{ MPa}$ for Circular section

D Outer diameter of the circular hollow steel section (mm)

H Maximum transverse dimension of rectangular section (mm)

t Thickness of steel plates (mm)

L_{in} Length of load introduction (mm)

R_n Nominal bond strength (N)

P_b Periphery of bond interface between concrete & steel along composite section (mm)

2.8.8.3 Shear Connection Force Mechanism

In case the forces are transferred by shear connection for encased composite or filled composite, the ultimate shear strength of the steel headed stud or steel channel anchors can be calculated from the following formula:

$$\phi_v R_c = \sum Q_{cv} = \phi_v \sum Q_{nv} \quad \text{Eqn. (2.39)}$$

The design shear strength (ϕQ_{nv}) can be calculated from the following formula if the breakout strength of the concrete is not governing the shear strength

$$Q_{nv} = F_u A_{sa} \quad \text{Eqn. (2.40)}$$

Where:

ΣQ_{cv}	Sum of Shear Strength of headed stud, or steel channel (N)
A_{sa}	Area of Steel Headed Stud (mm ²)
F_u	Tensile Strength of Steel Headed Stud (mm ²)
Q_{nv}	Nominal Shear Strength of Steel Headed Stud (N)
ϕ_v	Shear Strength Reduction Factor = 0.65

In case the design shear strength is governing by concrete breakout strength such as having the breakout prism not confined by steel plates, then adequate anchor reinforcement shall be added.

The design shear strength (Q_{nv}) shall be the minimum of the values calculated in equation (2.40) or the value calculated from ACI 318-11 provision which can be summarized as follow:

$$V_u \leq \phi V_{nv} \quad \text{Eqn. (2.41)}$$

For clean and rough contact surface,

$$V_{nv} = (1.8 + 0.6\rho_v f_y) \lambda b_v d \quad \text{Eqn. (2.42)}$$

$$V_{nv,max} = 0.55 b_v d \quad \text{Eqn. (2.43)}$$

$$V_{nv,max} = 3.5 b_v d \quad \text{Eqn. (2.44)}$$

If $V_u > \phi (3.5b_v d)$, shear-friction design method to be applied as per ACI 318-11

$$V_n = A_{vf} f_y \mu \quad \text{Eqn. (2.45)}$$

Or
$$V_n = A_{vf} f_y (\mu \sin \alpha + \cos \alpha) \quad \text{Eqn. (2.46)}$$

For normal weight concrete has been cast attached to existing rough surface concrete; then (V_n) shall not exceed the lowest value of the following:

$$V_{n,max} = 0.2 f'_c A_c \quad \text{Eqn. (2.47)}$$

$$V_{n,max} = (3.3 + 0.08 f'_c) A_c \quad \text{Eqn. (2.48)}$$

$$V_{n,max} = 11 A_c \quad \text{Eqn. (2.49)}$$

For other cases; (V_n) shall not exceed the lowest value of the following:

$$V_{n,max} = 0.2f'_c A_c \quad \text{Eqn. (2.50)}$$

$$V_{n,max} = 5.5 A_c \quad \text{Eqn. (2.51)}$$

$V_{n,min}$ can be calculated from the following formula

$$V_{n,min} = 0.062 (f'_c)^{0.5} (b_w S / f_{yt}) \quad \text{Eqn. (2.52)}$$

But it should not be greater 600mm and not exceed 4 times the least dimension of the supported element.

Where:

α	Angle between shear plane and provided shear friction rebar, refer to Fig. (2.8)
A_{vf}	Shear friction reinforcement (mm^2)
μ	Friction Coefficient
f_y	Reinforcement yield strength ≤ 420 MPa
λ	Concrete material factor = 1.0 for normal concrete
A_c	Area of concrete (mm^2)
ρ_v	Ratio between area of shear friction reinforcement and area of contact surface = $A_v / (b_v s)$
b_v	Cross section width at contact surface (mm)
S	Spacing between reinforcement (mm)
ϕ	Material Reduction Factor in Shear and Torsion = 0.75 as per ACI 318-11

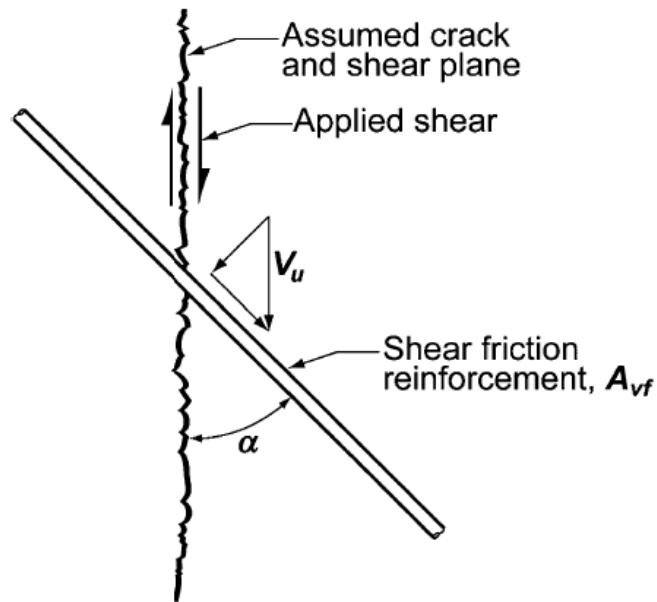


Fig. 2.8 Angle between Shear Friction Reinforcement and Crack Plane

2.8.8.4 Tensile Strength of Steel Headed Stud Anchor in Composite Members

ANCI / AISC highlights that the tensile strength of one stud can be calculated from Eqn. (2.53) equation subject to comply with the following conditions:

- The distance from the centroid of the stud to the concrete edge in the perpendicular direction to the stud height is equal to or more than 1.50 times the stud height.
- The distance between studs is equal to or more than 3.0 times the stud height.

$$Q_{nt} = F_u A_{sa} \quad \text{Eqn. (2.53)}$$

Where:

Q_{nt} Nominal Tensile Strength of Steel Headed Stud (N)

A_{sa} Area of Steel Headed Stud (mm²)

F_u Tensile Strength of Steel Headed Stud (mm²)

ϕ_t Tensile Strength Reduction Factor = 0.75

If one of the above two conditions is not met, then the tensile strength of the stud can be calculated by one of the following:

- As extracted from the ACI 318-11 provision and showing in clause 2.7.8.3 of this report.
- In case of having anchor, rebar provided as per ACI 318-11 on both sides of concrete breakout surface for the stud anchor, then the nominal tensile strength of the headed stud shall be the minimum of the tensile strength calculated from equation (2.52) or the nominal strength of the anchor reinforcement showing in clause 2.7.8.3 of this report.

2.8.8.5 *Strength of Steel Headed Stud Anchors for Interaction of Shear and Tension in Composite Members*

The design strength of the headed stud anchors subject to shear and torsional in composite member can be calculated from the following formula subject to comply with the following requirements:

- The shear strength is not governing by concrete breaking strength
- The distance from the centroid of the stud to the concrete edge in the perpendicular direction to the stud height is equal to or more than 1.50 times the stud height.
- The distance between studs is equal to or more than 3.0 times the stud height.

$$(Q_{rt} / Q_{ct})^{5/3} + (Q_{rv} / Q_{cv})^{5/3} \leq 1.0 \quad \text{Eqn. (2.54)}$$

Where:

Q_{rt}	Ultimate Tensile Force (N)
Q_{ct}	Design Tensile Strength (N)
Q_{rv}	Ultimate Shear Strength (N)
Q_{cv}	Design Shear Strength (N)
ϕ_t	Reduction factor for tension = 0.75
ϕ_v	Reduction Factor for shear = 0.65

If one of the above two conditions is not met, then the nominal strength for combined shear and tension of the steel stud can be calculated by one of the following:

- In case of having anchor reinforcement provided as per ACI 318-11 on two sides of concrete breakout surface for the stud anchor, then the nominal shear strength (Q_{nv}) of the headed stud shall be the minimum of the shear strength calculated from equation (2.40) or the nominal strength of the anchor reinforcement showing in clause 2.8.8.3, equation (2.41) to (2.52) of this report. The nominal tensile strength shall be the minimum of the tensile strength showing in equation (2.53) and the anchor reinforcement strength as specified in ACI 318-11 and described in clause 2.8.8.3 of this report
- As extracted from the ACI 318-11 provision and showing in clause 2.8.8.3 of this report.

2.8.8.6 *Shear Strength of Steel Channel Anchors in Composite Members*

The nominal shear strength (Q_n) of hot-rolled channel used as steel studs can be calculated from the following formula:

$$\phi_t Q_n = \phi_t [0.3 (t_f + 0.5t_w) L_a (f'_c E_c)^{0.5}] \quad \text{Eqn. (2.55)}$$

Where:

- t_f Flange thickness of the steel channel (mm)
- t_w Web thickness of the steel channel (mm)
- L_a Length of the steel channel
- ϕ_t Strength reduction factor = 0.75

2.8.8.7 *Detailing Requirements for the Steel Studs and Anchors in Composite Elements*

The following criteria shall be met in the composite members:

- a. Minimum concrete cover to steel anchors to follow ACI 318-11, (40mm).
- b. Minimum distance between steel stud is 4 times diameter.
- c. Maximum distance between steel stud is 32 times shank diameter.
- d. Maximum distance between steel channel anchors is 600mm.
- e. The ratio between shank length of the stud to the diameter shall not exceed 5.0 under shear loads and shall not exceed 8 under tension load and/or combined shear and tension.

2.9 COMPOSITE DESIGN PROVISION IN ACCORDANCE WITH EUROCODE 4 SPECIFICATIONS

The following criteria need to be adopted as per EUROCODE 4 for the design of composite columns subject to axial compression load with fully encased concrete sections, partially encased concrete sections, and concrete filled tube section as shown in Fig. (2.9).

- Steel Grades from S235 to S460.
- Concrete Grade from C20/25 to C50/60
- Steel Participation ratio (δ) shall not be less than 0.20 and not exceeding 0.90, ($0.20 \leq \delta \leq 0.90$)
- Composite Column under compression loads shall satisfy the Eurocode requirements for the local buckling, and shear resistance between steel and concrete elements. The influence of the local buckling might be ignored if the steel section is fully encased composite, otherwise it shall follow Eurocode 4 requirements as per Table [2.3].
- The 2nd order effect can be considered in the composite column design by adopting adequate amplification in the 1st order analysis, otherwise it should be included in the global analysis.
- the design of composite columns shall cover the influence of the imperfections including residual stresses, and geometry imperfections such as miss-alignment, miss-verticality, improper flatness, and joint eccentricities.
- The influence of concrete cracking, creep, shrinkage, heating, and construction methodology.

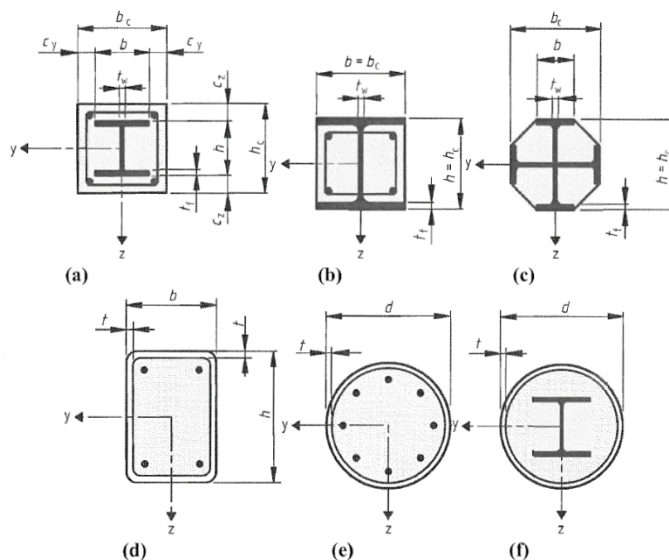


Fig. 2.9 Typical cross sections of different types of composite columns

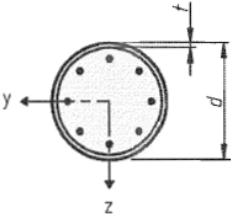
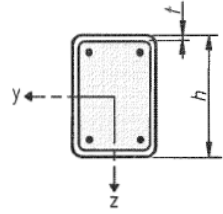
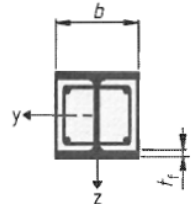
Cross-section	Max (d/t), max (h/t) and max (b/t)
Circular hollow steel sections 	$\max (d/t) = 90 \frac{235}{f_y}$
Rectangular hollow steel sections 	$\max (h/t) = 52 \sqrt{\frac{235}{f_y}}$
Partially encased I-sections 	$\max (b/t_f) = 44 \sqrt{\frac{235}{f_y}}$

Table [2.3] Local Buckling requirements, Maximum values (d/t) & (h/t) with f_y in N/mm² as extracted from Eurocode 4 Part 1.1.

The Eurocode provides two methods for the composite design, a general method for non symmetrical or non-uniform cross sectional along the member length taking into consideration second order influence, local stability, concrete creep and shrinkage, and yielding of the steel rebar and steel sections. And the 2nd method is a simplified method for symmetrical and uniform cross sectional along the column length.

The simplified method cannot be applied if the steel geometry comprises two or more unconnected [isolated] sections.

Eurocode recommends to limit the maximum concrete cover to 0.30h and 0.40b for each relevant direction. In addition, the longitudinal bars can be used shall not exceed 6% of the concrete cross sectional area, and the ratio of depth to the width of the composite section dimensions to be between 0.20 and 5.0.

2.9.1 EUROCODE 4 DESIGN PROVISION FOR COMPOSITE COLUMN SUBJECT TO AXIAL COMPRESSION LOADS

The simplified method can be applied for encased composite and filled composite column by determining the cross-sectional plastic resistance under axial compression load.

- a. Plastic Resistance of the encased composite column

$$N_{pl,Rd} = A_a f_{yd} + 0.85 A_c f_{cd} + A_s f_{sd} \quad \text{Eqn. (2.56)}$$

- b. Plastic Resistance of the filled composite column

$$N_{pl,Rd} = A_a f_{yd} + A_c f_{cd} + A_s f_{sd} \quad \text{Eqn. (2.57)}$$

Where:

$N_{pl,Rd}$	Plastic Resistance to Axial Compression Load	
A_a	Area of Structural Steel Cross-Sectional	
A_c	Area of Concrete Cross-Sectional	
A_s	Area of Steel Reinforcement	
f_{yd}	Yield Design Strength of the structural steel element	$= f_{yk} / \gamma_y$
f_{cd}	Cylinder Design Compressive Strength of Concrete	$= f_{ck} / \gamma_c$
f_{sd}	Yield Design Strength of the reinforcement bars	$= f_{sk} / \gamma_s$
f_{ck}	Cylinder Compressive Strength of the concrete at 28 days	
f_{sk}	Yield Strength of the reinforcement rebar	
f_{yk}	Yield Strength of the Steel section	
γ_y	Structural Steel strength reduction factor = 1.0	
γ_c	Concrete strength reduction factor = 1.50	
γ_s	Steel Reinforcement strength reduction factor = 1.15	

The Eurocode 4 allows to increase the concrete strength for the filled tube of circular steel section due to the confinement provided for the concrete as per the following equation

$$N_{pl,Rd} = \eta_a A_a f_{yd} + A_c f_{cd} [1 + (\eta_c * t f_y / d f_{ck})] + A_s f_{sd} \quad \text{Eqn. (2.58)}$$

Where:

t Thickness of Steel Tube Section

$$\eta_a = \eta_{ao} \quad \text{and} \quad \eta_c = \eta_{co} \quad \text{if } e=0.0$$

$$\eta_{ao} = 0.25 (3 + 2\lambda) \leq 1.0$$

$$\eta_{co} = 4.9 - 18.5\lambda + 17\lambda^2 \geq 0.0$$

$$\eta_a = \eta_{ao} + (1 - \eta_{ao})(10 e/d) \quad \text{if } 0 < e/d \leq 0.10$$

$$\eta_c = \eta_{co} [1 - (10 e/d)] \quad \text{if } 0 < e/d \leq 0.10$$

$$\eta_a = 1.0 \text{ and } \eta_c = 0.0 \quad \text{if } e/d > 0.10$$

The Eurocode 4 highlights that the steel contribution ratio $[\delta]$ to be in-between 0.20 and 0.90. If the

steel contribution is less than 0.20, then the column to be designed as conventional reinforced concrete column. If the steel contribution ratio is exceeding 0.90, then the column to be designed as steel column and concrete effect to be ignored.

$$\delta = (A_a f_{yd}) / N_{pl,Rd} \quad \text{Eqn. (2.59)}$$

$$\lambda = (N_{pl,Rd} / N_{cr})^{0.5} \quad \text{Eqn. (2.60)}$$

Where:

$N_{pl,Rd}$ Plastic Resistance to Axial Compression Load

N_{cr} The critical load causes buckling for the column associated with the effective stiffness of the composite column $(EI)_{eff}$.

2.9.2 EUROCODE 4 DESIGN PROVISION FOR COMPOSITE COLUMN SUBJECT TO AXIAL COMPRESSION AND UNIAXIAL FLEXURE BENDING

The following formula provides the composite section resistance in combined compression and uniaxial flexure bending based on the P-M interaction relationship showing in **Fig. (2.10)**

$$M_{Ed} / M_{pl,N,Rd} = M_{Ed} / (\mu_d M_{pl,Rd}) \leq \alpha_M \quad \text{Eqn. (2.61)}$$

Where:

M_{Ed} Maximum Bending Moments at the two ends and along the column length

$M_{pl,N,Rd}$ Plastic Resistance to flexure bending considering the normal force effect N_{Ed} as

shown in P-M Interaction Diagram in **Fig. (2.10)**

$M_{pl,Rd}$ Plastic Resistance to flexure bending at Point (B), where Axial Forces is equal to Zero

as per P-M Interaction Relationship Curve **Fig. (2.11)**

μ_d Design Factor related to compression and flexure as per **Fig. (2.12)**

α_M Bending Coefficient for Composite Column, equal to 0.90 for Steel Grade S235 & S355 and equal to 0.80 for Steel Grade S420 & S460

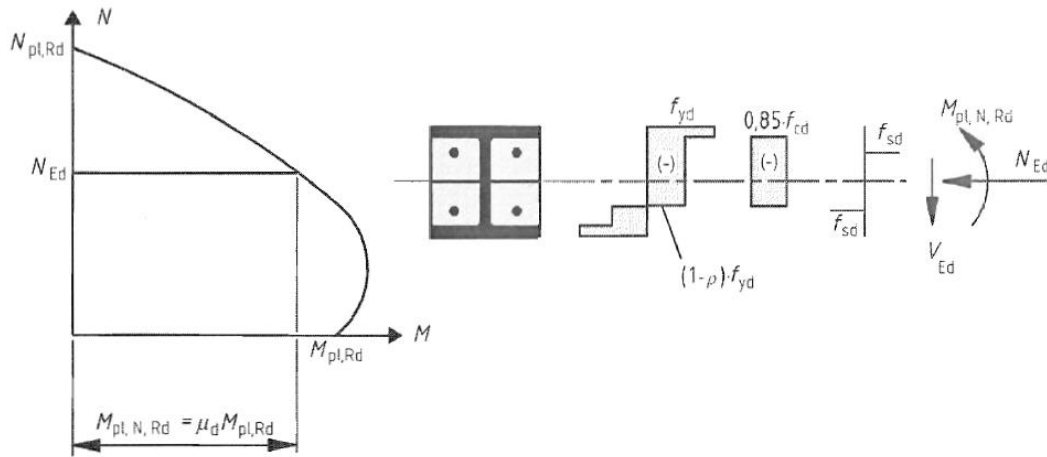


Fig. 2.10 P-M Interaction Diagram for Combined Compression and Uniaxial Flexure Bending

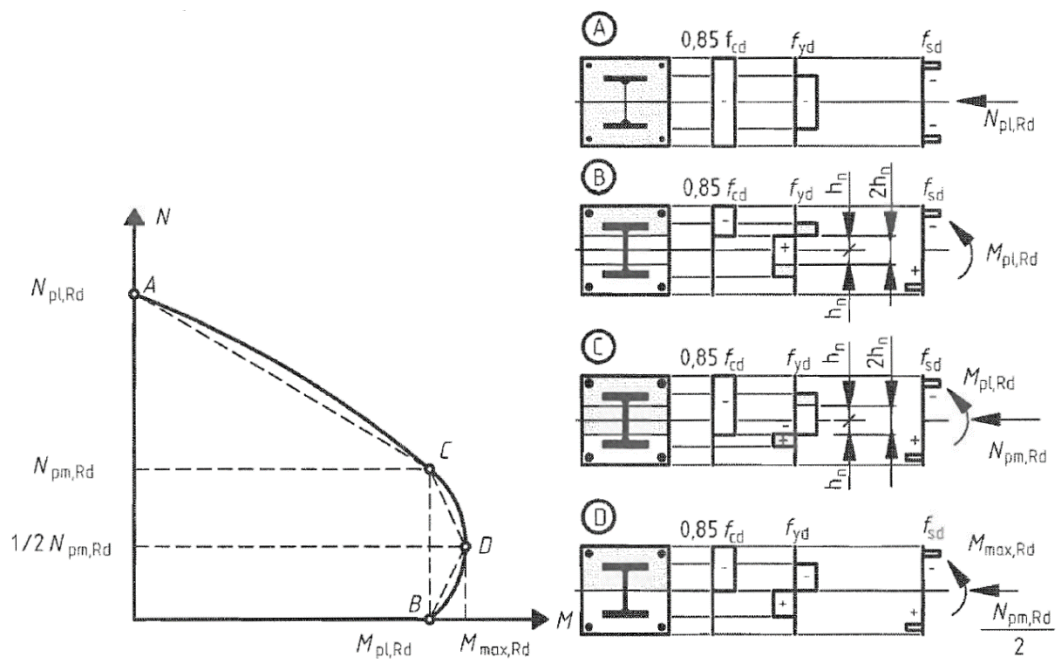


Fig. 2.11 Simplified P-M Interaction Diagram and corresponding stress distribution

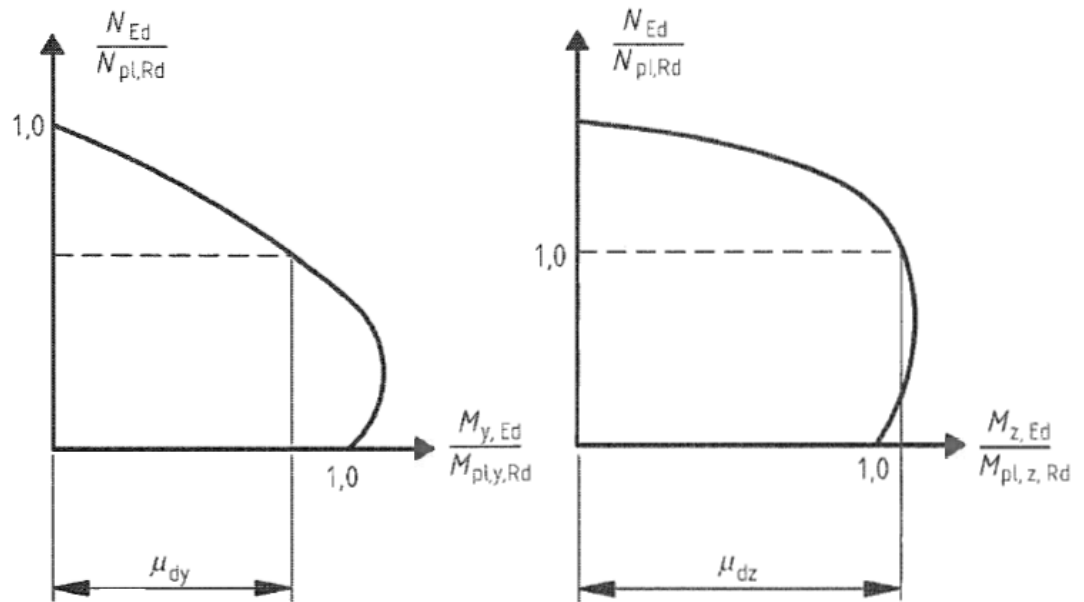


Fig. 2.12 Determination of Design Factor (μ_d) related to Compression and Flexure

2.9.3 EUROCODE 4 DESIGN PROVISION FOR COMPOSITE COLUMN SUBJECT TO AXIAL COMPRESSION AND BIAXIAL FLEXURE BENDING

The Eurocode 4 part 1.1 demonstrate the following conditions should be adopted for the composite columns design subject to axial compression and biaxial bending.

$$M_{y,Ed} / (\mu_{dy} M_{pl,y,Rd}) \leq \alpha_{M,y} \quad \text{Eqn. (2.62)}$$

$$M_{z,Ed} / (\mu_{dz} M_{pl,z,Rd}) \leq \alpha_{M,z} \quad \text{Eqn. (2.63)}$$

$$M_{y,Ed} / (\mu_{dy} M_{pl,y,Rd}) + M_{z,Ed} / (\mu_{dz} M_{pl,z,Rd}) \leq 1.0 \quad \text{Eqn. (2.64)}$$

Where:

$M_{pl,y,Rd}$ & $M_{pl,z,Rd}$ Plastic Resistance to Bending for relevant bending plane of the member

$M_{y,Ed}$ & $M_{z,Ed}$ Design Bending Moment taking into consideration the 2nd-order effect

And imperfections as per Eurocode 4 Part 1.1.

μ_{dy} & μ_{dz}	Design Factor related to compression and bending for the plane being considered as per Fig. (2.12)
$\alpha_{M,y}$ & $\alpha_{M,z}$	Bending Coefficient for Composite Column, equal to 0.90 for Steel Grade S235 & S355 and equal to 0.80 for Steel Grade S420 & S460

2.9.4 TRANSVERSE SHEAR FORCES EFFECT ON THE COMPOSITE COLUMN DESIGN RESISTANCE

The capacity of the composite section under combined axial compression and flexure bending can be determined considering the stress block presented in **Fig. (2.10)**, taking into consideration the effect of the shear force V_{Ed} . The concrete tensile strength shall be ignored.

The effect of the transverse shearing forces on the capacity of the composite section subject to axial compression and flexure bending should be reflected on the P-M interaction curve, if the shearing forces on the steel section is greater than 50% of the steel section capacity to shear

$$(V_{a,Ed} > 0.50V_{pl,a,Rd}).$$

The effect of the transverse shear on the capacity of the composite section under combined compression and flexure is leading to reduce the composite section capacity by $(1 - \rho) f_{yd}$.

The shear forces on the steel section shall not exceed the steel section capacity in the shear. The shear forces can be distributed into two components, $V_{a,Ed}$ received by the structural steel section and $V_{c,Ed}$ received by the reinforced concrete section.

Eurocode 4 Part 1.1 allows to apply the shear forces on the steel section only to simplify the design assumptions.

$$V_{a,Ed} = V_{Ed} \left[M_{pl,a,Rd} / M_{pl,Rd} \right] \quad \text{Eqn. (2.65)}$$

$$V_{Ed} = V_{a,Ed} + V_{c,Ed} \quad \text{Eqn. (2.66)}$$

Where:

$M_{pl,a,Rd}$	Plastic Resistance Moment of the Steel Section
$M_{pl,Rd}$	Plastic Resistance Moment of the Composite Section
V_{Ed}	Total Shear Forces on the Composite Column
$V_{a,Ed}$	Shear Forces received by Structural Steel
$V_{c,Ed}$	Shear Forces received by Concrete Section.

2.9.5 EUROCODE PROVISION FOR THE P-M INTERACTION DIAGRAM

A simplified P-M Interaction Relationship Curve for composite column under axial compression and bending moment.

The P-M interaction curve can be modeled using a polygonal diagram for four points A, B, C, and D

as per **Fig. (2.11)**. The design resistance of Concrete to axial compression load $[N_{pm,Rd}]$ is equal to $[0.85f_{cd} A_{cd}]$ for concrete fully encased and partially encased sections, while it is equal to $[f_{cd} A_c]$ for filled composite section.

Point (A) represents the composite section plastic resistance to axial compression load as defined in Eqn. (2.56) and (2.57). Point (B) represents the composite section plastic resistance to flexure only.

Point (C) represents the intersection between plastic resistance of the composite member in flexure and the design resistance of the Concrete section to axial compression load. Point (D) represents the intersection between plastic resistance of the composite section to flexure and half of the concrete resistance to axial compression $[0.50 N_{pm,Rd}]$.

2.9.6 EFFECTIVE FLEXURE STIFFNESS OF THE COMPOSITE COLUMNS

The effective flexure stiffness of the composite column cross sectional $[EI]_{\text{eff}}$ should be calculated in order to determine the relative stiffness $[\lambda]$, the axial compression load leading the column to buckle, and long-term effect on the characteristics of the concrete [Creep & Shrinkage].

The Eurocode 4 Part 1.1 provide the following formula to determine the effective stiffness.

$$(EI)_{\text{eff}} = E_a I_a + E_s I_s + K_e E_{c,\text{eff}} I_c \quad \text{Eqn. (2.67)}$$

$$E_{c,\text{eff}} = E_{\text{cm}} * [1 / \{1 + (\phi_t N_{G,\text{Ed}} / N_{\text{Ed}})\}] \quad \text{Eqn. (2.68)}$$

Where:

K_e	Correction Factor = 0.60
I_a	Moment of Inertia of structural steel section
I_c	Moment of Inertia of uncracked concrete cross sectional
I_s	Moment of Inertia of steel reinforcement
E_a	Modulus of Elasticity of structural steel section
E_s	Modulus of Elasticity of steel reinforcement
E_{cm}	Short term Modulus of Elasticity of concrete section
$E_{c,\text{eff}}$	Long-term Modulus of Elasticity considering creep and shrinkage
$N_{G,\text{Ed}}$	Sustained axial compression load
N_{Ed}	Total design axial compression load
ϕ_t	Concrete Creep Coefficient

The Eurocode 2 Part 1.1 provide a guidance to determine the concrete creep coefficient (ϕ_t) by following the charts showing in **Fig. (2.13)** for inside condition and **Fig. (2.14)** for outside condition.

The first step is to identify the intersecting point between age of concrete at the time of loading (t_0) and cement class (S, N, or R). The second step is to create straight line between the created point in step #1 and the zero-creep coefficient [$\phi(t_0) = 0.0$]. The third step is to calculate the theoretical size (h_0) as per Eqn. (2.69), and then determine the intersecting point between h_0 and design concrete strength. The fourth step is to create horizontal line from the created point in step #3. The last step is to define the concrete creep coefficient $\phi(t_0)$

which is representing the intersection point between the horizontal line created in Step #4 and the straight tangent line created in step #2. **Fig. (2.15)** showing the methodology of calculating the creep coefficient.

$$h_0 = 2 A_c / u \quad \text{Eqn. (2.69)}$$

$$u = 2 * (B + H) \quad \text{Eqn. (2.70)}$$

Where:

A_c Area of concrete cross sectional

u periphery of the portion exposed to humidity condition

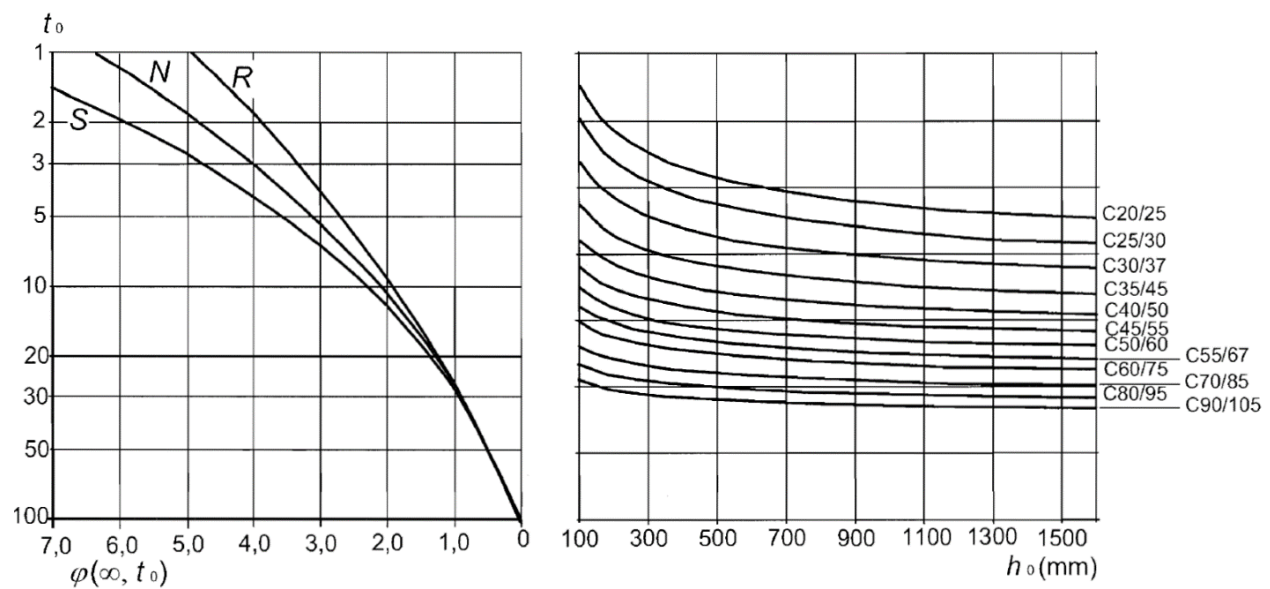


Fig. 2.13 Creep Coefficient $\phi(t_0)$ for Concrete in inside condition, Relative Humidity (RH=50%)

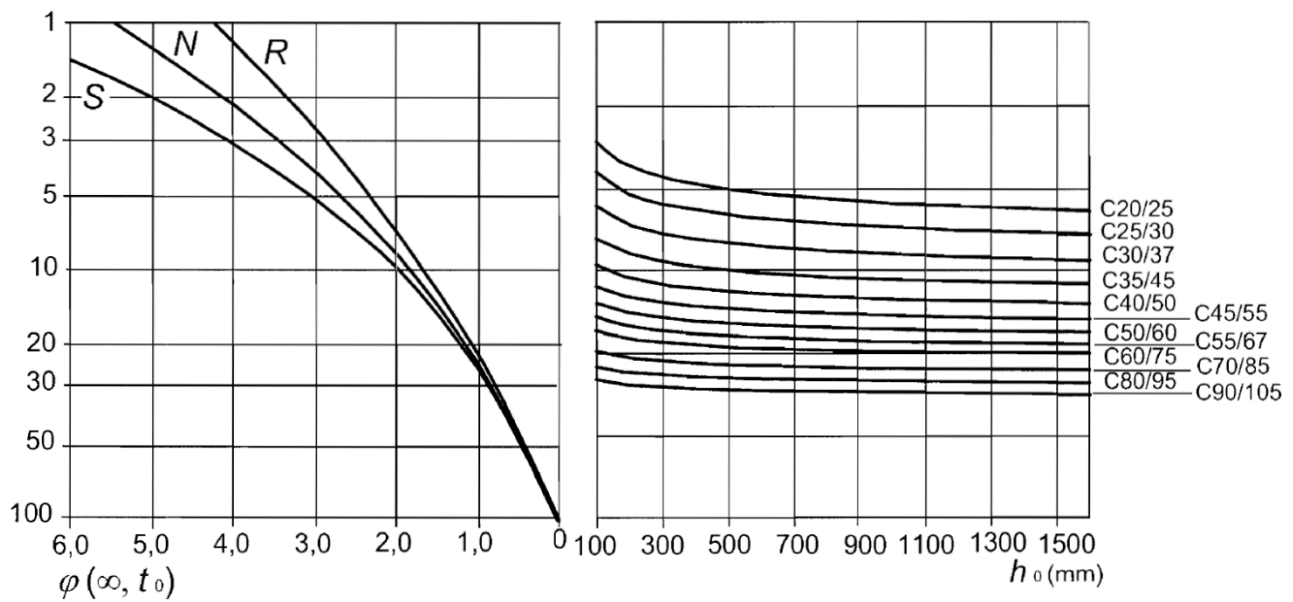


Fig. 2.14 Creep Coefficient $\phi(t_0)$ for Concrete in outside condition, Relative Humidity (RH=80%)

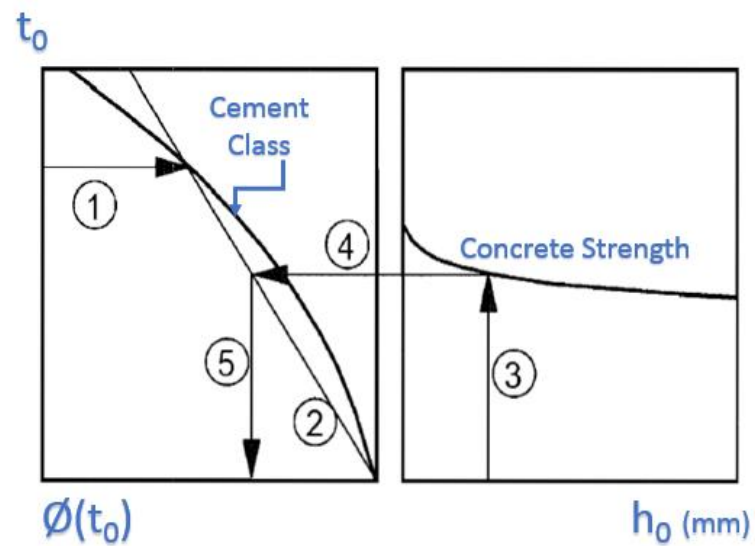


Fig. 2.15 Methodology of calculating the creep coefficient $\phi(t_0)$ in normal environment situation

2.9.7 SECOND ORDER INFLUENCE, GEOMETRICAL, AND MEMBER IMPERFECTIONS

Second order effect on the composite section capacity to be applied by multiplying the highest first-order bending moment (M_{Ed}) by a factor (K) determined by the following formula:

$$K = \beta / [1 - (N_{Ed} / N_{cr,eff})] \quad \text{Eqn. (2.71)}$$

The effective flexure stiffness can be defined as per the following formula:

$$(EI)_{eff,II} = K_0 (E_a I_a + E_s I_s + K_{e,II} E_{cm} I_c) \quad \text{Eqn. (2.72)}$$

For composite section subject to axial compression load, the following condition shall be met in-line with Eurocode 4 requirements.

$$N_{Ed} / (\chi * N_{pl,Rd}) \leq 1.0 \quad \text{Eqn. (2.73)}$$

$$\chi = 1 / [\phi + (\phi^2 - \lambda^2)^{0.5}] \quad \text{Eqn. (2.74)}$$

$$\phi = 0.50 [1 + \alpha(\lambda^2 - 0.20) + \lambda^2] \quad \text{Eqn. (2.75)}$$

Where:

$N_{cr,eff}$ Critical Buckling Load considering the effective stiffness as per Eqn. (2.72).

N_{cr} Critical Buckling Load considering the effective stiffness as per Eqn. (2.76).

$N_{pl,Rd}$ Plastic Resistance to Axial Compression Load as per Eqn. (2.56) or (2.57).

β Factor related to the second order moment fundamental as per [Table \[2.4\]](#).

$K_{e,II}$ Correction factor to be equal to 0.50

K_0 Calibration Factor to be equal to 0.90

χ Buckling Reduction Factor.

ϕ Reduced Value required to calculate the buckling reduction factor.

α Imperfection Factor for Buckling Modes as per [Table 2.5\]](#) and [Table \[2.6\]](#), where ρ_s represents the steel reinforcement ratio (A_s/A_c)

λ = $(A f_y / N_{cr})^{0.50}$ for cross section class 1, 2, and 3

λ = $(A_{eff} f_y / N_{cr})^{0.50}$ for cross section class 4

The second order effect can be neglected if the additional internal bending moments occurred due to the deformation calculated from the first order analysis is lower than 10%.

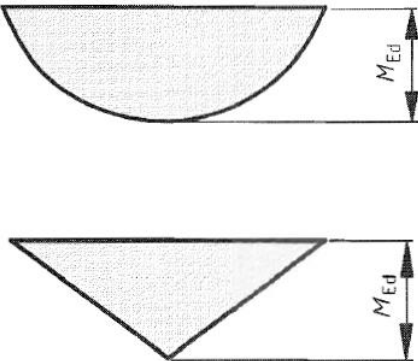
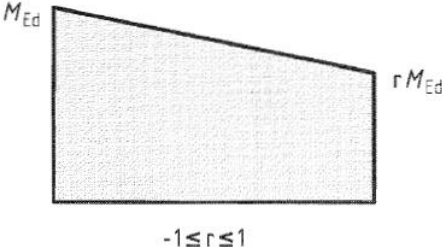
Moment distribution	Moment factors β	Comment
	<p>First-order bending moments from member imperfection or lateral load:</p> $\beta = 1,0$	<p>M_{Ed} is the maximum bending moment within the column length ignoring second-order effects</p>
	<p>End moments:</p> $\beta = 0,66 + 0,44r$ <p>but $\beta \geq 0,44$</p>	<p>M_{Ed} and $r M_{Ed}$ are the end moments from first-order or second-order global analysis</p>

Table [2.4] Determination of Factor β related to the second order analysis theory

Buckling curve	a_0	a	b	c	d
Imperfection factor α	0,13	0,21	0,34	0,49	0,76

Table [2.5] Imperfection Factor for Buckling Modes

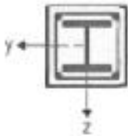
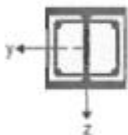
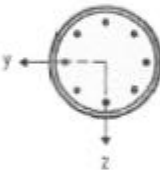
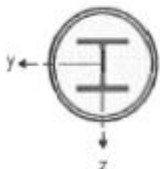
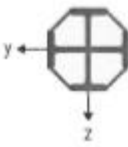
Cross-section	Limits	Axis of buckling	Buckling curve	Member imperfection
concrete encased section 		y-y	b	$L/200$
		z-z	c	$L/150$
partially concrete encased section 		y-y	b	$L/200$
		z-z	c	$L/150$
circular and rectangular hollow steel section 	$\rho_s \leq 3\%$	any	a	$L/300$
	$3\% < \rho_s \leq 6\%$	any	b	$L/200$
circular hollow steel sections with additional I-section 		y-y	b	$L/200$
		z-z	b	$L/200$
partially concrete encased section with crossed I-sections 		any	b	$L/200$

Table [2.6] Buckling Modes and Imperfections for Different types of Composite Columns

2.9.8 CRITICAL BUCKLING LOAD ON THE COMPOSITE COLUMN

The critical [Euler] buckling load can be calculated taking into consideration the end conditions of the composite columns. The following formula addressed the critical [Euler] buckling loads

$$N_{cr} = \pi^2 * (EI)_{eff} / (K.L)^2 \quad \text{Eqn. (2.76)}$$

Where:

K Effective Length of the Column, which is determined based on the end conditions.

L Overall Unsupported Length of the Composite Column

Fig. (2.16) represents the buckling mode and relevant effective lengths for each boundary condition.

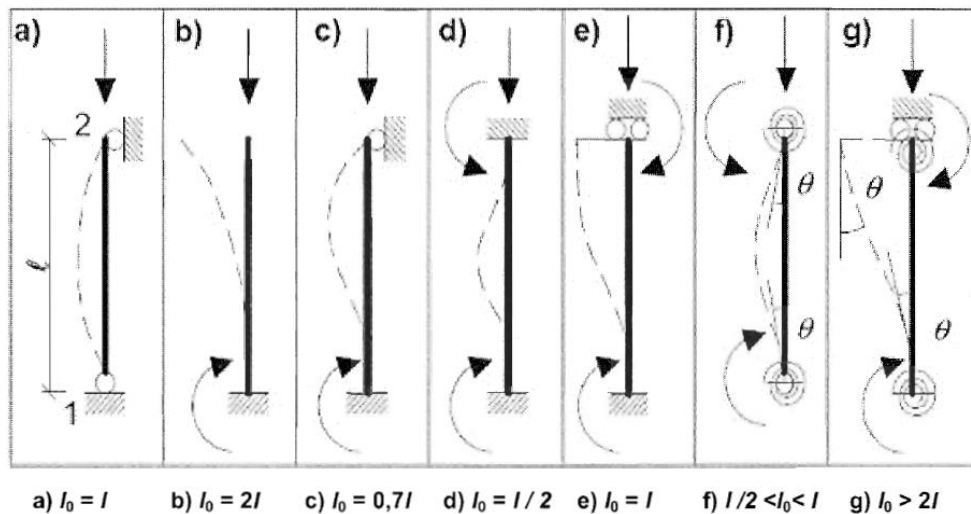


Fig. 2.16 Buckling Modes with relevant effective length for different boundary conditions

2.9.9 EUROCODE 4 PROVISION FOR SHEAR FORCES TRANSFER

The composite column affected by transverse shear forces [local transverse load] need to be carefully studied in order to evaluate the transfer of the longitudinal shear stress at the interface surface between concrete and steel.

The longitudinal shearing forces outside the introduced loaded area can be neglected for the composite column subject to axial compression load.

The shear connectors are required if the design shear strength (t_{Rd}) is increased at the interface surface between steel and concrete, and to be provided within the introduced loaded area and in the area with change of cross section. The design shear strength can be determined in [Table \[2.7\]](#).

Type of cross section	τ_{Rd} (N/mm ²)
Completely concrete encased steel sections	0,30
Concrete filled circular hollow sections	0,55
Concrete filled rectangular hollow sections	0,40
Flanges of partially encased sections	0,20
Webs of partially encased sections	0,00

Table [2.7] Design Shear Strength (t_{Rd}) as per Eurocode 4

The shear connectors to be distributed outside the area of load introduction if the longitudinal shear is greater than the design shear strength (t_{Rd}).

The shear forces can be determined using Elastic analysis method taking into account the effect of creep and shrinkage if the shear loads introduction applied to the concrete cross sectional only, otherwise elastic or plastic analysis method can be applied.

The length of the introduced load usually estimated as $2d$ or $L/3$, where d is the minimum transverse dimension of the column and L is the length of the column.

Eurocode 4 recommends not to provide shear connectors for the compression load introduced by endplates subject to achieving fully permanent interface between endplates and concrete section taking into consideration the long-term effect of the concrete [Creep and Shrinkage].

The effect of confinement on the concrete filled circular tube section calculated as per Eqn. (2.58) can be justified considering η_a and η_c are equal to zero.

The additional resistance introduced by the friction forces occurred from preventing the concrete to expand by the adjoining steel flanges shall be added to the shear stud resistance. The additional resistance due to friction can be estimated as $\mu P_{Rd} / 2$ on each flange and on

each single horizontal row of shear studs as presented in **Fig. (2.16)**. the friction coefficient factor $[\mu]$ is equal to 0.50, and the resistance of a single unit of shear stud $[P_{Rd}]$ is the smaller values Eqn. (2.77) and (2.78).

The maximum spacing between the flanges is specified in **Fig. (2.17)**.

$$P_{Rd} = 0.8 f_u \pi d^2 / 4 X_v \quad \text{Eqn. (2.77)}$$

$$\text{or} \quad P_{Rd} = 0.29 \alpha d^2 (f_{ck} E_{cm})^{0.5} / 4 X_v \quad \text{Eqn. (2.78)}$$

Where:

$$\alpha = 0.20 [1 + (h_{sc}/d)] \quad \text{for } 3 \leq h_{sc} / d \leq 4 \quad \text{and } \alpha = 1.0 \text{ for } h_{sc} / d > 4$$

X_v Partial Factor = 1.25

d Stud diameter, $16\text{mm} \leq d \leq 25\text{mm}$

f_u Tensile ultimate strength of the stud $\leq 500\text{MPa}$

f_{ck} Characteristic cylinder compressive strength of the concrete

h_{sc} overall nominal height of the stud.

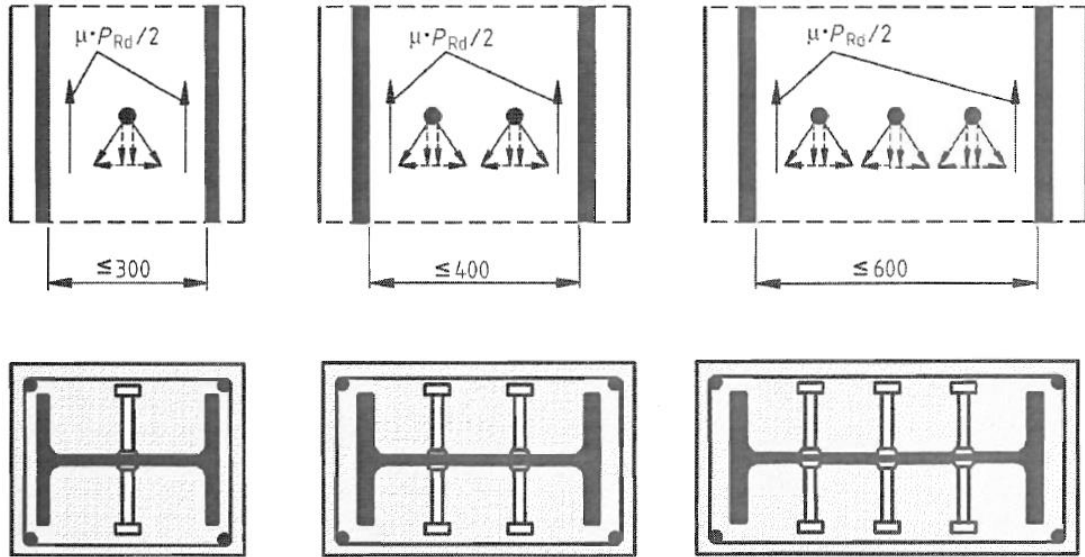


Fig. 2.17 Additional Frictional Forces introduced in the composite columns due to the use of headed studs

In case of having partially interface between endplates and concrete section in compression, then the loads can be re-distributed along the end plate thickness with a ratio of 1:2.5, and the concrete stresses to be limited to the introduced effective loaded area.

In case the concrete filled steel tube is partially loaded throughout gusset plates along the steel profile or throughout stiffener plates as shown in **Fig. (2.18)** the local design strength of the concrete ($\sigma_{c,Rd}$) introduced by the sectional forces of the concrete can be calculated as follow:

$$\sigma_{c,Rd} = f_{cd} \left[1 + (\eta_{cl} t.f_y / a.f_{ck}) \right] * \left[A_c / A_1 \right]^{0.5} \leq A_c f_{cd} / A_1 \leq f_{yd}$$

Eqn. (2.79)

Where:

t	Thickness of steel tube plate
a	diameter of circular tube or width of the square tube section
A_c	Area of concrete section
A_1	loaded area under gusset plate, refer to Fig. (2.18)
η_{cl}	4.90 for circular tube and equal to 3.50 for square tube.
A_c/A_1	≤ 20.0

The longitudinal reinforcement can be considered in the design resistance of the composite column and not required to be welded to the endplates or to have direct interface with the endplates. The gap distance between rebar and endplates shall not exceed 30mm, refer to **Fig. (2.18)**.

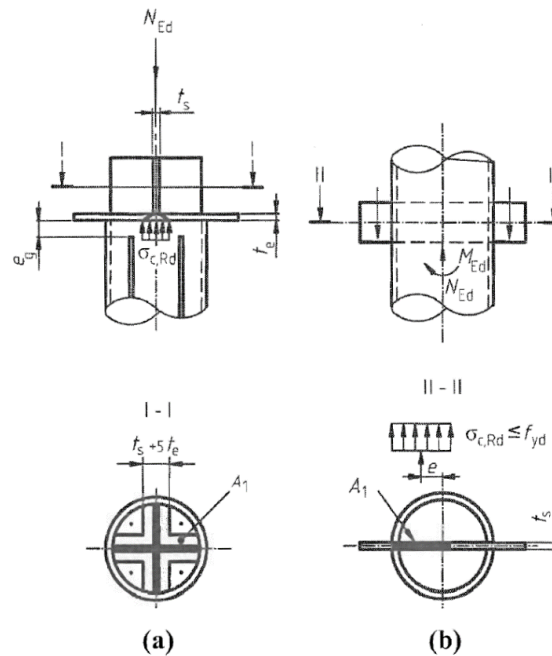


Fig. 2.18 Concrete Filled Circular Tube Section Partially Loaded

Transverse reinforcement should follow EN 1992-1-1, 9.5.3. For partially encased steel section, the concrete to be confined using transverse reinforcement in-line with **Fig. (2.19)** extracted from Eurocode4.

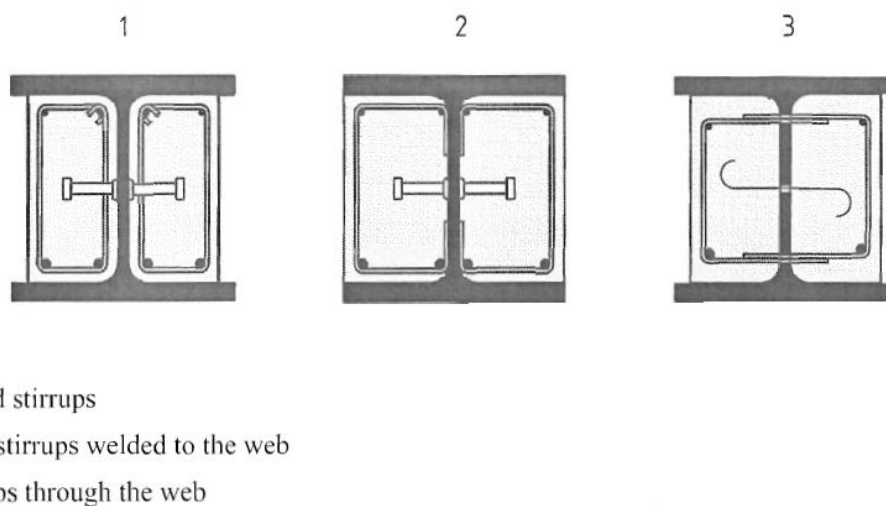


Fig. 2.19 Stirrups Arrangements for Partially Encased Steel Sections

The transverse reinforcement should be designed for the longitudinal shear forces introduced due to the transfer of the axial forces (N_{c1}) showing in **Fig. (2.20)** from the portion of concrete

directly connected by shear connectors into the portion of concrete without direct shear connectors. As per **Fig. (2.20)** the hatched area outside the steel flanges is assumed as in-direct connected, and the transverse steel reinforcement to be designed and distributed using a Strut and Tie Model of 45° angle between concrete compression strut and the member axis.

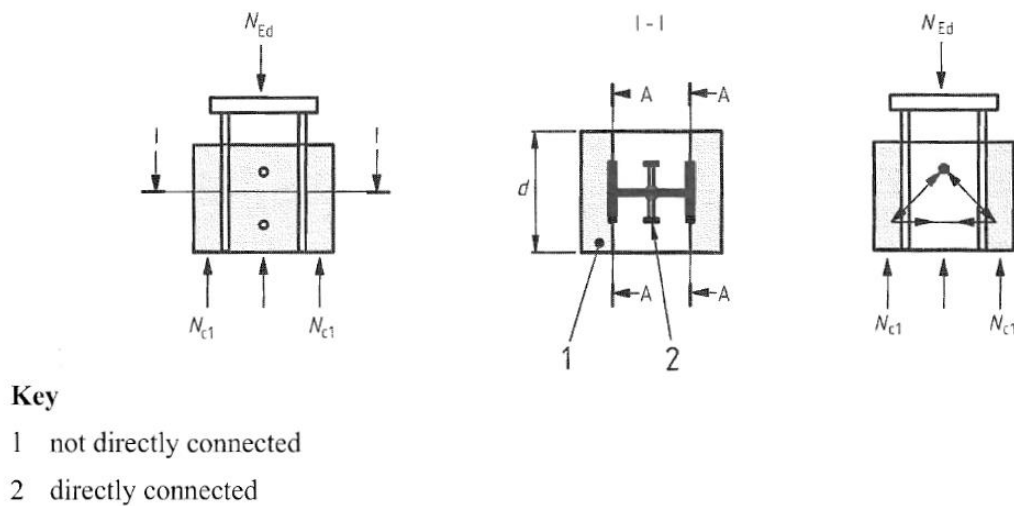


Fig. 2.20 Direct and in-direct connected to concrete areas for the transverse design reinforcement

The design shear strength (t_{Rd}) for fully encased composite column can be applied under the following conditions:

- a. A minimum concrete cover of 40mm.
- b. The longitudinal reinforcement for encased composite column shall be not less than 0.30% of the concrete cross sectional.
- c. No longitudinal reinforcement required for filled concrete composite column.
- d. The transverse reinforcement shall follow EN 1992-1-1, 9.5.3 summarized as follow:
 - Minimum diameter is 6mm or one quarter of the maximum diameter of the longitudinal rebar.
 - Minimum diameter of wires or welded fabric mesh is 5mm.
 - Distance between transverse reinforcement shall not exceed 20 times minimum diameter of the longitudinal reinforcement, the less column dimension, or 400mm.

The design shear strength (t_{Rd}) can be increased by (β_c) for fully encased composite columns as per the following equation;

$$\beta_c = 1 + 0.02 c_z \left[1 - (c_{z,min}/c_z) \right] \leq 2.50 \quad \text{Eqn. (2.80)}$$

Where:

c_z Concrete cover (mm)

$c_{z,min.}$ Minimum concrete cover (40mm)

In case the transverse reinforcement is carrying part of the transverse shear force ($V_{c,Ed}$), then it should be welded to the web of the steel section or should penetrate through the web of the steel section.

2.10 ISOLATED STEEL REINFORCED CONCRETE COLUMN (ISRC)

The Isolated Steel Reinforced Concrete Columns consist of multiple individual steel I Sections not connecting to each other. The use of the ISRC columns is leading to improve the construction quality and to facilitate the fabrication, erection, and execution of the composite mega columns. The design of the isolated steel reinforced concrete columns is not specified clearly in the international codes and there is no sufficient studies and testing conducted to evaluate the behavior of this type of composite columns.

China Academy of Building Research (CABR) has studied the performance of the ISRC columns by conducting two stages testing procedures on scaled columns designed for tall building in China.

The outcome from those testing and finite element analyses can be summarized as follow:

- a. The test results of the ISRC columns including 4 individual I steel sections are in-line with the finite element analysis and the simplified design method of the code.
- b. The composite action between concrete and isolated steel sections has been sufficiently developed, and the current code provisions for the composite column design are applicable to determine the flexure bending capacity of the ISRC columns with a maximum eccentricity not exceeding 15%.
- c. The performed testing has been evaluated by the current codes AISC, ACI 318, Eurocode 4m and China Code JGJ 138 and it is concluded that those codes are applicable to determine the axial compression and flexure bending capacities with appropriate factor of safety.
- d. The use of shear connectors has a slight effect on the nominal sectional capacities, since the shear demand on the concrete steel interface is quite tiny for the Composite Columns.
- e. The concrete confinement could improve the ductility, nominal strength and ultimate compressive strain of the concrete. In case of the ISRC columns, the concrete columns are robustly confined and surrounded by the steel sections

Fig. (2.21) showing the typical layout of 4 isolated steel reinforced concrete columns

Table [2.8] presenting different methods to design the shear studs in-line with Eurocode4 Code, Chinese Code, and AISC Code.

Code	Strength of shear studs	Specifications
Eurocode4	$V_u = \min\left\{\frac{0.8f_u\pi d^2}{4\gamma_v}, \frac{0.29\alpha d^2\sqrt{f_c E_c}}{\gamma_v}\right\}$ <p>where:</p> $\alpha = 0.2\left(\frac{h}{d} + 1\right), \text{ for } 3 \leq \frac{h}{d} \leq 4$ $\alpha = 1 \quad \text{for } \frac{h}{d} > 4$	<ul style="list-style-type: none"> $f_u \leq 500 \text{ MPa}$ $16\text{mm} \leq d \leq 25\text{mm}$ concrete density not less than 1750kg/m^3
Chinese GB50017	$V_u = \min\left\{0.7\gamma\frac{f_u\pi d^2}{4}, \frac{0.43\pi d^2}{4}\sqrt{f_c E_c}\right\}$ <p>where γ – ratio of tensile to yield strength of the stud</p>	<ul style="list-style-type: none"> $h/d \geq 4$ when the stud is not positioned right over the web: (1) $d \leq 1.5t_f$ if the flange is designed to be in tension; (2) $d \leq 2.5t_f$ if not.
AISC-LRFD	$V_u = \min\left\{\frac{f_u\pi d^2}{4}, \frac{0.5\pi d^2}{4}\sqrt{f_c E_c}\right\}$	<ul style="list-style-type: none"> $h/d \geq 4$ concrete density not less than 1440kg/m^3 $d \leq 2.5t_f$ if the stud is not positioned right over the web

Table [2.8] Different Methods to Design Shear Studs

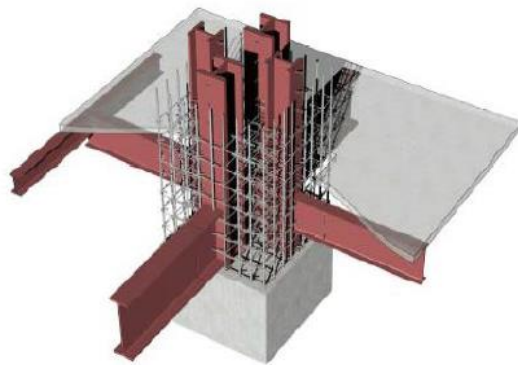
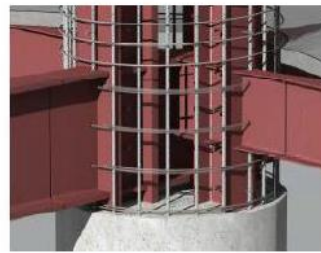
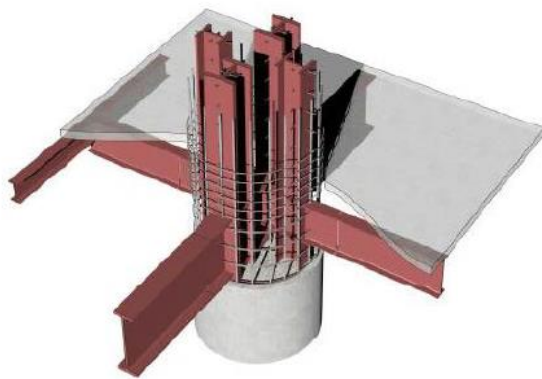
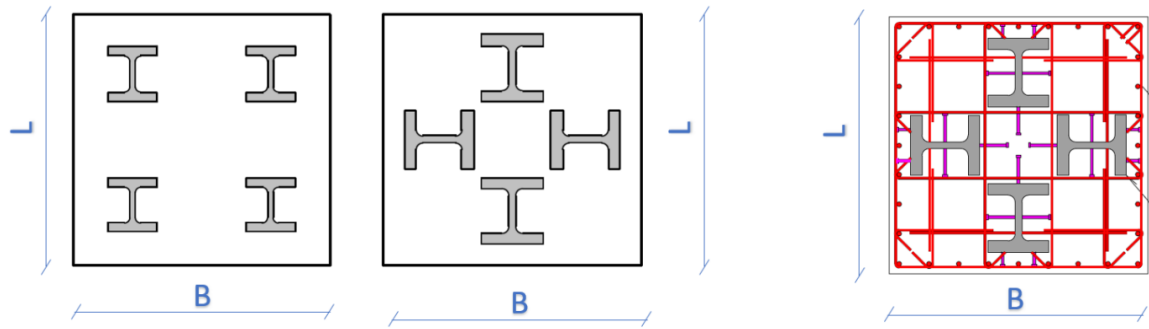


Fig. 2.21 Isolated Steel Reinforced Concrete Column (Layout & 3D View)

2.11 PRECEDING AND CURRENT RESEARCHES ON THE CONCRETE FILLED TUBE COLUMNS

There are many researches and studies performed in order to evaluate the behavior of concrete filled steel tube columns. Some of those studies have been highlighted in this research as follow:

Furlong [1967, 1968] performed one of the first testing in the United States on the concrete filled steel tube columns. The testing was including 52 CFST columns under different loading conditions. The CFST specimens have been formed from steel material of strength of 250MPa and concrete of low strength of 20MPa. The CFST columns have been categorized into two categories, 13 columns with square cross sectional and the remaining 31 CFST columns with circular tube. Thirty-Nine columns have been testes under bi-axial loading, and Thirteen columns have been tested under axial compression load.

The outcome of the test results as stated by Furlong is the strain in the CFST column is larger than hollow steel tube in the elastic zone and before local buckling happened.

The testing showed also that the columns' stiffnesses were less than the stiffness calculated based on the transformed area method, so Furlong concluded that the bond between steel and concrete is not exist.

The bond mechanism between concrete and steel was negligible to prevent splitting as a result of having variance in the Poisson Coefficient of Steel and Concrete.

The Poisson coefficient is defined as the ratio between lateral strain to the longitudinal strain under uniaxial load. The Poisson coefficient in the concrete is about 0.20 and in the steel is about 0.30, so the higher value of the steel material allows it to expand under lower values of uniaxial load and to mitigate bond between steel and concrete.

Once the concrete reached the crushing strain, the Poisson Coefficient increased leading the concrete to expand, so the steel tube can provide appropriate confinement to the concrete and consequently enhance ductility of the composite member.

Furlong advised that the stiffness of the concrete filled steel tube column can be calculated from the following formula:

1) Axial Stiffness

$$AE_{\text{composite}} = A_c E_c + A_s E_s \quad \text{Eqn. (2.81)}$$

2) Flexure Stiffness

$$IE_{\text{composite}} = I_c E_c + I_s E_s \quad \text{Eqn. (2.82)}$$

Furlong demonstrated that the theoretical stiffness of the CFST Columns is about 89% compare to the results of the experimental testing and recommended to calculate the stiffness accurately by using the interaction P-M chart considering the crushing strain of concrete is 0.003.

Tomii et. al. [1995] examined the confinement influence on the CFST columns by conducting more than 270 uniaxial compression experimental tests. There were many different parameters affecting the confinement such as slenderness ratio (kL/r), geometry of the cross section, concrete strength and its characteristics specifically the use of expanded cement.

The experimental study was conducted on two stages, the first stage was to evaluate the impact of the column lengths and geometry, while the second stage was focusing on the slenderness, concrete characteristics and cross-sectional geometry.

The outcome from those experimental works done by Tomii et al [1995] demonstrated that the flexure buckling caused a failure to the long columns, while the concrete is crushed in the short columns because of the confinement effect.

The experimental results have showed higher load capacities than the theoretical derived from the superposition of the material strength, and it was noticeable in the CFST columns with circular or octagonal cross sectional. The confinement influence introduced by the circular or octagonal geometry provides higher deformation capacities after reaching local buckling of the steel tubes compare to the square tube, the confinement effect of the square column cannot be predicted.

Tomi and his teammates concluded that the expanded cement has no influence on the In-Elastic behavior of the concrete filled steel tube columns.

Baba et al. [1995] studied the application of high strength material on a square CFST short column. There were 45 columns have been tested under uniaxial compression load. the steel strength was varying from 400 N/mm² up to 800N/mm² and the concrete strength was varying from 20MPa to 80MPa. The slenderness ratio (b/t) was in-between 18.5 to 17.

The test results illustrated that the ratio (b/t) and ($b/t \sqrt{F_y/E_s}$) have a noticeable influence on the composite section capacity. A high strength concrete provides a larger capacity for the CFST column.

Baba et al. [1995] demonstrating that the influence of the concrete confinement introduced by the steel tube reduces as the ratio of (b/t) increments, in addition the capacity of a high strength concrete filled tube columns was anticipated properly by adopting the superposition of the material strength.

Sakino [1995] studied the performance of a high strength circular concrete filled tube beam column under combined flexure bending and Axial compression. A total number of 28 specimens have been tested under fixed axial compression load with variable bending moments. The steel strength was varying from 408 N/mm² to 879 N/mm², and the concrete strength was varying from 24.50MPa to 77.6MPa. the ratio of diameter to thickness (D/t) ranging between 16.7 to 152.

The applied axial compression force was ranging between 15% to 80% of the anticipated nominal compression strength using the material strength superposition. The ratio of (D/t) had a great influence on the composite column flexure capacity and its ductility as well as a result of the local buckling of the steel tube and restricted deformation capacity of concrete. The circular CFST column became more brittle member when the D/t exceeding 100, while it became more ductile when D/t is less than 50, even under higher axial compression load. The anticipated flexure capacity increased with less ratio (D/t) inline with concrete stress block methodology presented in the ACI Code ($0.85f'_c$).

Fujimoto et al. [1995] evaluated the behavior of concrete filled square steel tube column under flexure loading based on different parameters of material and steel cross sections. The steel tubes examined were having b/t ratios ranging in-between 19 and 75 with steel strength grade ranging from 267MPa to 851MPa, and concrete grade between 26MPa to 82MPa. The magnitude of axial compression test load was ranging in between 13% and 60%

of the predicted nominal axial compression load. The test results illustrated that the anticipated flexure capacity of CFST column affected by the b/t ratio as noticed by Sakino [1995] for the tube circular column. it was noted; when b/t reduced, the ductility increased and consequently the flexure bending capacity increased. The tested columns executed with high strength steel display a reduction in the deformation capacity.

Sakino [1996] defined the axial compression capacity of CFST column taking into account the confinement effect and based on the following assumptions.

The first assumption considering the concrete failure criteria is derived by the following formula:

$$f_{cc} = f'_c + k \cdot \sigma_r \quad \text{Eqn. (2.83)}$$

Where:

K confinement factor (4.1)

σ_r Confining Stress

The second assumption was the criteria of the steel yielding derived by Von Mises theorem:

$$\sigma_y^2 = \sigma_z^2 + \sigma_z \sigma_\theta + \sigma_\theta^2 \quad \text{Eqn. (2.84)}$$

Where:

σ_y Yielding Stress of the Steel Tube

σ_z Axial Stress of the Steel Tube

σ_θ Hoop Stress of the Steel Tube

The third assumption addressed the axial and hoop stress in the steel tube from the following formulas

$$\sigma_z = \beta \sigma_y \quad \text{Eqn. (2.85)}$$

$$\sigma_\theta = \alpha \sigma_y \quad \text{Eqn. (2.86)}$$

Where:

β Factor from Experimental work results = -0.20

α Factor from Experimental work results = 0.88

The Axial compression Capacity of the CFST column taking into account the confinement influence can be derived from the following formula given by Sakino [1996].

$$N_u / N_o = \beta - 0.5 k . \alpha - 1.0 \quad \text{Eqn. (2.87)}$$

The above formula ignored the residual stresses, and it is not applicable for CFST column with a ratio of Length to Diameter (L/D) less than 6.0.

Inai and Sakino [1996] illustrated the flexure capacity if the CFST column using the stress-strain relationship for the concrete and steel tube considering the influence of the concrete confinement, and local buckling of the steel tube. The CFST member was subjected to fixed axial compression load with increasing flexure moments and shearing forces. The model of concrete has considered its stress-strain behavior similar to plain concrete up to reaching compressive material, thereafter the confinement influence to be considered using D Coefficient. The experimental model of the stress-strain relationship of the confined concrete of square CFST Column was derived by Inai and Sakino as follow:

$$f_c = \emptyset f'_c . AX + (D-1) X^2 / 1 + (A-2)X + DX^2 \quad \text{Eqn. (2.88)}$$

Where:

f_c Concrete Stress (kg/cm²)

\emptyset Factor for scale effect strength

f'_c compressive strength of plain concrete (kg/cm²)

$$X = \epsilon_c / \epsilon_o \quad \text{for } 0.0 \leq \epsilon_c \leq \epsilon_o \quad \text{Eqn. (2.89)}$$

$$X = [(\epsilon_c - \epsilon_o)] * K_c + 1.0 \quad \text{Eqn. (2.90)}$$

$$A = (E_c * \epsilon_o) / f_p \quad \text{Eqn. (2.91)}$$

Where:

ϵ_c Concrete Strain

ϵ_o	Strain at the strength of plain concrete ($0.52f'_c{}^{0.25} * 10^{-3}$) (kg/cm ²)
K_c	Scale Factor = 3/2
E_c	Concrete Modulus of Elasticity = ($0.703+0.106f'_c{}^{0.5}$) * 10^{-5} (kg/cm ²)
D	$= \alpha + \beta.f'_c + \chi.f_{re}$
f_{re}	Effective Confining Pressure = $0.5\rho_h f_{hs} (d'' / C)$
ρ_h	Volumetric ratio of steel tube
d''	Thickness of steel tube
C	Inner width of steel tube
f_{hs}	Yield strength of the steel (kg/cm ²)
α	= 1.50
β	= $-1.68*10^{-3}$
χ	0.75

There are some assumptions adopted by Inai and Sakino to develop the stress strain curve of the Steel tube of a square CFST column as follow:

- The stress strain curve of the steel tube is exactly the same of the hollow steel tube up to compressive strength limit of the steel tube.
- Local buckling of the steel tube is not occurred and eliminated by the concrete if the compressive strength of the steel tube is less than the yield strength of the steel tube.
- Once the compressive strength of the steel tube attained, the compressive strain reduces linearly to (ϵ_T) , then the compressive strain turn into constant value $(T.F_y)$, and those parameters have no relation to b/t ratio.

$$(\epsilon_T - \epsilon_B) / \epsilon_y = 2.0 + (6.73/\alpha) \quad \text{Eqn. (2.92)}$$

$$T = 1.14 - 0.21 \alpha^{0.5} \quad \text{Eqn. (2.93)}$$

$$\alpha = (b/t)^2 \cdot F_y/E_s \quad \text{Eqn. (2.94)}$$

Where:

ϵ_B Strain at compressive strain

ϵ_y Yield strain of the steel tube

The conclusion of Inai and Sakino Studies that the flexure performance of the concrete filled steel tube columns was sufficiently anticipated by the formulations.

Toshiyuki et al. [1996] examined the deformation capacity of CFST beam-columns by testing 165 rectangular CFST columns and 47 circular CFST columns comprising different material strengths from conventional strength to high strength. The deformation capacity of the CFST beam columns has been anticipated based on the angle of rotation of the beam columns. The boundary of rotation angle, R_{95} of the beam column has been determined by Toshiyuki et al. as the calculated rotation when 95% of the maximum load preserved after ultimate capacity. The main factors affecting the deformation capacity were the axial compression load and the ratio (b/t) based on the previous researches illustrated that the slope turns into steeper with the increase in the axial compression load, and the influence of the material strength is minimal. The following empirical formulas showing the angle of rotation of the beam-column

a. For Square tube cross sectional

$$R_{95}(\%) = 4.24 - 1.68(N/N_o) - 0.105Nb/N_o t \quad \text{Eqn. (2.95)}$$

b. For Circular tube cross sectional

$$R_{95}(\%) = 8.0 - 0.7(N/N_o) - 0.03D/t \quad \text{Eqn. (2.96)}$$

The anticipated angle of rotation using the above formulas was sufficiently inline with the previous experimental test results conducted for square and circular CFST columns.

Zhang and Shahrooz [1997] analyzed the behavior of the CFST columns under fixed axial compression load and consistently increasing flexure load. The analysis has been conducted on three models of CFST column formed from conventional strength concrete and high strength steel tubes. The first model was conducted based on the applicable method to analyze the reinforced concrete columns, which allows compressive strain to reach 0.003 at failure, taking into consideration the ultimate strength is equivalent to $0.85f'_c$, and the steel tube material shall comply with the elastic perfectly plastic stress-strain behavior. The second model is similar to the first model but the steel along cross section is considered to be completely yielded. The third model was conducted based on the fiber analysis. There were a variety of the uniaxial stress-strain curves of the concrete and steel for the fiber analysis have been examined in order to define the perfect material models can be adopted to anticipate the behavior of the CFST column. Those three models have been compared to the experimental test results conducted on the square CFST column by Tomii and Sakino [1979], Furlong [1967 & 1968], and Building Contractors Society (BCS) in Japan [Fujimoto et al., 1995]. The main factors of these studies are illustrated in **Table [2.9]**.

Specimen	b/t	f'_c		f_y		E_s		P/P _o
		(ksi)	(Mpa)	(ksi)	(Mpa)	(ksi)	(Mpa)	
I-0	44	3.4809977	24	28.138065	194	29870.587	205945	0.00
I-1	44	5.5405881	38.2	28.138065	194	29870.587	205945	0.13
I-2	44	5.5405881	38.2	28.138065	194	29870.587	205945	0.27
I-3	44	5.5405881	38.2	28.138065	194	29870.587	205945	0.33
I-5	44	5.5405881	38.2	28.138065	194	29870.587	205945	0.46
I-6	44	5.3230257	36.7	28.138065	194	29870.587	205945	0.58
II-0	44	3.132898	21.6	44.23768	305	30297.299	208887	0.00
II-1	44	3.132898	21.6	44.23768	305	30297.299	208887	0.09
II-2	45	3.132898	21.6	49.169093	339	31008.438	213790	0.18
II-3	45	3.132898	21.6	49.169093	339	31008.438	213790	0.26
II-4	45	3.132898	21.6	41.917014	289	31293.009	215752	0.38
II-5	45	3.132898	21.6	41.917014	289	31293.009	215752	0.48
II-6	45	3.132898	21.6	41.917014	289	31293.009	215752	0.57
III-0	34	2.9878564	20.6	41.917014	289	30581.725	210848	0.00
III-1	34	2.9878564	20.6	41.917014	289	30581.725	210848	0.09
III-2	34	2.9878564	20.6	41.917014	289	30581.725	210848	0.19
III-3	33	2.9878564	20.6	41.771973	288	29870.587	205945	0.28
III-4	33	2.9878564	20.6	41.771973	288	29870.587	205945	0.37
III-5	33	2.9878564	20.6	41.771973	288	29870.587	205945	0.47
III-6	33	2.9878564	20.6	41.771973	288	29870.587	205945	0.56
IV-0	24	2.6977732	18.6	41.191807	284	32715.432	225559	0.00
IV-1	24	2.6977732	18.6	41.191807	284	32715.432	225559	0.10
IV-2	24	2.6977732	18.6	41.191807	284	32715.432	225559	0.19
IV-3	24	2.6977732	18.6	41.336848	285	32715.432	225559	0.29
IV-4	24	2.8718231	19.8	41.336848	285	32715.432	225559	0.38
IV-5	24	2.8718231	19.8	41.336848	285	32715.432	225559	0.48
IV-6	23	2.8718231	19.8	41.771973	288	31293.009	215752	0.57

(a) Tomii and Sakino

Specimen	b/t	f'_c		f_y		E_s		P/P _o
		(ksi)	(Mpa)	(ksi)	(Mpa)	(ksi)	(Mpa)	
ER8-A-4-01	19	5.8741837	40.5	121.10971	835	31435.15	216732	0.08
ER8-C-2-04	27	3.6840559	25.4	121.10971	835	31719.722	218694	0.39
ER8-C-2-06	27	3.6985601	25.5	121.10971	835	31719.722	218694	0.59
ER8-C-4-025	27	5.8741837	40.5	121.10971	835	31719.722	218694	0.25
ER8-C-4-04	27	5.8741837	40.5	121.10971	835	31719.722	218694	0.40
ER8-C-4-06	27	5.8741837	40.5	121.10971	835	31719.722	218694	0.59
ER8-C-8-04	27	11.168201	77	121.10971	835	31719.722	218694	0.40
ER8-C-8-06	27	11.168201	77	121.10971	835	31719.722	218694	0.60
ER8-D-4-04	41	5.8741837	40.5	121.10971	835	31435.15	216732	0.41
ER8-D-4-06	41	5.8741837	40.5	121.10971	835	31435.15	216732	0.61
ER6-C-2-025	33	3.6840559	25.4	89.635692	618	32146.434	221636	0.25

(b) Building Contractors Society (BCS)

Specimen	b/t	f'_c		f_y		E_s		P/P _o
		(ksi)	(Mpa)	(ksi)	(Mpa)	(ksi)	(Mpa)	
F-I-1	26	6.5268708	45	70.345163	485	29001.788	199955	0.25
F-I-2	26	6.5268708	45	70.345163	485	29001.788	199955	0.38
F-I-3	26	6.5268708	45	70.345163	485	29001.788	199955	0.38
F-I-4	26	6.5268708	45	70.345163	485	29001.788	199955	0.63
F-II-1	48	3.3359562	23	48.008761	331	29001.788	199955	0.18
F-II-2	48	3.3359562	23	48.008761	331	29001.788	199955	0.18
F-II-3	48	3.3359562	23	48.008761	331	29001.788	199955	0.48
F-II-4	48	3.3359562	23	48.008761	331	29001.788	199955	0.74
F-II-5	48	3.3359562	23	48.008761	331	29001.788	199955	0.74
F-III-0	32	4.2062056	29	48.008761	331	29001.788	199955	0.00
F-III-1	32	4.2062056	29	48.008761	331	29001.788	199955	0.06
F-III-2	32	4.2062056	29	48.008761	331	29001.788	199955	0.19
F-III-3	32	4.2062056	29	48.008761	331	29001.788	199955	0.19
F-III-4	32	4.2062056	29	48.008761	331	29001.788	199955	0.39
F-III-5	32	4.2062056	29	48.008761	331	29001.788	199955	0.45
F-III-6	32	4.2062056	29	48.008761	331	29001.788	199955	0.45
F-III-7	32	4.2062056	29	48.008761	331	29001.788	199955	0.65

(c) Furlong

Table [2.9] Main Factors utilized by Zhang and Shahrooz

Zhang and Shahrooz [1997] concluded that the first model is acceptable for the CFST column comprising normal strength concrete and steel, and it is not appropriate and provide underestimates for the design strength limit of the CFST column executed from high strength steel. The second model was more precise, the third model of fiber analysis demonstrated the perfect method of anticipated the behavior of the CFST column, regardless the strength of the steel material. Zhang and Shhrooz [1997] recommended to use the confined concrete model proposed by Tomii and Sakino [1979] presenting in **Fig. (2.22)** when using the fiber analysis, where the following formula can be adopted up to strain of 0.002

$$f_c = f'_c [2(\epsilon_c/\epsilon_o) - (\epsilon_c/\epsilon_o)^2] \quad \text{Eqn. (2.97)}$$

Where:

- f_c Concrete stress
- f'_c Concrete compressive strength
- ϵ_c Concrete strain
- ϵ_o Strain at peak stress

Fig. (2.22) illustrated that the post-peak response of the concrete is influenced by b/t ratio.

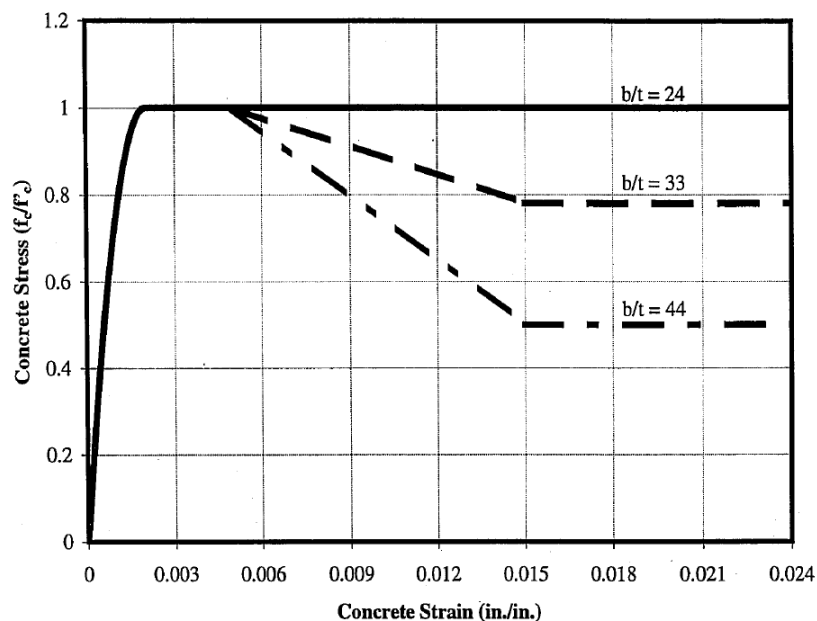


Fig. 2.22 Tomii and Skino's Model of Confined Concrete utilized by Zhang and Shahrooz [1997]

The conclusion from Zhang and Shahrooz researches that the elastic-perfectly plastic model of the steel compression fiber in CFST column can be adopted for modeling if the local buckling of the steel tube takes place.

Several studies have been performed by adopting the fiber analysis method in order to examine the influence of residual stresses and cold work stresses.

Zhang and Shahrooz [1997] noticed that the cold work effect is negligible on the behavior of the CFST column subject to large axial compression load combined with flexure bending.

Hull [1998] carried out experimental testing on a high strength concrete filled tube columns. A total number of 12 specimen have been tested as follow, 4 stub columns testing, and 8 columns has been tested with monotonic uniform flexure bending moments and fixed axial compression load. The steel yield stress was ranging between 317MPa and 551MPa with slenderness ratios between 32 and 48. The concrete strength was 110MPa. **Table [2.10]** illustrated the column stiffnesses defined from the experimental testing in comparison to the theoretical calculated stiffnesses using uncracked transformed section. **Table [2.11]** demonstrating the ratio between experimental capacities and theoretical calculated capacities.

Specimen	EA_{exp} (kips)	$\frac{EA_{exp}}{EA_{uncr, tr}}$
SC-32-46	$1.168 \cdot 10^6$	1.00
SC-48-46*	-NA-	-NA-
SC-32-80	$1.229 \cdot 10^6$	1.05
SC-48-80	$1.111 \cdot 10^6$	1.02
BC-48-46-20	$1.087 \cdot 10^6$	1.01
BC-48-46-22	$1.098 \cdot 10^6$	1.02

*Axial deformation instruments (LVDTs) gave unreliable data for specimen SC-48-46, therefore the axial stiffness of Specimen SC-48-46 was determined from data acquired when Specimens BC-48-46-20 and BC-48-46-22 were subjected to axial load.

Table [2.10] Tested Columns' Stiffnesses, Hull [1998]

Specimen	P_{exp} (kips)	P_{exp}	P_{exp}
		$\frac{A_s F_y + 0.85 A_c f'_c}{A_s F_y + 0.85 A_c f'_c}$	$\frac{A_s F_y + A_c f'_c}{A_s F_y + A_c f'_c}$
SC-32-46	2557	1.10	0.97
SC-48-46	2597	1.02	0.90
SC-32-80	3169	1.04	0.95
SC-48-80	2763	0.96	0.86

Table [2.11] Ratio between Experimental Capacities and Theoretical Capacities, Hull [1998]

Hull [1998] has concluded the following from his research;

- The average accuracy of the axial stiffness was 2% between experimental results and theoretical calculations using uncracked transformed section stiffness
- The average accuracy of the strength superposition was 3% between experimental results and theoretical calculations using equivalent compressive stress block of $0.85f'_c$.
- The local buckling of steel tube with higher slenderness ratio (b/t) prevent the steel section to achieve the full steel yield stress at peak load.

Nakahar and Sakino [1998] examined the behavior of high strength concrete filled steel tube columns by performing 14 experimental testing. There were 10 columns has been tested under combined axial compression load and unfirmed flexure bending, while the remaining four columns have been tested under uniaxial compression load. The yield strength of the steel tube was 310MPa, and the concrete strength was 119MPa. This research illustrated that the experimental compression capacity is exceeding the theoretical nominal load (N_o), where N_o can be calculated from the following formula:

$$N_o = A_s \sigma_{sy} + A_c \sigma_{cB} \quad \text{Eqn. (2.98)}$$

Where:

A_s Area of steel

A_c Area of concrete

σ_{sy}	Steel yield strength
σ_{cB}	Concrete compressive strength

The research demonstrated also that the behavior CFST column under uniform flexure bending and high axial compression with high value of (b/t) is being more brittle element, and the maximum bending moment realized in the experimental test is less than the plastic bending moment capacity of the column.

Kawaguchi et. al. [1998] gathered a lot of results of CFST experimental testing including different parameters in endeavor to identify appropriate formulas for the restoring force based on regression analysis. The collected data includes 209 sample from AIJ publications, with 143 of square tube geometry and 66 of circular tube geometry. The variable factors were the concrete compressive strength up to 50MPa, Steel yielding stress in-between 201MPa and 450MPa, the type of loading (Cycle and Monotonic), and b/t ratio ≤ 80 .

Fig. (2.23) demonstrate a multi-linear model progressed by Kawaguchi et. al. [1998] for iterating the forces of a CFT beam column for the application in pushover frame analysis. Point (A) is calculated as $M_{ult}/3K_e$ and $M_{ult}/3$, where M_{ult} is the hypothetical ultimate moment derived from the stress distribution of the full plastic moment, and K_e is the hypothetical elastic stiffness. Point B is determined as the intersection between R_{85} and $0.85M_{ult}$. Point C is determined as the intersection between R_{max} and M_{ult} , while Point D can be calculated as the intersection between R_u and M_{ult} .

Where:

$$R_{85} = 2.0 - 1.53(N/N_o) + [0.03(N/N_o) - 0.03]D/t \text{ for Square Tube} \quad \text{Eq. (2.99)}$$

$$R_{85} = 0.69 - 1.61(N/N_o) + [0.02 - 0.06(N/N_o)]D/t \text{ for Circular Tube} \quad \text{Eq. (2.100)}$$

$$R_{max} = 5.61 - 7.30(N/N_o) + [0.16(N/N_o) - 0.10]D/t \quad \text{for Square Tube} \quad \text{Eq. (2.101)}$$

$$R_{max} = -0.31 - 79.94(N/N_o) + [-0.12 + 0.131(N/N_o)]D/t \quad \text{for Circular Tube} \quad \text{Eq. (2.102)}$$

$$R_u = 5.5 - [(\sigma_b - 39)/120] - 0.45(D/t)(\sigma_y/324)^{0.5} - 5.0(N/N_o) \text{ for Square Tube} \quad \text{Eq. (2.103)}$$

$$R_u = 7.5 - [(\sigma_b - 39)/120] - 0.05(D/t)(\sigma_y/324)^{0.5} - 5.0(N/N_o) \text{ for Circular Tube} \quad \text{Eq. (2.104)}$$

σ_b Concrete Cylinder Strength (MPa)

σ_y Steel Yield Strength (MPa)

The conclusion from the test results in comparison with Static Pushover Analysis based on the above-mentioned equations demonstrating the anticipated average response is quite good for the square CFST column, while it shows less estimate for the circular CFS. The ratio between the ultimate moments extracted from the experimental studies and the theoretical ultimate bending moments ($M_{ult,exp}/M_{ult,theo}$) has been evaluated by Kawaguchi et. al. [1998] and it was noticed that the database of the square column specimens has a mean of 1.38 and a standard deviation of 0.34, while the circular column specimens have a mean of 1.20 and a standard deviation of 0.21.

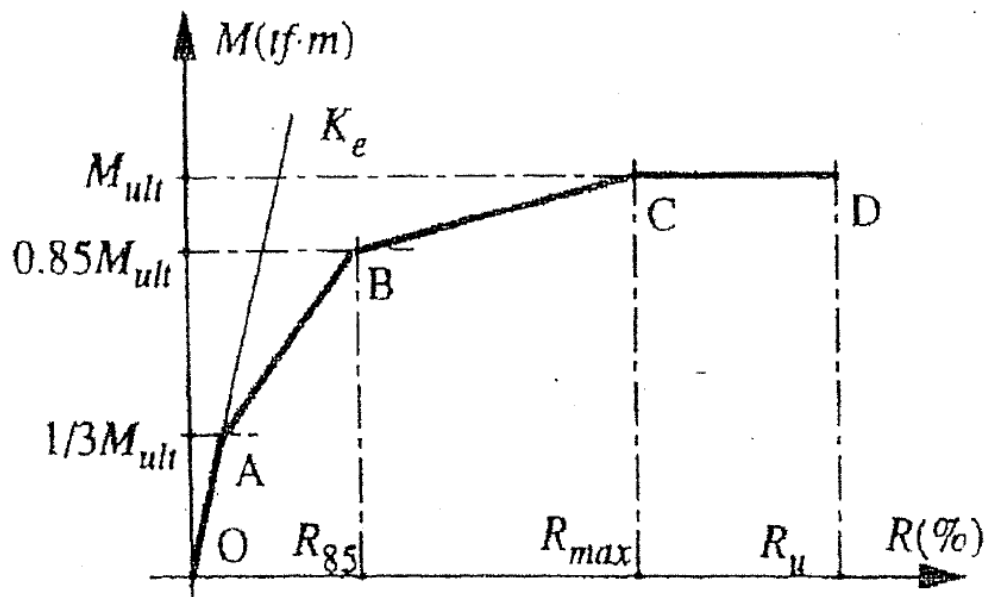


Fig. 2.23 Chart of Iterating Forces Characteristics, Kawaguchi et. al. [1998]

Sakino and Nakahara [2000] did a comparison between the test results conducted to evaluate flexure capacities of the CFST columns subject to eccentric axial compression load and the test results conducted to evaluate the flexure capacities of the CFST columns subject to combined fixed axial compression load and uniform flexure bending moment. The experimental testing comprises a total number of 67 square concrete filled steel tube column. The experimental test results have been compared with Japanese Code Provision (AIJ) and ACI code and the it was concluded that the AIJ provide overprediction to the ultimate capacity capacities of the CFST columns that behave in a brittle mode, while ACI Code provides conservative approach to the ultimate flexure capacities for those CFST behave in a brittle mode. Sakino and Nakahara [2000] impute the overestimation in the AIJ to the influence of local buckling on the square steel tubes with high ratio of b/t , and insufficient confinement provided by the square steel tubes, with increasing ratio of b/t . They highlighted three amendments to the AIJ provisions. The first amendment is to provide a reduction factor to the uniaxial compressive strength if the steel tube to accommodate the influence of the local buckling of the tube plate thicknesses. Where $\alpha \geq 4.11$,

Where:

$$\alpha = (b/t)^2 (F_y/E_s) \quad \text{Eq. (2.105)}$$

The following formula addressed the Coefficient (S):

$$1/S = 0.698 + 0.128 (\alpha) * 4.0/6.97 \quad \text{Eq. (2.106)}$$

The second amendment is considered for applying high strength concrete ($f'_c \geq 60\text{MPa}$) or a thin plate thickness ($\alpha \geq 4.11$). Sakino and Nakahara [2000] advised that the square tube did not create full confinement to the concrete, and there is no significant increase in the concrete ductility, thus the concrete compressive stress block to be reduced by a coefficient ($r_u f'_c$). The reduction factor is equal to 0.85 for the actual design of full-scale column, and for small scale model to be calculated from the following formula:

$$r_u = 1.67 (1.13B_c)^{-0.112} \quad \text{Eq. (2.107)}$$

The consequent concrete compressive strength shall be computed as ($K_2 X_n$), where X_n is the distance from the extreme compressive fiber to the neural axis, and K_2 can be calculated from the following formula:

$$K_2 = 0.429 - 0.010 (\sigma_c / 4.12) \quad \text{Eq. (2.108)}$$

Where:

$$\sigma_c = r_u f'_c$$

The third amendment is to implement a reduction coefficient of r_u for the concrete compressive strength.

Inai et. al. [2000] studied the experimental rotation capacity (R_{exp}) at post-peak limit of $0.95M_{max}$ on the concrete filled steel tube columns for Circular Tube and Square Tube. The outcome of this study demonstrated that the experimental rotation capacity ($R_{95,exp}$) of **circular** CFST column decreases as the slenderness b/t increased, the concrete strength reduced, and as the ratio N/N_o begin to be increased, where (N) the axial compression load and (N_o) is the axial compression capacity. Inai et. al. [2000] observed that the experimental rotation capacity ($R_{95,exp}$) of **square** CFST column decreases as the slenderness b/t increased, and as the ratio N/N_o begin to be increased, in addition they have noticed that no interrelationship between Experimental Rotation Capacity ($R_{95,exp}$) and concrete strength nor yield steel strength. The following formulas defined the maximum rotation capacity corresponding to $0.95M_{max}$ at post-peak in accordance with the experiments and regression analysis.

$$R_{95} = 8.8 - 6.7(N/N_o) - 0.04(D/t) - 0.012 \sigma_b \quad \text{for Circular Tube} \quad \text{Eq. (2.109)}$$

$$R_{95} = 100(t/b)^\beta / [0.15 + 3.79(N/N_o)] \quad \text{for Square Tube} \quad \text{Eq. (2.110)}$$

Where:

σ_b Compressive strength of concrete (MPa)

$$\beta = 1.0 - [(\sigma_b - 10.3)/566] \leq 1.0$$

Inai et. al. [2000] stated that the above formulas presenting a mean of 0.774 for Circular CFST Column and 0.668 for Square CFST column in comparison to the experimental testing database.

Sakino et. al. [2004] conducted extensive experimental testing for the CFST columns as part of the fifth phase of U.S. – Japan Cooperative Earthquake Research Program. They have tested total number of 114 hollow steel tube column and CFST column under centric axial compression load. the purpose of the experimental work is to examine the confinement influence on the local buckling and cross-sectional capacities. There were many factors considered in the research such as steel strength of the tube ranging from 400MPa to 800MPa, slenderness ratio (D/t) for the circular shape and/or (b/t) ratio for the square shape, and concrete design strength ranging from 20MPa to 80MPa. The diameter of circular sections was ranging from 122mm to 450mm, while the width of the square tubes was ranging from 120mm to 324mm. The circular tube has been made using cold formed plate and the square tube has been formed using couple of cold formed channels. They have used 4 different transducers to measure the longitudinal shortening in-between two end plates, consequently, identify the axial strain in the composite columns.

The mean longitudinal strain has been measured by using 4 different transducers that provide the axial shortening between two end plates.

The test results denote that the maximum experimental axial load is higher than the theoretical nominal axial load for the circular CFST column while it is lower in case of square CFST. They have imputed this to the confinement influence in the circular CFST column which enhance the capacity of the cross section under axial load, while the square CFST column affected by local buckling of the steel tube.

One of the key factors in the testing setup is the scale factor effect on the compressive concrete strength. The concrete compressive strength can be modified as recommended by Blanks and McNamara [1935] as illustrated in **Fig. (2.24)** for the circular and can be applied to the square tube assuming it as circular tube with equivalent sectional area.

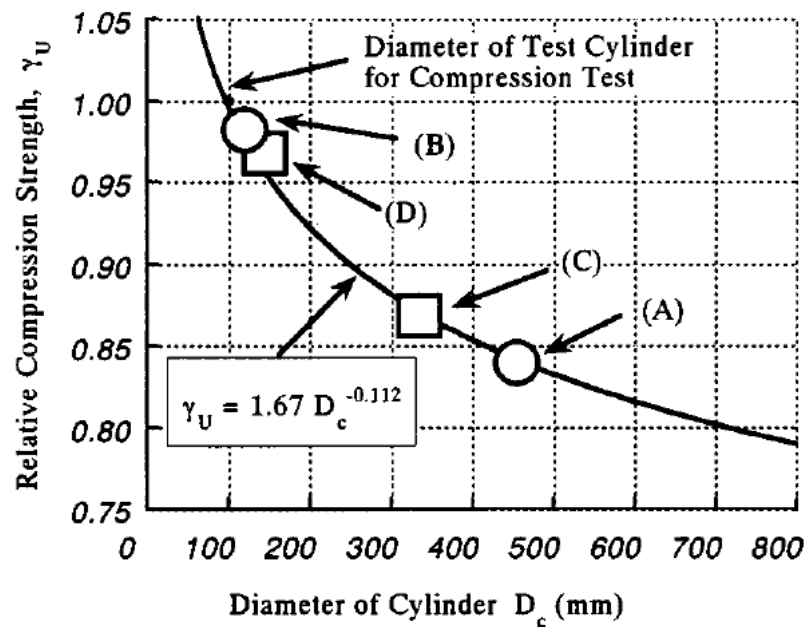


Fig. 2.24 Scale Effect on Compressive Strength of Circular Plain Concrete Column, McNamara [1935]

The outcome of the experimental work conducted for 114 columns can be summarized as follow:

- The relation between ultimate load and yield load of circular concrete filled steel tube columns can be calculated based on a linear function of the steel tube yield strength.
- The influence of local buckling on the capacity of the square CFST column can be determined based on the test results of the hollow steel square tube and then can be amended taking into consideration the restraining effect of the concrete in the CFST columns.
- The stress strain model of the confined concrete has been modeled based on Sakino-Sun's Model considering the steel tube expressible as transverse reinforcement to the concrete and can be named as steel jacket.
- The stress strain relationship of the steel tube has been calculated based on the test output.

Serkan and Cengiz [2010] did a comparative study between the behavior of concrete filled steel tube columns with plain concrete and CFST columns with steel fiber reinforced concrete, as denoted in **Fig. (2.25)**.

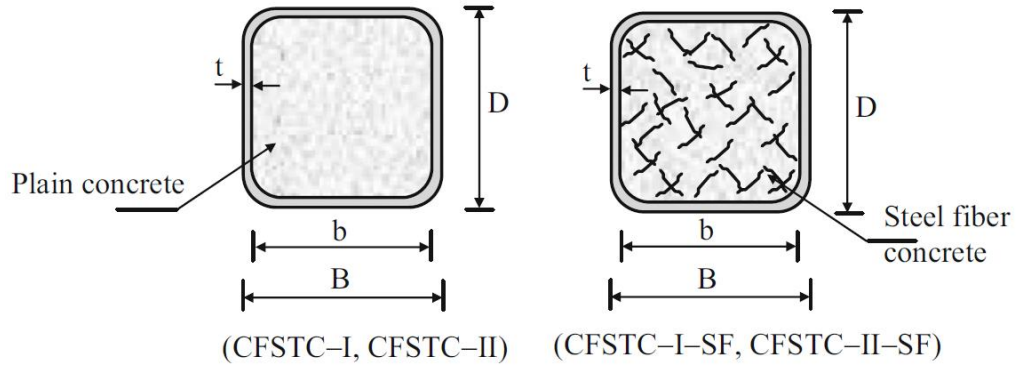


Fig. 2.25 Cross Sectional Details of CFST Column Specimens with Plain Concrete and Steel Fiber, Serkan Tokgoz & Cengiz Dunder [2010]

The experimental testing has been conducted using various parameters such as cross sections, slenderness, concrete strength and load eccentricity. They have tested 6 CFST column executed by plain and steel fiber reinforced concrete. The standard CFST column adopted for the experimental testing setup is described in **Fig. (2.26)**. The load, lateral deformation, and axial strain have been measured using appropriate measurement tools distributed among the column specimens as shown in **Fig. (2.26)**.

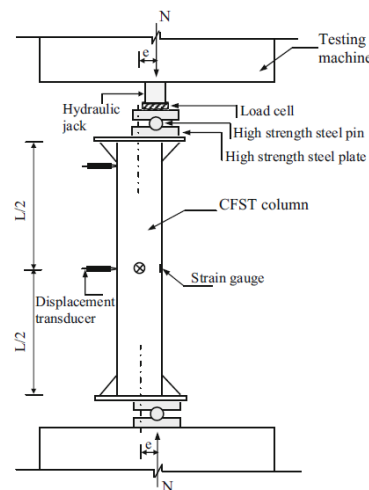


Fig. 2. The typical test setup for CFST column specimens.

Fig. 2.26 CFST Test Setup, Tokgoz & Cengiz Dunder [2010]

They have formulated the strain and deflection considering the plane of the cross section stay plain. The strain at any point (x_i, y_i) can be calculated using the following formula and inline with Fig. (2.27).

$$\epsilon_i = \epsilon_u [(y_i/c) + (x_i/a) - 1.0] \quad \text{Eq. (2.111)}$$

Where:

- a Horizontal distance between the origin of (x-y) axis system and neutral axis
- c Vertical distance between the origin of (x-y) axis system and neutral axis
- ϵ_u maximum compressive fiber strain of the section

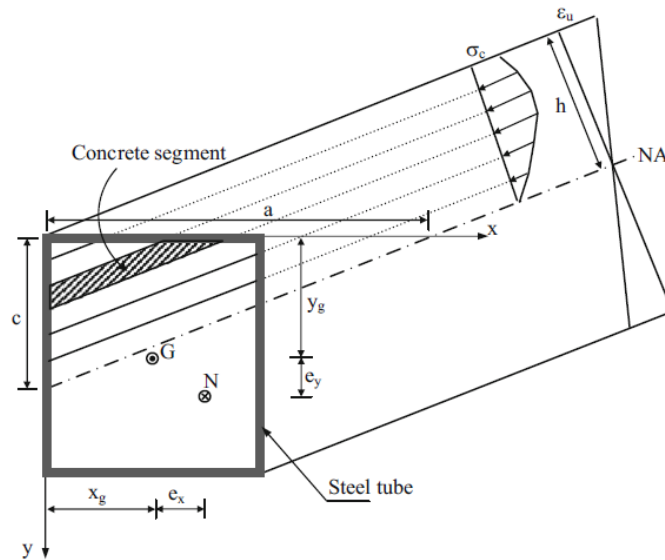


Fig. 2.27 CFST Column Cross Section and Stress Distribution, Tokgoz & Cengiz Dundar [2010]

The curvature (ψ) is calculated using the strain distribution as follow:

$$\psi = \epsilon_u / h \quad \text{Eq. (2.112)}$$

Where:

- h the distance from the maximum compressive fiber to the neutral axis.

The curvature at mid height of the CFST column can be determines using the linear strain distribution with the following equations;

$$\psi_x = \epsilon_t / c \quad \text{Eq. (2.113)}$$

$$\psi_y = \epsilon_t / a \quad \text{Eq. (2.114)}$$

Where:

- ϵ_t the strain at the most heavily stressed point

The deflection at the mid height of the column can be calculated from the following formulas inline with **Fig. (2.28)**.

$$\delta_x = \psi_x L_{ef}^2 / \pi^2 \quad \text{Eq. (2.115)}$$

$$\delta_y = \psi_y L_{ef}^2 / \pi^2 \quad \text{Eq. (2.116)}$$

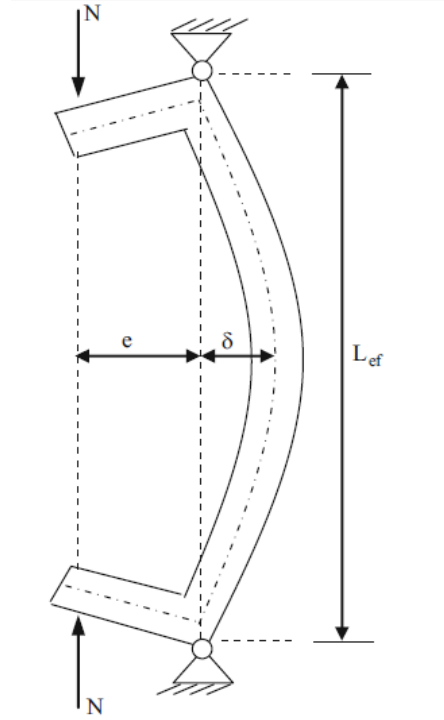
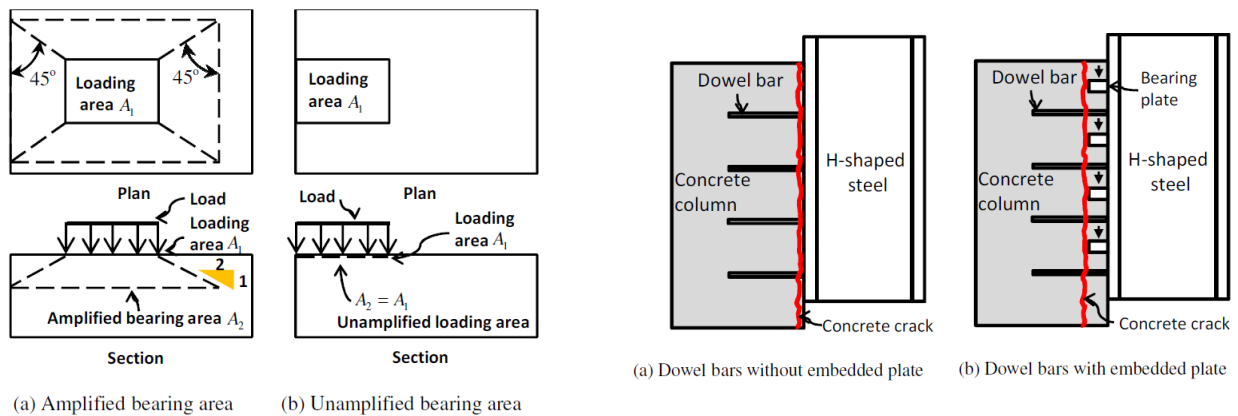


Fig. 2.28 Typical Deformation Geometry of CFST Column, Tokgoz & Cengiz Dundar [2010]

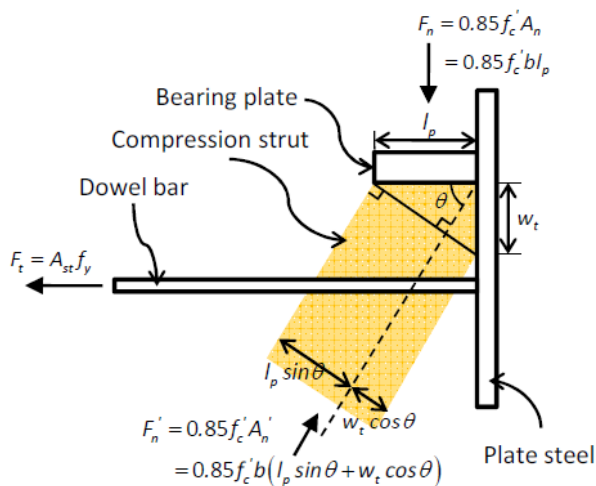
The output of the experimental work demonstrated that the concrete strength, CFST cross section, slenderness and load eccentricity have a major impact on the nominal strength capacity of the CFST columns. The introduction of steel fiber reinforcement concrete in the CFST column is improving the ductility and deformation behavior of the CFST but it does not have remarkable influence on the nominal strength capacity. The anticipated results based on the theoretical analysis was very close from the test results in terms ultimate strength and load-deflection curve.

Jang & Hyeon [2012] studied the shear connections and load transfer between steel members and concrete mega columns applied in one the tall buildings in Seoul. The research was focusing on the use of shear studs or dowel rebar and its strength effect by introducing embedment bearing plates. They have conducted experimental testing using Push-Out Test and analyze the experimental results in comparison with the theoretical findings derived from the concrete bearing, shear friction, stud strength, and strut-and-tie model.

Four failure mechanisms have been investigated, concrete bearing failure, shear friction over the vertical cracks, stud mechanism in the absence of bearing plates, and strut-and-tie mechanism. **Fig. (2.29)** depicted those four mechanism failures.



Concrete Bearing



Strut-and-tie Mechanism

Fig. 2.29 Four Failure Mechanism, Jang-Woon Beak and Hyeon-Jong Hwang [2012]

The bearing strength can be determined from the following equations as per ACI 318-11;

For Amplified Bearing Area; $P_n = 0.85 A_1 f'_c (\sqrt{A_2/A_1}) \leq 1.70 A_1 f'_c$ Eq. (2.117)

For Unamplified Bearing Area; $P_n = 0.85 A_1 f'_c$ Eq. (2.118)

The shear friction strength can be calculated from the following equations as per ACI 318-11;

For Dowel Rebar without Embedded Plate; $P_n = A_{vf} f_y \mu$ and $\mu=0.70$ Eq. (2.119)

For Dowel Rebar with Embedded Plate; $P_n = A_{vf} f_y \mu$ and $\mu=1.40$ Eq. (2.120)

Where:

A_{vf} Area of the dowel rebars (mm^2)

f_y Yield strength of the dowel rebars (MPa)

μ Coefficient of friction

The shear strength of the stud provided without embedment bearing plates can be calculated as follow;

$$P_n = 0.5 A_{sc} \sqrt{f'_c} E_c \leq A_{sc} f_u \quad \text{Eq. (2.121)}$$

Where:

A_{sc} Area of the stud (mm^2)

f_u Ultimate shear strength of the stud (MPa)

The strut-and-tie model can be adopted to calculate the strength of the connection as follow:

$$P_n = A_{st} f_y \tan \Theta = 2 A_{st} f_y < 0.85 f'_c A_1 \quad \text{Eq. (2.122)}$$

Where the angle of inclined strut was determined from the experimental test result.

The conclusion of the research can be outlined as follow:

- The behavior of shear connectors is the same for both types of shear connectors, studs or deformed rebar dowel.
- The traditional stud strength anticipated the nominal strength.
- Introducing bearing plates between dowel rebar or shear stud is leading to a remarkable increase the maximum transferred loads and the initial stiffness. Furthermore, the residual strength subsequent the nominal strength in the tested column with bearing plates has been increased twice compared to the other column tested without bearing plates. The residual strength was calculated using strut-and-tie model.
- There is no relation between the amount of steel reinforcement in the columns and the performance of the shear connectors.

- The increase in the embedment length is leading to augmentation in the design strength and residual strength.
- There are no cracks or quash damage noticed for the column samples with studs or dowels rebar without bearing plates, while the column samples with bearing plates immaterial cracks have been observed without quash damage. This behavior illustrates that local concrete quash occurred beneath the bearing plates.

Liang et. al. [2014] studied the preload influence on the behavior of biaxially loaded rectangular concrete filled steel tubular slender columns. A nonlinear analysis has been conducted using Fiber Element Model in order to represent the load-deflection curves and the capacity of thin-walled CFST column taking into consideration the preload effect on the steel tubes and its local buckling.

They did a comparison between finite element models and testing results. The cross sectional of the CFST column has been divided into small fiber elements as indicated in **Fig. (2.30)**. Each small fiber element can be defined as steel or concrete. It is presumed that the plane section stay plane after deformation. Stresses in the fiber elements can be determined using the fiber strains extracted from axial stress-strain curves. Uni-axial compression forces and flexure bending moments loaded by the CFST cross section are identified as stress resultants in the CFST cross section.

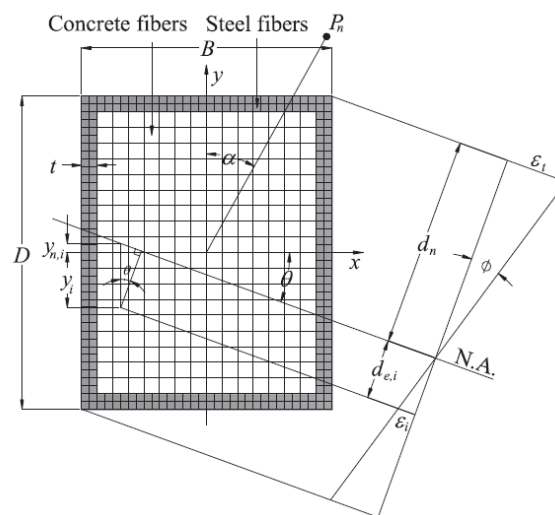


Fig. 2.30 Fiber Strain Distribution in CFST Column subject to Uniaxial and Biaxial Loading, Liang, et. al. [2014]

The conclusion of this research illustrated that the increase in the preloads has a remarkable effect on the strength and stiffness of a slender CFST columns. The research demonstrated that the preload effect on the short CFST column can be negligible in the design. The preload with significant effect was noticed for the CFST slender column of e/D ratio of 0.40.

The parametric studies illustrate that the fiber element model provide a good anticipation to the preload effect on the behavior of slender CFST column compared with the experimental test results.

Jin Won Kim et. al. [2014] studied the shear-head reinforcement for concrete slab to concrete filled steel tube column connections. They have conducted full-scale testing on ten CFST columns connected to RC flat plate with shear-heads and under axial gravity loads. The purpose of this research is to examine the punching shear at the interface between CFST column and connected RC slab. The experimental testing was conducted based on different parameters including columns cross section, shear-head length, and the sizing of the CFST column. The slab thickness was 200mm for all specimens except two specimens provided with 300mm and without shear-head. The cylinder concrete strength was 22.80MPa. the yield strength of the rebar was 400MPa and it was 235MPa for the steel sections. **Table [2.12]** summarizes the variable parameters utilized in the experimental work. **Fig. (2.31)** denotes the geometry of each tested column with its connection details.

	Slab thickness, mm	Shearhead arm length, mm (x slab thickness)	Shearhead dimension, mm	Column type and thickness, mm	Column size, mm
NSH-S200	200	No shearhead used	—	Built-up (40)	400 x 400
SH320-PR	200	320 (1.6h)	H-100 x 100 x 6 x 8 (Type S)	Built-up (40)	400 x 400
SH-AR1.5	200	290 (short face) x 370 (long face) (1.45h x 1.85h)	H-100 x 100 x 6 x 8 (Type S)	Built-up (40)	320 x 480
SH-AR2.0	200	230 (short face) x 340 (long face) (1.15h x 1.7h)	H-100 x 100 x 6 x 8 (Type S)	Built-up (40)	270 x 540
SH490-S200	200	490 (2.45h)	H-100 x 100 x 6 x 8 (Type S)	Built-up (40)	400 x 400
SH770-C500	200	770 (3.5h)	2H-100 x 100 x 6 x 8 (Type S)	Built-up (40)	500 x 500
SH320-WT19	200	320 (1.6h)	H-100 x 100 x 6 x 8 (Type S)	Rolled (19)	400 x 400
SH670-WT19	200	670 (3.35h)	2H-100 x 100 x 6 x 8 (Type S)	Rolled (19)	400 x 400
RC-S300	300	No shearhead used	—	Monolithic RC column	400 x 400
SH620-S300	300	620 (2.1h)	H-150 x 150 x 7 x 10 (Type L)	Built-up (40)	400 x 400

Table [2.12] Summary of Design Parameters for test specimens extracted from Jin-Won Kim et. al. [2014]

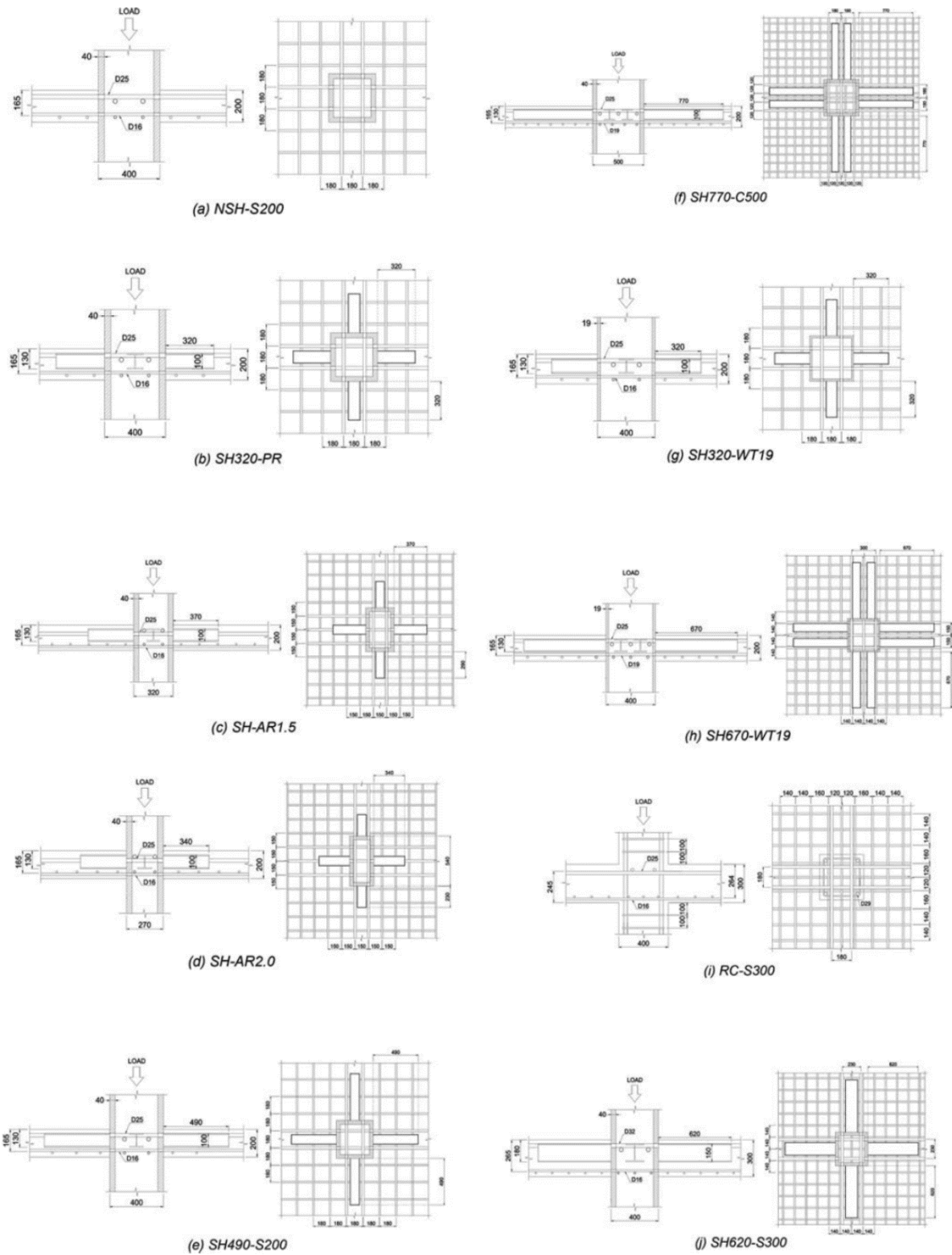


Fig. 2.31 Section Geometry and its Connection Details, Jin-Won Kim et. al. [2014]

The conclusion of this research illustrated that shear-head rebar increase the punching shear strength compare to the RC flat slab. Furthermore; it demonstrates the punching shear strength increases with the increase of the arm length of the shear-head. The minimum length of the shear-head shall be four times the slab thickness connected to the CFST column, and shall provide a maximum shear strength of $0.58 \sqrt{f'_c} b_o d$ at the upper cap. They have suggested the following formulas to define the punching shear strength;

$$V_n = \psi V_c + V_s = \psi \left[\frac{1}{6} \lambda \sqrt{f'_c \text{ (MPa)}} b_o d \right] + \frac{n M_p}{\left(l_v - \frac{c_1}{2} + h_v \right)}$$

Eq. (2.123)

$$\text{or } V_n = \psi V_c + V_s = \psi \left[2 \lambda \sqrt{f'_c \text{ (psi)}} b_o d \right] + \frac{n M_p}{\left(l_v - \frac{c_1}{2} + h_v \right)}$$

$$\psi = 0.7 \left[\frac{(l_v - c_1 - 320) \text{ mm}}{480 \text{ mm}} \right] + 0.5 \quad \text{or}$$

$$\psi = 0.7 \left[\frac{(l_v - c_1 - 12.6) \text{ in.}}{18.9 \text{ in.}} \right] + 0.5$$

Eq. (2.124)

$$M_p = \left(\frac{V_u}{n} - \frac{V_c}{n} \right) h_v + V_w \left(l_v - \frac{c_1}{2} \right)$$

Eq. (2.125)

Where:

V_n Nominal Shear Strength

ψ Factor related to the arm length of the shear-head

V_c Concrete resistance in shear

V_s punching shear resistance provided by shear reinforcement

λ Factor equal to 1.0 for normal concrete and equal to 0.75 for light weight concrete

f'_c Cylinder Concrete Strength at 28 days age.

b_o	The perimeter of the critical shear section at $d/2$ from the column edge
d	Effective depth of the RC slab
n	Number of shear-head
M_p	Plastic moment at the face of the column
L_v	The distance from the center of the CFST column to the end of the shear-head
C_1	Width of the CFST column
h_v	Height of Shear-head section
V_w	$\alpha_v V_c/n$
α_v	The ratio between stiffness of shear-head (EI) and stiffness of the surrounding composite slab.

Jing-ming Cai et. al. [2016] have evaluated the performance of Steel-Reinforced Square Concrete-Filled Steel Hollow Section (SRSCFSHS) columns subject to uniaxial compression load. The study was conducted using a nonlinear finite element analysis for twenty-six SRSCFSHS columns with variable parameters. The SRSCFSHS column comprises encased composite section confined with steel tube as denotes in **Fig. (2.32)**, so it is considered as integration of CFST and SRC.

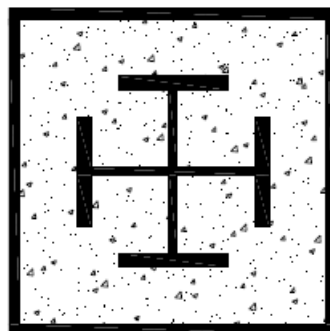


Fig. 2.32 Cross Section of SRSCFSHS Column, Jing-ming Cai et. al. [2016]

The finite element models were verified in comparison to the previous experimental testing performed by Zhu et. al. [2010]. They have chosen 4 SRSCFSHS columns tested with dimensions and properties indicated in Table [2.13].

Table 1. Dimensions and Material Properties of the SRSCFSHS Columns

Specimens	B×t×Le(mm)	L/B	f_c (MPa)	A_c (mm ²)	f_y (MPa)	f_u (MPa)	A_s (mm ²)	A_g (mm ²)	N_{u}^{ex}/N_{u}^{lim}
S5L10	195×5.5×600	3	48.4	30990	288	338	4169	2866	1.08
S5H10	195×5.5×600	3	70.8	30990	288	338	4169	2866	1.06
S4L10	195×4.5×600	3	48.4	31730	289	338	3429	2866	1.04
S4H14	195×4.5×600	3	70.8	30726	289	327	3429	4300	1.05

Table [2.13] Properties and Sizing of SRSCFSHS Column Jing-ming Cai et. al. [2016]

The axial load -strain curves of the SRSCFSHS columns from the test and theoretical results is shown in Fig. (2.33). The results of the finite element models were very close the experimental test results.

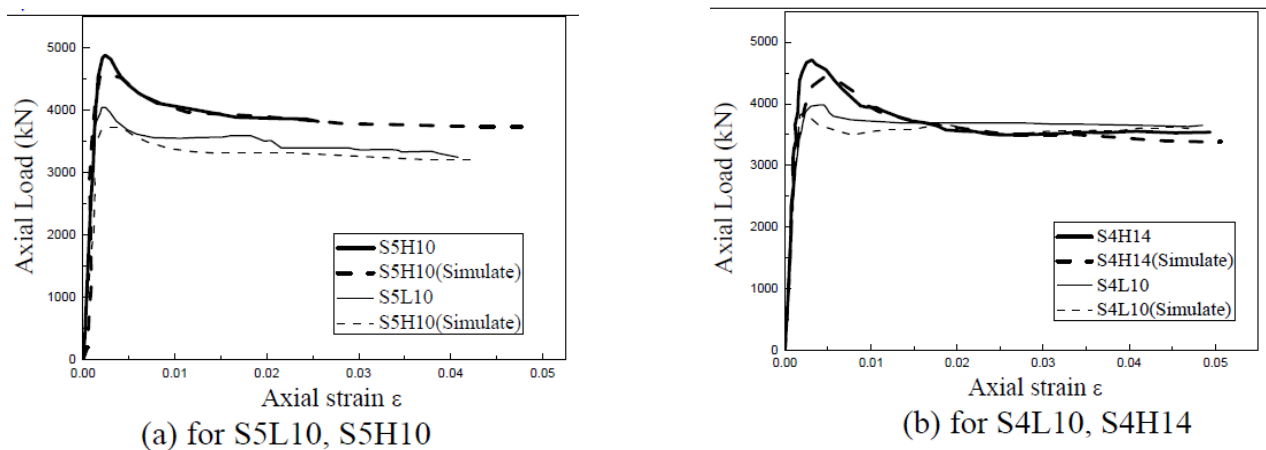


Fig. 2.33 Axial Load Strain Curve for Theoretical and Experimental, Jing-ming Cai et. al. [2016]

The research Highlighted that the Eurocode 4 underestimates the nominal load of the SRSCFSHS columns as a result of ignoring the confinement influence of the steel tube on the section design strength.

The conclusion of this research denotes that the SRSCFSHS columns are more ductile and robust than CFST column with similar cross section because of the presence of internal steel section.

Jiang Zhu et. al. [2017] illustrated a comparative research of circular CFST columns provided with three different geometry of stirrups; perpendicular stirrups, bi-directional stirrups, and circular stirrups as per Fig. (2.34).

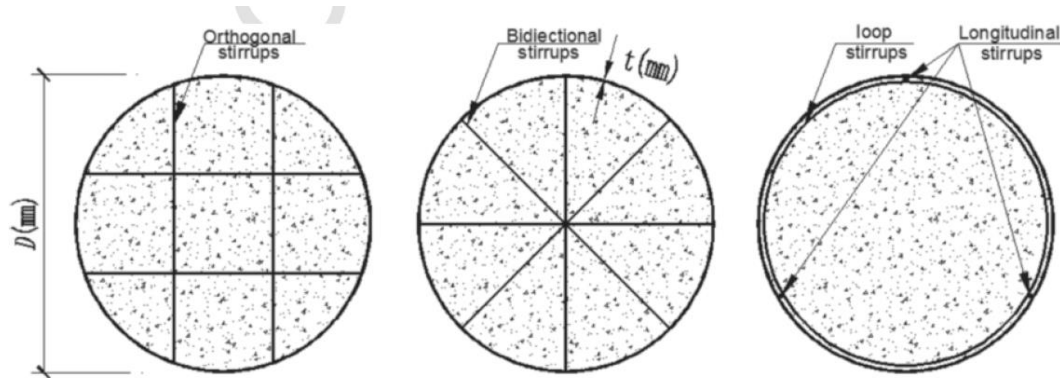


Fig. 2.34 Cross Sections of Tested Columns, Ziang Zhu et. al. [2017]

There were 10 specimens tested with different types of stirrups. The circular steel tube section was (500mm diameter x 4mm thickness x 1.20m height). The diameter of stirrups was ranging from 4mm to 8mm and the spacing between stirrups was 50-60mm. The columns were demonstrating an elastic behavior at loading test lower than 70% of the nominal load. Once the test load was about 70% of the nominal load, the column specimens behaved were behaving as elastic-plastic elements by introducing local buckling close to the two ends of the CFST circular column as a result of the end influence. As soon as the axial compression load attained the nominal loads, further local buckling has been observed in the middle height of the steel tube, despite of the increment in the buckling deformation of the perpendicular stirrups and bi-directional stirrups at the failure step was not as considerable as that of CFST columns with loop stirrups.

The CFST compression capacity steadily decreased after attained the ultimate load, whilst the axial strain was incessantly increased.

The ductility of the CFST column has been calculated based on L.H.Han et. al. [2005] which can be formulated as follow;

$$DI = \epsilon_{0.85} / \epsilon_b \quad \text{Eq. (2.126)}$$

Where:

$\epsilon_{0.85}$ The axial strain when the load descends to 85% of the nominal load after the peak load

$\epsilon_b = \epsilon_{0.75} / 0.75$, and $\epsilon_{0.75}$ is the axial strain at 75% of the nominal load prior to reaching the peak load

The CFST column with high value of Ductility Index (DI) represent less reduction in the axial load after the peak load stage, consequently it denotes to more ductile performance.

As a result of the theoretical and experimental testing the following was concluded from this research;

- The failure manner of the circular CFST column has not been influenced by the provided types of stirrups.
- The perpendicular stirrups provide large enhancement to the axial load capacity and ductility of the circular CFST columns compare to the other two types of stirrups, bi-directional and circular.
- The increase in the volumetric ratio of the stirrups is leading to increase the axial local capacity of the circular CFST columns.
- The composite action is highly increased as a result of increasing the volumetric ratio of the perpendicular stirrups in comparison with the other stirrup types.
- Radial stresses of the core concrete developed from the stirrups was higher than the steel tube.

T. Kibryia [2017] studied the performance of the circular and square concrete filled steel tubular columns. The experimental testing has been done for 36 specimens divided into 4 groups consisting of 2 groups for circular CFST columns and 2 groups for square CFST columns. Each group has 9 CFST column categorized into 3 CFST with hollow tube, 3 CFST unbraced tube filled with concrete, and 3 CFST braced tube and filled with concrete. the overall height of the tested column was 750mm. The hollow steel tube was braced by providing deformed rebar of 10mm diameter welded in the transverse direction. All specimens have been tested under uni-axial loads. [Table \[2.14\]](#) represents the geometry of the steel tubes used in the experimental work.

1. Geometric properties of steel tubes used

Ser #	Group	Column Type	Outer Dia mm	Inner Dia mm	Thickness mm	D/t or b/t	L/D or L/b	λ
1	A	Circular	160	155	2.5	64	4.69	19
2	B	Circular	111.25	106.25	2.5	44.5	6.74	27
3	C	Square	125.66	120.66	2.5	50.26	5.97	21
4	D	Square	87.38	82.38	2.5	34.95	8.58	30

2. Properties of concrete used

Specimen	Compressive strength f_c' (MPa)	Average f_c' (MPa)
1	32.61	31.82
2	29.74	
3	33.42	

3. Limiting values of b/t

Type	LRFD	Eurocode	ACI code
Square	40	50.6	49.16
Circular	40	85	80

4. Minimum steel check

Ser	Column type	Outer Dia mm	Inner Dia mm	Thickness mm	As sq mm	Ac sq mm	As %
1	A Circular	160	155	2.5	1237	18869	6.15
2	B Circular	111.25	106.25	2.5	854	8866	8.80
3	C Square	125.66	120.66	2.5	1231	14559	7.80
4	D Square	87.38	82.38	2.5	848	6786	11.11

Steel $f_y = 250$ Mpa
Concrete $f_c = 30$ Mpa.

Table [2.14] Geometry of the Steel Tubes used in the Experimental Work, T. Kibryia [2017]

The stress strain curves of the tested columns are described in **Fig. (2.35)** for hollow steel tube columns, **Fig. (2.36)** for filled columns and **Fig. (2.37)** for braced columns.

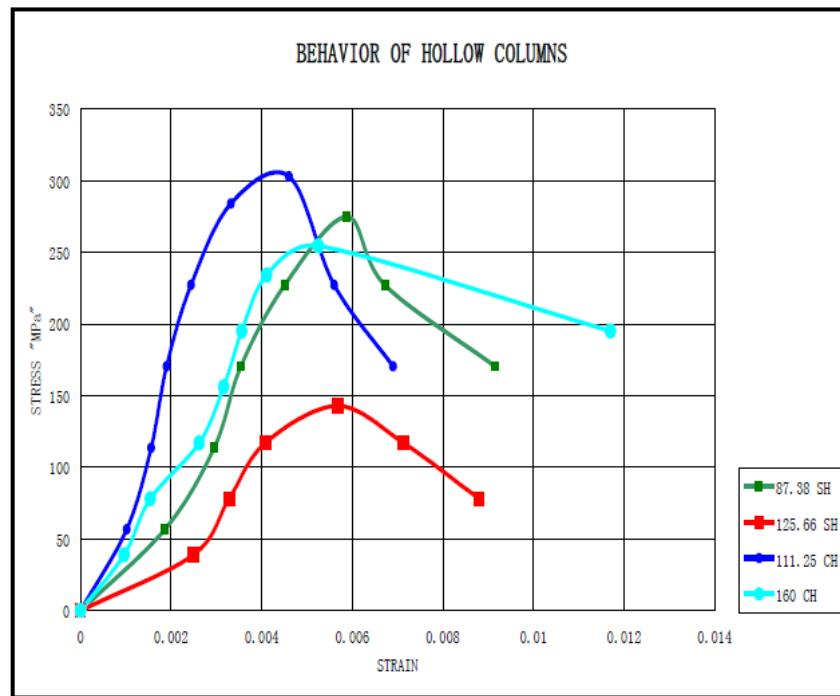


Fig. 2.35 Stress Strain Curve of Hollow Steel Columns, T. Kibryia [2017]

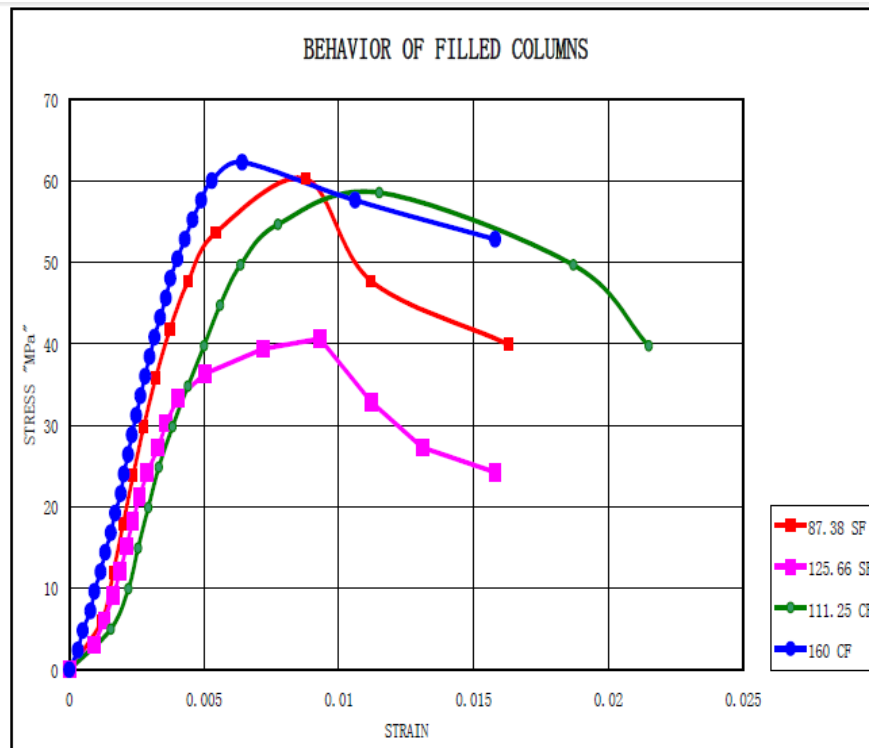


Fig. 2.36 Stress Strain Curve of Filled Columns, T. Kibryia [2017]

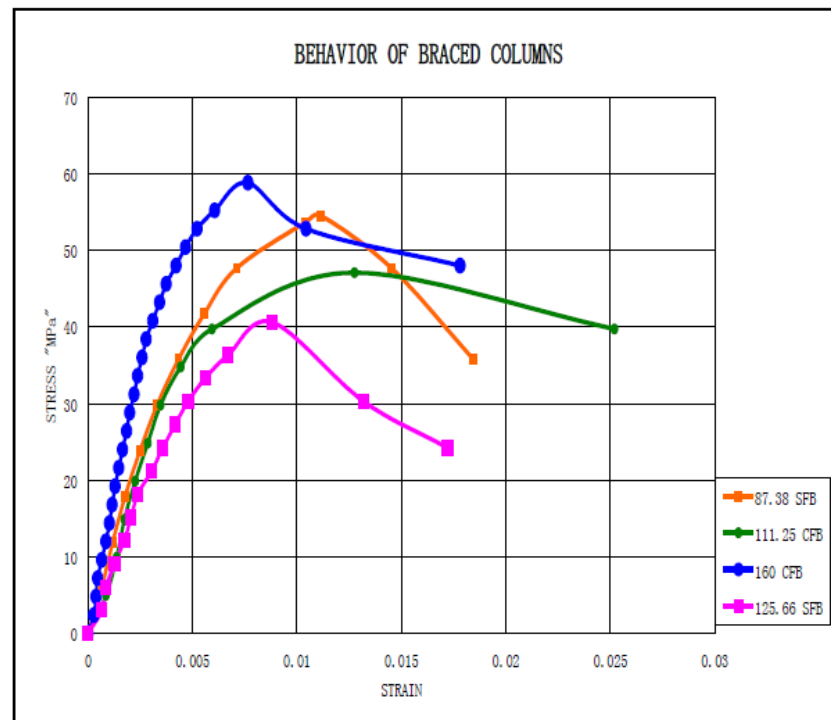


Fig. 2.37 Stress Strain Curve of Braced Columns, T. Kibryia [2017]

The outcome of the test results illustrated a failure because of local buckling and concrete crushing. It was noticed that the failure was identical for all columns at the bottom and top of the member, where the concrete core pushed out the steel tubes. In addition; the concrete core deformed inline with the steel tube deformation which is proofing the composite action between steel and concrete.

The research concluded also that the increase in the axial compressive strength of the circular concrete filled steel tube columns is higher than that of square concrete filled steel tube columns. The circular CFST columns is showing 400% higher capacity in comparison to 300% in the square CFST columns.

Jizhong Wang et. al. [2018] studied the behavior of the CFRP-steel composite tube steel reinforced columns with high strength concrete. the research was focusing on the experimental testing for circular and square CFRP-steel confined concrete-encased steel column under axial compression loads. The experimental work has been conducted taking into consideration various factors on the behavior of the FRP-steel composite tubed steel-reinforced columns (FSCSCs), including the cross-sectional geometry, the force-giving methods of wrapping tube, and the number of CFRP sheet layers. There were 14 number of columns confined by CFRP and steel tube have been tested, 6 square tubes and 8 circular tubes with 3mm thickness and 540mm length as denoted in **Fig. (2.38)**.

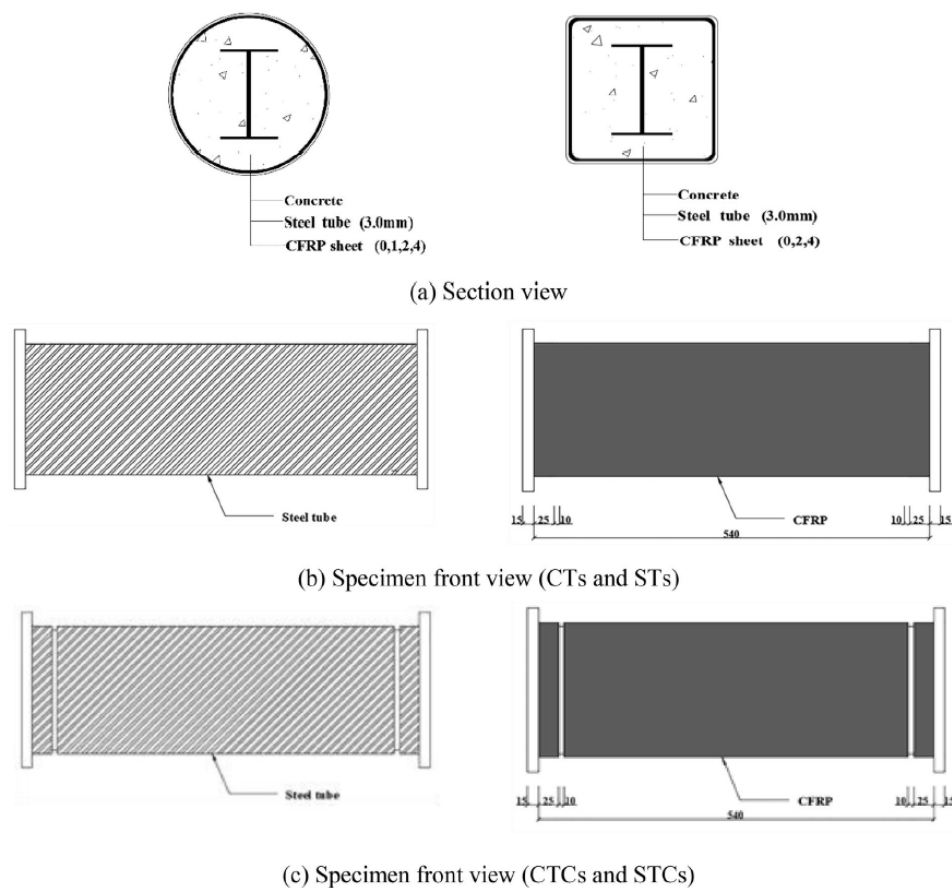


Fig. 2.38 Tested Column Arrangements, T. Kibryia [2017]

The diameter of the circular tube was 180mm and the width if the square tube was 160mm. the yield strength of the steel structure element was 280MPa. The carbon fiber sheets have a hoop tension strength (f_{frp}) of 4.216GPa, Elasticity modulus (E_f) of 252GPa, 1.76% Elongation percent, 0.167mm each layer thickness, and jacket density of 300g/m². The test load utilized with load control attained at 80% of the predicted axial load capacity,

then the test load has been controlled by average deformation loading of 0.3mm/min till the test is completed. They have installed two linear variable displacement transducer (LVDTs) to measure the axial displacement of the column specimens. Jizhong Wang et. al. installed with glue 16 strain gauges to each column specimen, 12 strain gauge in the hoop direction arranged equally at the top, mid height and bottom along each side of the column as per **Fig. (2.39)**, and 4 strain gauges in the mid height of the column in the axial direction. Two grooves of 10mm have been created close the top and bottom end of the column to ensure no axial forces transferred direct to the tube.

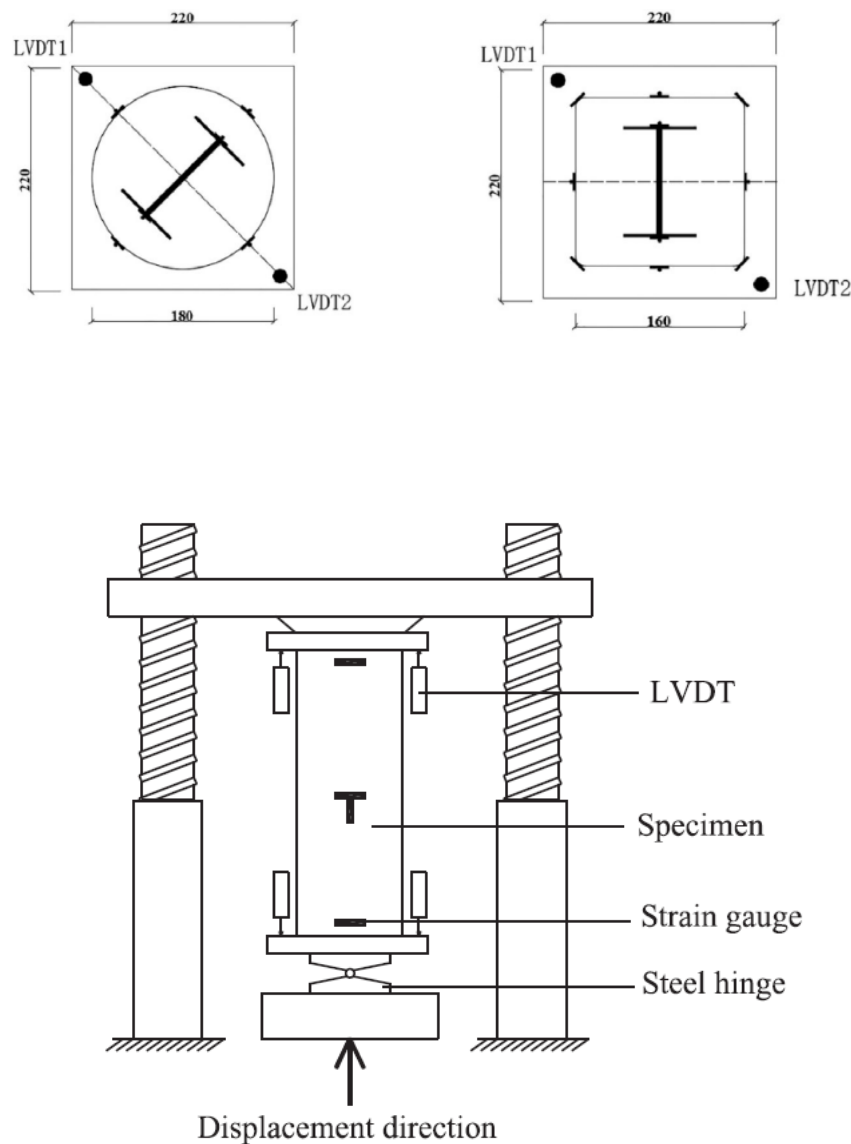


Fig. 2.39 Strain Gauge Arrangements, T. Kibryia [2017]

The test results illustrate the cross-sectional capacity under axial compression load, the load deformation curve, failure mode, and sectional ductility. Based on parametric analysis conducted for 54 different case for FSCSCs with high strength concrete, various steel tube ratio, various yield strength of the steel tube, various concrete strength, and various number of FRP layers, the following was summarized from this research:

- The uniaxial compression capacity of the circular tube and its deformation capacity increases as the number of CFRP layers increases, while the square tube has not the same performance.
- The confinement achieved by the CFRP and steel tube is more functional if the compression load is not transferred directly to the external steel tube, because it delays the local buckling of the steel tube.
- The results of the finite element models were inline with the experimental test results.
- The influence of the confinement on the FRP-steel composite tube has been highly observed with a thinner steel tube, and it has been significantly reduced with ultra-high strength concrete.
- The research results are appropriate for short circular FSCSCs subject to axial compression load.
- Extensive researches and detailed investigations are required for the stress-strain model of the FSCSCs and Square FSCSCs.

2.12 PRECEDING AND CURRENT RESEARCHES ON ENCASED COMPOSITE COLUMNS

There are many researches and studies performed in order to evaluate the behavior of the encased composite columns. Some of those studies have been highlighted in this research as follow:

Morino, et. al. [1984] studied the behavior of the encased composite columns (SRC) subject to biaxially compression loads. The tested column has square geometry of (160x160) mm consist of hot rolled I steel section of (100x100x6x8). There were three different factors controlling the experiential test, columns slenderness ($\lambda=20, 50, 75$, and 100), load eccentricity ($e=40$, and 75mm), and angle determined from the main axis of the column cross section ($\theta=0^\circ, 30^\circ, 45^\circ, 60^\circ$, and 90°).

The test load was conducted using 300-ton hydraulic spherical supports. The tested columns were verified by controlling lateral deformation at the mid height to lower than $h/1000$ in the two directions under one-third of the ultimate compression load. after that the specified eccentricities applied to each sample, and the lateral deformation were measured using displacement meter at $h/4$, $h/2$, and $3h/4$ from the base of the tested columns. Strain gauges have been installed to measure strain on the concrete surface and steel flanges at the same 3 points heighted for the lateral deformation. **Fig. (2.40)** depicted the column test with the applied loads.

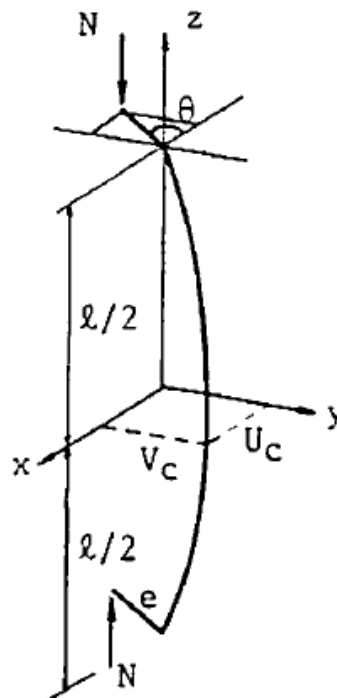


Fig. (2.40) Column Test Setup, Morino, et. al. [1984]

The following was concluded from this research:

- The ultimate capacity of the short encased composite column is inline with concrete quash.

- The encased composite columns under biaxially compression load are laterally deformed in both direction due to bending effect. It was noticed that the lateral deformation in the weak stiffness direction increases with high increase in the load, while the lateral deformation in the other strong direction does not increase and might be reduced in some conditions as a result of the P delta influence. As a conclusion the encased column performed similar to the column under uniaxial flexure. However, with $\Theta \leq 60^\circ$ there is no significant benefit from considering it under uniaxial bending. **Fig. (2.41)** demonstrating the load-deflection curves with $\Theta = 60^\circ$ for all specimens.
- The ultimate capacity of a slender column under biaxially bending and compression is less than that of the short column due to the influence of P-delta bending and gradual transfer to uniaxial flexure about the weak stiffness axis.
- The variance between experimental test results and theoretical analysis is lower than 10% for most cases.

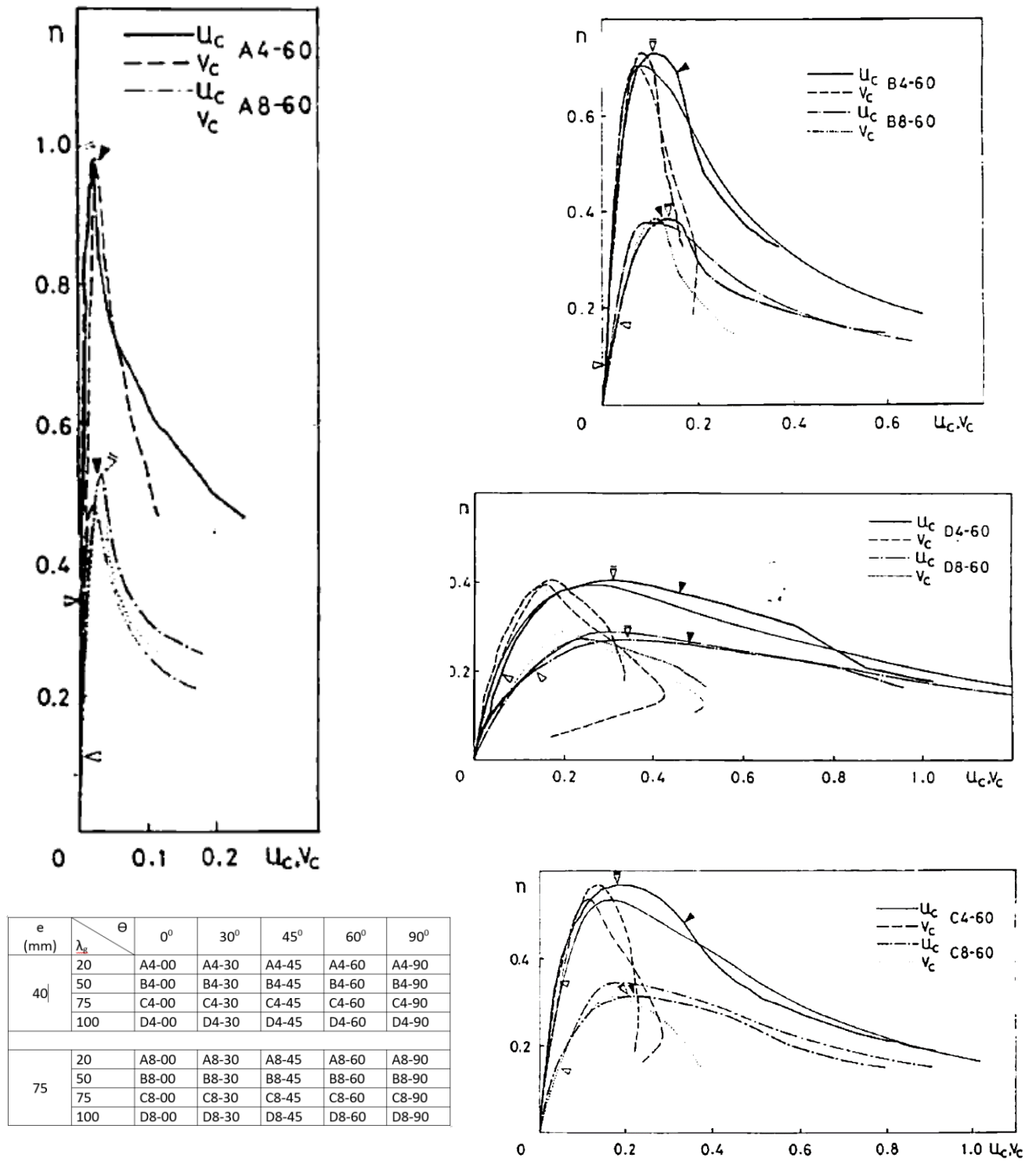


Fig. (2.41) Load -Deflection Curve, Morino, et. al. [1984]

El-Tawil, et. al. [1999] studied the ductility and strength of encased composite columns by utilizing a Non-Linear Fiber Element Model for normal strength and high strength concrete.

AISC-LRFD and ACI 318 include specific details for the encased composite columns located in low seismic region. Further detailing requirements have been introduced for medium and high seismic regions, specifically for the vertical and horizontal reinforcement for the concrete section as per ACI 318 Chapter 21 in order to improve the ductility of the column sections under high seismic effect.

The minimum tie horizontal reinforcement (A_{sh}) for high seismic zone can be determined from the following formula inline with AISC-LRFD.

$$A_{sh} = 0.09h_c S [1 - (F_{ys}A_s/P_n)] [f'_c/F_{yh}] \quad \text{Eq. (2.127)}$$

Where:

h_c Dimension of the confined core taken from center to center of the tie reinforcement

S Vertical spacing between tie reinforcement

F_{ys} Yield strength of the steel section

A_s Area of steel section

P_n Ultimate compressive strength of the composite column

f'_c Cylinder concrete compressive strength

F_{yh} Yield strength of the horizontal tie reinforcement

A fiber model analysis has been adopted in this research to address the strength and stiffness of the encased composite columns by generating numerous small areas to evaluate the behavior of each small area based on its own axial compression stress strain model. Each small area can be defined as steel, reinforcing steel, or concrete with different level of confinement. **Fig. (2.42)** described the fiber section model utilized in this research.

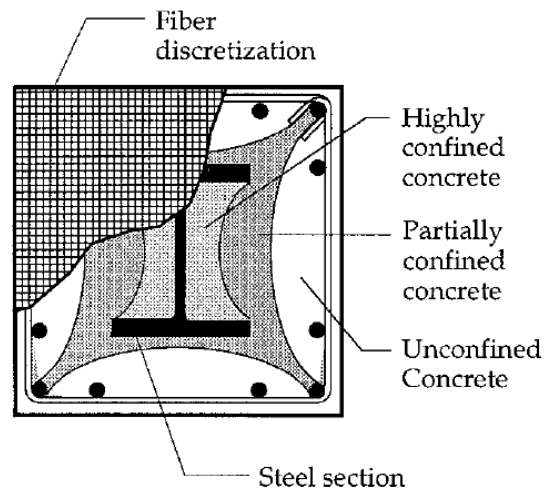


Fig. (2.42) Fiber Model of Encase Composite Column

They have first analyzed three variable encased composite sections as shown in **Fig. (2.43)**. the sizing of the encased composite section was (700 x 700) mm with a vertical reinforcement of 12T25 and non-seismic horizontal tie of T16-320mm with yield strength of 414MPa. each column has different steel section with yield strength of 345MPa as shown in **Fig. (2.43)**, which represent 4%, 8%, and 16% of the gross section of the encased composite column. The concrete strength specified for the three columns was 28, 69, and 110MPa in order evaluate the influence of different concrete strength on the behavior of the composite columns.

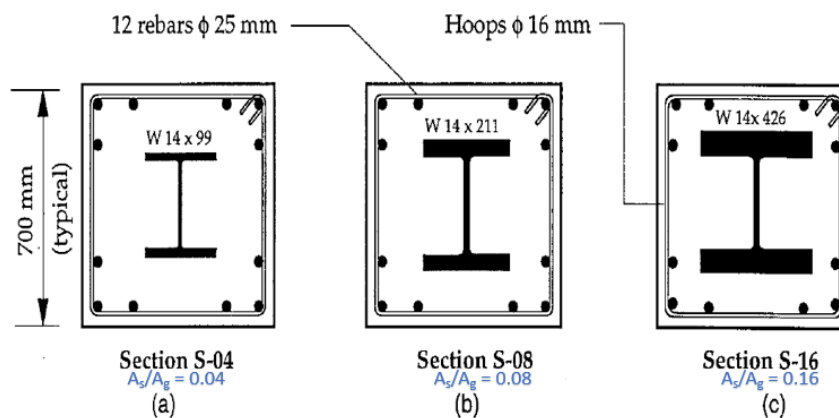
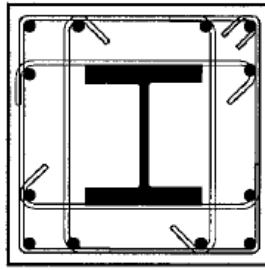


Fig. (2.43) Encased Composite Column Section utilized in the study by El-Tawil, et. al. [1999]

The next approach is to analyze the seismic horizontal tie requirements in order to examine the confinement influence on the ultimate strength and ductility of the encased composite column by providing T16-100 tie for $f'_c=28$, and 69MPa, and to provide T16-75mm for $f'_c=110$ MPa as shown in **Fig. (2.44)**.



4-Legged Hoops
 ϕ 16 mm @ 100 mm

Fig. (2.44) Encased Composite Column with Seismic Tie Requirements (S-08)

The following points have been concluded from this research:

- It was noticed a considerable variance between ACI 318-95 and AISC-93 related to the ultimate strength of the encased columns subject to biaxially loading, and the variance will continue increase with the increase in the concrete strength.
- The comparison between both codes and fiber element model was illustrating that the provision of ACI 318 is about 10% unconservative for encased composite column with concrete cylinder strength of 110MPa, while the AISC provision was demonstrating more than 63% conservative for the same column with a steel section area of 4% of the gross sectional area as summarized in [Table \[2.15\]](#)
- The outcome of the analysis asserted the necessity to review the big variance between ACI 318 and AISC-LRFD for the ultimate strength if the encased composite columns.
- The AISC-LRFD provision turns into more precise when the concrete participation reduced by increase steel sections, reduce concrete strength, and flexure bending behavior governs.
- The provision of ACI 318 and AISC-LRFD for the composite columns can be applied when the provided steel sectional area is 4% of the total gross area of the column. By applying this ratio, the crush load of the steel section is equal to (12-32) % of the crush load of the entire composite section. The increase in strength of the steel section (P_{ys}/P_0) to 50% of the entire composite section provide more accurate results with the provision of ACI 318 and AISC-LRFD.
- Ductility of the encased composite column can be enhanced by implementing transvers reinforcement (stirrups), however the use of high strength concrete of 110MPa Cylinder Strength provide remarkable reduction in the ductility.
- The use of a big steel section enhances ductility and residual strength after concrete quashing. [Table \[2.16\]](#) summarized the curvature ductilities for all different specimens.

Section (1)	P_{ys}/P_0 (2)	$e/h = 1$		$e/h = 1/5$	
		M_{ACI}/M_f (3)	M_{AISC}/M_f (4)	M_{ACI}/M_f (5)	M_{AISC}/M_f (6)
S-04-L	0.32	0.98	0.73	1.02	0.62
S-04-M	0.18	0.98	0.69	1.09	0.48
S-04-H	0.12	1.00	0.73	1.10	0.37
S-08-L	0.51	0.95	0.87	1.01	0.81
S-08-M	0.33	0.99	0.80	1.06	0.69
S-08-H	0.24	1.01	0.74	1.10	0.63
S-16-L	0.70	0.97	0.96	1.00	0.88
S-16-M	0.52	1.00	0.89	1.04	0.83
S-16-H	0.41	1.02	0.82	1.08	0.76

Legend	
L	Low Strength Concrete
M	Moderate Strength Concrete
H	High Strength Concrete
M_f	Moments extracted from the Fiber Model

Table [2.15] Ultimate Strength of Encased Composite Columns Specimens, El-Tawil, et. al. [1999]

Section (1)	P/P_0		
	0 (2)	0.3 (3)	0.6 (4)
S-04-M	—	2	2
S-04-H	—	2	2
S-08-L	>12	>12 (>12)	4 (>12)
S-08-M	>12	2 (11)	2 (8)
S-08-H	>12	2 (6)	<2 (5)
S-16-M	—	>12	2
S-16-H	—	2–4	<2

Note: Values in parentheses are for sections with seismic hoop reinforcements.

Table [2.16] Curvature Ductilities

Dundar, et. al. [2007] investigated the behavior of conventional reinforced concrete columns and encased composite columns under bi-direction flexure and axial compression load.

They have tested 15 reinforced concrete columns subject to flexure and axial compression load. the main purpose of this test program is to illustrate the nominal strength capacity and load deflection action for short and slender conventional reinforced concrete columns and to emulate the test results with the numerical analysis conducted based on the stress-strain relationships for the materials.

The column specimens have different varieties in terms of sizing and distribution of the vertical and horizontal reinforcement. **Fig. (2.45)** denotes the cross sectional of the conventional reinforced concrete columns utilized in the experimental program.

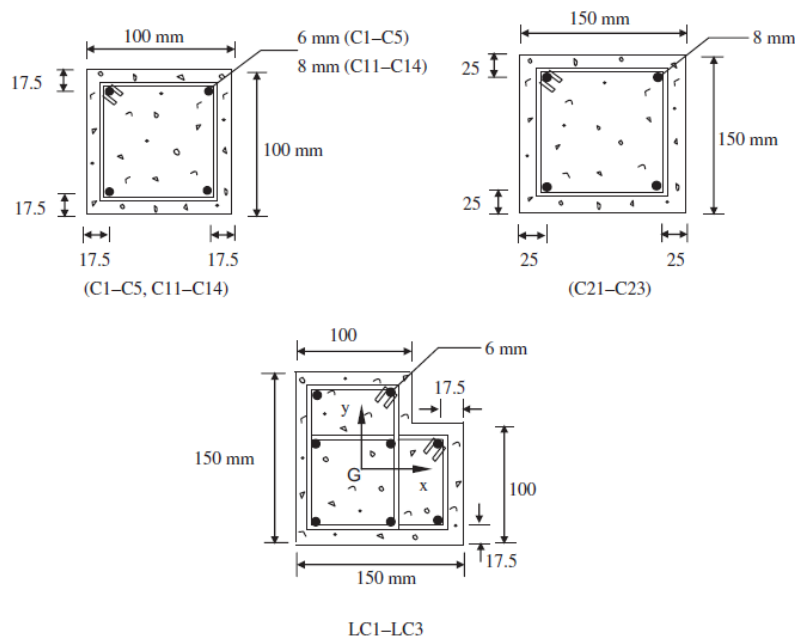


Fig. (2.45) Cross Sectional Tested by Dundar, et. al. [2007]

Table [2.17] is showing the details of the columns' specimens. All columns are built with hinged at the two ends and have been examined using H-Tech Magnus hydraulic equipment of 400kN capacity as depicted in **Fig. (2.46)**.

The concrete section capacities have been addressed using different stress-strain relationship models, Hognestad E & Hanson [1995] (HOG), Commission of the European Communities [1984] (CEC), Kent & Park for Confined Concrete [1969] (K&P^c), Kent & Park for Unconfined Concrete [1969] (K&P^u), Saatcioglu & Razvi [1992] (S&R), Whitney Stress Block [1940] (WSP), and the experimental stress-strain curve defined from the cylinder sample of the columns (EXP). The comparison between experimental works and theoretical analysis showing high level of accuracy for the behavior of the concrete columns under biaxially loaded as depicted in **Table [2.18]**.

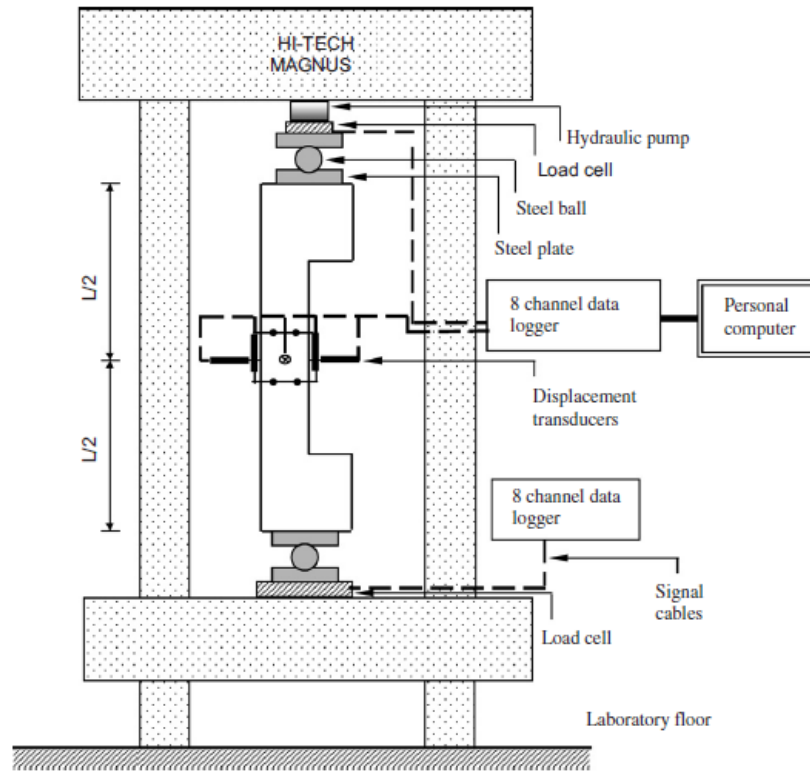


Fig. (2.46) Experimental Testing Setup, Dundar, et. al. [2007]

Specimen no.	L (mm)	f_c (MPa)	e_x (mm)	e_y (mm)	ϕ/s (mm/cm)
C1	870	19.18	25	25	6/12.5
C2	870	31.54	25	25	6/15
C3	870	28.13	25	25	6/10
C4	870	26.92	30	30	6/8
C5	870	25.02	30	30	6/10
C11	1300	32.27	35	35	6.5/10.5
C12	1300	47.86	40	40	6.5/10.5
C13	1300	33.10	35	35	6.5/10.5
C14	1300	29.87	45	45	6.5/12.5
C21	1300	31.70	40	40	6.5/10.5
C22	1300	40.76	50	50	6.5/10.5
C23	1300	34.32	50	50	6.5/10.5
LC1	1300	35.12	36.25	36.25	6/10
LC2	1300	32.77	41.25	41.25	6/11
LC3	1300	44.88	46.25	46.25	6/13

Table [2.17] Details of Columns Specimens, Dundar, et. al. [2007]

Ultimate strength capacities of reinforced concrete columns

Column no.	N_{test} (kN) (A)	N_u (theoretical)						
		HOG (B)	CEC (C)	K&P ^(u) (D)	K&P ^(c) (E)	S&R (F)	WSB (G)	EXP (H)
C1	89	90.45	88.95	89.75	104.44	88.18	79.66	—
C2	121	127.98	126.78	118.76	130.29	110.15	114.04	119.85
C3	125	117.83	116.51	111.45	127.00	105.63	104.71	109.45
C4	99	95.21	93.57	91.25	107.14	87.76	83.67	94.46
C5	94	90.47	88.83	87.70	100.42	83.78	79.55	89.46
C11	104	90.53	88.81	86.86	92.54	82.38	80.71	83.45
C12	95	99.24	91.39	93.74	98.96	87.63	82.38	88.31
C13	98	91.51	90.00	87.58	94.73	83.22	81.81	83.23
C14	58	63.46	63.02	61.38	67.88	59.51	60.57	64.10
C21	238	236.45	233.41	219.86	224.17	197.44	211.89	205.46
C22	199	208.82	208.83	188.86	205.71	183.00	187.88	204.78
C23	192	189.46	189.38	176.12	188.41	167.15	176.35	175.26
LC1	196	187.47	179.96	190.02	256.35	—	170.68	194.54
LC2	182	160.30	153.38	163.21	215.52	—	153.23	158.53
LC3	178	166.28	158.53	169.61	215.40	—	149.91	164.47

Table [2.18] Experimental and Theoretical Results of RC Columns, Dundar, et. al. [2007]

Dundar et. al. analyzed 4 encased composite columns tested by Munoz and Hsu [1994]. Those four columns classified into two categories, three slender columns and one short column. The analytical models have been created using different stress-strain models such as (HOG, CEC, K&P^u, and WSB). The comparison between each stress-strain model showing that the analysis models provides high level of accuracy compare to the experimental work done by Munoz and Hsu [1994] except WSB model which showing ultimate strength less than the test loads.

Z. Huang, et. al. [2018] investigated the performance of a very high strength concrete-encased steel composite column affected by combined axial compression and flexure bending at the end.

They have categorized the concrete strength to normal strength ($<50\text{MPa}$), high strength ($50\text{--}100\text{MPa}$), very high strength ($100\text{--}150\text{MPa}$), and ultra-strength concrete ($>150\text{MPa}$).

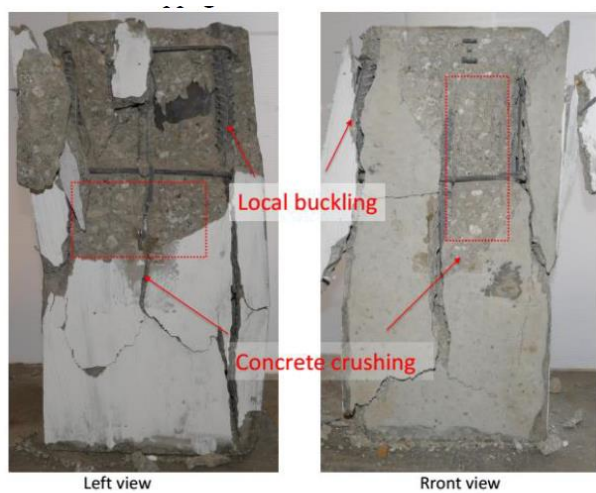
They have tested 6 encased composite columns with concrete strength ranging $50\text{--}100\text{MPa}$ by utilizing 10MN testing actuator performed in displacement control mechanism. The tested columns were having pin condition at the two ends. All composite column specimens provided with linear displacement transducers (LVDT).

The test results demonstrated that the failure of very high concrete encased steel started with concrete spalling and after that the rebar will buckle locally as result of de-bonding developed between concrete and rebar after concrete spalling. The encased composite columns with normal strength concrete were failing due to concrete crushing, then the rebar will be yielded. The use of fiber-reinforced was leading to combined failure mode of concrete crushing and splitting. The use of steel fiber in the concrete enhance the section capacity in compression and tension and mitigating the cracks in the composite section. **Fig. (2.47)** illustrating the failure mode of each different concrete strength. **Table [2.19]** presenting the failure load for each specimen and its failure mechanism.

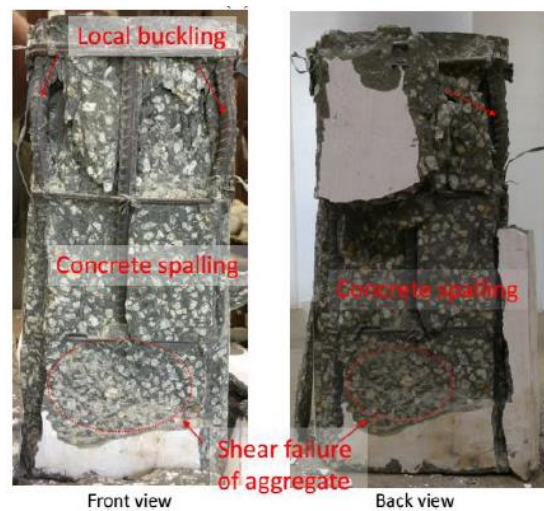
The load displacement curves are showing in **Fig. (2.48)** for the encased columns under compression with/without eccentricity. For encased column under flexure the load displacement curve is illustrated in **Fig. (2.49)**.

The following was concluded from this research:

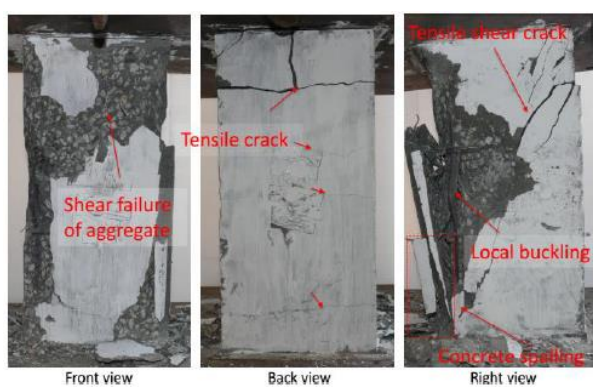
- A very high strength concrete encased composite column display brittle failure mechanism. The column subject to compression is failing the experimental testing by concrete spalling, then local buckling to the vertical rebar. The use of confined stirrups improves the ductility of the concrete.
- The use of steel fiber instead of normal rebar in the very high strength concrete provides brittle failure mode in case the concrete is unconfined and no horizontal stirrups surrounding provided.
- The encased column under uniaxial compression or eccentric compression can be displayed using plastic resistance approach, while the encased column with flexure or axial compression with remarkable eccentricity the plastic resistance approach is not achievable. The current standards overestimate the section capacity of very high strength concrete encased composite, so the section capacity can be predicted by using stress-strain compatibility.



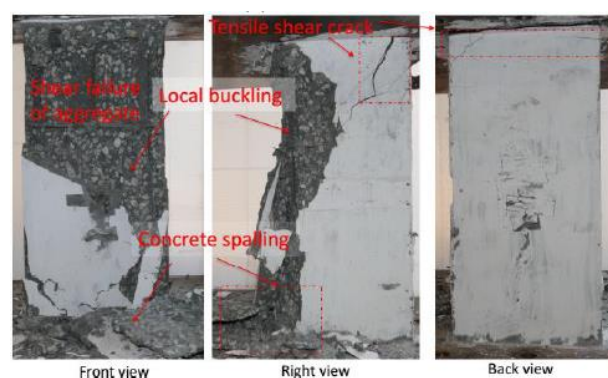
(a) C50e0.



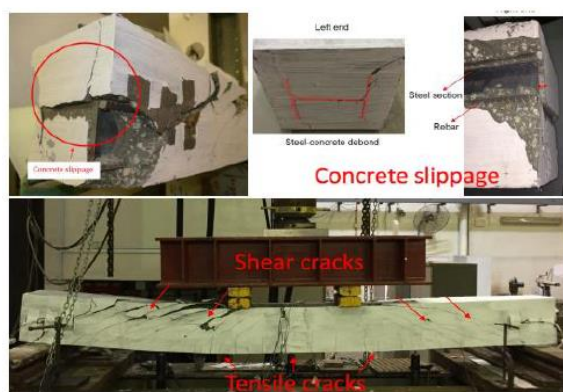
(b) C100e0.



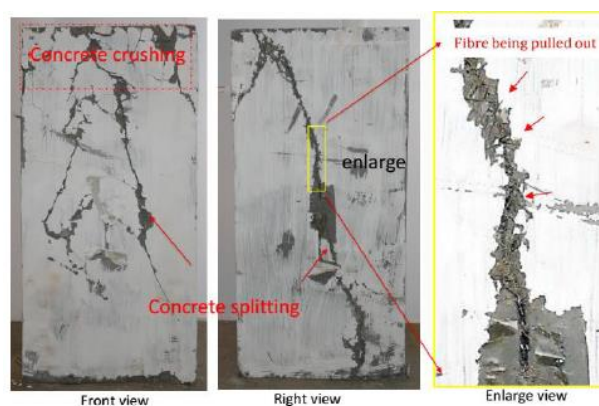
(c) C100e50.



(d) C100e105.



(e) C100B.



(f) C100F.

Fig. (2.47) Failure Modes of the Tested Column, Z. Huang, et. al. [2018]

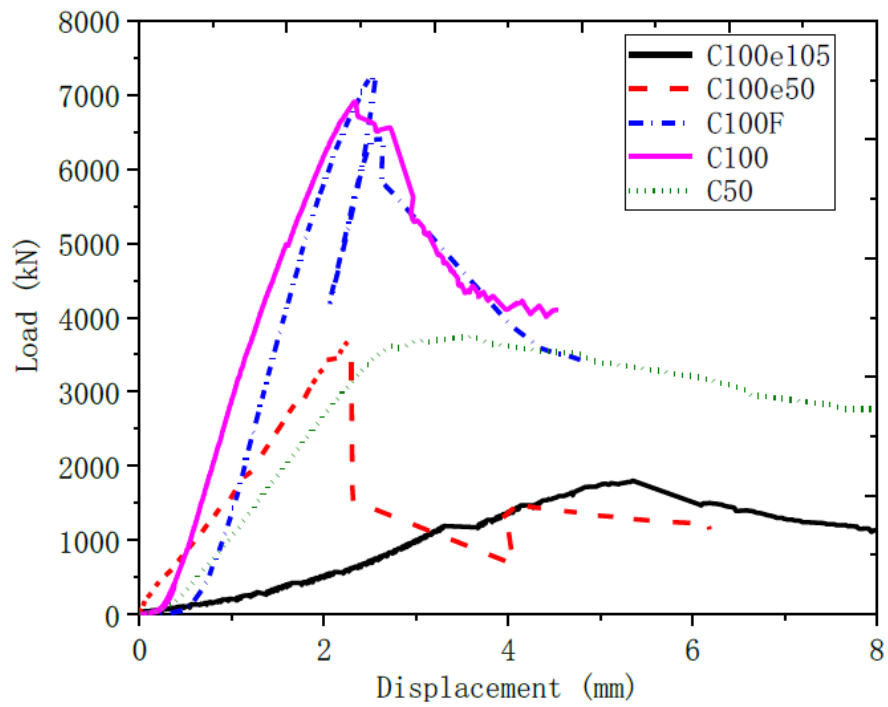


Fig. (2.48) Load-Displacement Relationship for Tested Columns under Compression

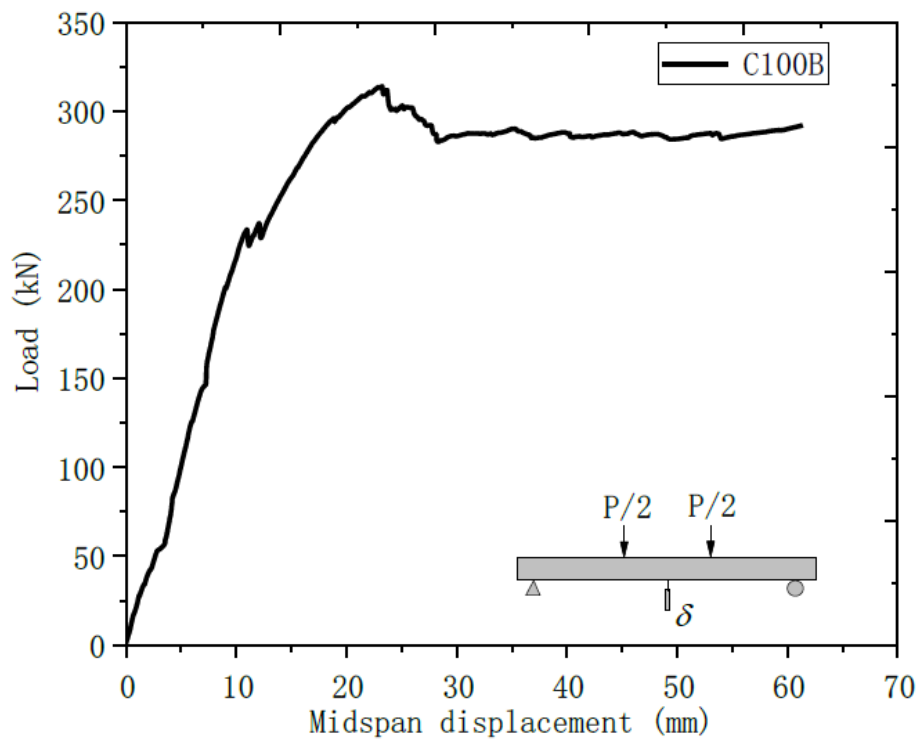


Fig. (2.49) Load-Midspan Displacement Relationship for Tested Columns under Flexure

Specimen	P (kN)	M (kN·m)	Primary failure	Other failure	f_c (MPa)	f_{fiber} (MPa)	f_s (MPa)	e (mm)
C50e0	3744.1	-	CC	LBR	51.1	-	356.8	0
C100e0	6913.4	-	CS	LBR	109.3	-	356.8	0
C100e50	3686.7	242.8	CS	LBR	109.3	-	356.8	50
C100e105	1800.5	209.7	TF	CC	109.3	-	356.8	105
C100B	314.0	149.1	FF	SF, CSl	109.3	-	356.8	-
C100F	7256.9	-	CSp	CS	123.8	1600	-	0

CC= Concrete crushing; CS= Concrete spalling; TF= Tension failure; FF= Flexural failure; CSp= Concrete

Table [2.19] Failure Loads for each Specimen and its Failure Mechanism, Z. Huang, et. al. [2018]

CHAPTER 3

RESEARCH METHODOLOGY

3.1 INTRODUCTION

This chapter illustrates the research approach, methodology, and strategy adopted to accomplish its objective.

It demonstrates a case study considered in this research and outlines the analysis procedures and the anticipated sectional capacities under axial compression loads and bi-axial bending moments.

Furthermore, it presents the experimental approach vs the theoretical by conducting a study for 1/5 scaled Columns compared to the actual size extracted for the case study.

3.2 RESEARCH APPROACH

The literature review introduced in this research has displayed a guidance to the behavior of the concrete filled steel tube (CFST) columns and encased composite (SRC) columns under different types of loading taking into considerations the influence of many factors such as the local buckling of the steel sections, bond between concrete and steel, concrete confinement, load transfer between steel and concrete, and high strength materials.

It demonstrates the design approach of the composite columns using the provision of the American Standard and Euro Code.

It also provides an insight into the performance of the Isolated Steel Reinforced Concrete Columns (ISRC) studied by China Academy of Building Research (CABR), which is recently used in the high-rise buildings.

The research approach will focus on the behavior of Biaxially loaded of Tapered High Strength Concrete Filled Steel Tube (CFST) Column connected to Encased Composite (SRC) Columns based on a case study from existing High-Rise Building.

For ease of study a model of 1/5 scaled column compared to the actual size indicated in the case study will be adopted in this research.

The data of the case study has been collected from the Structural Engineer including drawings, calculations, analysis, and construction methodology of the composite columns. The experimental works will be used to challenge and evaluate the accuracy compared to the theoretical analysis and to emphasize the composite action between CFST column and SRC column.

3.3 RESEARCH STRATEGY

The main objective of this study is to investigate the behavior of two different elements connected to each other under different type of loading and taking into account some factors such as the use of high strength concrete vs normal concrete, local buckling of the steel sections, the bond between steel and concrete, the use of shear connectors, concrete confinement, and load path and stresses along the height of the column.

The analysis will be carried out based on an existing high-rise building in Dubai constructed in 2019.

The following points outlines the research strategy adopted to achieve its objectives;

- Demonstrate a case study and the actual straining actions on the composite columns utilized in this research.
- Determine the sectional capacity using American Standard and Euro-Code
- Theoretical analysis of 1/5 scaled column model compared to the actual size specified in the case study using appropriate software.
- Comparison of the Theoretical Results between 3D Fiber (Solid) Model and simplified method adopted by AISC316-16, ACI 318-11, and Eurocode-4.
- Provide a conclusion and summary for the study presented in this research

3.4 DATA COLLECTION

The data presented the case study were collected from the Structural Engineer based on 3D finite element models performed for the entire high-rise building including gravity and lateral loads (Seismic & Wind).

The data collected from the existing case study was including the following:

- As- Built Drawings and Detailing of all connections.
- Construction Methodology and erection of the composite columns.
- A 3D-Finite Element Models (ETAB and SAP) performed by the Structural Engineer for the existing high-rise building.

CHAPTER 4

RESEARCH RESULTS

4.1 INTRODUCTION

This chapter demonstrates the numerical analysis of the tapered CFST columns connected to the Encased Composite (SRC) columns as per the selected case study of an existing high-rise building located in Dubai, UAE.

Thereafter, it provides the numerical analysis of 1/5 scaled column model under different type of loading with different concrete compressive strengths.

The results from the 3D-finite element models will be compared to the simplified formulas adopted by Eurocode-4, AISC/ANCI, and ACI318-11.

The results are demonstrating the stress and strain distribution along the column height under different type of loadings, uni-axial compression, axial compression with uni-direction moments, and axial compression with bi-direction moments.

4.2 CASE STUDY

The case study utilized in this research was an existing high rise building of 250m height (3B+G+60) with a major transfer floor at level 11. There were two encased composite columns from the foundation up to level 10, then those two columns have been changed to tapered CFST columns from level 10 to 11 in order to withstand a significant increase in the bi-axial bending moments at the interface with the transfer slab. Level 10 was MEP floor, so it was accepted by the architect to have tapered column geometry. The encased composite column was (1400 x 1400) mm with embedded heavy I steel Section of (1000 x 1000 x 100) mm. The concrete of the encased column was confined by a closed stirrup of T16 @ every 200mm. the vertical rebar used in the encased column was 40T40. The steel tube of the tapered CFST column was varying from (1400 x 1400 x 100) mm at the interface with the encased column to (2250 x 2250 x 100) mm at the top part embedded into the transfer slab. The size of the CFST column is (2000x2000x100) at the interface with the Transfer slab which has been considered in the design of the column under gravity and bi-axially bending. The concrete cylinder strength used in the composite columns was C70MPa. The depth of the transfer slab was 2.50m and it is supporting about 50 floors above the transfer level. The steel grade used in this element was S355, and the rebar has been provided with grade 500MPa.

Fig. (4.1) demonstrates the elevation of the case study of the tapered CFST column connected to the encased SRC column with variable cross sections along the column height.

Fig. (4.2) illustrates the 3D geometry of the case study (Design vs Construction)

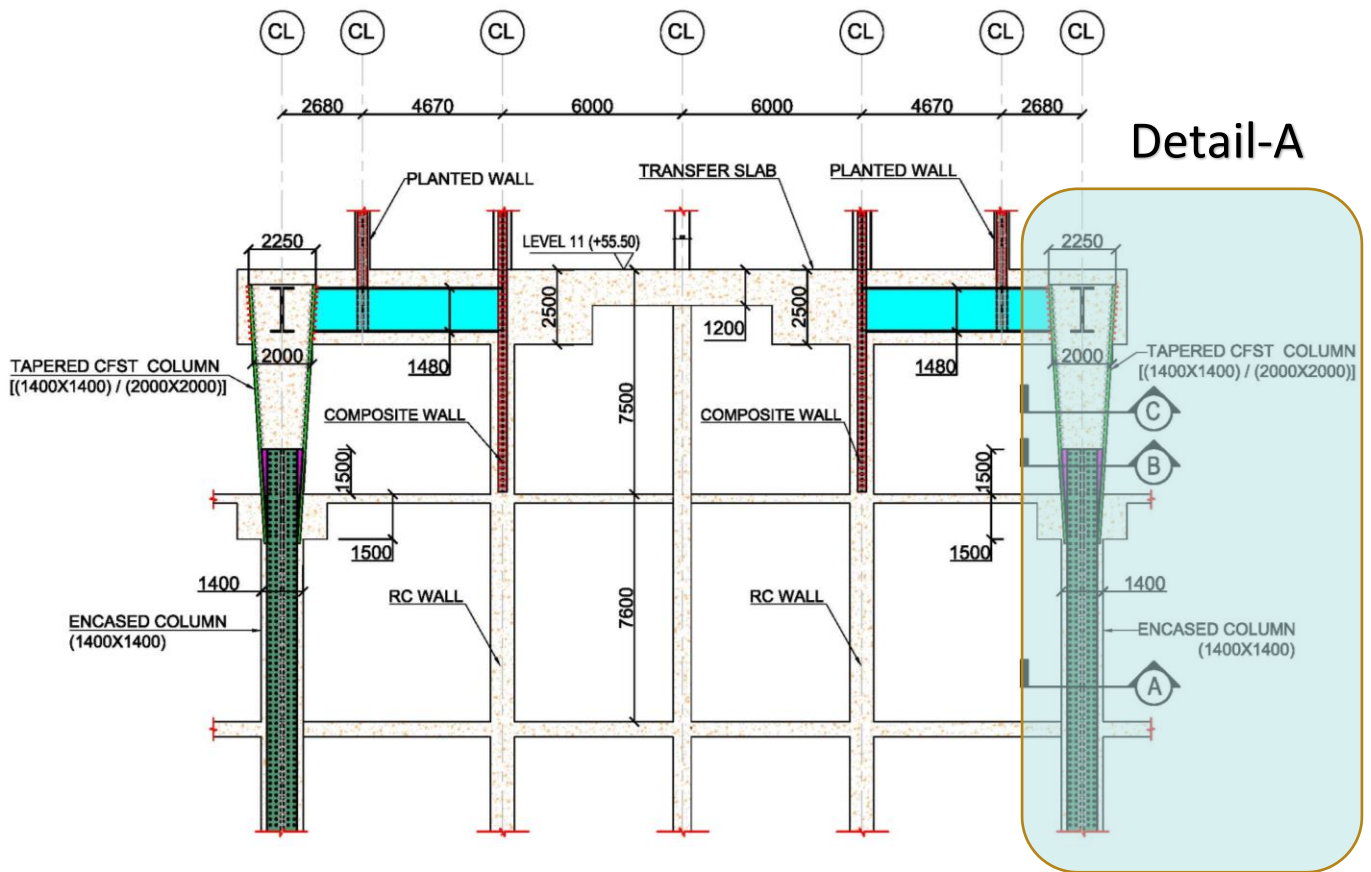


Fig. (4.1) Case Study of Tapered CFST Column connected to Encased Composite Column

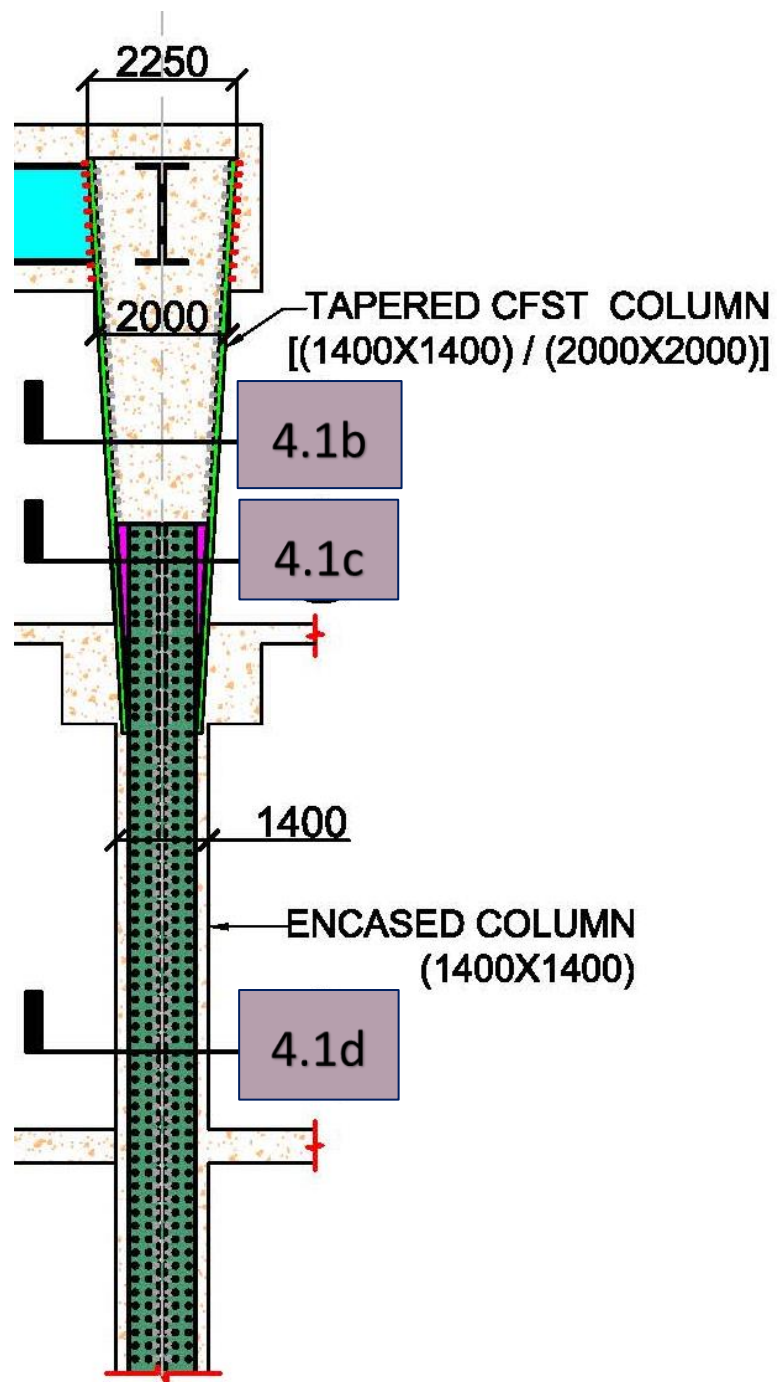


Fig. (4.1a) Detail-A Case Study, Enlarged Column Elevation

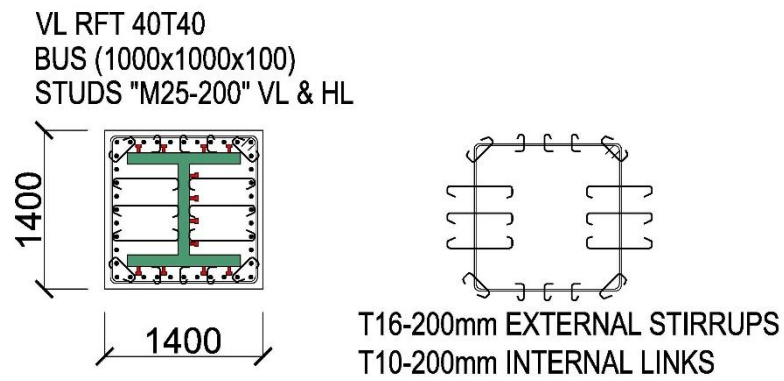


Fig. (4.1b) Case Study, Encased Composite Column

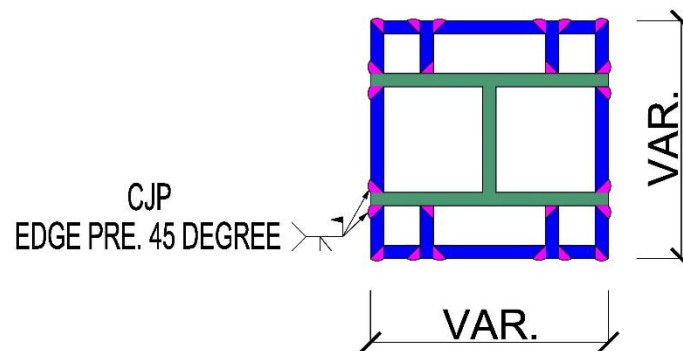


Fig. (4.1c) Case Study, Connection between CFST Column and Encased Composite Column

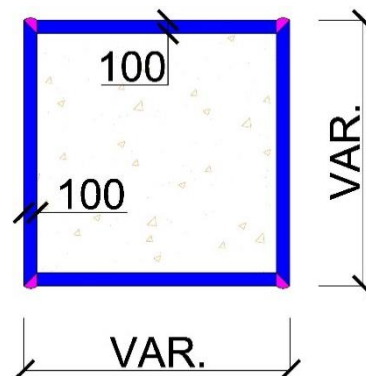
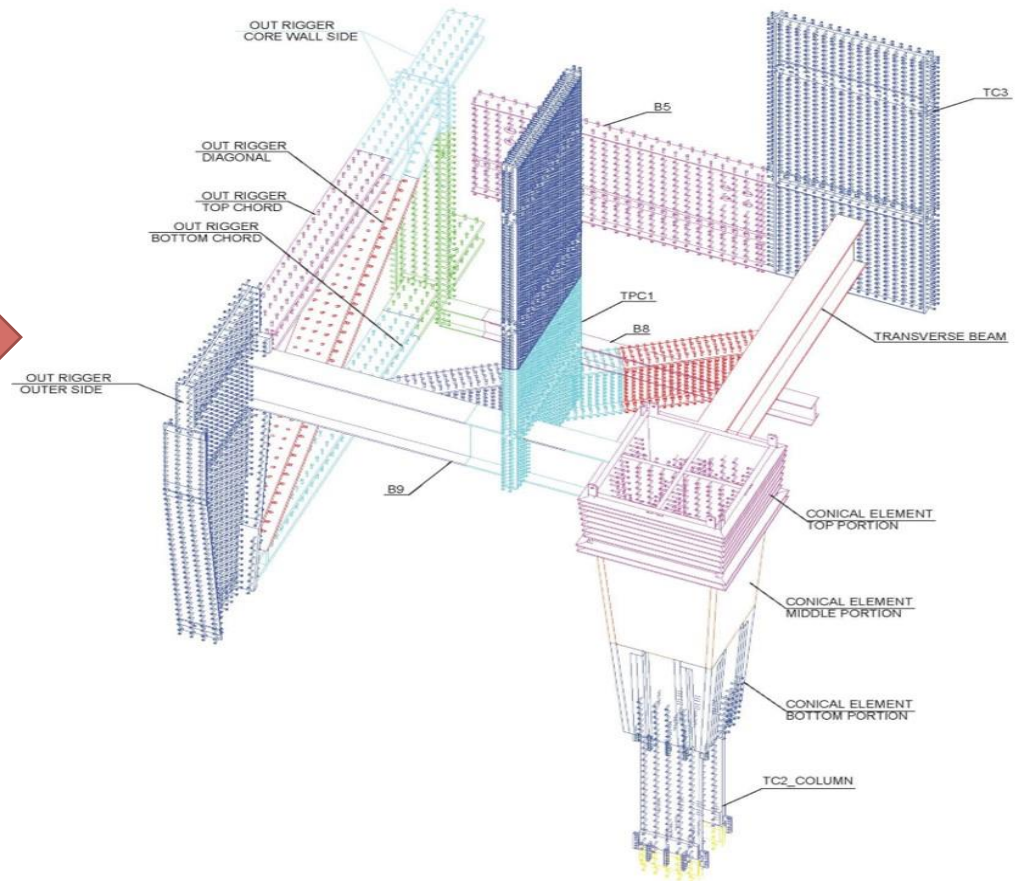
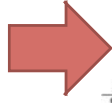


Fig. (4.1d) Case Study, Concrete Filled Steel Tube (CFST) Column

Design



Construction

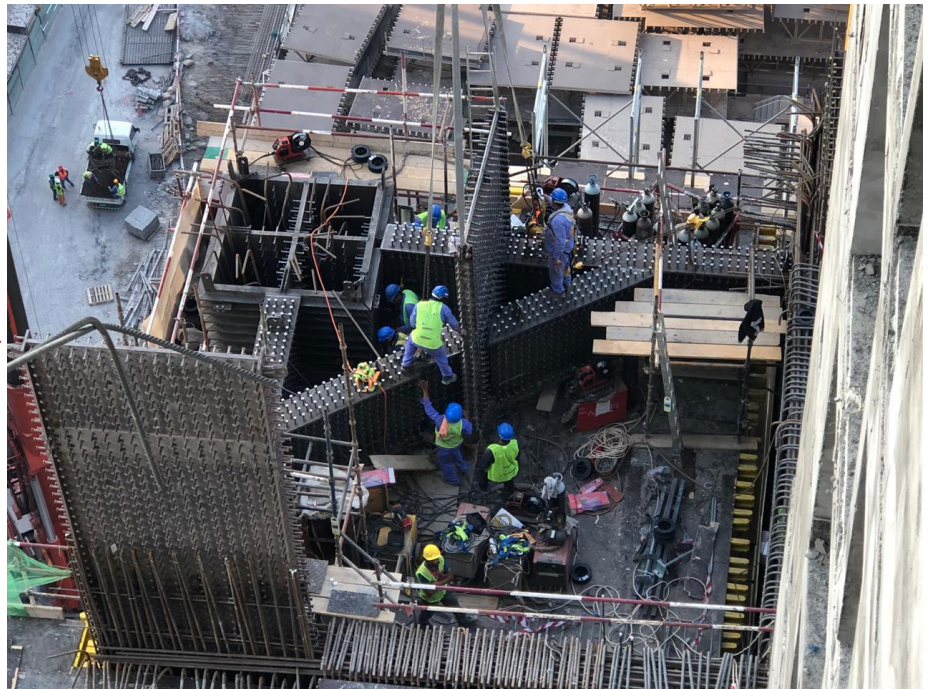


Fig. (4.2) Case Study, 3D geometry of the case study (Design vs Construction)

The composite column is subjected to axial compression loads and bi-axial bending moments at the top edge, while it is mainly subjected to Axial forces at the bottom edge with significant reduction in the bending moments compared to the top part.

The maximum bending moments on the Encased Composite Column is not exceeding 10% from the maximum bending moments on the top edge of the CFST column.

The axial forces on the top edge of the CFST column is 116,000 kN with corresponding moments of 100,000 kN.m in (X) direction and 55,000 kN.m in (Y) direction.

The axial forces on the bottom edge of the Encased columns is 119,000 kN with corresponding moments of 11,900 kN.m in (X) direction and 2,400 kN.m in (Y) direction.

It is noted that the bending moments in (X) direction at the bottom of the encased section is 11.9% of the bending moments at the top of the CFST column, while in (Y) direction, the bending moments at the bottom of the Encased section is about 4.4% of the bending moments at the top of the CFST section.

Table [4.1] summarize the factored straining actions along the column height to provide a clear understanding to the straining actions diagrams inline with the changing in the tapered column cross sectional size as well as changing the composite columns type.

The CFST column is classified as compact section since $b/t = 20 < 54 (2.26E/F_y)$.

The ultimate axial force is equal to 33% of the nominal compressive strength of the CFST column

$(P_u / \phi_c P_n)$.

As illustrated in the Literature Review, the CFST provides larger capacities to the axial and flexure compare to the encased composite section, so it was an efficient solution to change the column section from encased section to CFST section for one level only rather than having CFST column in all levels from the Foundations until the Transfer Floor.

The challenge of this idea was to assemble the CFST column components and to provide a rigid and appropriate connection details to the transfer slabs and Encased Column section to ensure a smooth load path to the tapered CFST throughout Transfer Slabs and subsequently to the below Encased Composite Column and Foundations.

Factored Straining Action on the Top of the CFST Column		
Axial Forces	P_u (kN)	116,000
Bending Moments around (X) Direction	M_x (kN.m)	100,000
Bending Moments around (Y) Direction	M_y (kN.m)	55,000
Shearing Forces along (X) Direction	V_x (kN)	15,900
Shearing Forces along (Y) Direction	V_y (kN)	9,100
Torsional Moments	T_u (kN.m)	475

Factored Straining Action on the Bottom of the CFST Column		
Axial Forces	P_u (kN)	117,000
Bending Moments around (X) Direction	M_x (kN.m)	17,000
Bending Moments around (Y) Direction	M_y (kN.m)	12,900
Shearing Forces along (X) Direction	V_x (kN)	15,900
Shearing Forces along (Y) Direction	V_y (kN)	9,100
Torsional Moments	T_u (kN.m)	475

Factored Straining Action on the Top of Encased Composite Columns		
Axial Forces	P_u (kN)	119,000
Bending Moments around (X) Direction	M_x (kN.m)	4,100
Bending Moments around (Y) Direction	M_y (kN.m)	2,800
Shearing Forces along (X) Direction	V_x (kN)	2,100
Shearing Forces along (Y) Direction	V_y (kN)	300
Torsional Moments	T_u (kN.m)	0.00

Factored Straining Action on the Bottom of Encased Composite Columns		
Axial Forces	P_u (kN)	119,000
Bending Moments around (X) Direction	M_x (kN.m)	11,900
Bending Moments around (Y) Direction	M_y (kN.m)	2,400
Shearing Forces along (X) Direction	V_x (kN)	2,100
Shearing Forces along (Y) Direction	V_y (kN)	300
Torsional Moments	T_u (kN.m)	0.00

Table [4.1] Straining Actions Along Column Height

4.3 SIMPLIFIED METHOD FOR THE CFST COLUMN CAPACITY OF THE CASE STUDY

4.3.1 ANCI/ AISC PROVISION

The following formula extracted from the AISC presents the design strength of the CFST under axial compression and bi-axial bending.

$$D/ C = [Pr / Pc] + [8/9 \{ (Mrx/Mcx) + (Mry/Mcy) \}] \leq 1.0$$

By applying the above formula, the D/C = **1.0** under the specified straining action, so the ultimate load was equivalent to the strength load.

4.3.2 EUROCODE 4 PROVISION

The following formula extracted from the AISC presents the design strength of the CFST under axial compression and bi-axial bending.

$$D/ C = M_{y,Ed} / (\mu_{dy} M_{pl,y,Rd}) + M_{z,Ed} / (\mu_{dz} M_{pl,z,Rd}) \leq 1.0$$

By applying the above formula, the D/C = 0.94 under the specified straining action.

4.4 RESEARCH DESIGN MODEL

A scaled 1:5 of the case study presented in clause 4.2 has been selected to study the behavior of the tapered CFST column connected to the encased composite column.

The overall height of the column is 2175mm divided into 3 different shapes, the lower part of 900mm height is encased composite element, the upper part of 850mm is tapered CFST elements, and the intermediate part of 425mm is the overlapping between encased composite element and tapered CFST element.

The tapered CFST element has a slope angle of 3° . The wider CFST section at the top is (340 x 340) mm and the smaller CFST section at the bottom is (210 x 210) mm. The steel tube cross section is (340 x 340 x 6) mm and the clear sizing of the concrete cross section confined by the steel tube is (328 x 328) mm.

The size of the encased composite element is (210 x 210) mm with steel I section of (120 x 120 x 15) mm. The concrete element of the encased column is confined by closed stirrups of T10@200mm. The vertical reinforcement provided for the encased column is 4T10. The concrete clear cover of the encased element is 20mm.

All steel connections supposed to be full penetration butt weld.

The overlapping length between encased composite column and CFST column is 425mm. the steel I section is connected to the tapered CFST column throughout 6 stiffener plates fully welded to the steel tube plates.

The steel section used in the research design model has been studied using two different grades, steel grade S275 with a yield strength of 375MPa and steel grade S355 with a yield strength of 355MPa.

The steel reinforcement used in the model has a yield strength of 500MPa.

The concrete cylinder strength utilized in the research was varying from C40MPa to C70MPa.

Fig. (4.3) presents the overall design model adopted for the research study.

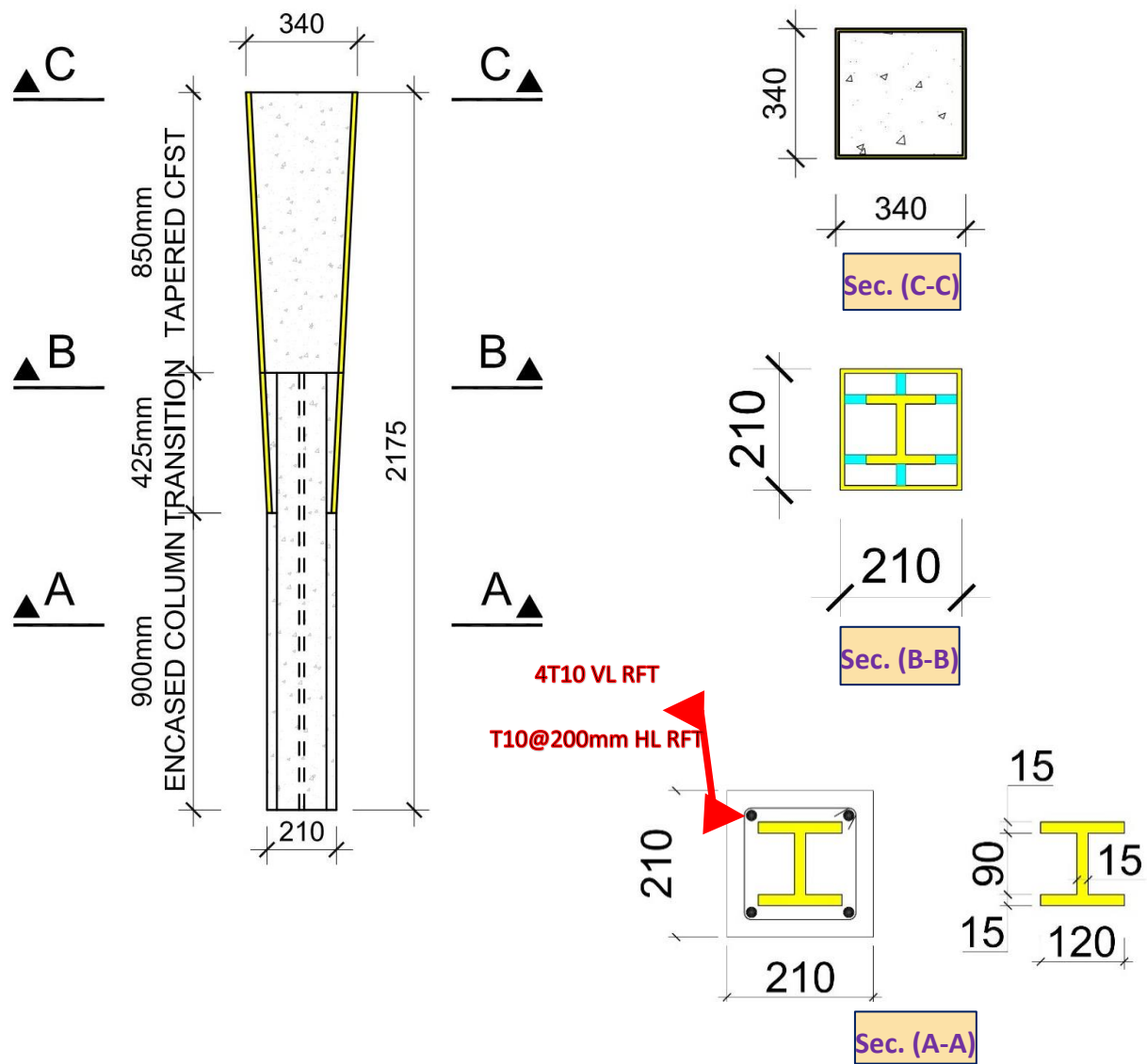


Fig. (4.3) Research Design Model Geometry

4.4.1 3D-FIBER (SOLID) FINITE ELEMENT MODEL

The column has been modeled using fiber (Solid) element method. The cross section of the columns has been divided into tiny fiber (solid) elements as shown in Fig. (4.4).

The advantage of using a fiber (solid) element is to easily assign the tiny element as concrete or steel. It allows also to have full detailed and more accurate 3D-Model including overlapping between Encased Column and CFST Columns. Even the stiffeners provided between Steel I Element and Steel Tube Element within the overlapping zone can be modeled easily modeled.

The maximum size of the fiber (solid) element is (10mm x 10mm) which warrant more accurate results in terms of stress and strain. The vertical rebar was ignored from the 3D Fiber Model.

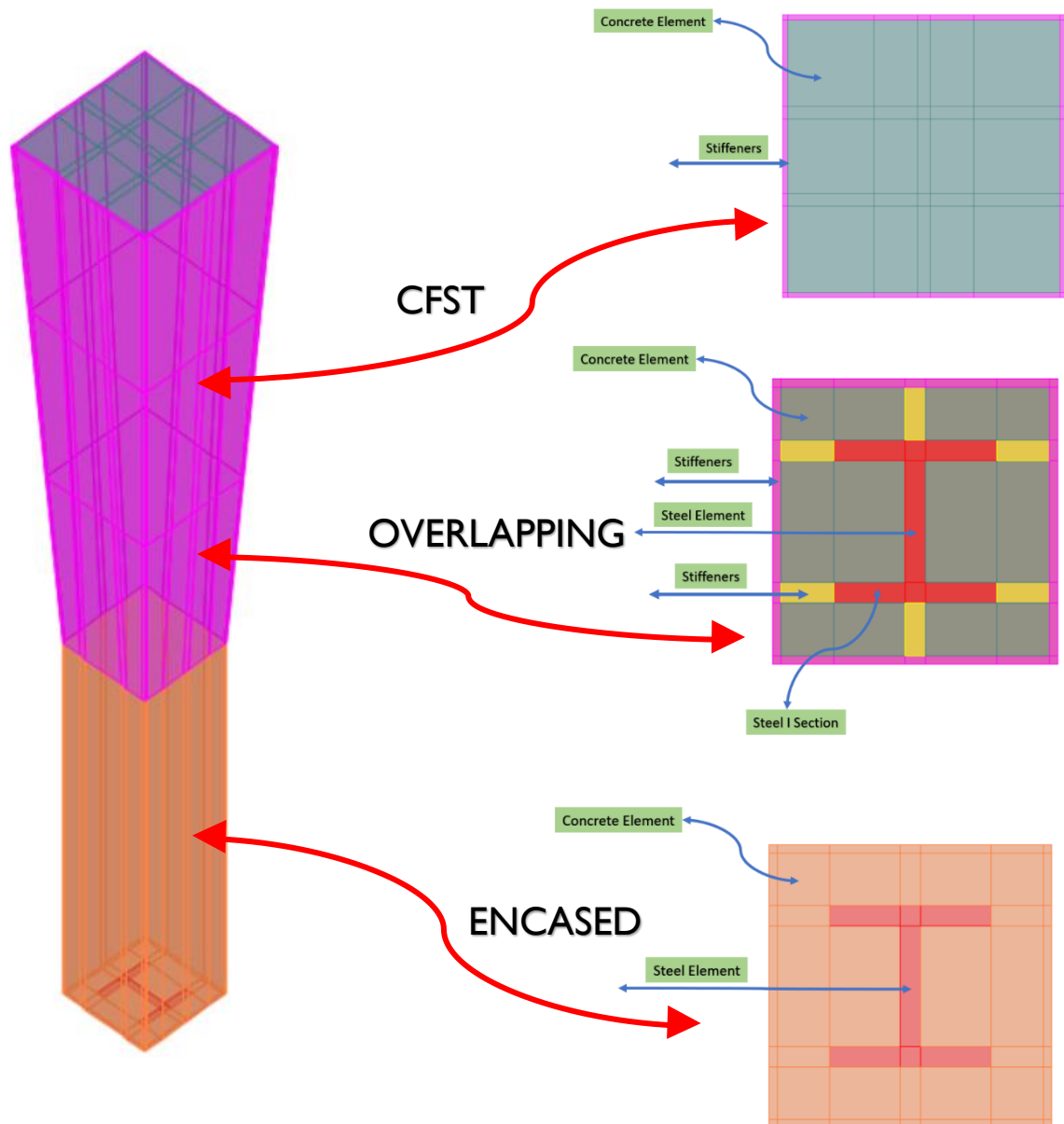


Fig. (4.4) 3D Fiber (Solid) Finite Element Model

4.4.2 BOUNDARY CONDITIONS

The boundary conditions for the 3D-Fiber (Solid) element are a vital to represent the actual behavior of the structural element under different type of loading

The top node of the element is roller support which is free to rotate and allow for a vertical movement while it provides restrain the two-horizontal direction, however; the purpose of having roller support is to transfer axial forces uniformly along element height and to transfer the minimum amount of the moments to the bottom node in case of having uni-direction or bi-direction moments.

The bottom node of the column element is fixed support in order to withstand vertical and horizontal forces, as well as the moment.

Fig. (4.5) presents the boundary conditions and straining action diagrams due to axial and flexure.

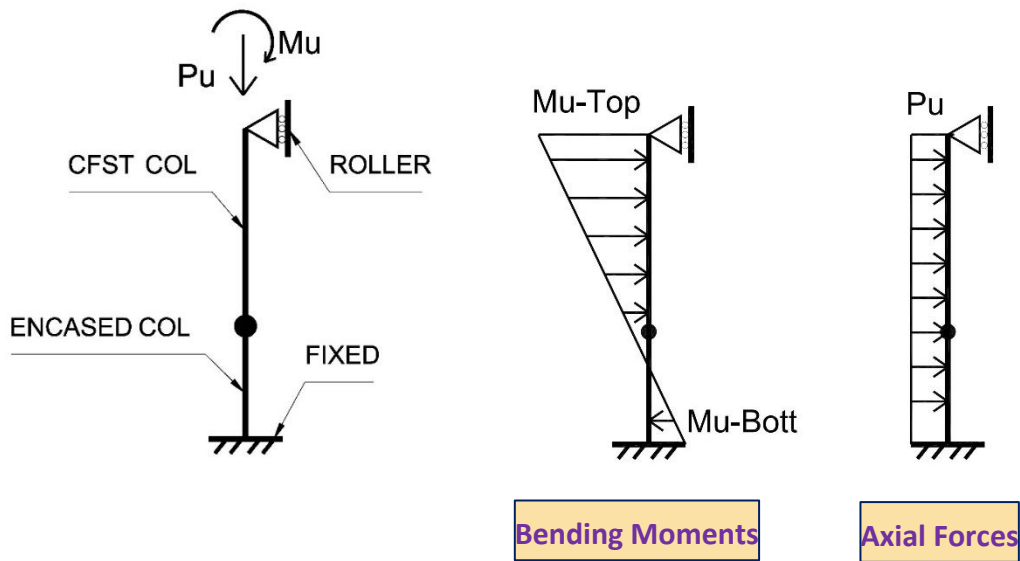


Fig. (4.5) Design Model Boundary Conditions and Straining Action Diagram

4.4.3 COLUMN RESISTANCE TO AXIAL COMPRESSION LOADS

The first approach in this research is to examine the column under pure axial gravity loads. The column has been modeled using four different cylinder concrete strengths, 40, 50, 60, and 70MPa.

Each concrete strength has been analyzed using two different steel strength, S275MPa and S355MPa inline with EN 1993-1-1.

The nominal strength of the composite columns has been checked using AISC 360-16, ACI 318-11, Eurocode-4 and compared with the output from the 3D-Fiber (Solid) Element Model.

The Finite element has been divided into 3 parts, the first part is the encased column, the second part is the CFST column, and the third part is the stiffener plates connecting I section to CFST tube.

The Concrete Modulus of Elasticity has been determined as follow:

- C40MPa, $E_c = 29,725 \text{ MPa}$
- C50MPa, $E_c = 33,234 \text{ MPa}$
- C60MPa, $E_c = 40,022 \text{ MPa}$
- C70MPa, $E_c = 42,079 \text{ MPa}$

The Steel Modulus of Elasticity is equal to 200,000 MPa

4.4.3.1 Stresses on of the Encased Composite Column subject to Axial Compression Loads

This clause describes the analysis of the encased Composite Column subject to pure axial compression loads. the stresses and strains on the concrete and steel section have been evaluated and compared to the simplified methods adopted by ACI 318-11, AISC 360-16, and Eurocode-4.

It was vital to understand the sectional behavior under different concrete cylinder strengths ranging from C40MPa to C70MPa, with different Young's Modulus of Elasticity as summarized in **clause 4.4.3**.

Furthermore; the capacity of the composite section has been evaluated using two different steel grades, S275MPa and S355MPa.

4.4.3.1.1 Encased Column Analysis under Axial Compression Load, C40MPa, S355MPa

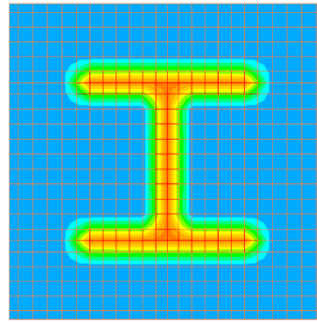
The following [table \[4.2\]](#) summarizes the nominal compressive loads using simplified approach adopted by AISC 360-16, ACI 318-11, and Eurocode-4. In addition; it shows the stresses and strains of the concrete and steel elements extracted from the 3D -Fiber (Solid) Model. The analysis showing in the below [table \[4.2\]](#) has been performed using Concrete Cylinder Strength of C40MPa, and Steel Grade of S355MPa.

Fig. (4.6) presents the stress contours along the height of the encased columns as extracted from the 3D Fiber (Solid) Model.

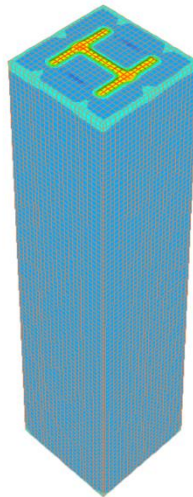
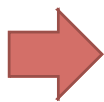
Analysis Approach	AISC 360-16	ACI 318-11	Eurocode-4	3D-Fiber (Solid) Element Model	
Concrete Cylinder Strength (MPa)	40	40	40	40	
Steel Grade (MPa)	S355	S355	S355	S355	
Nominal Compressive Strength (kN)	2,880	2749	2,774	2,500	
Stresses (MPa)				Concrete Stress (MPa)	Steel Stress (MPa)
Average Stresses on the Encased Column				40	225
Maximum Stresses at the Top of the Encased column connected to CFST				60	348
Strain (ϵ)				Concrete Strain	Steel Strain
Average Strain on the Encased Column				0.00135	0.0011
Maximum Strain at the Top of the Encased column connected to CFST				0.002	0.0017

Table [4.2] Nominal Compressive Strength of the Encased Composite Column, C40MPa, S355

Stresses of Encased Column



Stress of Concrete Section



Stress of Steel I Section

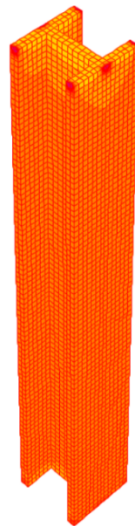


Fig. (4.6) Stresses of the Encased Column under Axial Compression Load

$P_u = 2,500 \text{ kN}$

Concrete Cylinder Strength, C40MPa

Steel Grade, S355MPa

4.4.3.1.2 Encased Column Analysis under Axial Compression Load, C50MPa, S355MPa

The following [table \[4.3\]](#) summarizes the nominal compressive loads using simplified approach adopted by AISC 360-16, ACI 318-11, and Eurocode-4. In addition; it shows the stresses and strains of the concrete and steel elements extracted from the 3D -Fiber (Solid) Model.

The analysis showing in the below [table \[4.3\]](#) has been performed using Concrete Cylinder Strength of C50MPa, and Steel Grade of S355MPa.

Fig. (4.7) presents the stress contours along the height of the encased columns as extracted from the 3D Fiber (Solid) Model.

Analysis Approach	AISC 360-16	ACI 318-11	Eurocode-4	3D-Fiber (Solid) Element Model	
Concrete Cylinder Strength (MPa)	50	50	50	50	
Steel Grade (MPa)	S355	S355	S355	S355	
Nominal Compressive Strength (kN)	3,162	3,030	2,994	3,125	
Stresses (MPa)				Concrete Stress (MPa)	Steel Stress (MPa)
Average Stresses on the Encased Column				50	250
Maximum Stresses at the Top of the Encased column connected to CFST				75	385
Strain (ϵ)				Concrete Strain	Steel Strain
Average Strain on the Encased Column				0.0015	0.0013
Maximum Strain at the Top of the Encased column connected to CFST				0.0023	0.0019

Table [4.3] Nominal Compressive Strength of the Encased Composite Column, C50MPa, S355

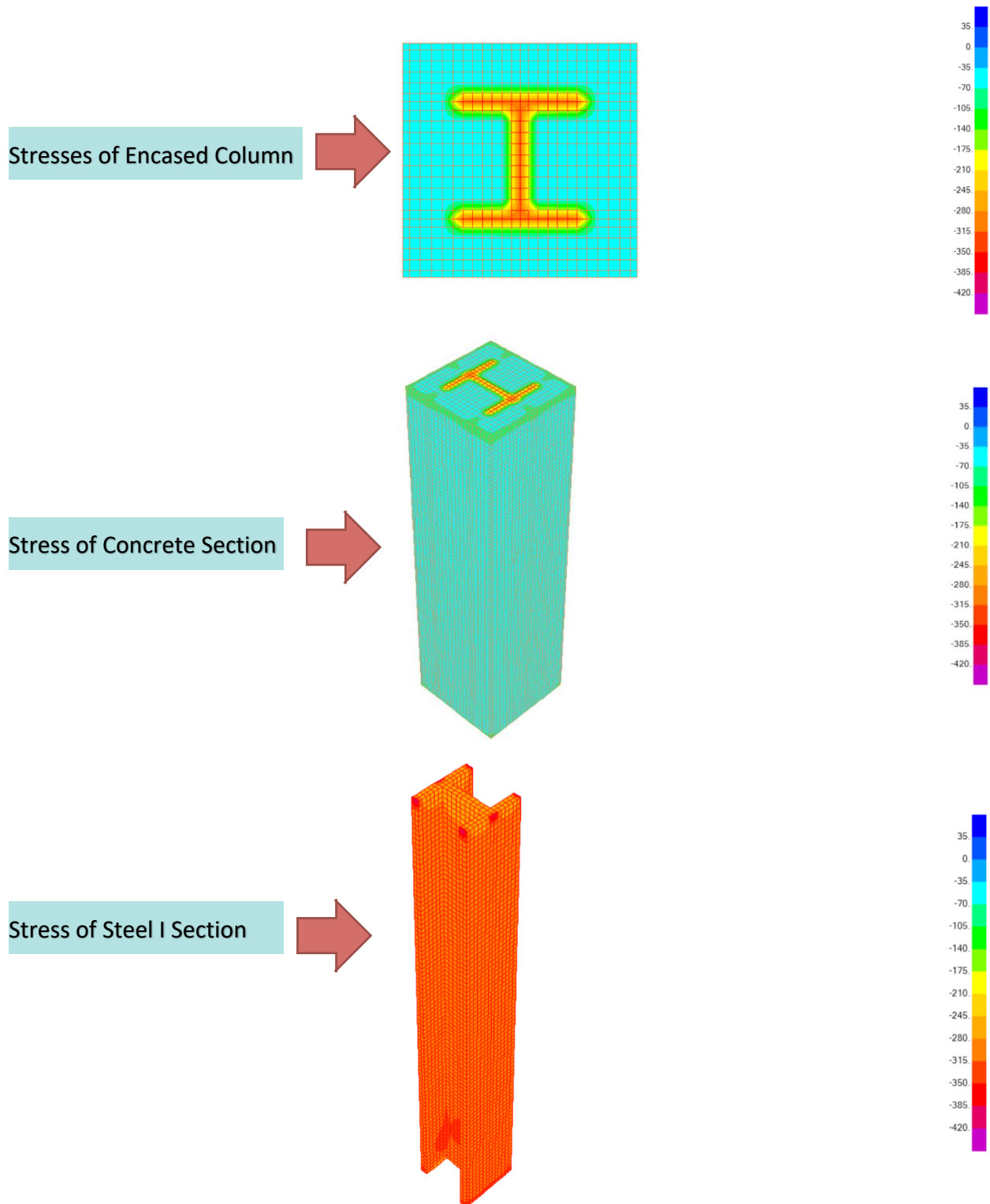


Fig. (4.7) Stresses of the Encased Column under Axial Compression Load

$P_u = 3,125 \text{ kN}$

Concrete Cylinder Strength, C50MPa

Steel Grade, S355MPa

4.4.3.1.3 Encased Column Analysis under Axial Compression Load, C60MPa, S355MPa

The following [table \[4.4\]](#) summarizes the nominal compressive loads using simplified approach adopted by AISC 360-16, ACI 318-11, and Eurocode-4. In addition; it shows the stresses and strains of the concrete and steel elements extracted from the 3D -Fiber (Solid) Model.

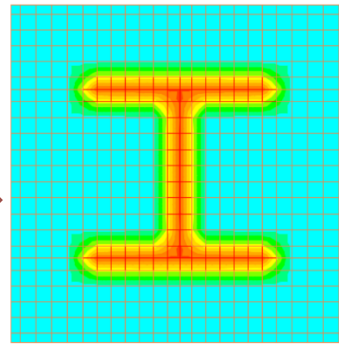
The analysis showing in the below [table \[4.4\]](#) has been performed using Concrete Cylinder Strength of C60MPa, and Steel Grade of S355MPa.

Fig. (4.8) presents the stress contours along the height of the encased columns as extracted from the 3D Fiber (Solid) Model.

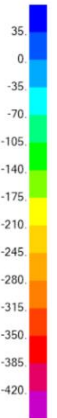
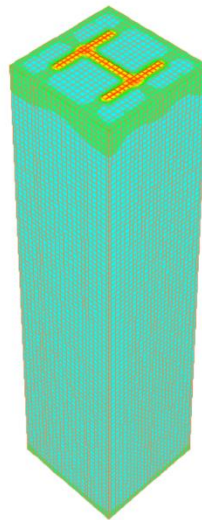
Analysis Approach	AISC 360-16	ACI 318-11	Eurocode-4	3D-Fiber (Solid) Element Model	
Concrete Cylinder Strength (MPa)	60	60	60	60	
Steel Grade (MPa)	S355	S355	S355	S355	
Nominal Compressive Strength (kN)	3,465	3,311	3,214	3,500	
Stresses (MPa)				Concrete Stress (MPa)	Steel Stress (MPa)
Average Stresses on the Encased Column				60	265
Maximum Stresses at the Top of the Encased column connected to CFST				90	390
Strain (ϵ)				Concrete Strain	Steel Strain
Average Strain on the Encased Column				0.0015	0.00133
Maximum Strain at the Top of the Encased column connected to CFST				0.0022	0.00195

Table [4.4] Nominal Compressive Strength of the Encased Composite Column, C60MPa, S355

Stresses of Encased Column



Stress of Concrete Section



Stress of Steel I Section

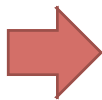


Fig. (4.8) Stresses of the Encased Column under Axial Compression Load

$P_u = 3,500 \text{ kN}$

Concrete Cylinder Strength, C60MPa

Steel Grade, S355MPa

4.4.3.1.4 Encased Column Analysis under Axial Compression Load, C70MPa, S355MPa

The following [table \[4.5\]](#) summarizes the nominal compressive loads using simplified approach adopted by AISC 360-16, ACI 318-11, and Eurocode-4. In addition; it shows the stresses and strains of the concrete and steel elements extracted from the 3D -Fiber (Solid) Model.

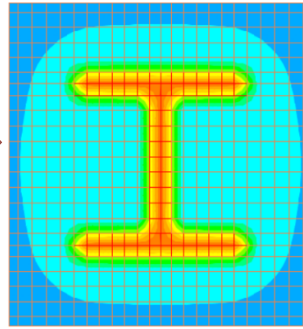
The analysis showing in the below [table \[4.5\]](#) has been performed using Concrete Cylinder Strength of C70MPa, and Steel Grade of S355MPa.

Fig. (4.9) presents the stress contours along the height of the encased columns as extracted from the 3D Fiber (Solid) Model.

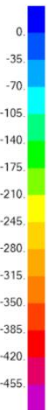
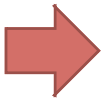
Analysis Approach	AISC 360-16	ACI 318-11	Eurocode-4	3D-Fiber (Solid) Element Model	
Concrete Cylinder Strength (MPa)	70	70	70	70	
Steel Grade (MPa)	S355	S355	S355	S355	
Nominal Compressive Strength (kN)	3,736	3,591	3,434	4,000	
Stresses (MPa)				Concrete Stress (MPa)	Steel Stress (MPa)
Average Stresses on the Encased Column				70	290
Maximum Stresses at the Top of the Encased column connected to CFST				105	428
Strain (ϵ)				Concrete Strain	Steel Strain
Average Strain on the Encased Column				0.0017	0.00145
Maximum Strain at the Top of the Encased column connected to CFST				0.0025	0.00214

Table [4.5] Nominal Compressive Strength of the Encased Composite Column, C70MPa, S355

Stresses of Encased Column



Stress of Concrete Section



Stress of Steel I Section

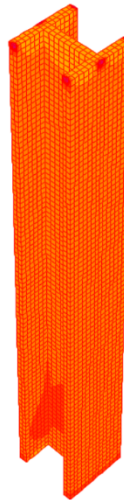


Fig. (4.9) Stresses of the Encased Column under Axial Compression Load

$P_u = 4,000 \text{ kN}$

Concrete Cylinder Strength, C70MPa

Steel Grade, S355MPa

4.4.3.1.5 Encased Column Analysis under Axial Compression Load, C40MPa, S275MPa

The following [table \[4.6\]](#) summarizes the nominal compressive loads using simplified approach adopted by AISC 360-16, ACI 318-11, and Eurocode-4. In addition; it shows the stresses and strains of the concrete and steel elements extracted from the 3D -Fiber (Solid) Model.

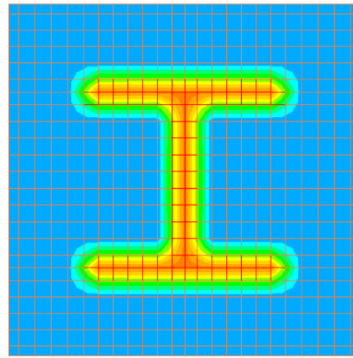
The analysis showing in the below [table \[4.6\]](#) has been performed using Concrete Cylinder Strength of C40MPa, and Steel Grade of S275MPa.

Fig. (4.10) presents the stress contours along the height of the encased columns as extracted from the 3D Fiber (Solid) Model.

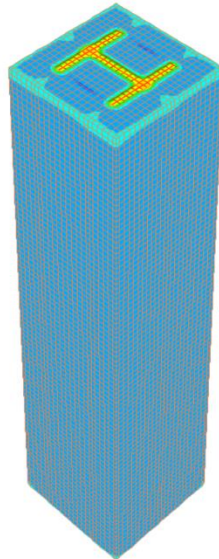
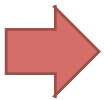
Analysis Approach	AISC 360-16	ACI 318-11	Eurocode-4	3D-Fiber (Solid) Element Model	
Concrete Cylinder Strength (MPa)	40	40	40	40	
Steel Grade (MPa)	S275	S275	S275	S275	
Nominal Compressive Strength (kN)	2,564	2,412	2,378	2,500	
Stresses (MPa)				Concrete Stress (MPa)	Steel Stress (MPa)
Average Stresses on the Encased Column				40	225
Maximum Stresses at the Top of the Encased column connected to CFST				60	348
Strain (ϵ)				Concrete Strain	Steel Strain
Average Strain on the Encased Column				0.00135	0.0011
Maximum Strain at the Top of the Encased column connected to CFST				0.002	0.0017

Table [4.6] Nominal Compressive Strength of the Encased Composite Column, C40MPa, S275

Stresses of Encased Column



Stress of Concrete Section



Stress of Steel I Section

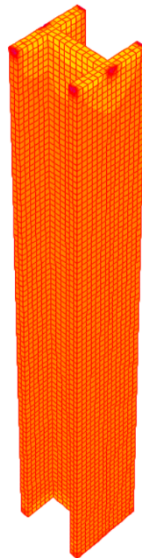


Fig. (4.10) Stresses of the Encased Column under Axial Compression Load

$P_u = 2,500 \text{ kN}$

Concrete Cylinder Strength, C40MPa

Steel Grade, S275MPa

4.4.3.1.6 Encased Column Analysis under Axial Compression Load, C50MPa, S275MPa

The following [table \[4.7\]](#) summarizes the nominal compressive loads using simplified approach adopted by AISC 360-16, ACI 318-11, and Eurocode-4. In addition; it shows the stresses and strains of the concrete and steel elements extracted from the 3D -Fiber (Solid) Model.

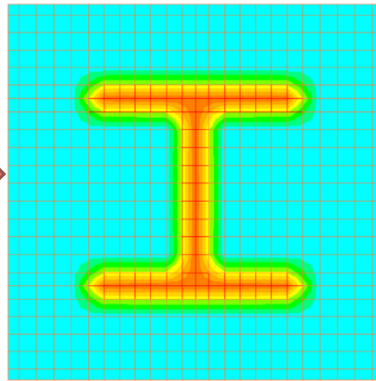
The analysis showing in the below [table \[4.7\]](#) has been performed using Concrete Cylinder Strength of C50MPa, and Steel Grade of S275MPa.

Fig. (4.11) presents the stress contours along the height of the encased columns as extracted from the 3D Fiber (Solid) Model.

Analysis Approach	AISC 360-16	ACI 318-11	Eurocode-4	3D-Fiber (Solid) Element Model	
Concrete Cylinder Strength (MPa)	50	50	50	50	
Steel Grade (MPa)	S275	S275	S275	S275	
Nominal Compressive Strength (kN)	2848	2693	2,598	3,125	
Stresses (MPa)				Concrete Stress (MPa)	Steel Stress (MPa)
Average Stresses on the Encased Column				50	250
Maximum Stresses at the Top of the Encased column connected to CFST				75	385
Strain (ϵ)				Concrete Strain	Steel Strain
Average Strain on the Encased Column				0.0015	0.0013
Maximum Strain at the Top of the Encased column connected to CFST				0.0023	0.0019

Table [4.7] Nominal Compressive Strength of the Encased Composite Column, C50MPa, S275

Stresses of
Encased Column



Stress of Concrete Section



Stress of Steel I Section

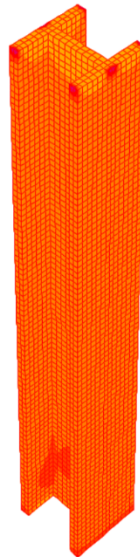


Fig. (4.11) Stresses of the Encased Column under Axial Compression Load

$P_u = 3,125 \text{ kN}$

Concrete Cylinder Strength, C50MPa

Steel Grade, S275MPa

4.4.3.1.7 Encased Column Analysis under Axial Compression Load, C60MPa, S275MPa

The following [table \[4.8\]](#) summarizes the nominal compressive loads using simplified approach adopted by AISC 360-16, ACI 318-11, and Eurocode-4. In addition; it shows the stresses and strains of the concrete and steel elements extracted from the 3D -Fiber (Solid) Model.

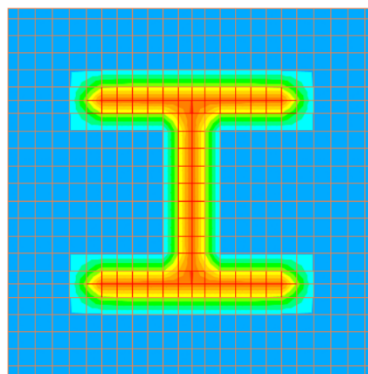
The analysis showing in the below [table \[4.8\]](#) has been performed using Concrete Cylinder Strength of C60MPa, and Steel Grade of S275MPa.

Fig. (4.12) presents the stress contours along the height of the encased columns as extracted from the 3D Fiber (Solid) Model.

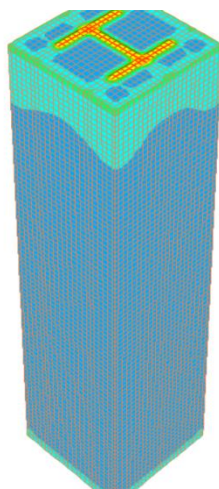
Analysis Approach	AISC 360-16	ACI 318-11	Eurocode-4	3D-Fiber (Solid) Element Model	
Concrete Cylinder Strength (MPa)	60	60	60	60	
Steel Grade (MPa)	S275	S275	S275	S275	
Nominal Compressive Strength (kN)	3,150	2974	2,818	3,500	
Stresses (MPa)				Concrete Stress (MPa)	Steel Stress (MPa)
Average Stresses on the Encased Column				60	265
Maximum Stresses at the Top of the Encased column connected to CFST				90	390
Strain (ϵ)				Concrete Strain	Steel Strain
Average Strain on the Encased Column				0.0015	0.00133
Maximum Strain at the Top of the Encased column connected to CFST				0.0022	0.00195

Table [4.8] Nominal Compressive Strength of the Encased Composite Column, C60MPa, S275

Stresses of Encased Column



Stress of Concrete Section



Stress of Steel I Section

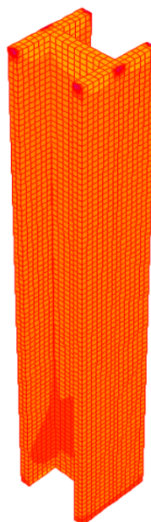


Fig. (4.12) Stresses of the Encased Column under Axial Compression Load

$P_u = 3,500 \text{ kN}$

Concrete Cylinder Strength, C60MPa

Steel Grade, S275MPa

4.4.3.1.8 Encased Column Analysis under Axial Compression Load, C70MPa, S275MPa

The following [table \[4.9\]](#) summarizes the nominal compressive loads using simplified approach adopted by AISC 360-16, ACI 318-11, and Eurocode-4. In addition; it shows the stresses and strains of the concrete and steel elements extracted from the 3D -Fiber (Solid) Model.

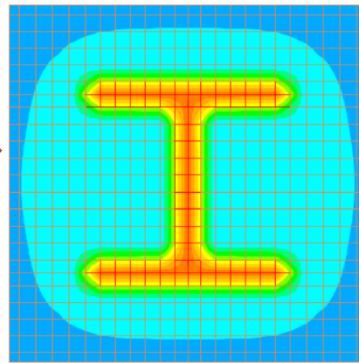
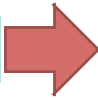
The analysis showing in the below [table \[4.9\]](#) has been performed using Concrete Cylinder Strength of C70MPa, and Steel Grade of S275MPa.

Fig. (4.13) presents the stress contours along the height of the encased columns as extracted from the 3D Fiber (Solid) Model.

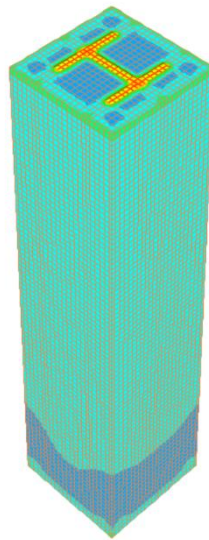
Analysis Approach	AISC 360-16	ACI 318-11	Eurocode-4	3D-Fiber (Solid) Element Model	
Concrete Cylinder Strength (MPa)	70	70	70	70	
Steel Grade (MPa)	S275	S275	S275	S275	
Nominal Compressive Strength (kN)	3,425	3,254	3,038	3,790	
Stresses (MPa)				Concrete Stress (MPa)	Steel Stress (MPa)
Average Stresses on the Encased Column				66	275
Maximum Stresses at the Top of the Encased column connected to CFST				99	405
Strain (ϵ)				Concrete Strain	Steel Strain
Average Strain on the Encased Column				0.00157	0.00138
Maximum Strain at the Top of the Encased column connected to CFST				0.0024	0.00203

Table [4.9] Nominal Compressive Strength of the Encased Composite Column, C70MPa, S275

Stresses of Encased Column



Stress of Concrete Section



Stress of Steel I Section

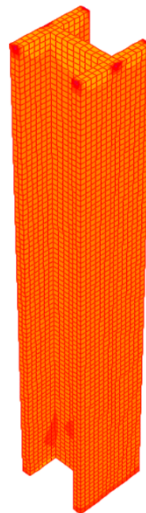


Fig. (4.13) Stresses of the Encased Column under Axial Compression Load

$P_u = 4,000 \text{ kN}$

Concrete Cylinder Strength, C70MPa

Steel Grade, S275MPa

4.4.3.2 Stresses on of the CFST Composite Column subject to Axial Compression Loads.

This clause describes the analysis of the CFST Composite Column under pure axial compression loads. the stresses and strains on the concrete and steel section have been evaluated and compared to the simplified methods adopted by ACI 318-11, AISC 360-16, and Eurocode-4. It was vital to understand the sectional behavior under different concrete cylinder strengths ranging from C40MPa to C70MPa, with different Young's Modulus of Elasticity as summarized in clause 4.4.3.

Furthermore; the capacity of the composite section has been evaluated using two different steel grades, S275MPa and S355MPa.

4.4.3.2.1 CFST Column Analysis under Axial Compression Load, C40MPa, S355MPa

The following [table \[4.10\]](#) summarizes the nominal compressive loads using simplified approach adopted by AISC 360-16, ACI318-11, and Eurocode-4. In addition; it shows the stresses and strains of the concrete and steel elements extracted from the 3D -Fiber (Solid) Model. The analysis showing in the below [table \[4.10\]](#) has been performed using Concrete Cylinder Strength of C40MPa, and Steel Grade of S355MPa.

[Fig. \(4.14\)](#) presents the stress contours along the height of the CFST columns as extracted from the 3D Fiber (Solid) Model.

Analysis Approach	AISC 360-16	ACI 318-11	Eurocode-4	3D-Fiber (Solid) Element Model	
Concrete Cylinder Strength (MPa)	40	40	40	40	
Steel Grade (MPa)	S355	S355	S355	S355	
Nominal Compressive Strength (kN)	3,071	2,610	2,783	3,500	
Stresses (MPa)				Concrete Stress	Steel Stress
Average Stresses on the CFST Column				40	240
Maximum Stresses at the interface with the Stiffener Plates.				75	355
Strain (ϵ)				Concrete Strain	Steel Strain
Average Strain on the CFST Column				0.001346	0.001200
Maximum Strain at the interface with the stiffener plates				0.002523	0.001775

[Table \[4.10\]](#) Nominal Compressive Strength of the CFST Composite Column, C40MPa, S355

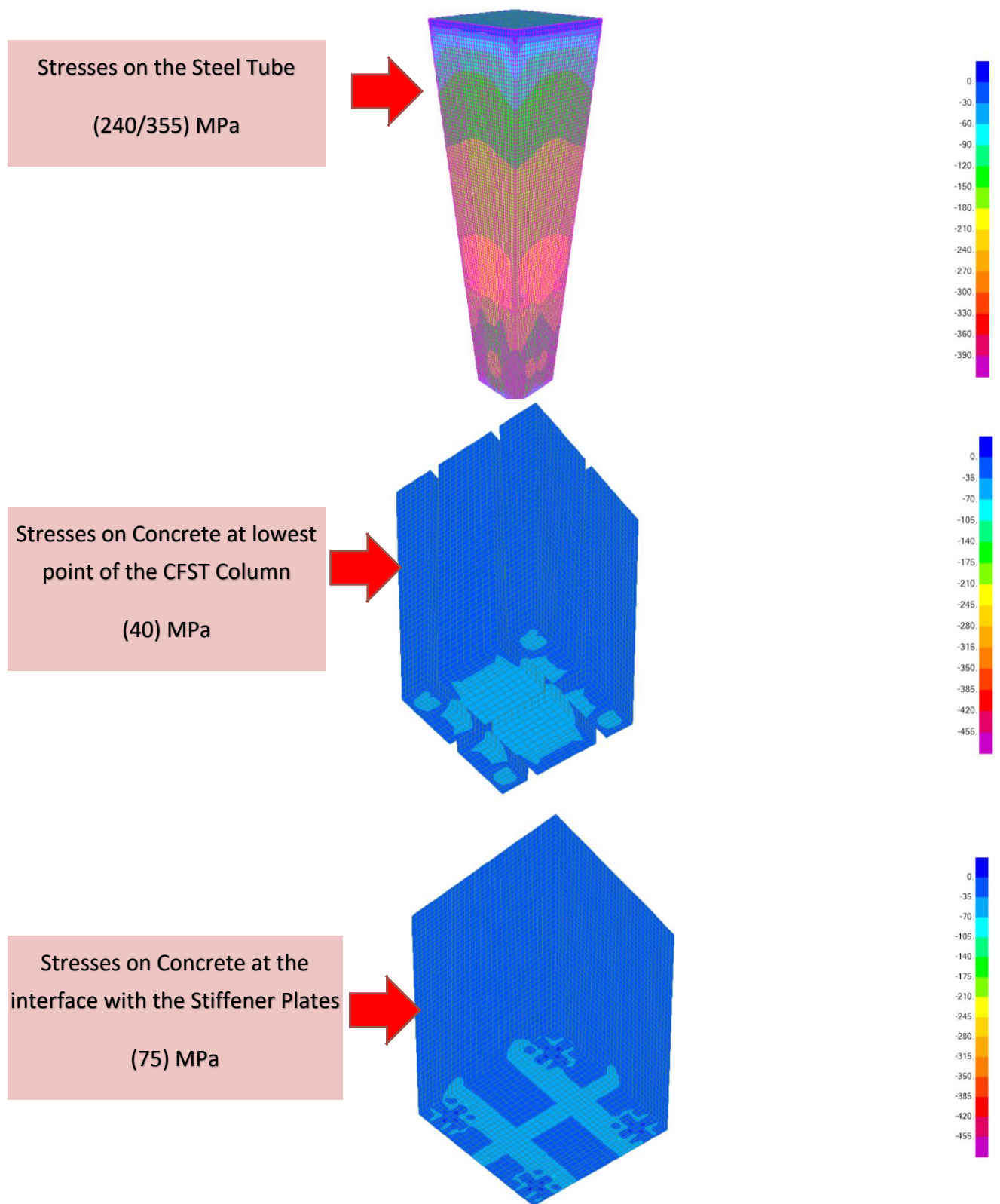


Fig. (4.14) Stresses along CFST Column, C40MPa, S335MPa

4.4.3.2.2 CFST Column Analysis under Axial Compression Load, C50MPa, S355MPa

The following [table \[4.11\]](#) summarizes the nominal compressive loads using simplified approach adopted by AISC 360-16, ACI 318-11, and Eurocode-4. In addition; it shows the stresses and strains of the concrete and steel elements extracted from the 3D -Fiber (Solid) Model.

The analysis showing in the below [table \[4.11\]](#) has been performed using Concrete Cylinder Strength of C50MPa, and Steel Grade of S355MPa.

[Fig. \(4.15\)](#) presents the stress contours along the height of the CFST columns as extracted from the 3D Fiber (Solid) Model.

Analysis Approach	AISC 360-16	ACI 318-11	Eurocode-4	3D-Fiber (Solid) Element Model	
Concrete Cylinder Strength (MPa)	50	50	50	50	
Steel Grade (MPa)	S355	S355	S355	S355	
Nominal Compressive Strength (kN)	3,404	2,893	3,044	4,000	
Stresses (MPa)				Concrete Stress (MPa)	Steel Stress (MPa)
Average Stresses on the CFST Column				50	260
Maximum Stresses at the interface with the Stiffener Plates.				86	375
Strain (ϵ)				Concrete Strain	Steel Strain
Average Strain on the CFST Column				0.001504	0.0013
Maximum Strain at the interface with the stiffener plates				0.002588	0.001875

Table [4.11] Nominal Compressive Strength of the CFST Composite Column, C50MPa, S355

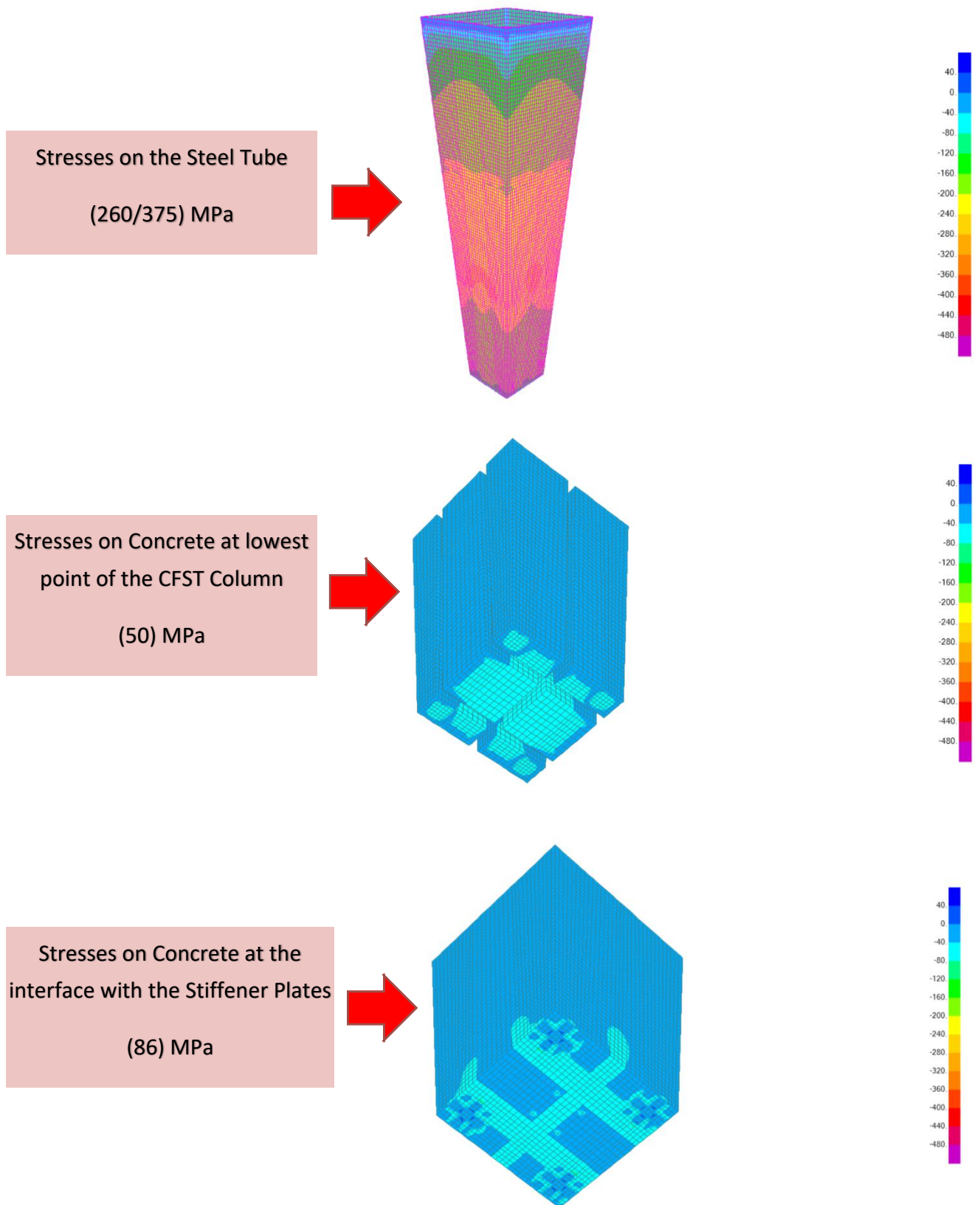


Fig. (4.15) Stresses along CFST Column, C50MPa, S355MPa

4.4.3.2.3 CFST Column Analysis under Axial Compression Load, C60MPa, S355MPa

The following [table \[4.12\]](#) summarizes the nominal compressive loads using simplified approach adopted by AISC 360-16, ACI 318-11, and Eurocode-4. In addition; it shows the stresses and strains of the concrete and steel elements extracted from the 3D -Fiber (Solid) Model.

The analysis showing in the below [table \[4.12\]](#) has been performed using Concrete Cylinder Strength of C60MPa, and Steel Grade of S355MPa.

[Fig. \(4.16\)](#) presents the stress contours along the height of the CFST columns as extracted from the 3D Fiber (Solid) Model.

Analysis Approach	AISC 360-16	ACI 318-11	Eurocode-4	3D-Fiber (Solid) Element Model	
Concrete Cylinder Strength (MPa)	60	60	60	60	
Steel Grade (MPa)	S355	S355	S355	S355	
Nominal Compressive Strength (kN)	3,737	3,176	3,306	4,500	
Stresses (MPa)				Concrete Stress (MPa)	Steel Stress (MPa)
Average Stresses on the CFST Column				60	260
Maximum Stresses at the interface with the Stiffener Plates.				99	367
Strain (ϵ)				Concrete Strain	Steel Strain
Average Strain on the CFST Column				0.001499	0.0013
Maximum Strain at the interface with the stiffener plates				0.002474	0.00184

Table [4.12] Nominal Compressive Strength of the CFST Composite Column, C60MPa, S355

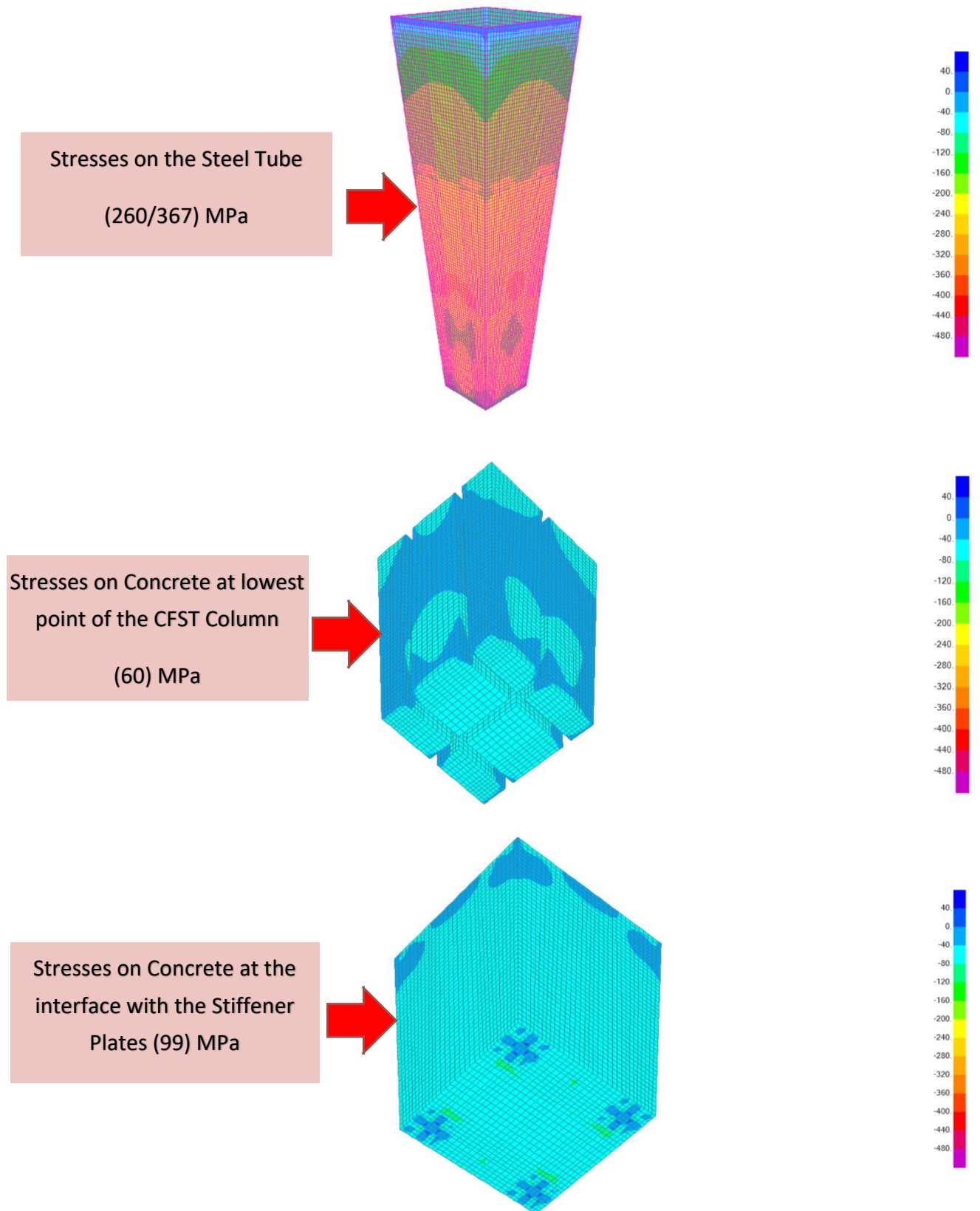


Fig. (4.16) Stresses along CFST Column, C60MPa, S355MPa

4.4.3.2.4 CFST Column Analysis under Axial Compression Load, C70MPa, S355MPa

The following [table \[4.13\]](#) summarizes the nominal compressive loads using simplified approach adopted by AISC 360-16, ACI 318-11, and Eurocode-4. In addition; it shows the stresses and strains of the concrete and steel elements extracted from the 3D -Fiber (Solid) Model.

The analysis showing in the below [table \[4.13\]](#) has been performed using Concrete Cylinder Strength of C70MPa, and Steel Grade of S355MPa.

[Fig. \(4.17\)](#) presents the stress contours along the height of the CFST columns as extracted from the 3D Fiber (Solid) Model.

Analysis Approach	AISC 360-16	ACI 318-11	Eurocode-4	3D-Fiber (Solid) Element Model	
Concrete Cylinder Strength (MPa)	70	70	70	70	
Steel Grade (MPa)	S355	S355	S355	S355	
Nominal Compressive Strength (kN)	4,070	3,460	3,567	5,000	
Stresses (MPa)				Concrete Stress (MPa)	Steel Stress (MPa)
Average Stresses on the CFST Column				70	282
Maximum Stresses at the interface with the Stiffener Plates.				110	392
Strain (ϵ)				Concrete Strain	Steel Strain
Average Strain on the CFST Column				0.00166	0.00141
Maximum Strain at the interface with the stiffener plates				0.00261	0.00196

Table [4.13] Nominal Compressive Strength of the CFST Composite Column, C70MPa, S355

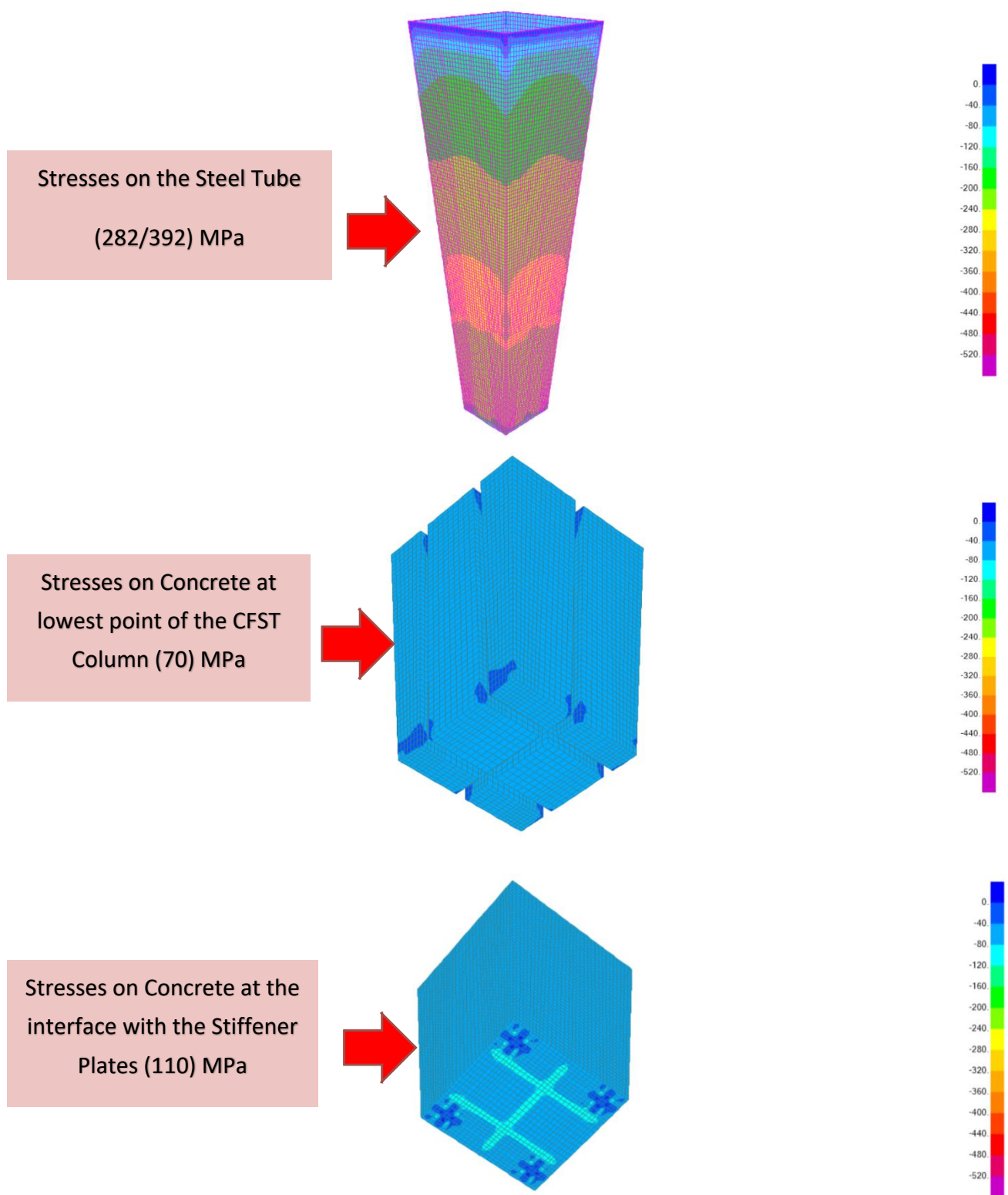


Fig. (4.17) Stresses along CFST Column, C70MPa, S355MPa

4.4.3.2.5 CFST Column Analysis under Axial Compression Load, C40MPa, S275MPa

The following [table \[4.14\]](#) summarizes the nominal compressive loads using simplified approach adopted by AISC 360-16, ACI 318-11, and Eurocode-4. In addition; it shows the stresses and strains of the concrete and steel elements extracted from the 3D -Fiber (Solid) Model.

The analysis showing in the below [table \[4.14\]](#) has been performed using Concrete Cylinder Strength of C40MPa, and Steel Grade of S275MPa.

[Fig. \(4.18\)](#) presents the stress contours along the height of the CFST columns as extracted from the 3D Fiber (Solid) Model.

Analysis Approach	AISC 360-16	ACI 318-11	Eurocode-4	3D-Fiber (Solid) Element Model	
Concrete Cylinder Strength (MPa)	40	40	40	40	
Steel Grade (MPa)	S275	S275	S275	S275	
Nominal Compressive Strength (kN)	2,679	2,277	2,391	3,500	
Stresses (MPa)				Concrete Stress (MPa)	Steel Stress (MPa)
Average Stresses on the CFST Column				40	240
Maximum Stresses at the interface with the Stiffener Plates.				75	355
Strain (ε)				Concrete Strain	Steel Strain
Average Strain on the CFST Column				0.001346	0.00123
Maximum Strain at the interface with the stiffener plates				0.002523	0.00180

Table [4.14] Nominal Compressive Strength of the CFST Composite Column, C40MPa, S275

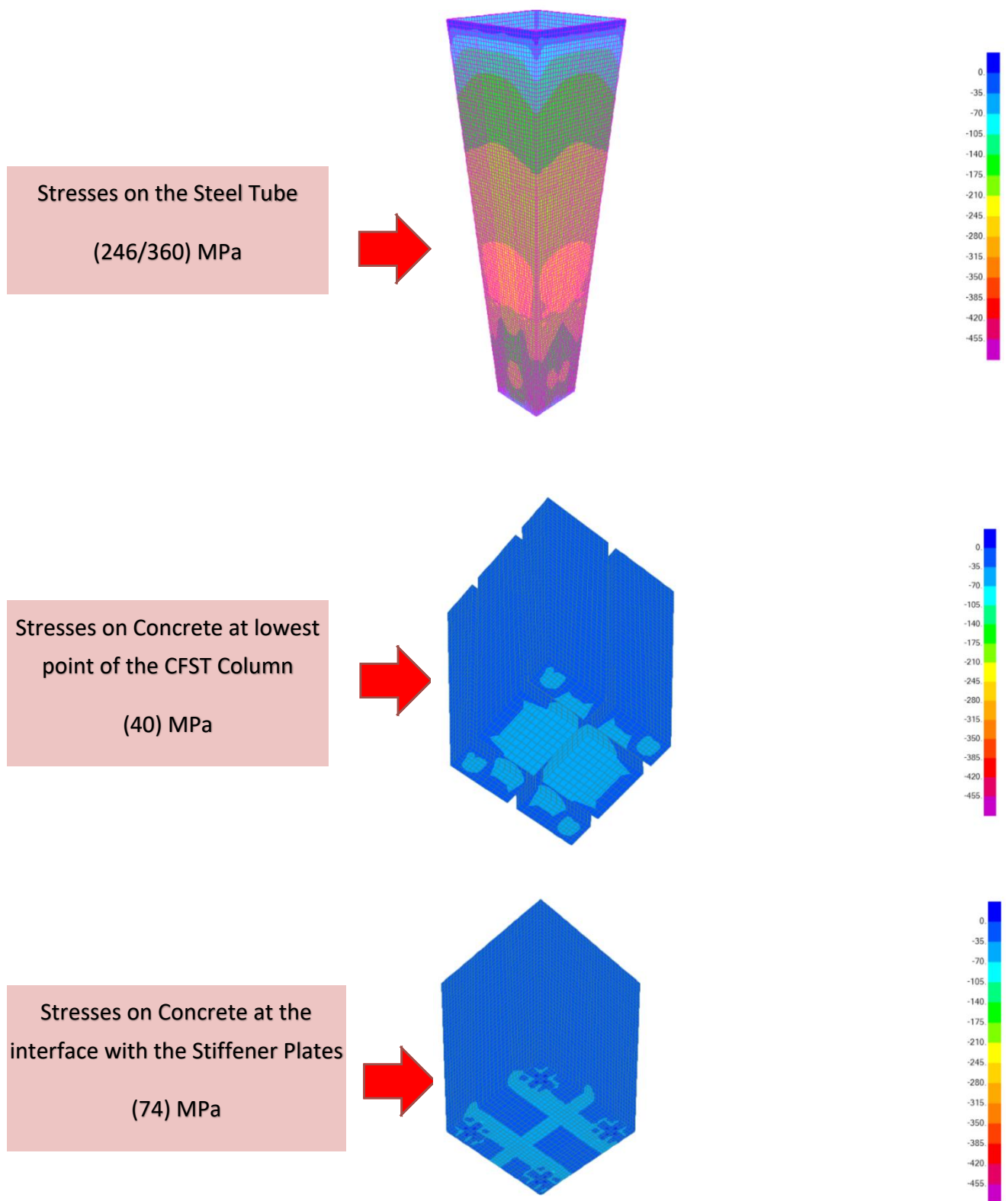


Fig. (4.18) Stresses along CFST Column, C40MPa, S275MPa

4.4.3.2.6 CFST Column Analysis under Axial Compression Load, C50MPa, S275MPa

The following [table \[4.15\]](#) summarizes the nominal compressive loads using simplified approach adopted by AISC 360-16, ACI 318-11, and Eurocode-4. In addition; it shows the stresses and strains of the concrete and steel elements extracted from the 3D -Fiber (Solid) Model.

The analysis showing in the below [table \[4.15\]](#) has been performed using Concrete Cylinder Strength of C50MPa, and Steel Grade of S275MPa.

Fig. (4.19) presents the stress contours along the height of the CFST columns as extracted from the 3D Fiber (Solid) Model.

Analysis Approach	AISC 360-16	ACI 318-11	Eurocode-4	3D-Fiber (Solid) Element Model	
Concrete Cylinder Strength (MPa)	50	50	50	50	
Steel Grade (MPa)	S275	S275	S275	S275	
Nominal Compressive Strength (kN)	3,012	2,560	2,653	4,000	
Stresses (MPa)				Concrete Stress (MPa)	Steel Stress (MPa)
Average Stresses on the CFST Column				50	260
Maximum Stresses at the interface with the Stiffener Plates.				86	375
Strain (ϵ)				Concrete Strain	Steel Strain
Average Strain on the CFST Column				0.001504	0.001315
Maximum Strain at the interface with the stiffener plates				0.002588	0.00189

Table [4.15] Nominal Compressive Strength of the CFST Composite Column, C50MPa, S275

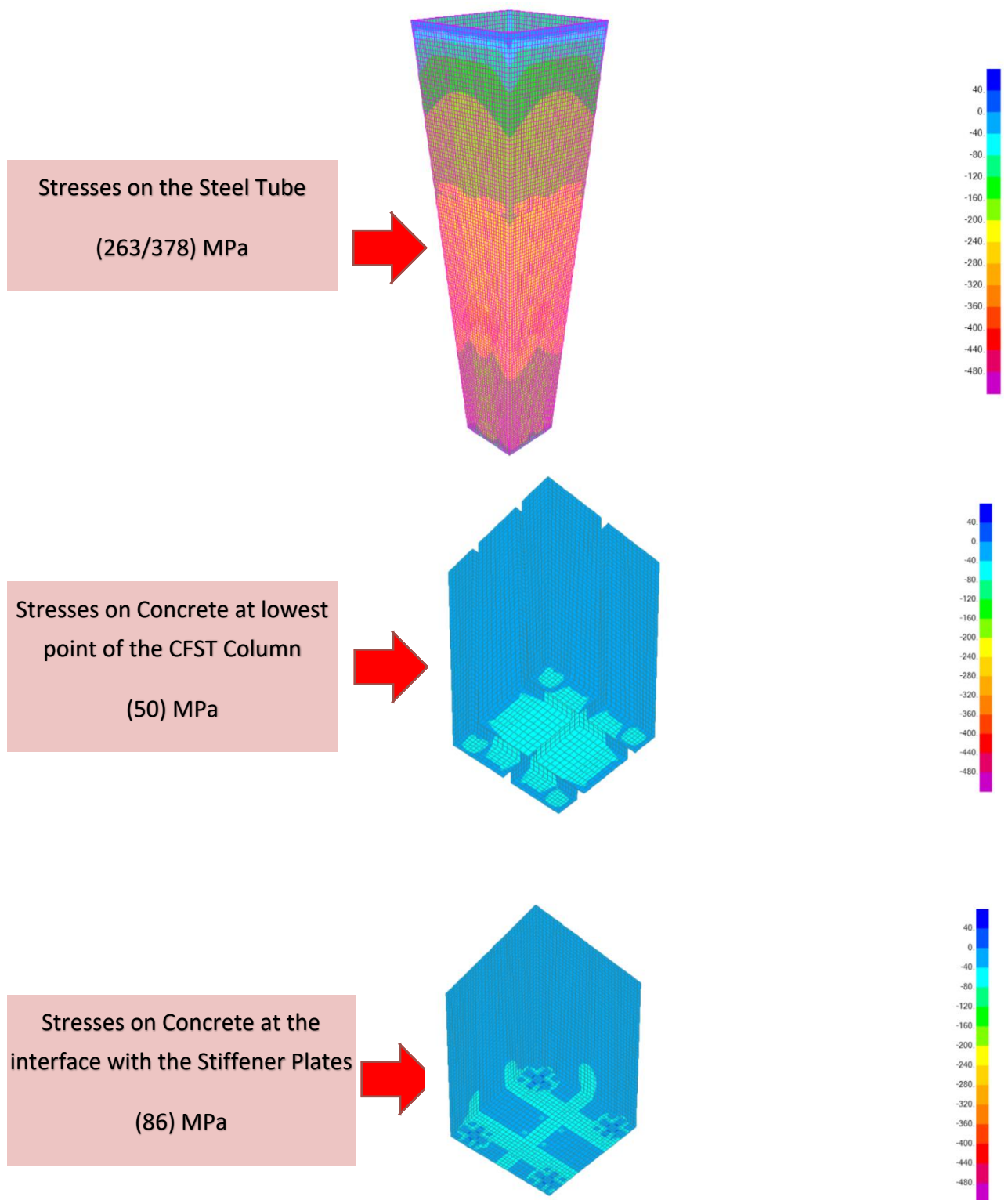


Fig. (4.19) Stresses along CFST Column, C50MPa, S275MPa

4.4.3.2.7 CFST Column Analysis under Axial Compression Load, C60MPa, S275MPa

The following [table \[4.16\]](#) summarizes the nominal compressive loads using simplified approach adopted by AISC 360-16, ACI 318-11, and Eurocode-4. In addition; it shows the stresses and strains of the concrete and steel elements extracted from the 3D -Fiber (Solid) Model.

The analysis showing in the below [table \[4.16\]](#) has been performed using Concrete Cylinder Strength of C60MPa, and Steel Grade of S275MPa.

[Fig. \(4.20\)](#) presents the stress contours along the height of the CFST columns as extracted from the 3D Fiber (Solid) Model.

Analysis Approach	AISC 360-16	ACI 318-11	Eurocode-4	3D-Fiber (Solid) Element Model	
Concrete Cylinder Strength (MPa)	60	60	60	60	
Steel Grade (MPa)	S275	S275	S275	S275	
Nominal Compressive Strength (kN)	3,345	2,843	2,914	4,500	
Stresses (MPa)				Concrete Stress (MPa)	Steel Stress (MPa)
Average Stresses on the CFST Column				60	260
Maximum Stresses at the interface with the Stiffener Plates.				99	367
Strain (ϵ)				Concrete Strain	Steel Strain
Average Strain on the CFST Column				0.0015	0.00132
Maximum Strain at the interface with the stiffener plates				0.00247	0.00184

Table [4.16] Nominal Compressive Strength of the CFST Composite Column, C60MPa, S275

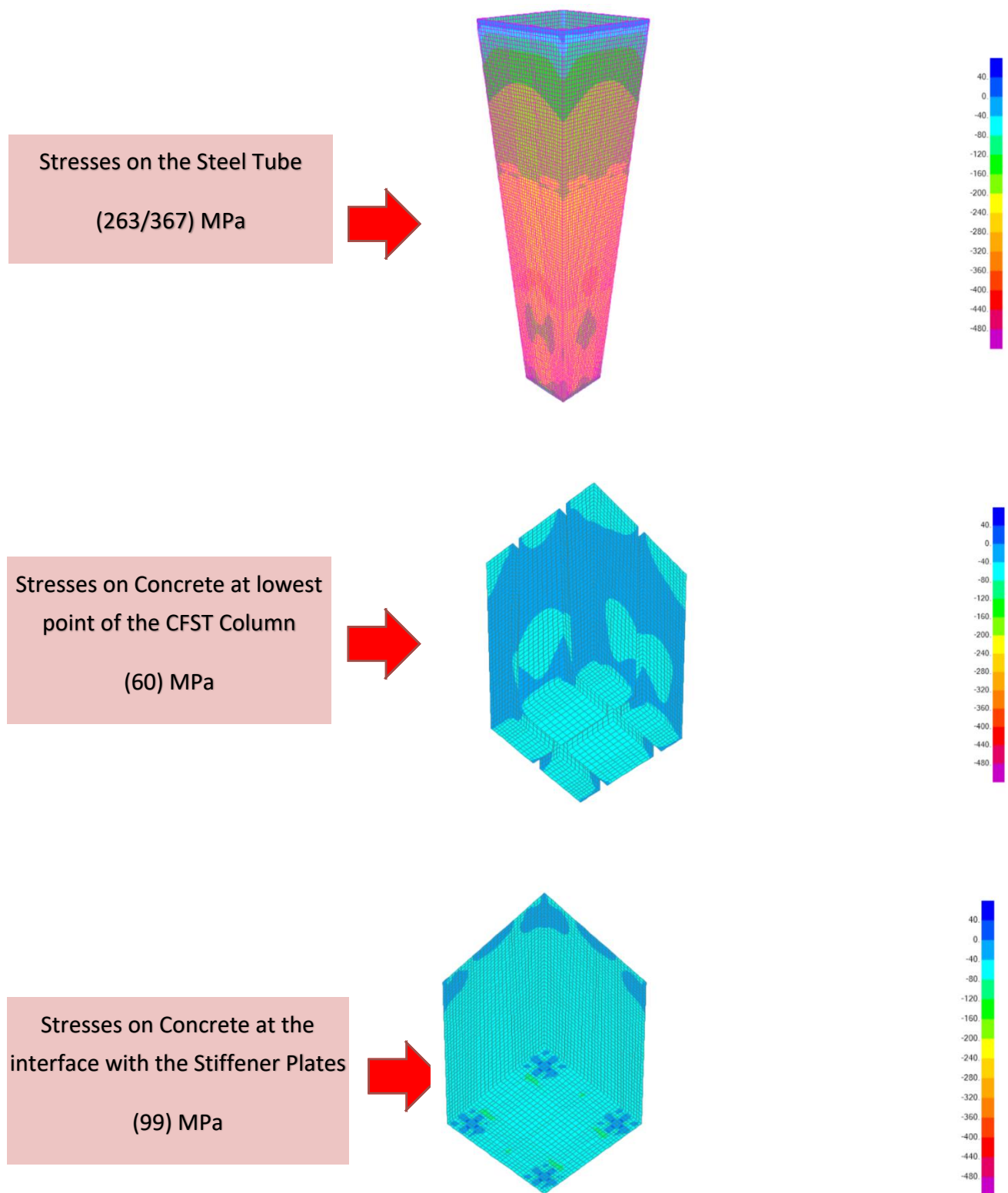


Fig. (4.20) Stresses along CFST Column, C60MPa, S275MPa

4.4.3.2.8 CFST Column Analysis under Axial Compression Load, C70MPa, S275MPa

The following [table \[4.17\]](#) summarizes the nominal compressive loads using simplified approach adopted by AISC 360-16, ACI 318-11, and Eurocode-4. In addition; it shows the stresses and strains of the concrete and steel elements extracted from the 3D -Fiber (Solid) Model.

The analysis showing in the below [table \[4.17\]](#) has been performed using Concrete Cylinder Strength of C70MPa, and Steel Grade of S275MPa.

[Fig. \(4.21\)](#) presents the stress contours along the height of the CFST columns as extracted from the 3D Fiber (Solid) Model.

Analysis Approach	AISC 360-16	ACI 318-11	Eurocode-4	3D-Fiber (Solid) Element Model	
Concrete Cylinder Strength (MPa)	70	70	70	70	
Steel Grade (MPa)	S275	S275	S275	S275	
Nominal Compressive Strength (kN)	3,679.04	3,127.18	3,175.92	4,875	
Stresses (MPa)				Concrete Stress (MPa)	Steel Stress (MPa)
Average Stresses on the CFST Column				68	275
Maximum Stresses at the interface with the Stiffener Plates.				107	390
Strain (ϵ)				Concrete Strain	Steel Strain
Average Strain on the CFST Column				0.00162	0.001375
Maximum Strain at the interface with the stiffener plates				0.00254	0.00195

Table [4.17] Nominal Compressive Strength of the CFST Composite Column, C70MPa, S275

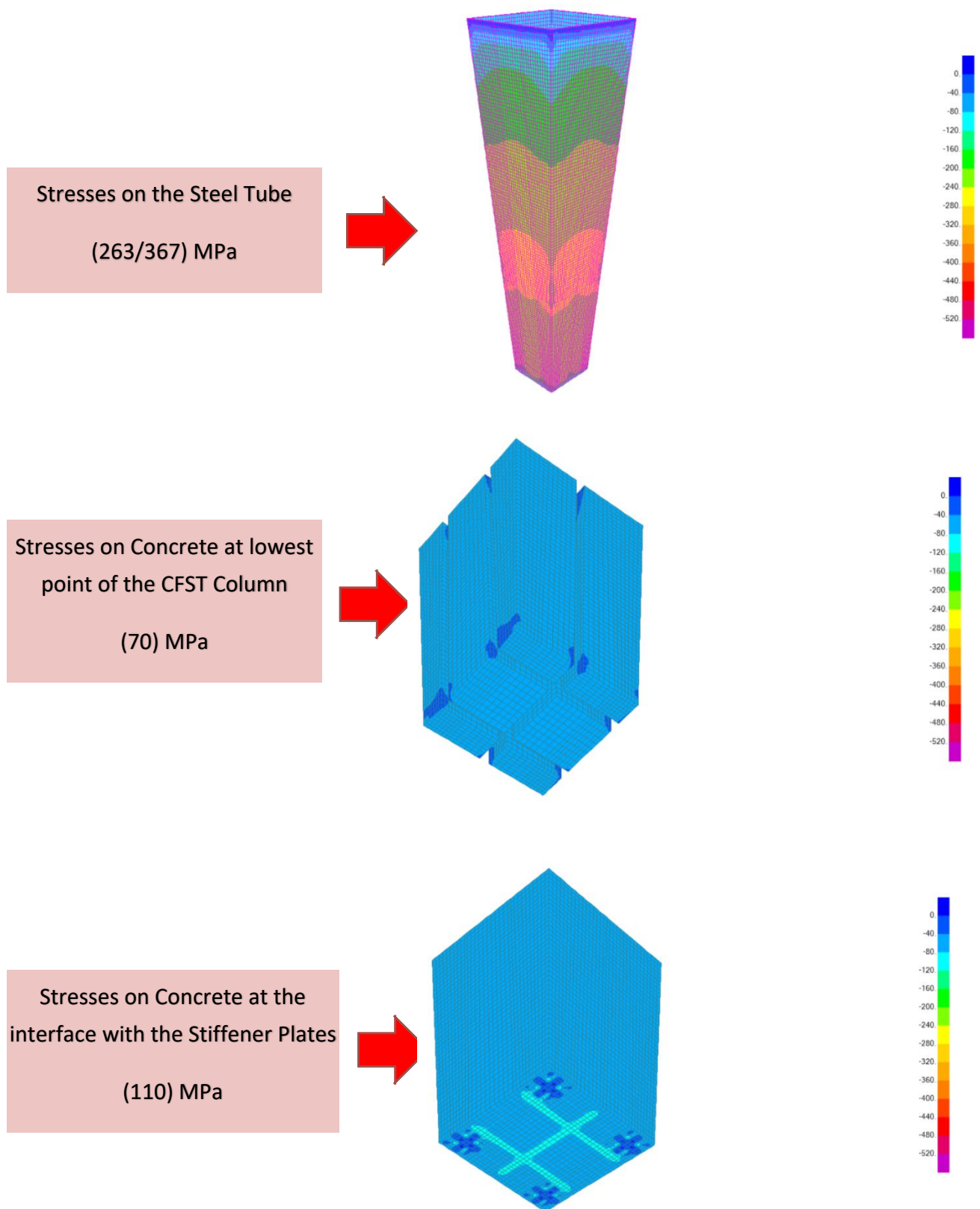


Fig. (4.21) Stresses along CFST Column, C70MPa, S275MPa

4.4.3.3 Stresses on the Stiffener Plates welded to the CFST and Encased Element under Axial Compression Loads.

This clause describes the analysis of stiffener plates connected to the CFST Tube and I section under pure axial compression loads. The stresses and strains on the steel plates have been presented in the below table

It was vital to understand the stresses transferred through stiffener plates using different concrete cylinder strengths ranging from C40MPa to C70MPa, with different Young's Modulus of Elasticity as summarized in clause 4.4.3.

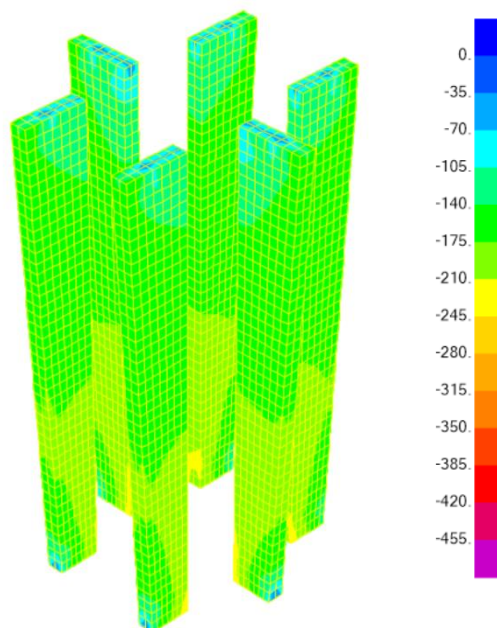
Furthermore; the stresses have been evaluated using two different steel grades, S275MPa and S355MPa.

Table [4.18] illustrates the stresses on the steel stiffener plates under different concrete strengths and using two different steel grades.

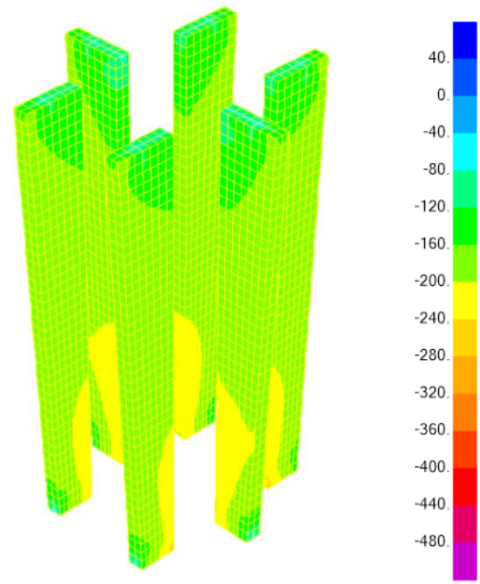
Fig. (4.22) demonstrates the stress contours along the height of the stiffener plates as extracted from the 3D Fiber (Solid) Model.

Steel Grade, (MPa)	S355	S355	S355	S355
Concrete Cylinder Strength (MPa)	C40MPa	C50MPa	C60MPa	C70MPa
Steel Stresses (MPa)	238	260	270	293
Steel Strain	0.00119	0.0013	0.00135	0.001465
Steel Grade, (MPa)	S275	S275	S275	S275
Concrete Cylinder Strength (MPa)	C40MPa	C50MPa	C60MPa	C70MPa
Steel Stresses (MPa)	238	260	270	293
Steel Strain	0.00119	0.0013	0.00135	0.001465

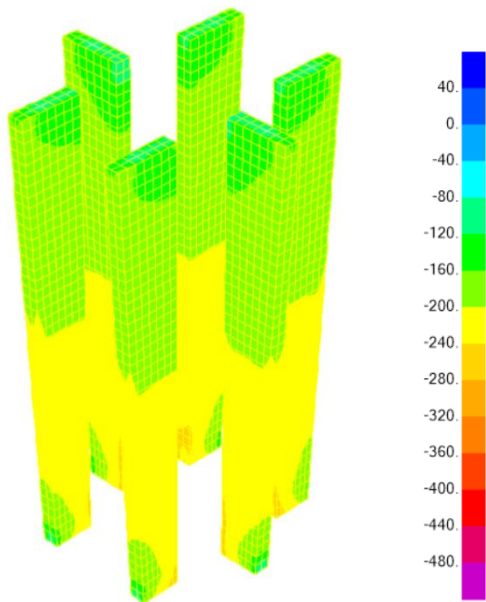
Table [4.18] Stresses on the Steel Stiffener Plates



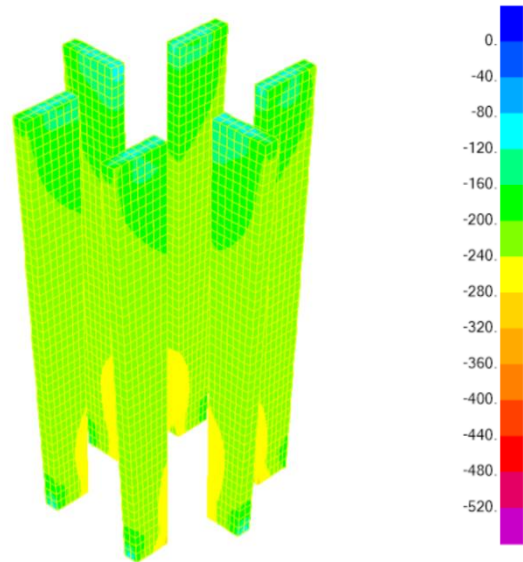
C40MPa



C50MPa



C60MPa



C70MPa

Fig. (4.22) Stresses' Contours Along Stiffener Plates under Axial Compression Loads

4.4.4 COLUMN RESISTANCE TO AXIAL COMPRESSION AND UNI-DIRECTION MOMENTS

The second approach in this research is to examine the column under axial compression and uni-direction bending moments.

The column has been modeled using four different cylinder concrete strengths, 40, 50, 60, and 70MPa.

Each concrete strength has been analyzed using two different steel strength, S275MPa and S355MPa inline with EN 1993-1-1.

The sectional capacity has been checked using AISC 360-16, Eurocode-4 and compared with the output from the 3D-Fiber (Solid) Element Model.

The Finite element has been divided into 3 parts, the first part is the encased column, the second part is the CFST column, and the third part is the stiffener plates connecting I section to CFST tube.

The Concrete Modulus of Elasticity has been determined as follow:

- C40MPa, $E_c = 29,725 \text{ MPa}$
- C50MPa, $E_c = 33,234 \text{ MPa}$
- C60MPa, $E_c = 40,022 \text{ MPa}$
- C70MPa, $E_c = 42,079 \text{ MPa}$

The Steel Modulus of Elasticity is equal to 200,000 MPa

4.4.4.1 Stresses on the Encased Composite Column subject to Axial Compression and Uni-Direction Moments

This clause describes the analysis of the encased Composite Column subject to axial compression loads and uni-direction moments. The stresses and strains on the concrete and steel section have been evaluated and compared to the simplified methods adopted by AISC 360-16, and Eurocode-4.

It was vital to understand the sectional behavior under different concrete cylinder strengths ranging from C40MPa to C70MPa, with different Young's Modulus of Elasticity as summarized in **clause 4.4.4**.

Furthermore; the capacity of the composite section has been evaluated using two different steel grades, S275MPa and S355MPa.

4.4.4.1.1 Encased Column Analysis under Axial Compression and Uni-Direction Moments, C40MPa, S355MPa.

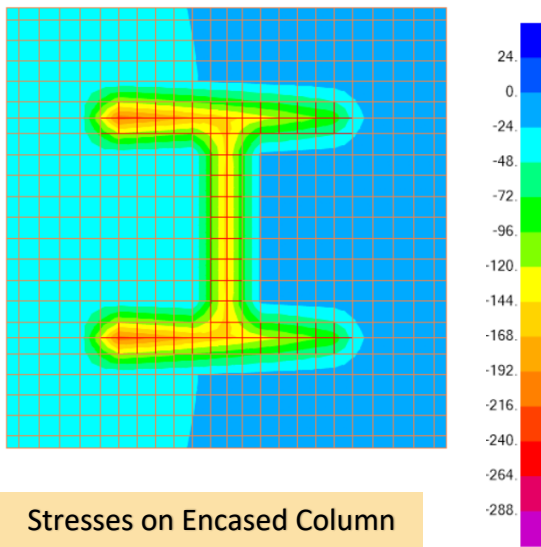
The following [table \[4.19\]](#) summarizes the Encased Column Sectional Capacity under Axial compression and uni-direction moments. The section capacity has been determined using simplified approach adopted by AISC 360-16, and Eurocode-4. In addition; it shows the stresses and strains of the concrete and steel elements extracted from the 3D -Fiber (Solid) Model. The load eccentricity was constant of 85.75mm from the cross-sectional centroid.

The analysis showing in the below [table \[4.19\]](#) has been performed using Concrete Cylinder Strength of C40MPa, and Steel Grade of S355MPa.

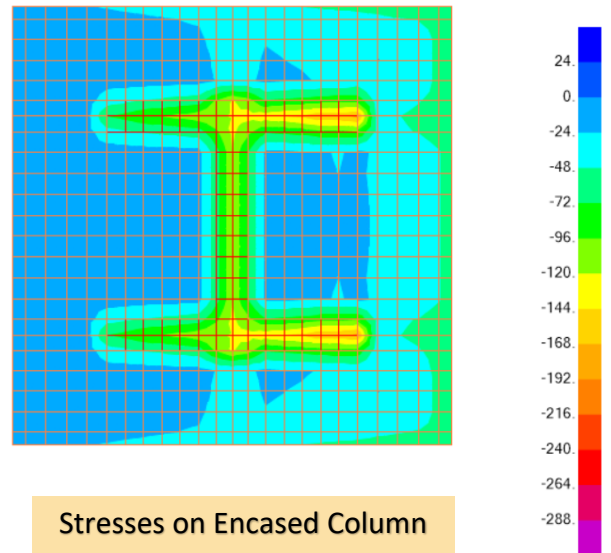
[Fig. \(4.23\)](#) presents the stress contours along the height of the encased columns as extracted from the 3D Fiber (Solid) Model.

Analysis Approach	AISC 360-16	Eurocode-4	3D-Fiber (Solid) Element Model	
Concrete Cylinder Strength (MPa)	40	40	40	
Steel Grade (MPa)	S355	S355	S355	
Nominal Compressive Strength, P_u (kN)	1,625	1,525	1,625	
Load Eccentricity, e (mm)	85.75	85.75	85.75	
Bending Moments at the Top of the Column, $M = P.e$ (kN.m)	139.34	130.77	139.34	
Section Capacity (D/C)	1.0	1.0		
Stresses on the Fiber (Solid) Model under 1,625 kN			Concrete Stress (MPa)	Steel Stress (MPa)
Average Stresses on the Encased Column			(40) Bottom of the Concrete	(220) Top of the Steel Section
Maximum Stresses			(76.89) Bottom of Concrete	(311.73) Top of Steel Section
Strain (ϵ)			Concrete Strain	Steel Strain
Average Strain on the Encased Column			0.001346	0.0011
Maximum Strain at the Top of the Encased column connected to CFST			0.002587	0.001559

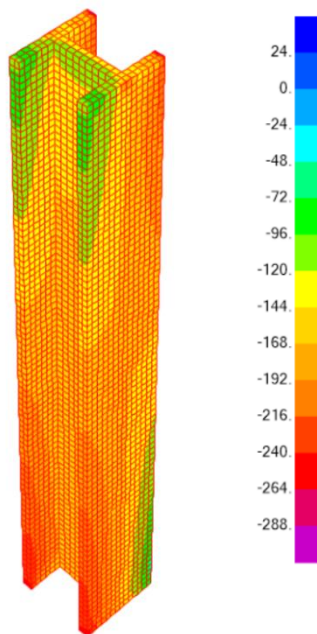
Table [4.19] Encased Column Section Capacity under Axial Compression and Uni-Direction Bending, C40MPa, S355



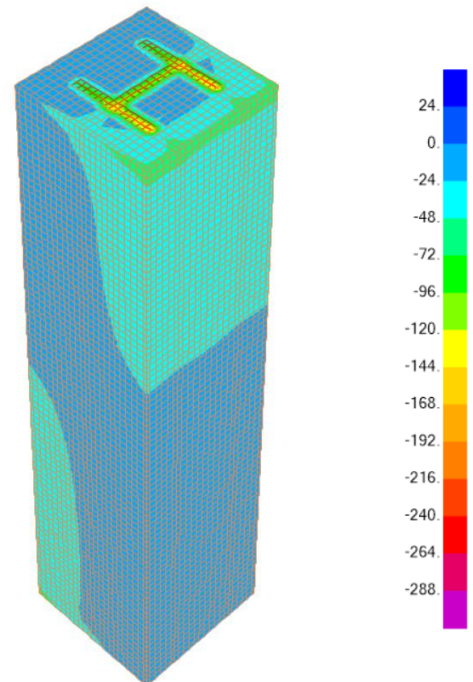
Stresses on Encased Column
Bottom View



Stresses on Encased Column
Top View



Stresses on Steel I Section



Stresses on Encased Column

Fig. (4.23) Stresses' Contours Along Encased Composite Column, C40MPa, S355MPa

4.4.4.1.2 Encased Column Analysis under Axial Compression and Uni-Direction Moments, C50MPa, S355MPa.

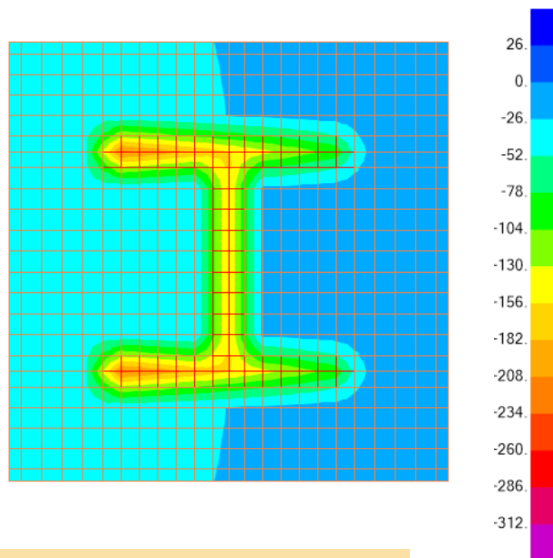
The following [table \[4.20\]](#) summarizes the Encased Column Sectional Capacity under Axial compression and uni-direction moments. The section capacity has been determined using simplified approach adopted by AISC 360-16, and Eurocode-4. In addition; it shows the stresses and strains of the concrete and steel elements extracted from the 3D -Fiber (Solid) Model. The load eccentricity was constant of 85.75mm from the cross-sectional centroid.

The analysis showing in the below [table \[4.20\]](#) has been performed using Concrete Cylinder Strength of C50MPa, and Steel Grade of S355MPa.

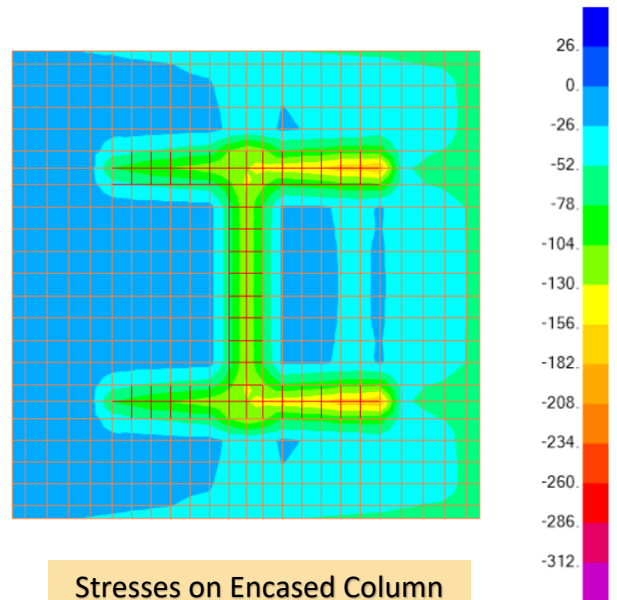
[Fig. \(4.24\)](#) presents the stress contours along the height of the encased columns as extracted from the 3D Fiber (Solid) Model.

Analysis Approach	AISC 360-16	Eurocode-4	3D-Fiber (Solid) Element Model	
Concrete Cylinder Strength (MPa)	50	50	50	
Steel Grade (MPa)	S355	S355	S355	
Nominal Compressive Strength, P_u (kN)	1,775	1,665	1,775	
Load Eccentricity, e (mm)	85.75	85.75	85.75	
Bending Moments at the Top of the Column, $M = P.e$ (kN.m)	152.21	142.77	152.21	
Section Capacity (D/C)	1.0	--		
Stresses on the Fiber (Solid) Model under 1,775 kN			Concrete Stress (MPa)	Steel Stress (MPa)
Average Stresses on the Encased Column			(50) Top and bottom of concrete	(225) Top and Bottom of Steel Section
Maximum Stresses			(87.38) Bottom of Concrete Section	(311.47) Top of Steel Section
Strain (ϵ)			Concrete Strain	Steel Strain
Average Strain on the Encased Column			0.00263	0.00156
Maximum Strain at the Top of the Encased column connected to CFST			0.00150	0.001125

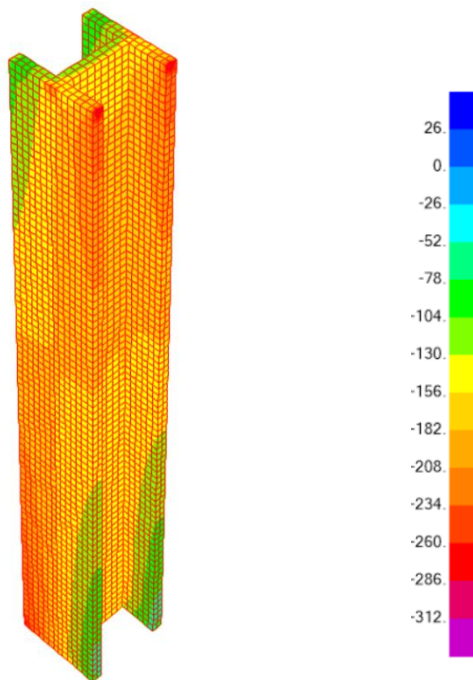
Table [4.20] Encased Column Section Capacity under Axial Compression and Uni-Direction Bending, C50MPa, S355



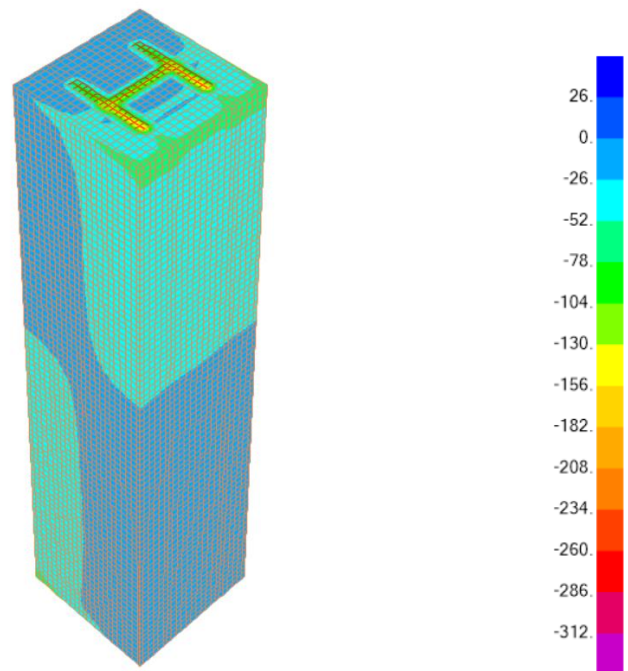
Stresses on Encased Column
Bottom View



Stresses on Encased Column
Top View



Stresses on Steel I Section



Stresses on Encased Column

Fig. (4.24) Stresses' Contours Along Encased Composite Column, C50MPa, S355MPa

4.4.4.1.3 Encased Column Analysis under Axial Compression and Uni-Direction Moments, C60MPa, S355MPa.

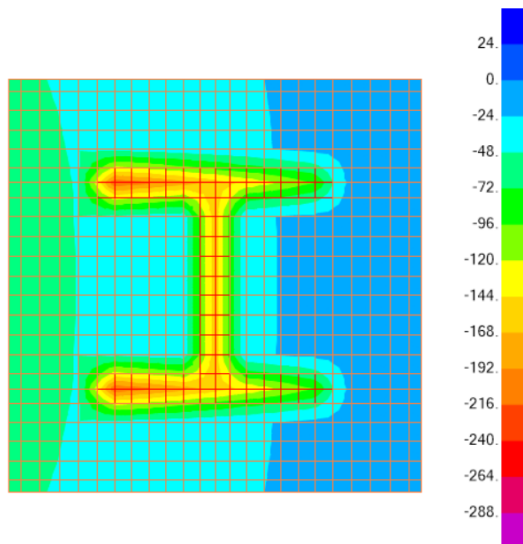
The following [table \[4.21\]](#) summarizes the Encased Column Sectional Capacity under Axial compression and uni-direction moments. The section capacity has been determined using simplified approach adopted by AISC 360-16, and Eurocode-4. In addition; it shows the stresses and strains of the concrete and steel elements extracted from the 3D -Fiber (Solid) Model. The load eccentricity was constant of 85.75mm from the cross-sectional centroid.

The analysis showing in the below [table \[4.21\]](#) has been performed using Concrete Cylinder Strength of C60MPa, and Steel Grade of S355MPa.

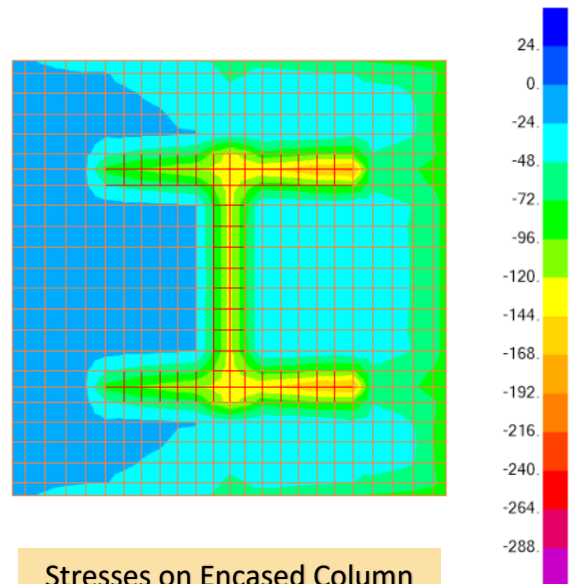
[Fig. \(4.25\)](#) presents the stress contours along the height of the encased columns as extracted from the 3D Fiber (Solid) Model.

Analysis Approach	AISC 360-16	Eurocode-4	3D-Fiber (Solid) Element Model	
Concrete Cylinder Strength (MPa)	60	60	60	
Steel Grade (MPa)	S355	S355	S355	
Nominal Compressive Strength, P_u (kN)	1,975	1,855	1,975	
Load Eccentricity, e (mm)	85.75	85.75	85.75	
Bending Moments at the Top of the Column, $M = P \cdot e$ (kN.m)	169.36	159.07	169.36	
Section Capacity (D/C)	1.0	--		
Stresses on the Fiber (Solid) Model under 1,975 kN			Concrete Stress (MPa)	Steel Stress (MPa)
Average Stresses on the Encased Column			(60) Top and bottom of concrete	(235) Bottom of Steel Section
Maximum Stresses			(103.36) Bottom of Concrete	(296.97) Bottom of Steel Section
Strain (ϵ)			Concrete Strain	Steel Strain
Average Strain on the Encased Column			0.0015	0.001175
Maximum Strain at the Top of the Encased column connected to CFST			0.0026	0.00148

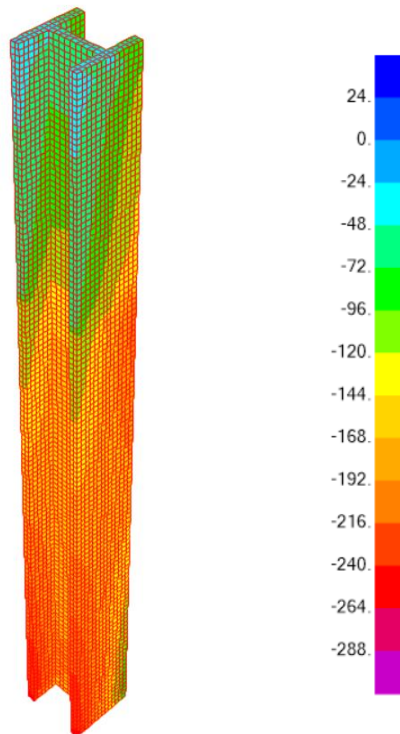
Table [4.21] Encased Column Section Capacity under Axial Compression and Uni-Direction Bending, C60MPa, S355



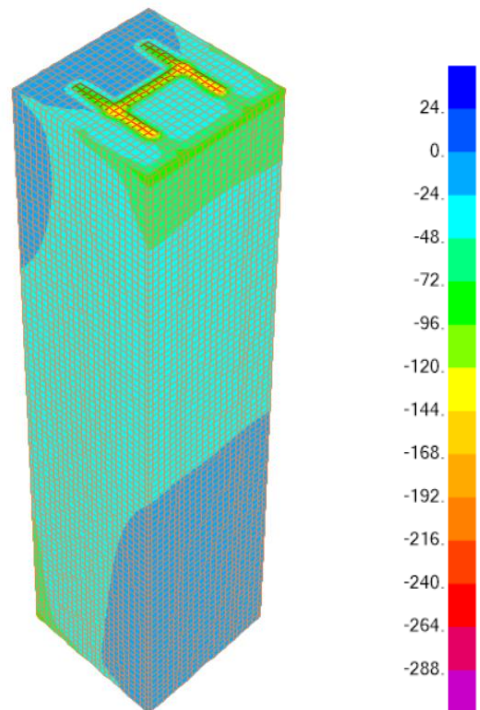
Stresses on Encased Column
Bottom View



Stresses on Encased Column
Top View



Stresses on Steel I Section



Stresses on Encased Column

Fig. (4.25) Stresses' Contours Along Encased Composite Column, C60MPa, S355MPa

4.4.4.1.4 Encased Column Analysis under Axial Compression and Uni-Direction Moments, C70MPa, S355MPa.

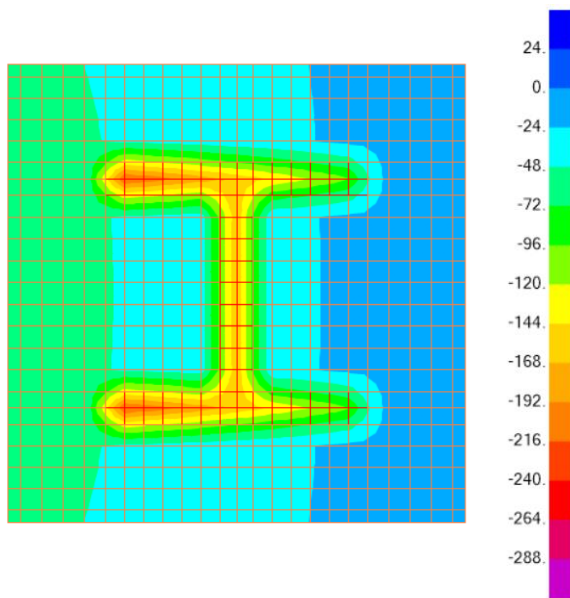
The following [table \[4.22\]](#) summarizes the Encased Column Sectional Capacity under Axial compression and uni-direction moments. The section capacity has been determined using simplified approach adopted by AISC 360-16, and Eurocode-4. In addition; it shows the stresses and strains of the concrete and steel elements extracted from the 3D -Fiber (Solid) Model. The load eccentricity was constant of 85.75mm from the cross-sectional centroid.

The analysis showing in the below [table \[4.22\]](#) has been performed using Concrete Cylinder Strength of C70MPa, and Steel Grade of S355MPa.

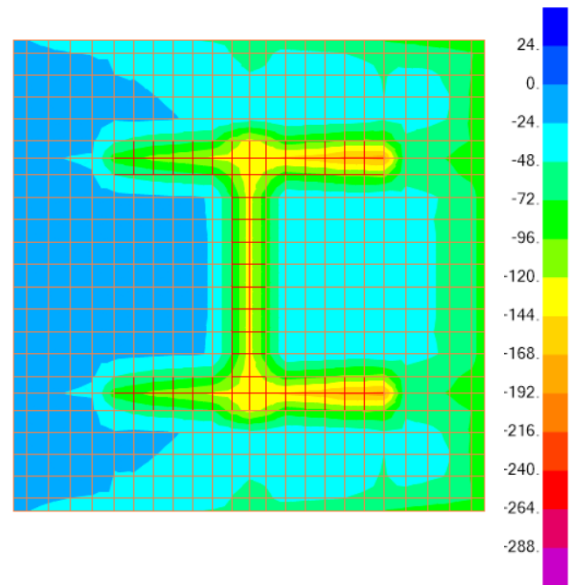
[Fig. \(4.26\)](#) presents the stress contours along the height of the encased columns as extracted from the 3D Fiber (Solid) Model.

Analysis Approach	AISC 360-16	Eurocode-4	3D-Fiber (Solid) Element Model	
Concrete Cylinder Strength (MPa)	70	70	70	
Steel Grade (MPa)	S355	S355	S355	
Nominal Compressive Strength, P_u (kN)	2,075	1,950	2,075	
Load Eccentricity, e (mm)	85.75	85.75	85.75	
Bending Moments at the Top of the Column, $M = P.e$ (kN.m)	177.93	167.21	177.93	
Section Capacity (D/C)	1.0	--		
Stresses on the Fiber (Solid) Model under 2,075 kN			Concrete Stress (MPa)	Steel Stress (MPa)
Average Stresses on the Encased Column			(70) Top & Bottom of concrete	(220) Top & Bottom of Steel Section
Maximum Stresses			(110.28) Bottom of Concrete	(298.89) Top & Bottom of Steel Section
Strain (ϵ)			Concrete Strain	Steel Strain
Average Strain on the Encased Column			0.00166	0.0011
Maximum Strain at the Top of the Encased column connected to CFST			0.00262	0.00149

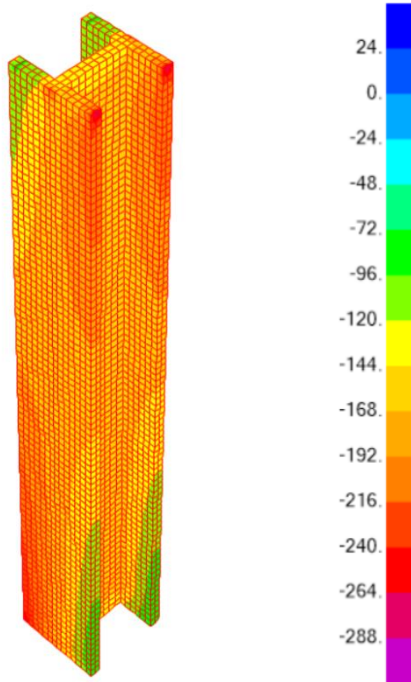
Table [4.22] Encased Column Section Capacity under Axial Compression and Uni-Direction Bending, C70MPa, S355



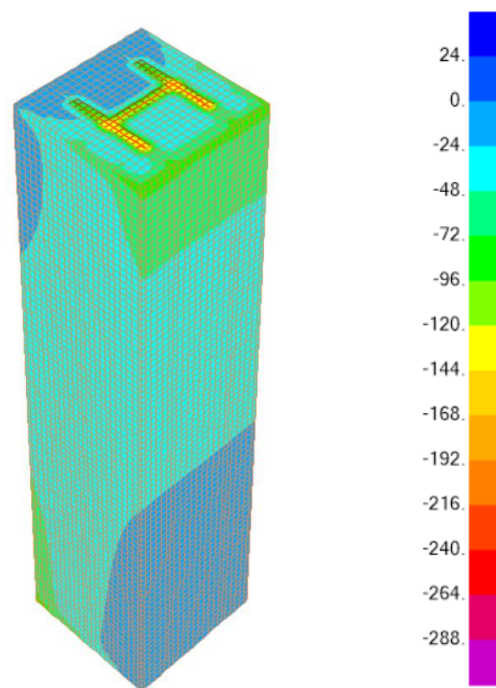
Stresses on Encased Column
Bottom View



Stresses on Encased Column
Top View



Stresses on Steel I Section



Stresses on Encased Column

Fig. (4.26) Stresses' Contours Along Encased Composite Column, C70MPa, S355MPa

4.4.4.1.5 Encased Column Analysis under Axial Compression and Uni-Direction Moments, C40MPa, S275MPa.

The following [table \[4.23\]](#) summarizes the Encased Column Sectional Capacity under Axial compression and uni-direction moments. The section capacity has been determined using simplified approach adopted by AISC 360-16, and Eurocode-4. In addition; it shows the stresses and strains of the concrete and steel elements extracted from the 3D -Fiber (Solid) Model.

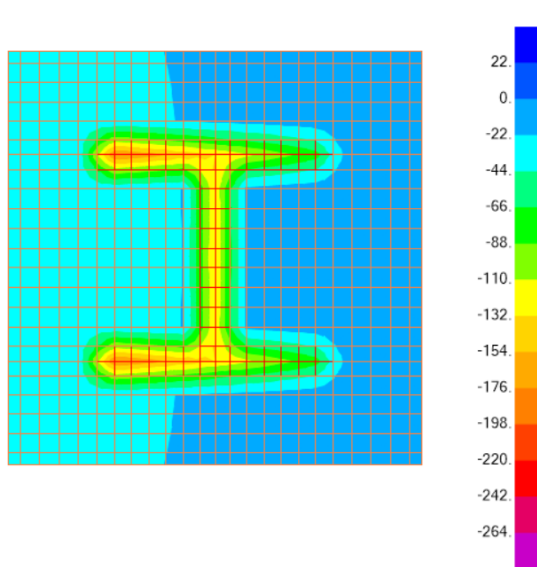
The load eccentricity was constant of 85.75mm from the cross-sectional centroid.

The analysis showing in the below [table \[4.23\]](#) has been performed using Concrete Cylinder Strength of C40MPa, and Steel Grade of S275MPa.

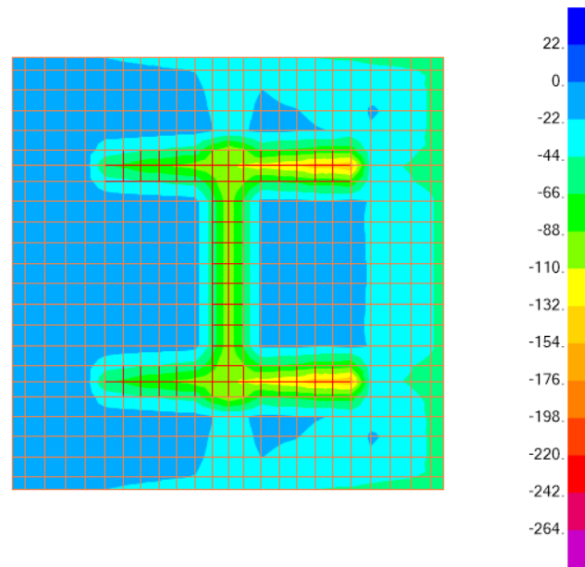
[Fig. \(4.27\)](#) presents the stress contours along the height of the encased columns as extracted from the 3D Fiber (Solid) Model.

Analysis Approach	AISC 360-16	Eurocode-4	3D-Fiber (Solid) Element Model	
Concrete Cylinder Strength (MPa)	40	40	40	
Steel Grade (MPa)	S275	S275	S275	
Nominal Compressive Strength, P_u (kN)	1,375	1,290	1,625	
Load Eccentricity, e (mm)	85.75	85.75	85.75	
Bending Moments at the Top of the Column, $M = P.e$ (kN.m)	117.91	110.62	139.34	
Section Capacity (D/C)	1.0	--		
Stresses on the Fiber (Solid) Model under 1,625 kN			Concrete Stress (MPa)	Steel Stress (MPa)
Average Stresses on the Encased Column			(40) Bottom of the Concrete	(220) Top of the Steel Section
Maximum Stresses			(76.89) Bottom of the Concrete	(311.73) Top of the Steel Section
Strain (ϵ)			Concrete Strain	Steel Strain
Average Strain on the Encased Column			0.001346	0.0011
Maximum Strain at the Top of the Encased column connected to CFST			0.002587	0.001559

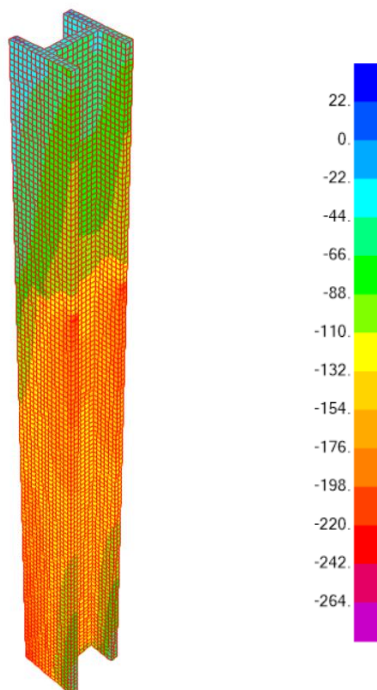
Table [4.23] Encased Column Section Capacity under Axial Compression and Uni-Direction Bending, C40MPa, S275



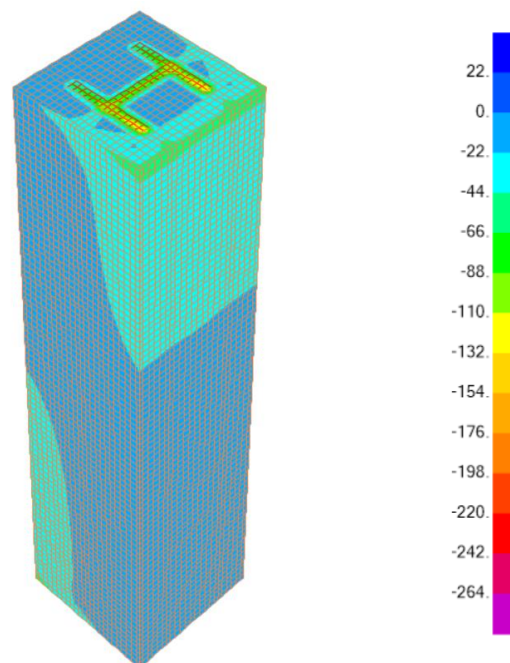
Stresses on Encased Column
Bottom View



Stresses on Encased Column
Top View



Stresses on Steel I Section



Stresses on Encased Column

Fig. (4.27) Stresses' Contours Along Encased Composite Column, C40MPa, S275MPa

4.4.4.1.6 Encased Column Analysis under Axial Compression and Uni-Direction Moments, C50MPa, S275MPa.

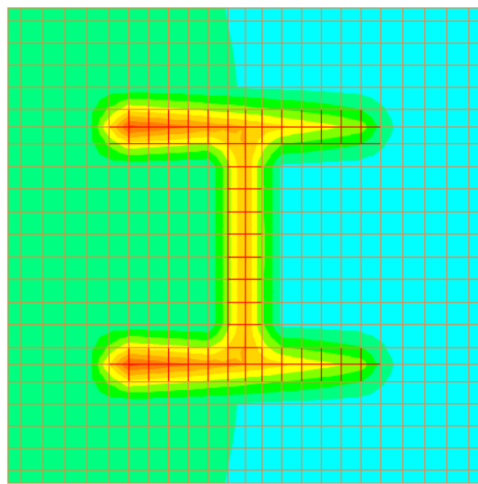
The following [table \[4.24\]](#) summarizes the Encased Column Sectional Capacity under Axial compression and uni-direction moments. The section capacity has been determined using simplified approach adopted by AISC 360-16, and Eurocode-4. In addition; it shows the stresses and strains of the concrete and steel elements extracted from the 3D -Fiber (Solid) Model. The load eccentricity was constant of 85.75mm from the cross-sectional centroid.

The analysis showing in the below [table \[4.24\]](#) has been performed using Concrete Cylinder Strength of C50MPa, and Steel Grade of S275MPa.

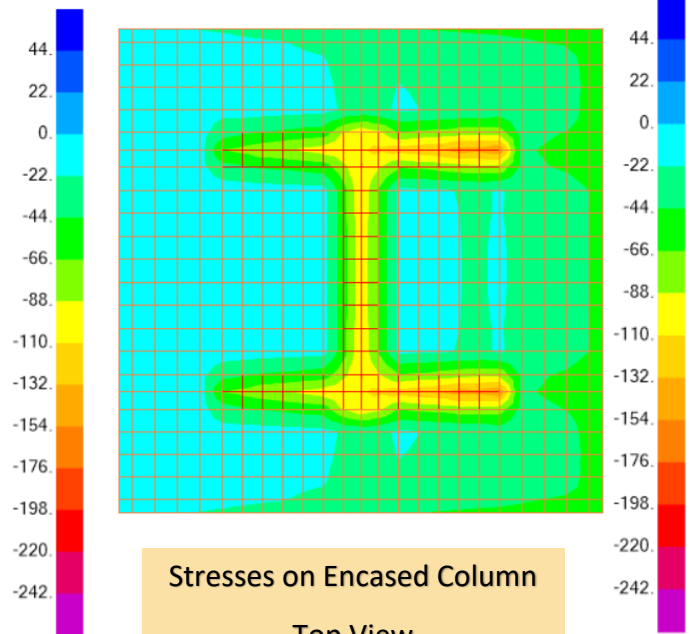
[Fig. \(4.28\)](#) presents the stress contours along the height of the encased columns as extracted from the 3D Fiber (Solid) Model.

Analysis Approach	AISC 360-16	Eurocode-4	3D-Fiber (Solid) Element Model	
Concrete Cylinder Strength (MPa)	50	50	50	
Steel Grade (MPa)	S275	S275	S275	
Nominal Compressive Strength, P_u (kN)	1,500	1,400	1,775	
Load Eccentricity, e (mm)	85.75	85.75	85.75	
Bending Moments at the Top of the Column, $M = P.e$ (kN.m)	128.63	120.05	152.21	
Section Capacity (D/C)	1.0	--		
Stresses on the Fiber (Solid) Model under 1,775 kN			Concrete Stress (MPa)	Steel Stress (MPa)
Average Stresses on the Encased Column			(50) Top & Bottom of the concrete	(225) Top and Bottom of Steel Section
Maximum Stresses			(87.38) Bottom of Concrete Section	(311.47) Top of Steel Section
Strain (ϵ)			Concrete Strain	Steel Strain
Average Strain on the Encased Column			0.00263	0.00156
Maximum Strain at Top of the Encased column connected to CFST			0.00150	0.001125

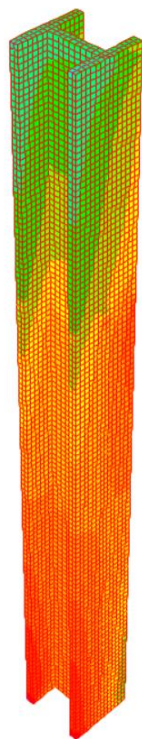
Table [4.24] Encased Column Section Capacity under Axial Compression and Uni-Direction Bending, C50MPa, S275



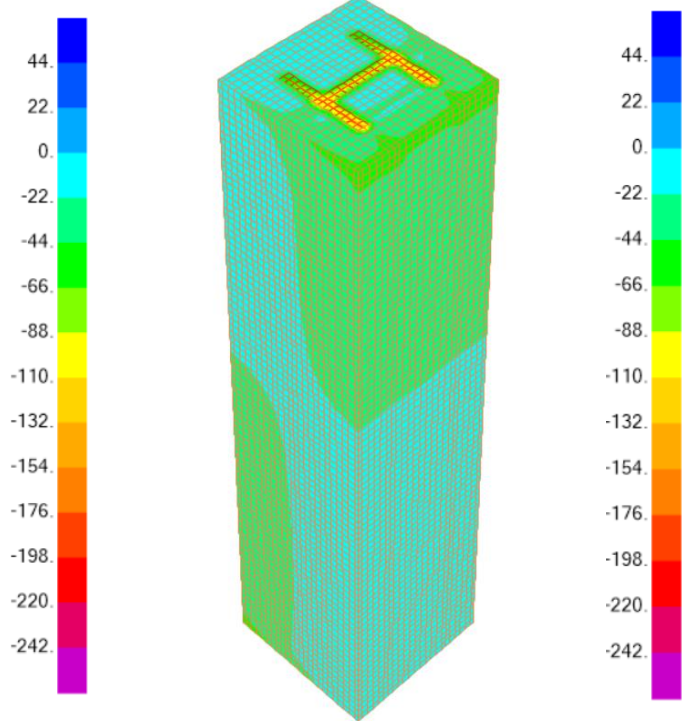
Stresses on Encased Column
Bottom View



Stresses on Encased Column
Top View



Stresses on Steel I Section



Stresses on Encased Column

Fig. (4.28) Stresses' Contours Along Encased Composite Column, C50MPa, S275MPa

4.4.4.1.7 Encased Column Analysis under Axial Compression and Uni-Direction Moments, C60MPa, S275MPa.

The following [table \[4.25\]](#) summarizes the Encased Column Sectional Capacity under Axial compression and uni-direction moments. The section capacity has been determined using simplified approach adopted by AISC 360-16, and Eurocode-4. In addition; it shows the stresses and strains of the concrete and steel elements extracted from the 3D -Fiber (Solid) Model.

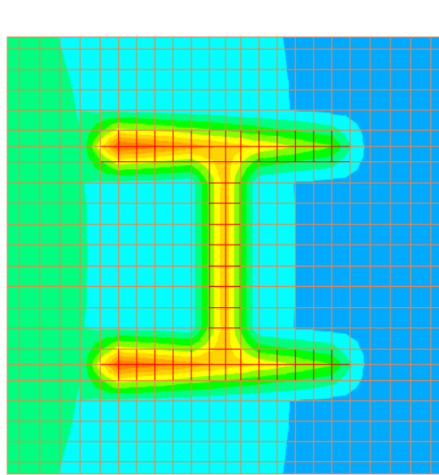
The load eccentricity was constant of 85.75mm from the cross-sectional centroid.

The analysis showing in the below [table \[4.25\]](#) has been performed using Concrete Cylinder Strength of C60MPa, and Steel Grade of S275MPa.

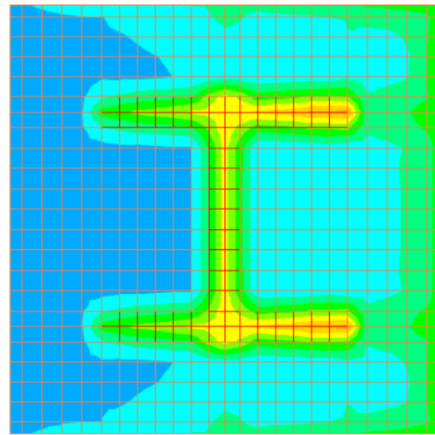
[Fig. \(4.29\)](#) presents the stress contours along the height of the encased columns as extracted from the 3D Fiber (Solid) Model.

Analysis Approach	AISC 360-16	Eurocode-4	3D-Fiber (Solid) Element Model	
Concrete Cylinder Strength (MPa)	60	60	60	
Steel Grade (MPa)	S275	S275	S275	
Nominal Compressive Strength, P_u (kN)	1,650	1,550	1,975	
Load Eccentricity, e (mm)	85.75	85.75	85.75	
Bending Moments at the Top of the Column, $M = P \cdot e$ (kN.m)	137.20	133	169.36	
Section Capacity (D/C)	1.0	--		
Stresses on the Fiber (Solid) Model under 1,975 kN			Concrete Stress (MPa)	Steel Stress (MPa)
Average Stresses on the Encased Column			(60) Top and bottom of the concrete	(235) Bottom of the Steel Section
Maximum Stresses			(103.36) Bottom of the Concrete	(296.97) Bottom of the Steel Section
Strain (ϵ)			Concrete Strain	Steel Strain
Average Strain on the Encased Column			0.0015	0.001175
Maximum Strain at Top of the Encased column connected to CFST			0.0026	0.00148

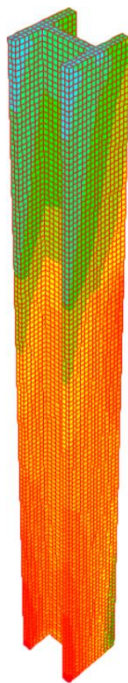
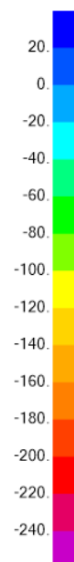
[Table \[4.25\]](#) Encased Column Section Capacity under Axial Compression and Uni-Direction Bending, C60MPa, S275



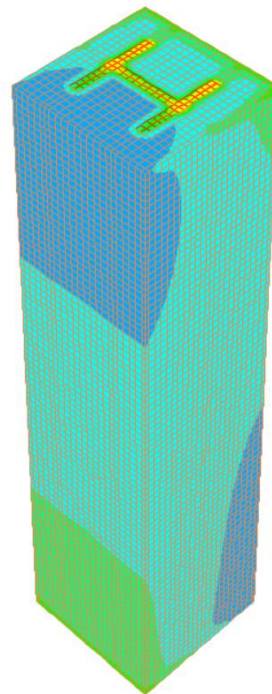
Stresses on Encased Column
Bottom View



Stresses on Encased Column
Top View



Stresses on Steel I Section



Stresses on Encased Column



Fig. (4.29) Stresses' Contours Along Encased Composite Column, C60MPa, S275MPa

4.4.4.1.8 Encased Column Analysis under Axial Compression and Uni-Direction Moments, C70MPa, S275MPa.

The following [table \[4.26\]](#) summarizes the Encased Column Sectional Capacity under Axial compression and uni-direction moments. The section capacity has been determined using simplified approach adopted by AISC 360-16, and Eurocode-4. In addition; it shows the stresses and strains of the concrete and steel elements extracted from the 3D -Fiber (Solid) Model.

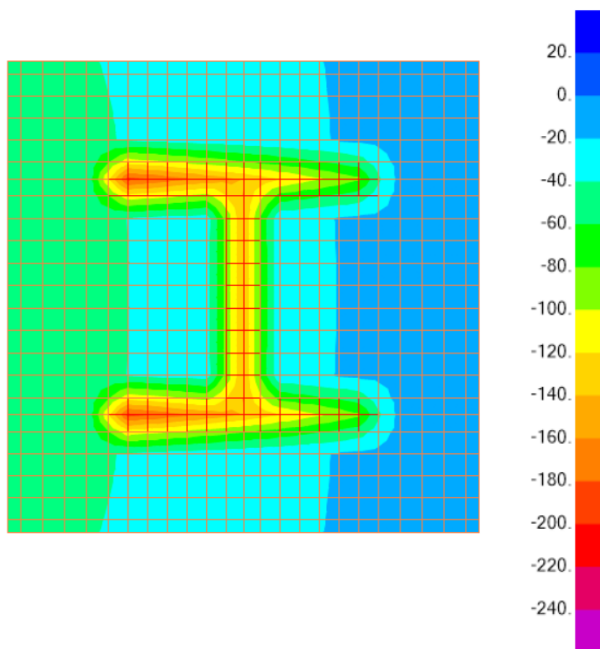
The load eccentricity was constant of 85.75mm from the cross-sectional centroid.

The analysis showing in the below [table \[4.26\]](#) has been performed using Concrete Cylinder Strength of C70MPa, and Steel Grade of S275MPa.

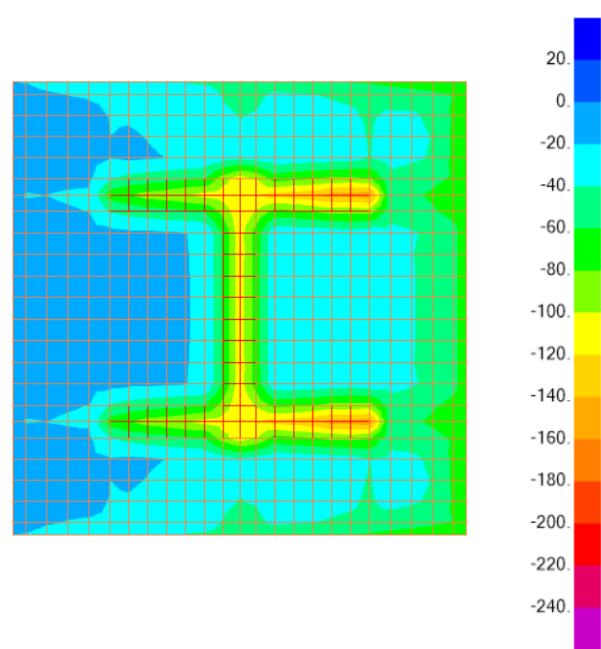
[Fig. \(4.30\)](#) presents the stress contours along the height of the encased columns as extracted from the 3D Fiber (Solid) Model.

Analysis Approach	AISC 360-16	Eurocode-4	3D-Fiber (Solid) Element Model	
Concrete Cylinder Strength (MPa)	70	70	70	
Steel Grade (MPa)	S275	S275	S275	
Nominal Compressive Strength, P_u (kN)	1,750	1,645	2,075	
Load Eccentricity, e (mm)	85.75	85.75	85.75	
Bending Moments at the Top of the Column, $M = P \cdot e$ (kN.m)	150.06	141.06	177.93	
Section Capacity (D/C)	1.0	--		
Stresses on the Fiber (Solid) Model under 2,075 kN			Concrete Stress (MPa)	Steel Stress (MPa)
Average Stresses on the Encased Column			(70) Top & Bottom of Concrete	(220) Top & Bottom of Steel Section
Maximum Stresses			(110.28) Bottom of Concrete	(298.89) Top & Bottom of Steel Section
Strain (ϵ)			Concrete Strain	Steel Strain
Average Strain on the Encased Column			0.00166	0.0011
Maximum Strain at Top of the Encased column connected to CFST			0.00262	0.00149

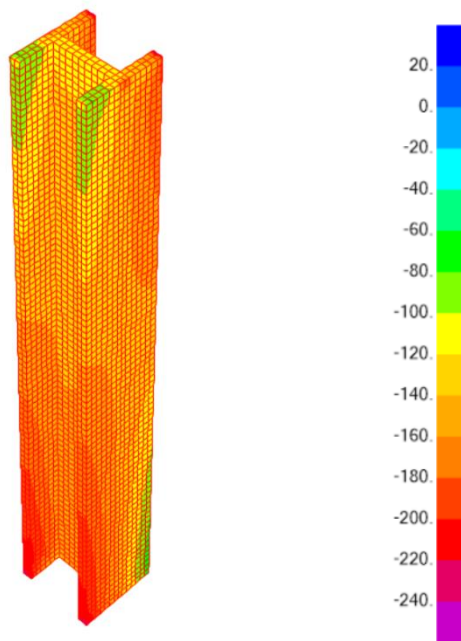
Table [4.26] Encased Column Section Capacity under Axial Compression and Uni-Direction Bending, C70MPa, S275



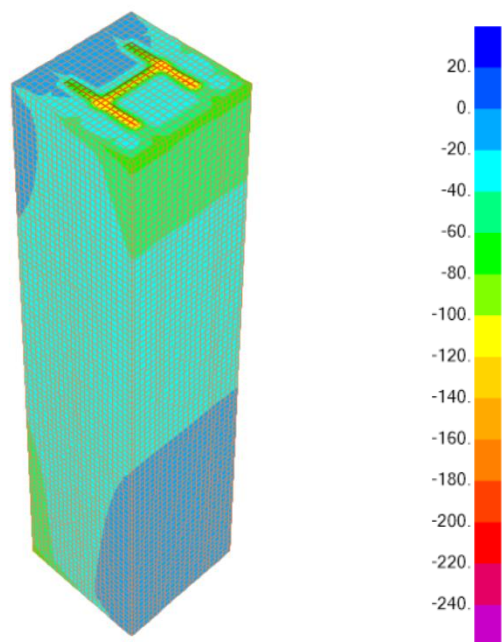
Stresses on Encased Column
Bottom View



Stresses on Encased Column
Top View



Stresses on Steel I Section



Stresses on Encased Column

Fig. (4.30) Stresses' Contours Along Encased Composite Column, C70MPa, S275MPa

4.4.4.2 Stresses on of the CFST Composite Column subject to Axial Compression and Uni-Direction Moments

This clause describes the analysis of the CFST Composite Column subject to axial compression loads and uni-direction moments. The stresses and strains on the concrete and steel section have been evaluated and compared to the simplified methods adopted by AISC 360-16, and Eurocode-4.

It was vital to understand the sectional behavior under different concrete cylinder strengths ranging from C40MPa to C70MPa, with different Young's Modulus of Elasticity as summarized in **clause 4.4.4.**

Furthermore; the capacity of the composite section has been evaluated using two different steel grades, S275MPa and S355MPa.

4.4.4.2.1 CFST Column Analysis under Axial Compression and Uni-Direction Moments, C40MPa, S355MPa.

The following [table \[4.27\]](#) summarizes the Encased Column Sectional Capacity under Axial compression and uni-direction moments. The section capacity has been determined using simplified approach adopted by AISC 360-16, and Eurocode-4. In addition; it shows the stresses and strains of the concrete and steel elements extracted from the 3D -Fiber (Solid) Model.

The load eccentricity was constant of 85.75mm from the cross-sectional centroid.

The analysis showing in the below [table \[4.27\]](#) has been performed using Concrete Cylinder Strength of C40MPa, and Steel Grade of S355MPa.

[Fig. \(4.31\)](#) presents the stress contours along the height of the CFST columns as extracted from the 3D Fiber (Solid) Model.

Analysis Approach	Encased Column Capacity	AISC 360-16 / Eurocode-4	3D-Fiber (Solid) Element Model	
Concrete Cylinder Strength (MPa)	40	40	40	
Steel Grade (MPa)	S355	S355	S355	
Axial Compression Load, Pu (kN)	1,625	1,750 / 1,625	1,825 However, the applied load shall not exceed the Encased Column capacity of 1,625kN	
Load Eccentricity, e (mm)	85.75	85.75	85.75	
Bending Moments at the Top of the Column, M = P.e (kN.m)	139.34	150.06 / 139.34	156.49	
Section Capacity (D/C)	0.925	1.0		
Stresses on the Fiber (Solid) Model, Applied Load 1,625kN			Concrete Stress (MPa)	Steel Stress (MPa)
Compression Stresses on the CFST Column (MPa)			(53.90) 40MPa Local Concentration (35.60) MPa Average Stresses	(255) MPa
Tensile Stresses on the CFST Column (MPa)			(10.08) MPa	(39.27) MPa
Strain (ε)			Concrete Strain	Steel Strain
Compression Strain on the CFST Column			0.00181 / 0.00120	0.001275
Tensile Strain on the CFST Column			0.00034	0.00020

Table [4.27] CFST Column Section Capacity under Axial Compression and Uni-Direction Bending, C40MPa, S355

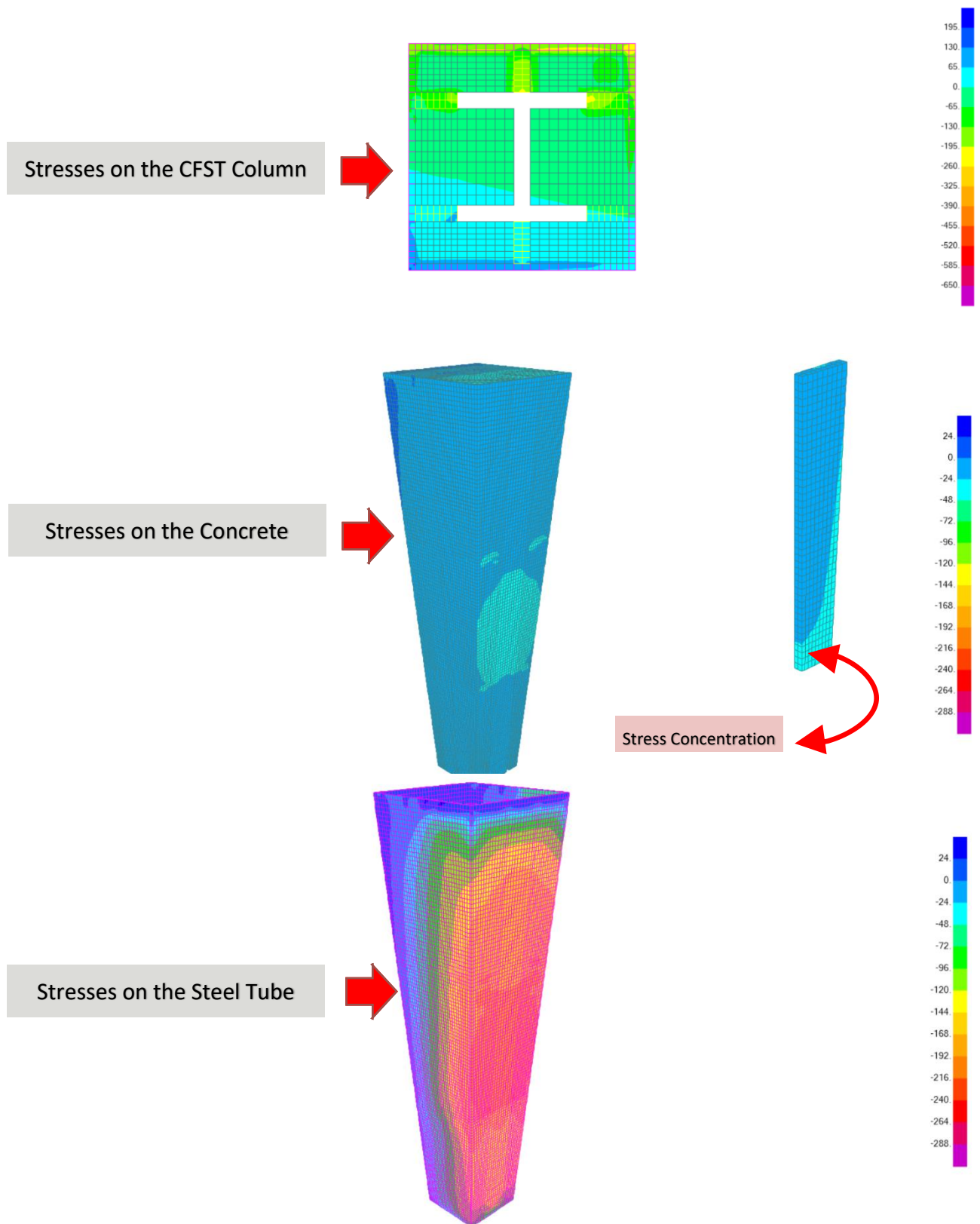


Fig. (4.31) Stresses' Contours Along CFST Composite Column, C40MPa, S355MPa

4.4.4.2.2 CFST Column Analysis under Axial Compression and Uni-Direction Moments, C50MPa, S355MPa.

The following [table \[4.28\]](#) summarizes the Encased Column Sectional Capacity under Axial compression and uni-direction moments. The section capacity has been determined using simplified approach adopted by AISC 360-16, and Eurocode-4. In addition; it shows the stresses and strains of the concrete and steel elements extracted from the 3D -Fiber (Solid) Model.

The load eccentricity was constant of 85.75mm from the cross-sectional centroid.

The analysis showing in the below [table \[4.28\]](#) has been performed using Concrete Cylinder Strength of C50MPa, and Steel Grade of S355MPa.

[Fig. \(4.32\)](#) presents the stress contours along the height of the CFST columns as extracted from the 3D Fiber (Solid) Model.

Analysis Approach	Encased Column Capacity	AISC 360-16 / Eurcode-4	3D-Fiber (Solid) Element Model	
Concrete Cylinder Strength (MPa)	50	50	50	
Steel Grade (MPa)	S355	S355	S355	
Axial Compression Load, Pu (kN)	1,775	1,925 / 1,790	2,160 However, the applied load shall not exceed the Encased Column capacity of 1,775kN	
Load Eccentricity, e (mm)	85.75	85.75	85.75	
Bending Moments at the Top of the Column, M = P.e (kN.m)	152.021	165.07 / 153.51	185.22	
Section Capacity (D/C)	0.925	1.0		
Stresses on the Fiber (Solid) Model, Applied Load 1,775kN			Concrete Stress (MPa)	Steel Stress (MPa)
Compression Stresses on the CFST Column (MPa)			(60.00) 40MPa Local Concentration (41.10) MPa Average Stresses	(262) MPa
Tensile Stresses on the CFST Column (MPa)			(11.00) MPa	(40.33) MPa
Strain (ε)			Concrete Strain	Steel Strain
Compression Strain on the CFST Column			0.00181 / 0.00124	0.00131
Tensile Strain on the CFST Column			0.000331	0.00121

Table [4.28] CFST Column Section Capacity under Axial Compression and Uni-Direction Bending, C50MPa, S355

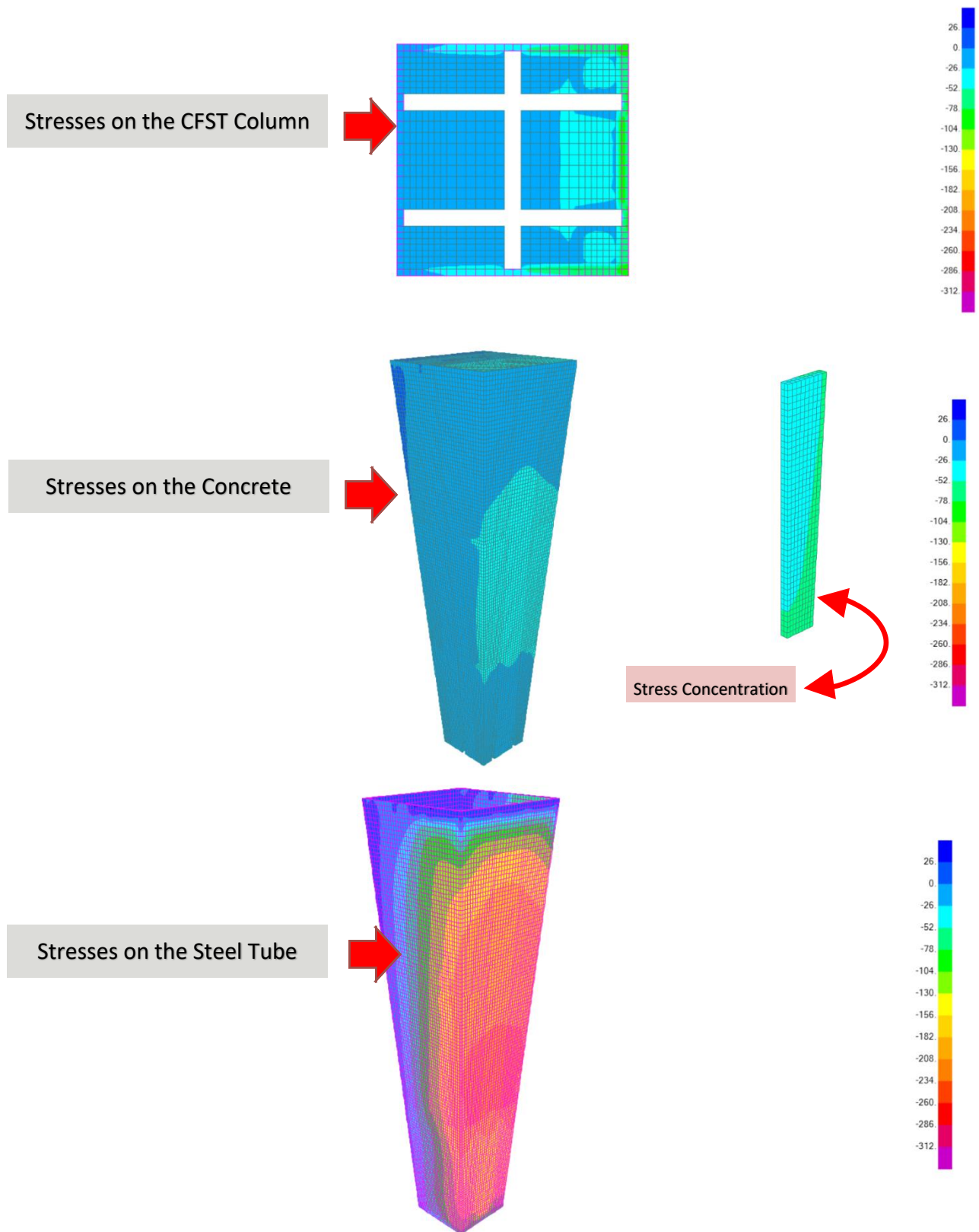


Fig. (4.32) Stresses' Contours Along CFST Composite Column, C50MPa, S355MPa

4.4.4.2.3 CFST Column Analysis under Axial Compression and Uni-Direction Moments, C60MPa, S355MPa.

The following [table \[4.29\]](#) summarizes the Encased Column Sectional Capacity under Axial compression and uni-direction moments. The section capacity has been determined using simplified approach adopted by AISC 360-16, and Eurocode-4. In addition; it shows the stresses and strains of the concrete and steel elements extracted from the 3D -Fiber (Solid) Model. The load eccentricity was constant of 85.75mm from the cross-sectional centroid.

The analysis showing in the below [table \[4.29\]](#) has been performed using Concrete Cylinder Strength of C60MPa, and Steel Grade of S355MPa.

[Fig. \(4.33\)](#) presents the stress contours along the height of the CFST columns as extracted from the 3D Fiber (Solid) Model.

Analysis Approach	Encased Column Capacity	AISC 360-16 / Eurocode-4	3D-Fiber (Solid) Element Model	
Concrete Cylinder Strength (MPa)	60	60	60	
Steel Grade (MPa)	S355	S355	S355	
Axial Compression Load, Pu (kN)	1,975	2,100 / 1,950	2,500 However, the applied load shall not exceed the Encased Column capacity of 1,975kN	
Load Eccentricity, e (mm)	85.75	85.75	85.75	
Bending Moments at the Top of the Column, M = P.e (kN.m)	169.36	180.08 / 167.21	185.22	
Section Capacity (D/C)	0.94	1.0		
Stresses on the Fiber (Solid) Model, Applied Load 1,975kN			Concrete Stress (MPa)	Steel Stress (MPa)
Compression Stresses on the CFST Column (MPa)			(68.56) 40MPa Local Concentration (48.00) MPa Average Stresses	(252) MPa
Tensile Stresses on the CFST Column (MPa)			(12.23) MPa	(39.55) MPa
Strain (ε)			Concrete Strain	Steel Strain
Compression Strain on the CFST Column			0.00171 / 0.00144	0.00126
Tensile Strain on the CFST Column			0.00031	0.0002

Table [4.29] CFST Column Section Capacity under Axial Compression and Uni-Direction Bending, C60MPa, S355

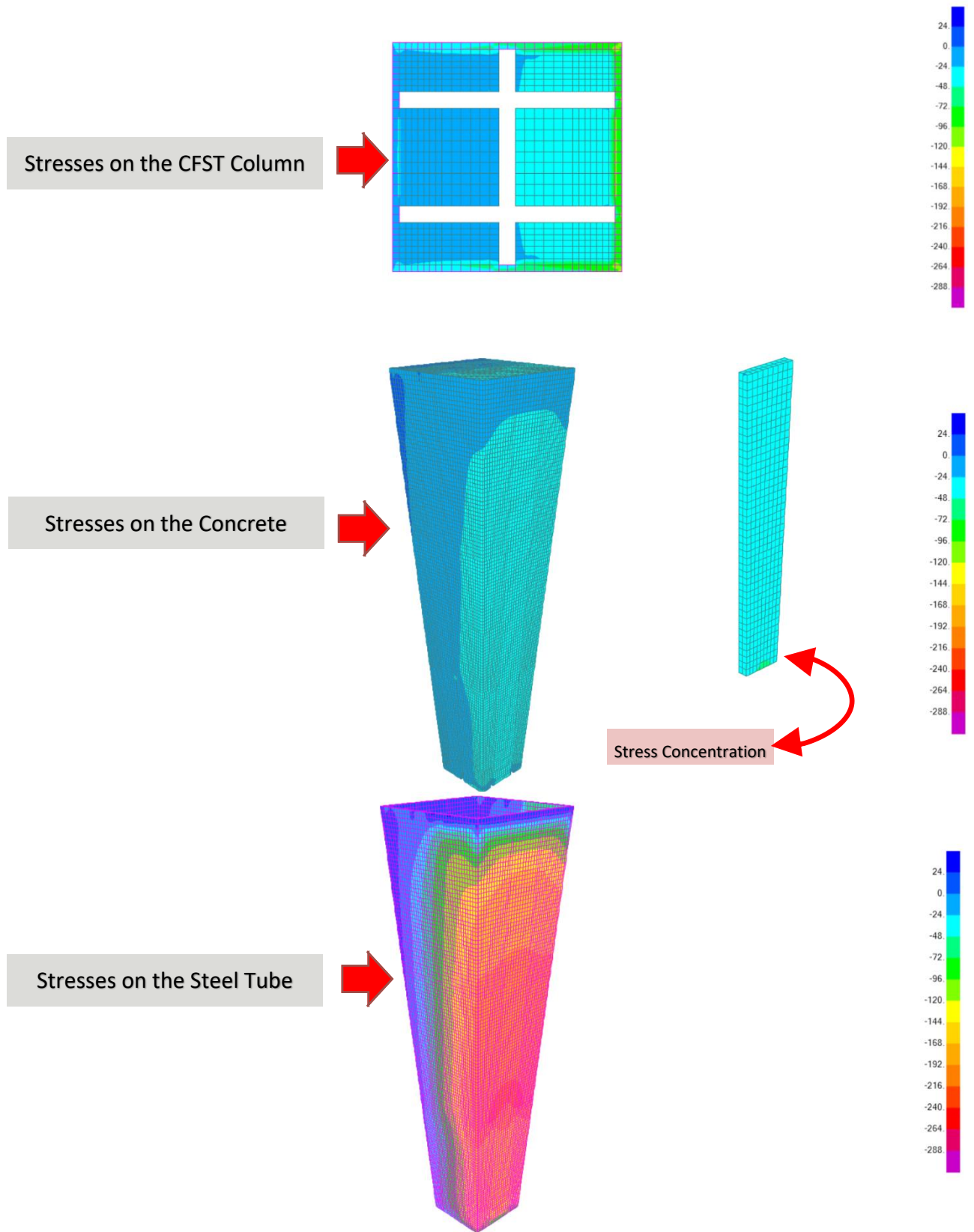


Fig. (4.33) Stresses' Contours Along CFST Composite Column, C60MPa, S355MPa

4.4.4.2.4 CFST Column Analysis under Axial Compression and Uni-Direction Moments, C70MPa, S355MPa.

The following [table \[4.30\]](#) summarizes the Encased Column Sectional Capacity under Axial compression and uni-direction moments. The section capacity has been determined using simplified approach adopted by AISC 360-16, and Eurocode-4. In addition; it shows the stresses and strains of the concrete and steel elements extracted from the 3D -Fiber (Solid) Model.

The load eccentricity was constant of 85.75mm from the cross-sectional centroid.

The analysis showing in the below [table \[4.30\]](#) has been performed using Concrete Cylinder Strength of C70MPa, and Steel Grade of S355MPa.

[Fig. \(4.34\)](#) presents the stress contours along the height of the CFST columns as extracted from the 3D Fiber (Solid) Model.

Analysis Approach	Encased Column Capacity	AISC 360-16 / Eurocode-4	3D-Fiber (Solid) Element Model	
Concrete Cylinder Strength (MPa)	70	70	70	
Steel Grade (MPa)	S355	S355	S355	
Axial Compression Load, Pu (kN)	2,075	2,250 / 2,090	2,900 However, the applied load shall not exceed the Encased Column capacity of 2,075kN	
Load Eccentricity, e (mm)	85.75	85.75	85.75	
Bending Moments at the Top of the Column, M = P.e (kN.m)	177.93	192.94 / 179.22	248.68	
Section Capacity (D/C)	0.925	1.0		
Stresses on the Fiber (Solid) Model, Applied Load 2,075kN			Concrete Stress (MPa)	Steel Stress (MPa)
Compression Stresses on the CFST Column (MPa)			(72.46) 40MPa Local Concentration (50) MPa Average Stresses	(255) MPa
Tensile Stresses on the CFST Column (MPa)			(12.84) MPa	(40.35) MPa
Strain (ε)			Concrete Strain	Steel Strain
Compression Strain on the CFST Column			0.00172 / 0.00120	0.001275
Tensile Strain on the CFST Column			0.00031	0.000202

Table [4.30] CFST Column Section Capacity under Axial Compression and Uni-Direction Bending, C70MPa, S355

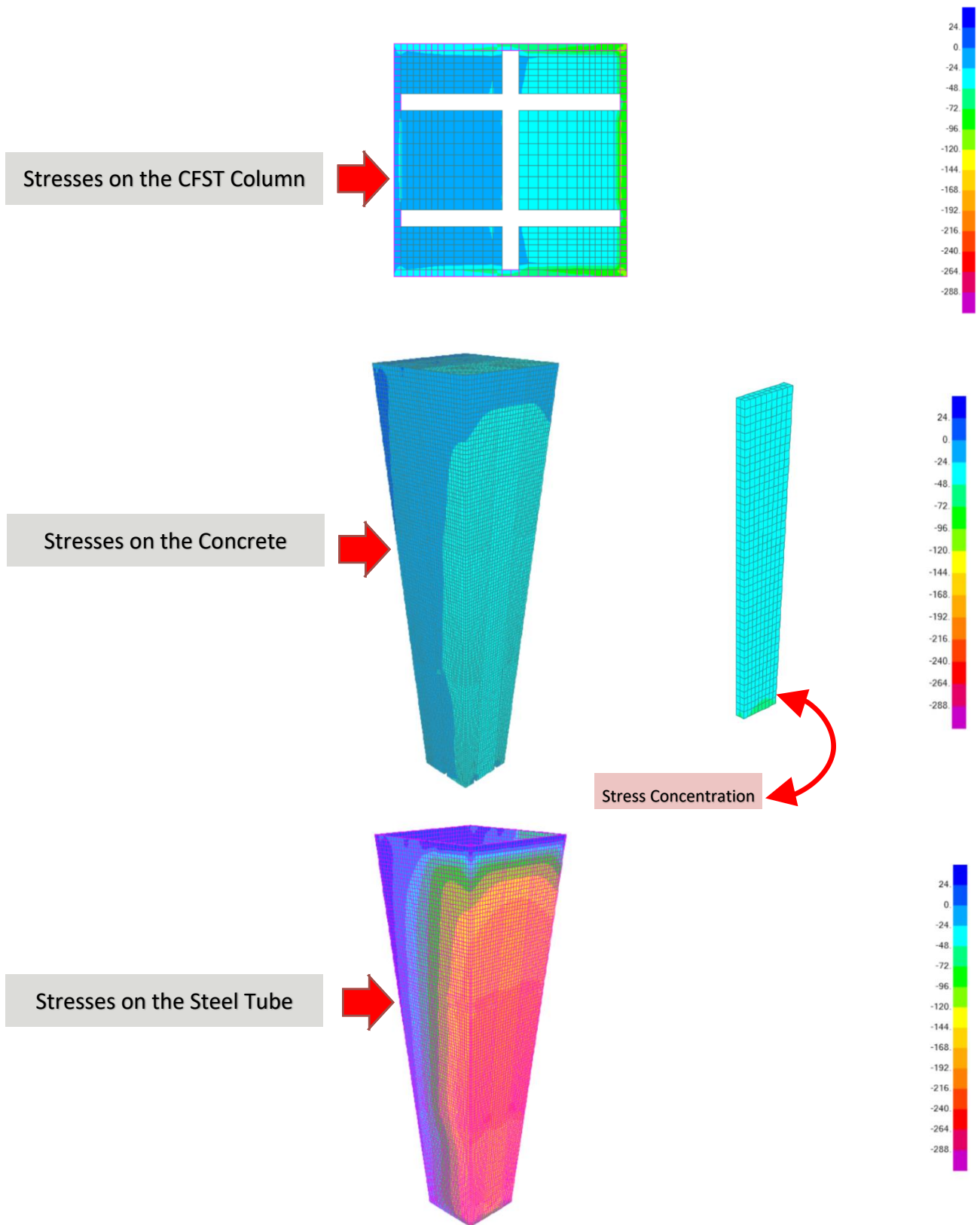


Fig. (4.34) Stresses' Contours Along CFST Composite Column, C70MPa, S355MPa

4.4.4.2.5 CFST Column Analysis under Axial Compression and Uni-Direction Moments, C40MPa, S275MPa.

The following [table \[4.31\]](#) summarizes the Encased Column Sectional Capacity under Axial compression and uni-direction moments. The section capacity has been determined using simplified approach adopted by AISC 360-16, and Eurocode-4. In addition; it shows the stresses and strains of the concrete and steel elements extracted from the 3D -Fiber (Solid) Model.

The load eccentricity was constant of 85.75mm from the cross-sectional centroid.

The analysis showing in the below [table \[4.31\]](#) has been performed using Concrete Cylinder Strength of C40MPa, and Steel Grade of S275MPa.

[Fig. \(4.35\)](#) presents the stress contours along the height of the CFST columns as extracted from the 3D Fiber (Solid) Model.

Analysis Approach	Encased Column Capacity	AISC 360-16 / Eurocode-4	3D-Fiber (Solid) Element Model	
Concrete Cylinder Strength (MPa)	40	40	40	
Steel Grade (MPa)	S275	S275	S275	
Axial Compression Load, Pu (kN)	1,625	1,500 / 1,395	1,775 However, the applied load shall not exceed the Encased Column capacity of 1,625 kN	
Load Eccentricity, e (mm)	85.75	85.75	85.75	
Bending Moments at the Top of the Column, M = P.e (kN.m)	139.34	128.63 / 119.62	152.21	
Section Capacity (D/C)	0.912	1.0		
Stresses on the Fiber (Solid) Model, Applied Load 1,625kN			Concrete Stress (MPa)	Steel Stress (MPa)
Compression Stresses on the CFST Column (MPa)			(53.90) 40MPa Local Concentration (35.60) MPa Average Stresses	(255) MPa
Tensile Stresses on the CFST Column (MPa)			(10.08) MPa	(39.27) MPa
Strain (ε)			Concrete Strain	Steel Strain
Compression Strain on the CFST Column			0.00181 / 0.00120	0.001275
Tensile Strain on the CFST Column			0.00034	0.00020

Table [4.31] CFST Column Section Capacity under Axial Compression and Uni-Direction Bending, C40MPa, S275

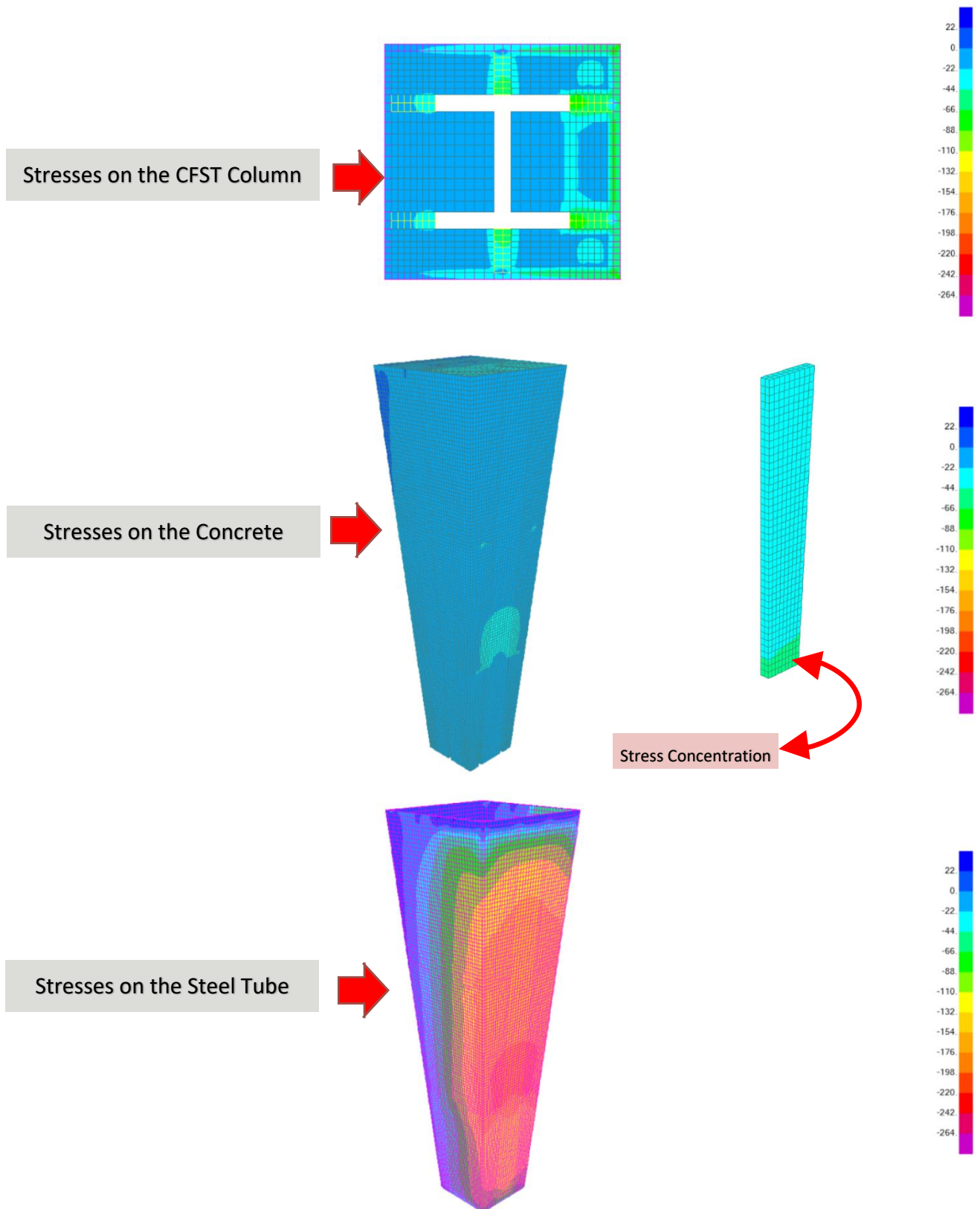


Fig. (4.35) Stresses' Contours Along CFST Composite Column, C40MPa, S275MPa

4.4.4.2.6 CFST Column Analysis under Axial Compression and Uni-Direction Moments, C50MPa, S275MPa.

The following [table \[4.32\]](#) summarizes the Encased Column Sectional Capacity under Axial compression and uni-direction moments. The section capacity has been determined using simplified approach adopted by AISC 360-16, and Eurocode-4. In addition; it shows the stresses and strains of the concrete and steel elements extracted from the 3D -Fiber (Solid) Model.

The load eccentricity was constant of 85.75mm from the cross-sectional centroid.

The analysis showing in the below [table \[4.32\]](#) has been performed using Concrete Cylinder Strength of C50MPa, and Steel Grade of S275MPa.

[Fig. \(4.36\)](#) presents the stress contours along the height of the CFST columns as extracted from the 3D Fiber (Solid) Model.

Analysis Approach	Encased Column Capacity	AISC 360-16 / Eurocode-4	3D-Fiber (Solid) Element Model	
Concrete Cylinder Strength (MPa)	50	50	50	
Steel Grade (MPa)	S275	S275	S275	
Axial Compression Load, Pu (kN)	1,775	1,650 / 1,535	2,225 However, the applied load shall not exceed the Encased Column capacity of 1,775 kN	
Load Eccentricity, e (mm)	85.75	85.75	85.75	
Bending Moments at the Top of the Column, M = P.e (kN.m)	152.21	141.49 / 131..63	190.79	
Section Capacity (D/C)	0.90	1.0		
Stresses on the Fiber (Solid) Model, Applied Load 1,775 kN			Concrete Stress (MPa)	Steel Stress (MPa)
Compression Stresses on the CFST Column (MPa)			(60.00) 40MPa Local Concentration (41.10) MPa Average Stresses	(262) MPa
Tensile Stresses on the CFST Column (MPa)			(11.00) MPa	(40.33) MPa
Strain (ε)			Concrete Strain	Steel Strain
Compression Strain on the CFST Column			0.00181 / 0.00124	0.00131
Tensile Strain on the CFST Column			0.000331	0.00121

Table [4.32] CFST Column Section Capacity under Axial Compression and Uni-Direction Bending, C50MPa, S275

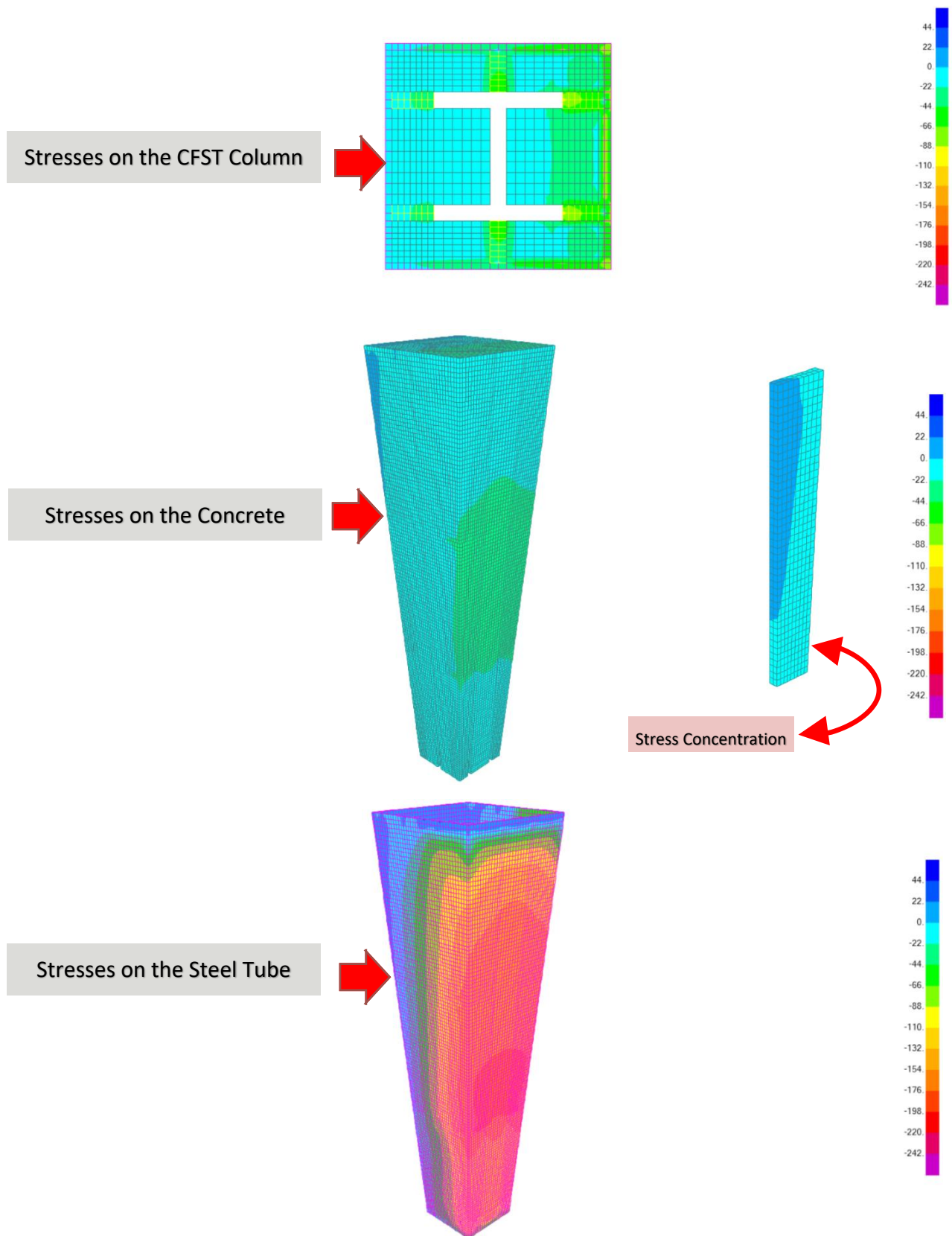


Fig. (4.36) Stresses' Contours Along CFST Composite Column, C50MPa, S275MPa

4.4.4.2.7 CFST Column Analysis under Axial Compression and Uni-Direction Moments, C60MPa, S275MPa.

The following [table \[4.33\]](#) summarizes the Encased Column Sectional Capacity under Axial compression and uni-direction moments. The section capacity has been determined using simplified approach adopted by AISC 360-16, and Eurocode-4. In addition; it shows the stresses and strains of the concrete and steel elements extracted from the 3D -Fiber (Solid) Model.

The load eccentricity was constant of 85.75mm from the cross-sectional centroid.

The analysis showing in the below [table \[4.33\]](#) has been performed using Concrete Cylinder Strength of C60MPa, and Steel Grade of S275MPa.

[Fig. \(4.37\)](#) presents the stress contours along the height of the CFST columns as extracted from the 3D Fiber (Solid) Model.

Analysis Approach	Encased Column Capacity	AISC 360-16 / Eurocode-4	3D-Fiber (Solid) Element Model	
Concrete Cylinder Strength (MPa)	60	60	60	
Steel Grade (MPa)	S275	S275	S275	
Axial Compression Load, Pu (kN)	1,975	1,825 / 1,695	2,475 However, the applied load shall not exceed the Encased Column capacity of 1,975 kN	
Load Eccentricity, e (mm)	85.75	85.75	85.75	
Bending Moments at the Top of the Column, M = P.e (kN.m)	169.36	156.49 / 145.35	212.23	
Section Capacity (D/C)	0.90	1.0		
Stresses on the Fiber (Solid) Model, Applied Load 1,975 kN			Concrete Stress (MPa)	Steel Stress (MPa)
Compression Stresses on the CFST Column (MPa)			(68.56) 40MPa Local Concentration (48.00) MPa Average Stresses	(252) MPa
Tensile Stresses on the CFST Column (MPa)			(12.23) MPa	(39.55) MPa
Strain (ε)			Concrete Strain	Steel Strain
Compression Strain on the CFST Column			0.00171 / 0.00144	0.00126
Tensile Strain on the CFST Column			0.00031	0.0002

Table [4.33] CFST Column Section Capacity under Axial Compression and Uni-Direction Bending, C60MPa, S275

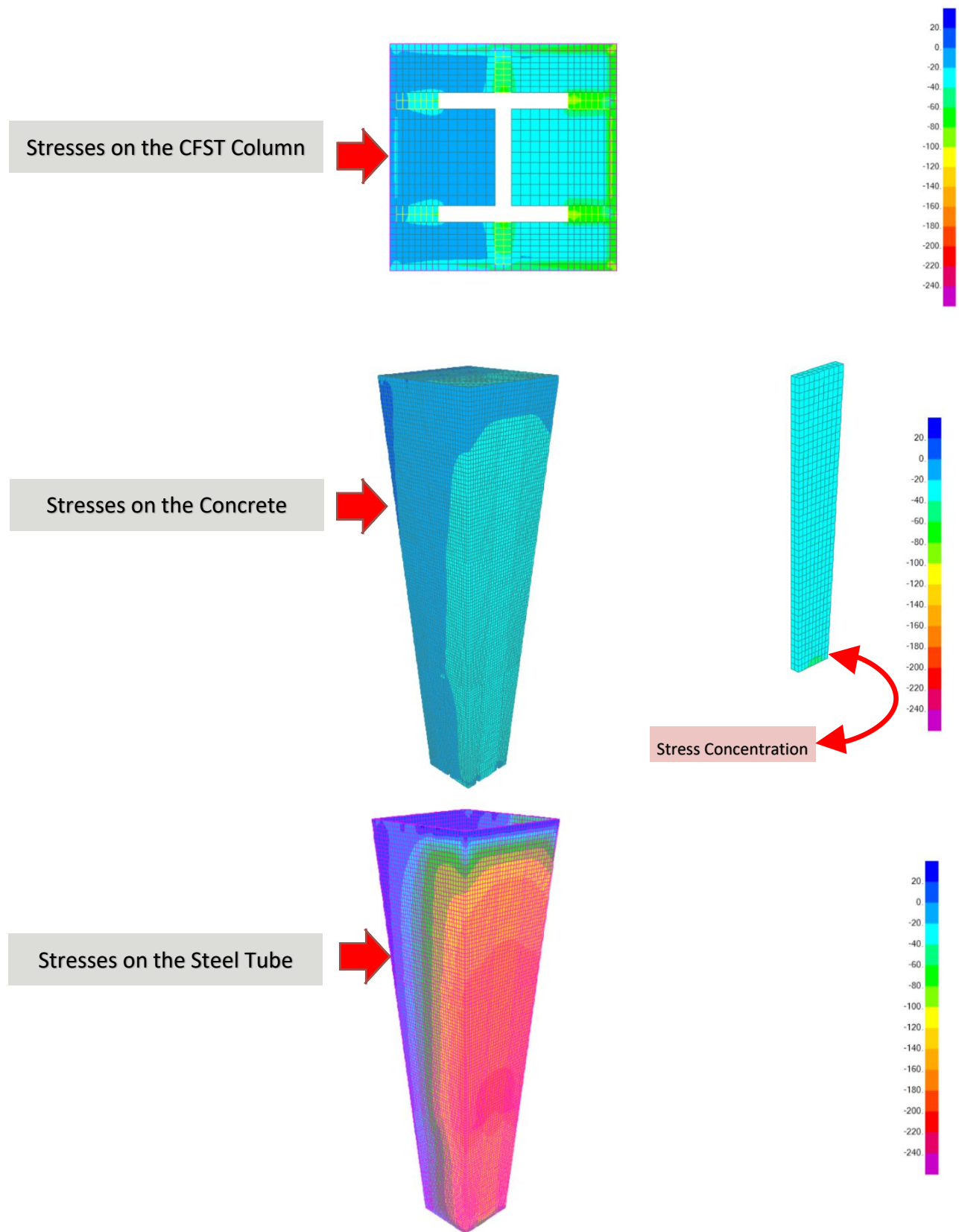


Fig. (4.37) Stresses' Contours Along CFST Composite Column, C60MPa, S275MPa

4.4.4.2.8 CFST Column Analysis under Axial Compression and Uni-Direction Moments, C70MPa, S275MPa.

The following [table \[4.34\]](#) summarizes the Encased Column Sectional Capacity under Axial compression and uni-direction moments. The section capacity has been determined using simplified approach adopted by AISC 360-16, and Eurocode-4. In addition; it shows the stresses and strains of the concrete and steel elements extracted from the 3D -Fiber (Solid) Model.

The load eccentricity was constant of 85.75mm from the cross-sectional centroid.

The analysis showing in the below [table \[4.34\]](#) has been performed using Concrete Cylinder Strength of C70MPa, and Steel Grade of S275MPa.

[Fig. \(4.38\)](#) presents the stress contours along the height of the CFST columns as extracted from the 3D Fiber (Solid) Model.

Analysis Approach	Encased Column Capacity	AISC 360-16 / Eurocode-4	3D-Fiber (Solid) Element Model	
Concrete Cylinder Strength (MPa)	70	70	70	
Steel Grade (MPa)	S275	S275	S275	
Axial Compression Load, Pu (kN)	2,075	1,975 / 1835	2,800 However, the applied load shall not exceed the Encased Column capacity of 2,075 kN	
Load Eccentricity, e (mm)	85.75	85.75	85.75	
Bending Moments at the Top of the Column, M = P.e (kN.m)	177.93	169.36 / 157.35	240.10	
Section Capacity (D/C)	0.89	1.0		
Stresses on the Fiber (Solid) Model, Applied Load 2,075 kN			Concrete Stress (MPa)	Steel Stress (MPa)
Compression Stresses on the CFST Column (MPa)			(72.46) 40MPa Local Concentration (50) MPa Average Stresses	(255) MPa
Tensile Stresses on the CFST Column (MPa)			(12.84) MPa	(40.35) MPa
Strain (ε)			Concrete Strain	Steel Strain
Compression Strain on the CFST Column			0.00172 / 0.00120	0.001275
Tensile Strain on the CFST Column			0.00031	0.000202

Table [4.34] CFST Column Section Capacity under Axial Compression and Uni-Direction Bending, C70MPa, S275

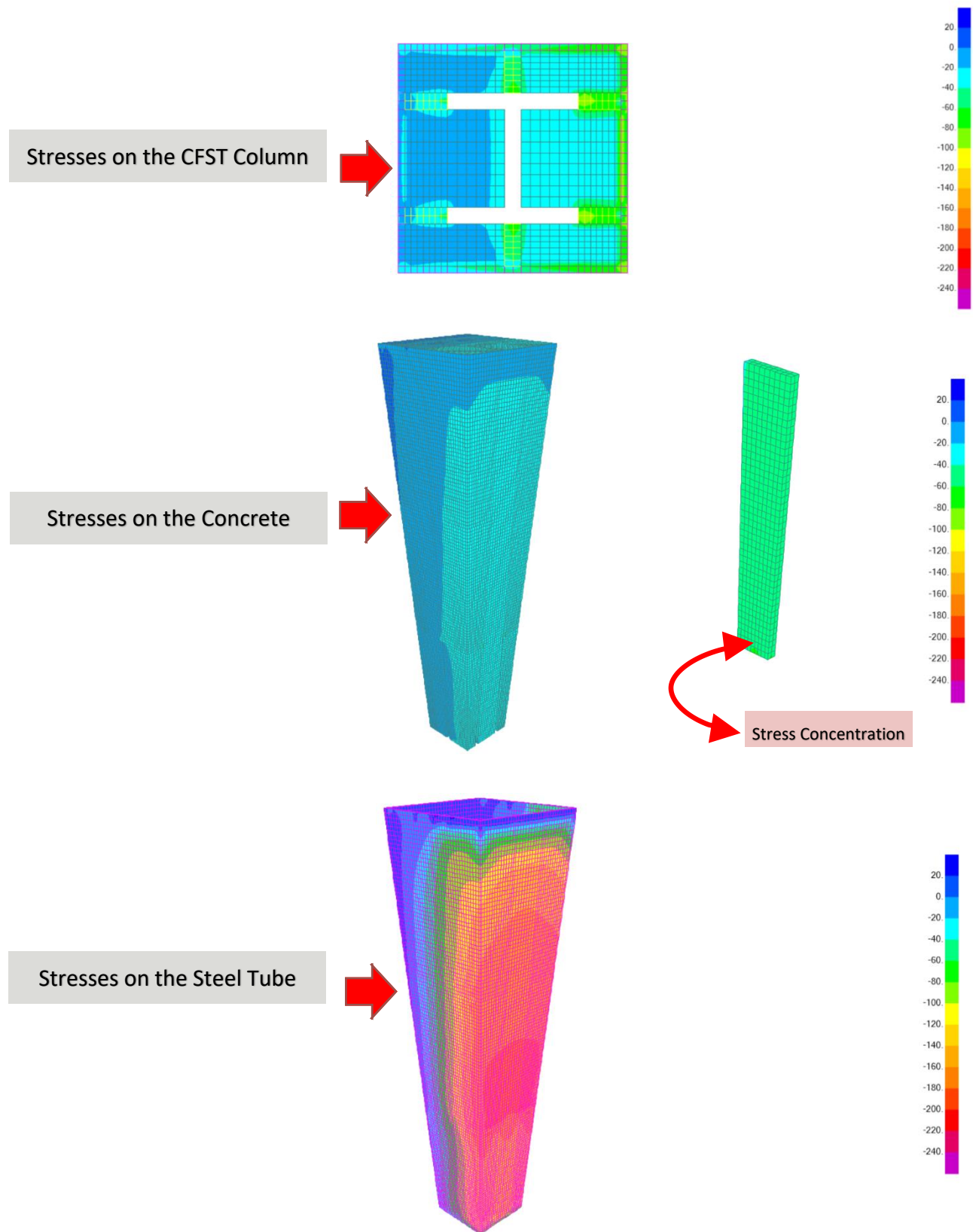


Fig. (4.38) Stresses' Contours Along CFST Composite Column, C70MPa, S275MPa

4.4.4.3 Stresses on the Stiffener Plates welded to the CFST and Encased Element, under Axial Compression and Uni-Direction Bending Moments

This clause describes the analysis of stiffener plates connected to the CFST Tube and I section under axial compression loads and uni-direction bending. The stresses and strains on the steel plates have been presented in the below table

It was vital to understand the stresses transferred through stiffener plates using different concrete cylinder strengths ranging from C40MPa to C70MPa, with different Young's Modulus of Elasticity as summarized in clause 4.4.3.

Furthermore; the stresses have been evaluated using two different steel grades, S275MPa and S355MPa.

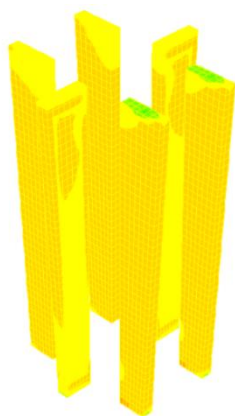
Table [4.35] illustrates the stresses on the steel stiffener plates under different concrete strengths and using two different steel grades.

Fig. (4.39) demonstrates the stress contours along the height of the stiffener plates with steel grade of **S355MPa** as extracted from the 3D Fiber (Solid) Model.

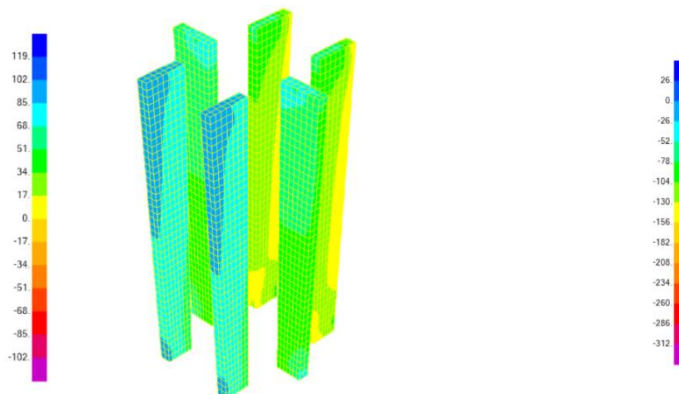
Fig. (4.40) demonstrates the stress contours along the height of the stiffener plates with steel grade of **S275MPa** as extracted from the 3D Fiber (Solid) Model.

Steel Grade, (MPa)	S355	S355	S355	S355
Concrete Cylinder Strength (MPa)	C40MPa	C50MPa	C60MPa	C70MPa
Steel Stresses (MPa)	151.40	156.41	158.27	161.97
Steel Strain	0.00076	0.00078	0.00079	0.00081
Steel Grade, (MPa)	S275	S275	S275	S275
Concrete Cylinder Strength (MPa)	C40MPa	C50MPa	C60MPa	C70MPa
Steel Stresses (MPa)	128.13	132.21	132.25	136.63
Steel Strain	0.00064	0.00066	0.00066	0.00068

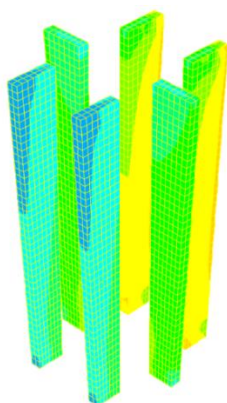
Table [4.35] Stresses on the Steel Stiffener Plates due to Axial Compression and Uni-Direction Bending



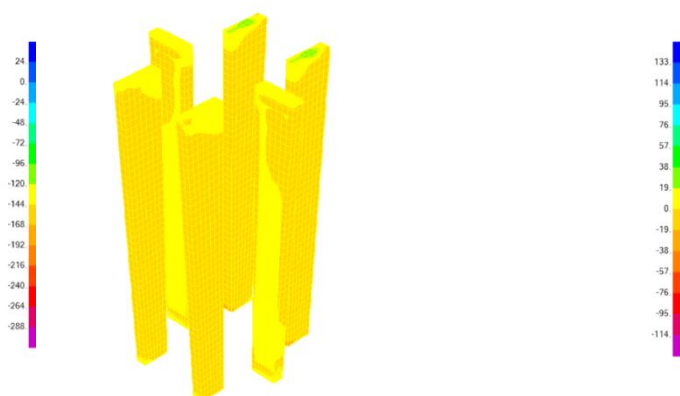
C40MPa, S355MPa



C50MPa, S355MPa

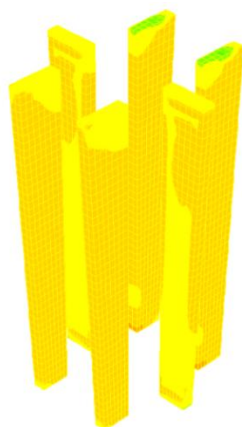


C60MPa, S355MPa

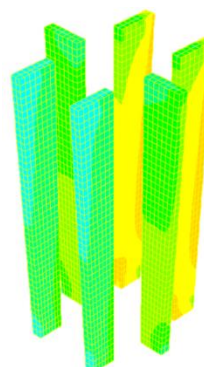


C70MPa, S355MPa

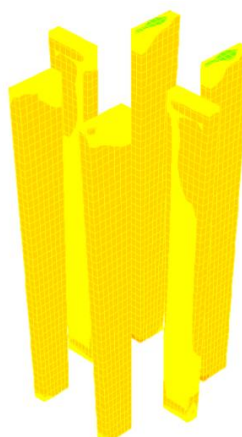
Fig. (4.39) Stresses' Contours Along Stiffener Plates, under Axial Compression and Uni-Direction Bending S355MPa



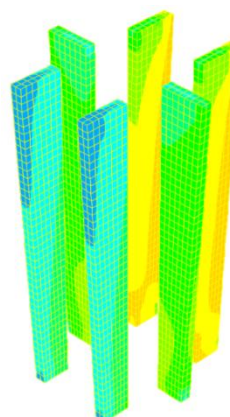
C40MPa, S275MPa



C50MPa, S275MPa



C60MPa, S275MPa



C70MPa, S275MPa



Fig. (4.40) Stresses' Contours Along Stiffener Plates, under Axial Compression and Uni-Direction Bending S275MPa

4.4.5 COLUMN RESISTANCE TO AXIAL COMPRESSION AND BI-AXIAL BENDING MOMENTS

The third approach in this research is to examine the column under axial compression and bi-axial bending moments.

The column has been modeled using four different cylinder concrete strengths, 40, 50, 60, and 70MPa.

Each concrete strength has been analyzed using two different steel strength, S275MPa and S355MPa inline with EN 1993-1-1.

The sectional capacity has been checked using AISC 360-16, , Eurocode-4 and compared with the output from the 3D-Fiber (Solid) Element Model.

The Finite element has been divided into 3 parts, the first part is the encased column, the second part is the CFST column, and the third part is the stiffener plates connecting I section to CFST tube.

The Concrete Modulus of Elasticity has been determined as follow:

- C40MPa, $E_c = 29,725 \text{ MPa}$
- C50MPa, $E_c = 33,234 \text{ MPa}$
- C60MPa, $E_c = 40,022 \text{ MPa}$
- C70MPa, $E_c = 42,079 \text{ MPa}$

The Steel Modulus of Elasticity is equal to 200,000 MPa

4.4.5.1 Stresses on the Encased Composite Column subject to Axial Compression and Bi-Axial Bending

This clause describes the analysis of the Encased Composite Column subject to axial compression loads and bi-axial bending moments. The stresses and strains on the concrete and steel section have been evaluated and compared to the simplified methods adopted by AISC 360-16, and Eurocode-4.

It was vital to understand the sectional behavior under different concrete cylinder strengths ranging from C40MPa to C70MPa, with different Young's Modulus of Elasticity as summarized in [clause 4.4.5](#).

Furthermore; the capacity of the composite section has been evaluated using two different steel grades, S275MPa and S355MPa.

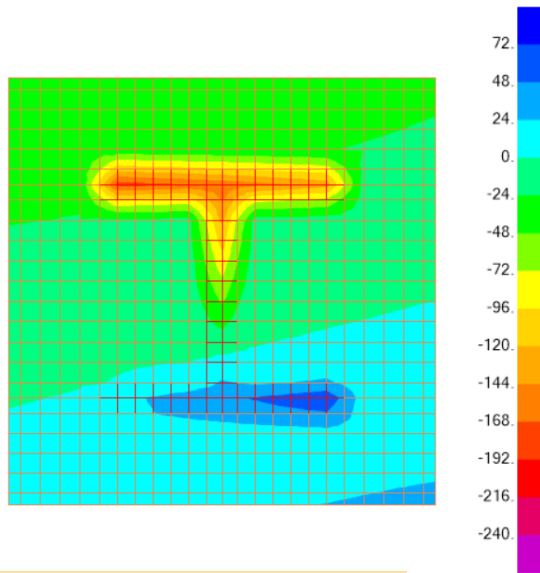
4.4.5.1.1 Encased Column Analysis under Axial Compression and Bi-Axial Moments, C40MPa, S355MPa.

The following [table \[4.36\]](#) summarizes the Encased Column Sectional Capacity under Axial compression and bi-axial bending moments. The section capacity has been determined using simplified approach adopted by AISC 360-16, and Eurocode-4. In addition; it shows the stresses and strains of the concrete and steel elements extracted from the 3D -Fiber (Solid) Model. The load eccentricities were constant of 85.75mm in X-direction and 104.50mm in Y-direction. The analysis showing in the below [table \[4.36\]](#) has been performed using Concrete Cylinder Strength of C40MPa, and Steel Grade of S355MPa.

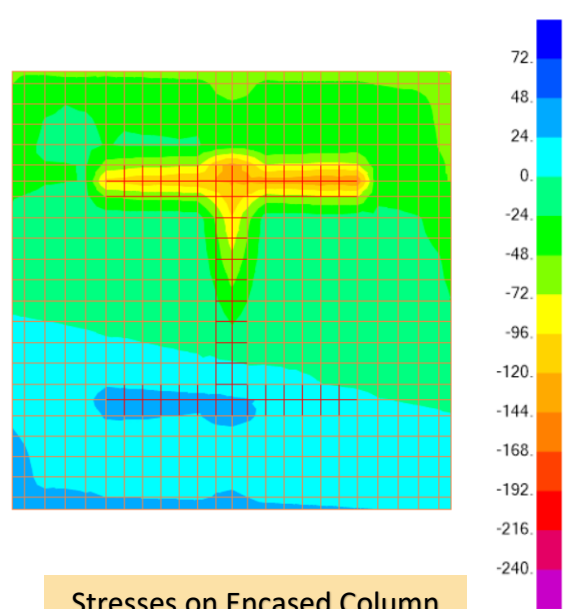
[Fig. \(4.41\)](#) presents the stress contours along the height of the encased columns as extracted from the 3D Fiber (Solid) Model.

Analysis Approach	AISC 360-16	Eurocode-4	3D-Fiber (Solid) Element Model	
Concrete Cylinder Strength (MPa)	40	40	40	
Steel Grade (MPa)	S355	S355	S355	
Axial Compression Load, P (kN)	900	835	600	
Load Eccentricity, e_x (mm)	85.75	85.75	85.75	
Load Eccentricity, e_y (mm)	104.50	104.50	104.50	
Bending Moments at the Top of the Column, M = P.e (kN.m)	M _x = 94.05 M _y = 77.18	M _x = 87.26 M _y = 71.60	M _x = 62.70 M _y = 51.45	
Section Capacity (D/C)	1.0	1.0		
Stresses on the Fiber (Solid) Model under 600 kN			Concrete Stress (MPa)	Steel Stress (MPa)
Compression Stresses on the Encased Column			(75 MPa) At Top & Bottom of Col (40 MPa) Average Stresses	(252.40 MPa) At the middle of the section
Tensile Stresses on the Encased Column			(42.11 MPa) At Top and Bottom	(94.30 MPa) At Bottom of Sec
Strain (ϵ)			Concrete Strain	Steel Strain
Compression Strain on the Encased Column			0.0025 / 0.0013	0.0013
Tensile Strain on the Encased Column			0.0014	0.0005

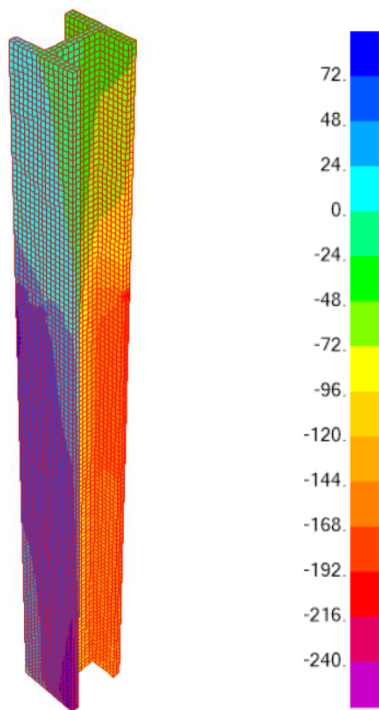
Table [4.36] Encased Column Section Capacity under Axial Compression and Bi-Axial Bending, C40MPa, S355



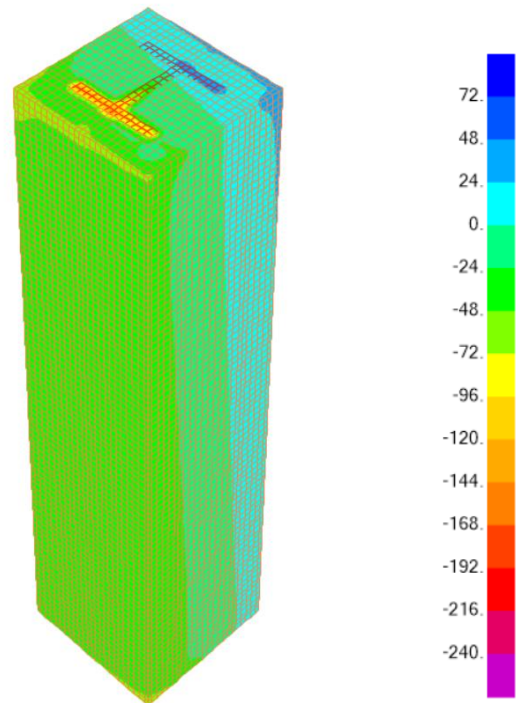
Stresses on Encased Column
Bottom View



Stresses on Encased Column
Top View



Stresses on Steel I Section



Stresses on Encased Column

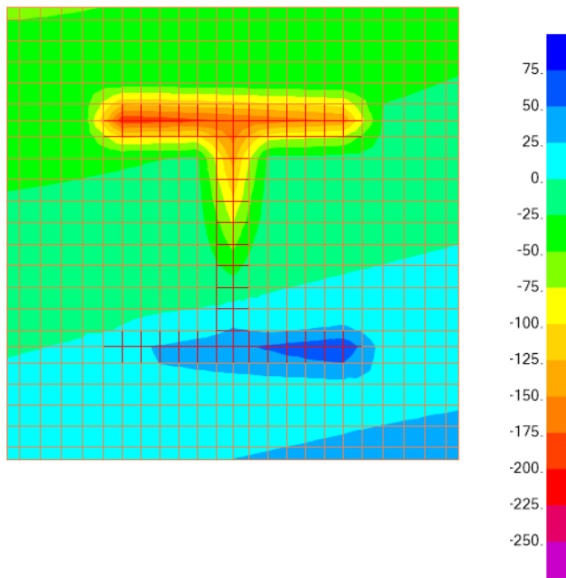
Fig. (4.41) Stresses' Contours Along Encased Composite Column, C40MPa, S355MPa

4.4.5.1.2 Encased Column Analysis under Axial Compression and Bi-Axial Moments, C50MPa, S355MPa.

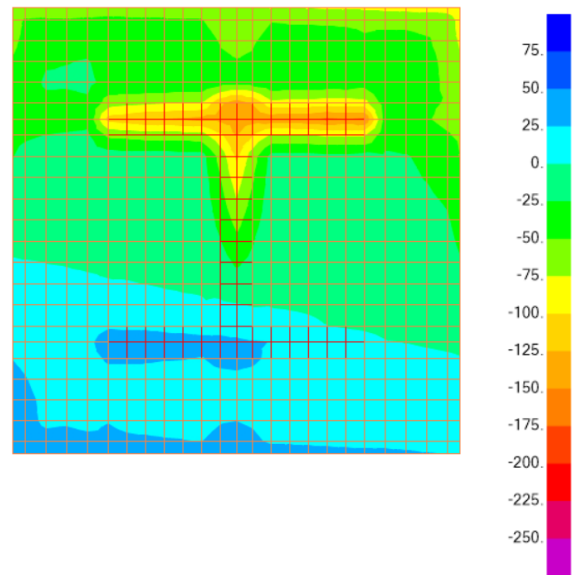
The following [table \[4.37\]](#) summarizes the Encased Column Sectional Capacity under Axial compression and bi-axial bending moments. The section capacity has been determined using simplified approach adopted by AISC 360-16, and Eurocode-4. In addition; it shows the stresses and strains of the concrete and steel elements extracted from the 3D -Fiber (Solid) Model. The load eccentricities were constant of 85.75mm in X-direction and 104.50mm in Y-direction. The analysis showing in the below [table \[4.37\]](#) has been performed using Concrete Cylinder Strength of C50MPa, and Steel Grade of S355MPa. [Fig. \(4.42\)](#) presents the stress contours along the height of the encased columns as extracted from the 3D Fiber (Solid) Model.

Analysis Approach	AISC 360-16	Eurocode-4	3D-Fiber (Solid) Element Model	
Concrete Cylinder Strength (MPa)	50	50	50	
Steel Grade (MPa)	S355	S355	S355	
Axial Compression Load, P (kN)	1,150	1,065	700	
Load Eccentricity, e_x (mm)	85.75	85.75	85.75	
Load Eccentricity, e_y (mm)	104.50	104.50	104.50	
Bending Moments at the Top of the Column, M = P.e (kN.m)	M _x = 120.18 M _y = 98.61	M _x = 111.30 M _y = 91.23	M _x = 73.15 M _y = 60.03	
Section Capacity (D/C)	1.0	1.0		
Stresses on the Fiber (Solid) Model under 700 kN			Concrete Stress (MPa)	Steel Stress (MPa)
Compression Stresses on the Encased Column			(88.94 MPa) At Top & Bottom of Col (50 MPa) Average Stresses	(269.23 MPa) At the middle of the section
Tensile Stresses on the Encased Column			(49.60 MPa) At Top & Bottom	(99.90 MPa) At Bottom of Sec
Strain (ϵ)			Concrete Strain	Steel Strain
Compression Strain on the Encased Column			0.0027 / 0.0015	0.0013
Tensile Strain on the Encased Column			0.0015	0.0005

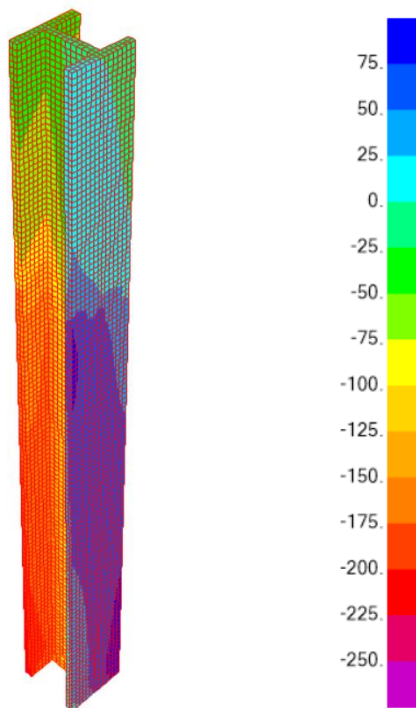
Table [4.37] Encased Column Section Capacity under Axial Compression and Bi-Axial Bending, C50MPa, S355



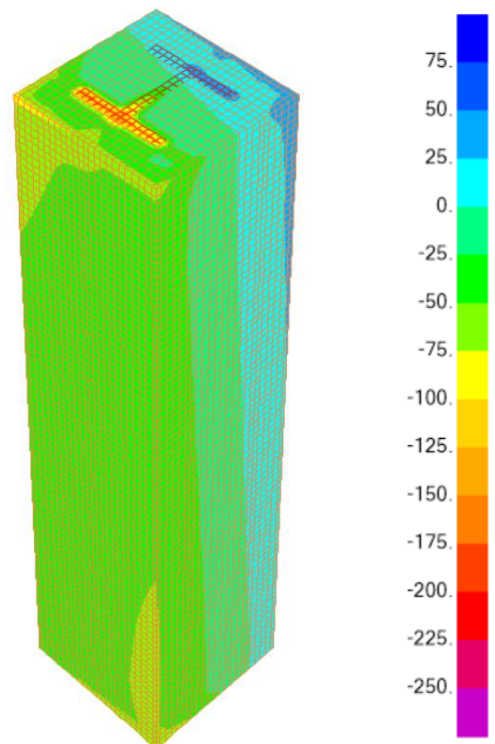
Stresses on Encased Column
Bottom View



Stresses on Encased Column
Top View



Stresses on Steel I Section



Stresses on Encased Column

Fig. (4.42) Stresses' Contours Along Encased Composite Column, C50MPa, S355MPa

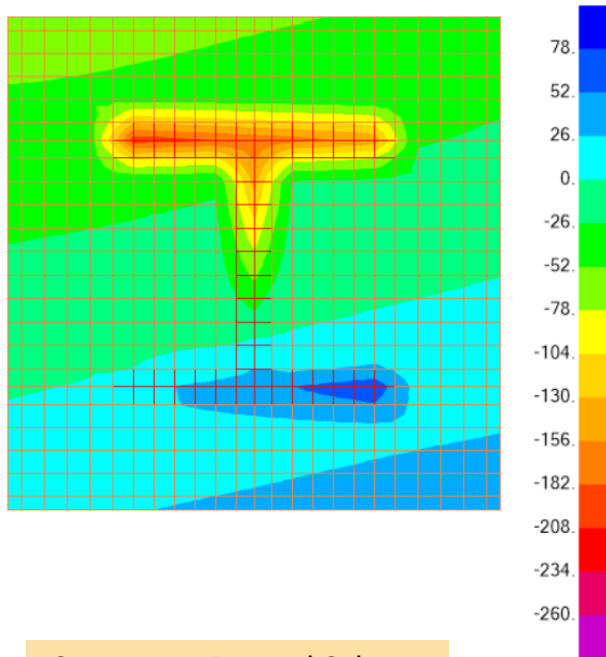
4.4.5.1.3 Encased Column Analysis under Axial Compression and Bi-Axial Moments, C60MPa, S355MPa.

The following [table \[4.38\]](#) summarizes the Encased Column Sectional Capacity under Axial compression and bi-axial bending moments. The section capacity has been determined using simplified approach adopted by AISC 360-16, and Eurocode-4. In addition; it shows the stresses and strains of the concrete and steel elements extracted from the 3D -Fiber (Solid) Model. The load eccentricities were constant of 85.75mm in X-direction and 104.50mm in Y-direction. The analysis showing in the below [table \[4.38\]](#) has been performed using Concrete Cylinder Strength of C60MPa, and Steel Grade of S355MPa.

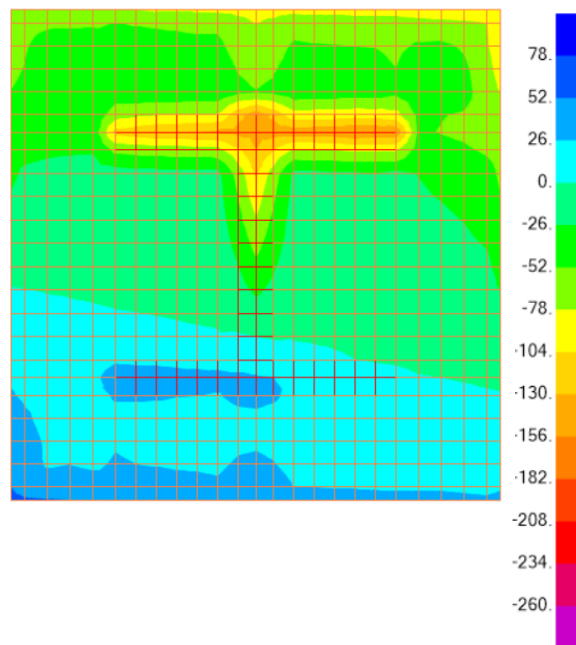
[Fig. \(4.43\)](#) presents the stress contours along the height of the encased columns as extracted from the 3D Fiber (Solid) Model.

Analysis Approach	AISC 360-16	Eurocode-4	3D-Fiber (Solid) Element Model	
Concrete Cylinder Strength (MPa)	60	60	60	
Steel Grade (MPa)	S355	S355	S355	
Axial Compression Load, P (kN)	1,275	1,185	800	
Load Eccentricity, e_x (mm)	85.75	85.75	85.75	
Load Eccentricity, e_y (mm)	104.50	104.50	104.50	
Bending Moments at the Top of the Column, M = P.e (kN.m)	M _x = 133.24 M _y = 109.33	M _x = 123.83 M _y = 101.61	M _x = 83.60 M _y = 68.60	
Section Capacity (D/C)	1.0	1.0		
Stresses on the Fiber (Solid) Model under 800 kN			Concrete Stress (MPa)	Steel Stress (MPa)
Compression Stresses on the Encased Column			(107.21 MPa) At Top & Bottom of Col (60 MPa) Average Stresses	(263.55 MPa) At the middle of the section
Tensile Stresses on the Encased Column			(57.33 MPa) At Top and Bottom	(96.79 MPa) At Bottom of Sec
Strain (ϵ)			Concrete Strain	Steel Strain
Compression Strain on the Encased Column			0.0027 / 0.0015	0.0013
Tensile Strain on the Encased Column			0.0014	0.0005

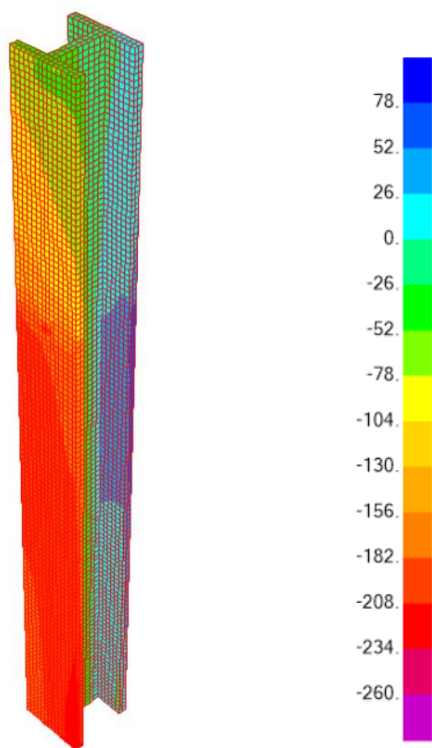
Table [4.38] Encased Column Section Capacity under Axial Compression and Bi-Axial Bending, C60MPa, S355



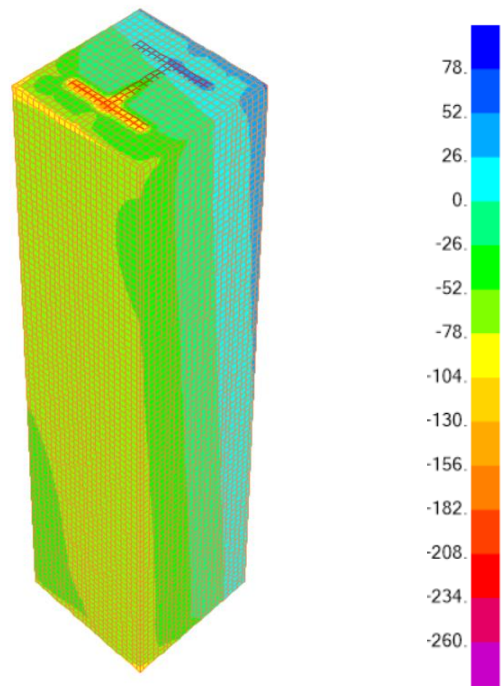
Stresses on Encased Column
Bottom View



Stresses on Encased Column
Top View



Stresses on Steel I Section



Stresses on Encased Column

Fig. (4.43) Stresses' Contours Along Encased Composite Column, C60MPa, S355MPa

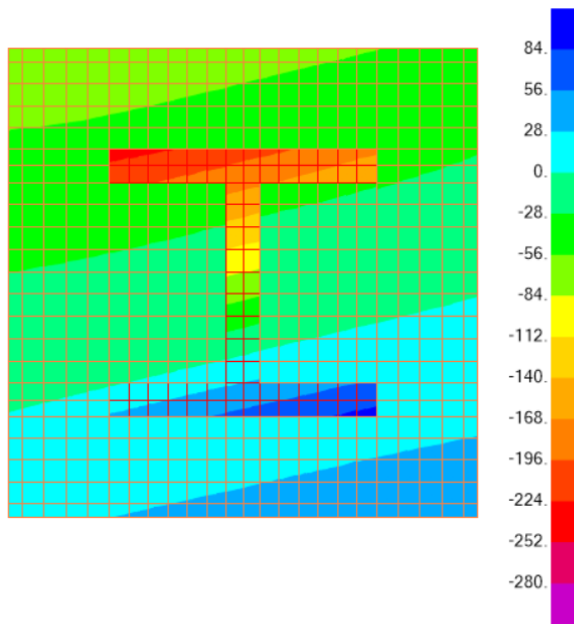
4.4.5.1.4 Encased Column Analysis under Axial Compression and Bi-Axial Moments, C70MPa, S355MPa.

The following [table \[4.39\]](#) summarizes the Encased Column Sectional Capacity under Axial compression and bi-axial bending moments. The section capacity has been determined using simplified approach adopted by AISC 360-16, and Eurocode-4. In addition; it shows the stresses and strains of the concrete and steel elements extracted from the 3D -Fiber (Solid) Model. The load eccentricities were constant of 85.75mm in X-direction and 104.50mm in Y-direction. The analysis showing in the below [table \[4.39\]](#) has been performed using Concrete Cylinder Strength of C70MPa, and Steel Grade of S355MPa.

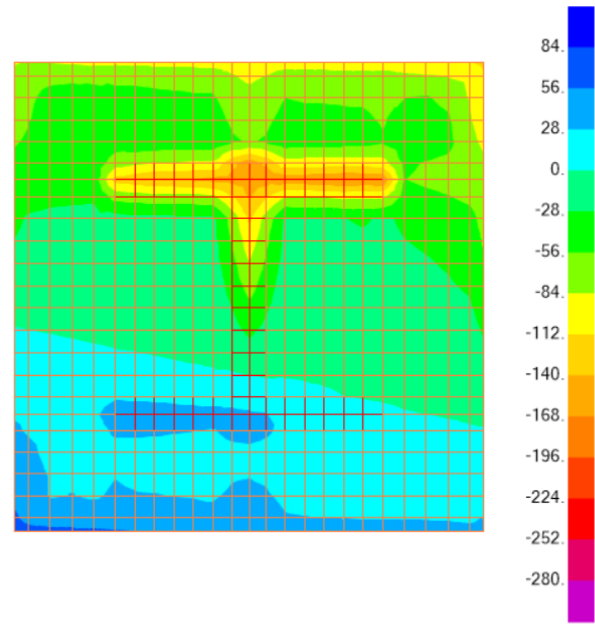
[Fig. \(4.44\)](#) presents the stress contours along the height of the encased columns as extracted from the 3D Fiber (Solid) Model.

Analysis Approach	AISC 360-16	Eurocode-4	3D-Fiber (Solid) Element Model	
Concrete Cylinder Strength (MPa)	70	70	70	
Steel Grade (MPa)	S355	S355	S355	
Axial Compression Load, P (kN)	1,350	1,255	925	
Load Eccentricity, ex (mm)	85.75	85.75	85.75	
Load Eccentricity, ey (mm)	104.50	104.50	104.50	
Bending Moments at the Top of the Column, M = P.e (kN.m)	Mx = 115.76 My = 141.08	Mx = 131.15 My = 107.62	Mx = 83.60 My = 79.32	
Section Capacity (D/C)	1.0	1.0		
Stresses on the Fiber (Solid) Model under 925 kN			Concrete Stress (MPa)	Steel Stress (MPa)
Compression Stresses on the Encased Column			(125.67 MPa) At Top & Bottom of Col (70MPa) Average Stresses	(291.80 MPa) At the middle of the section
Tensile Stresses on the Encased Column			(66.56 MPa) At Top and Bottom	(107.0 MPa) At Bottom of Sec
Strain (ε)			Concrete Strain	Steel Strain
Compression Strain on the Encased Column			0.003	0.0015
Tensile Strain on the Encased Column			0.0016	0.0005

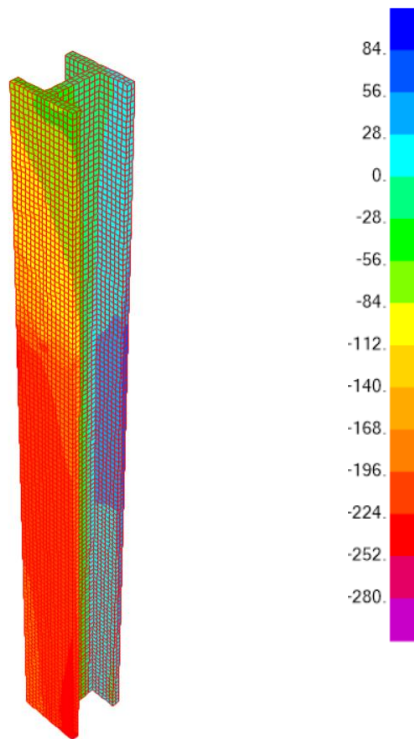
[Table \[4.39\]](#) Encased Column Section Capacity under Axial Compression and Bi-Axial Bending, C70MPa, S355



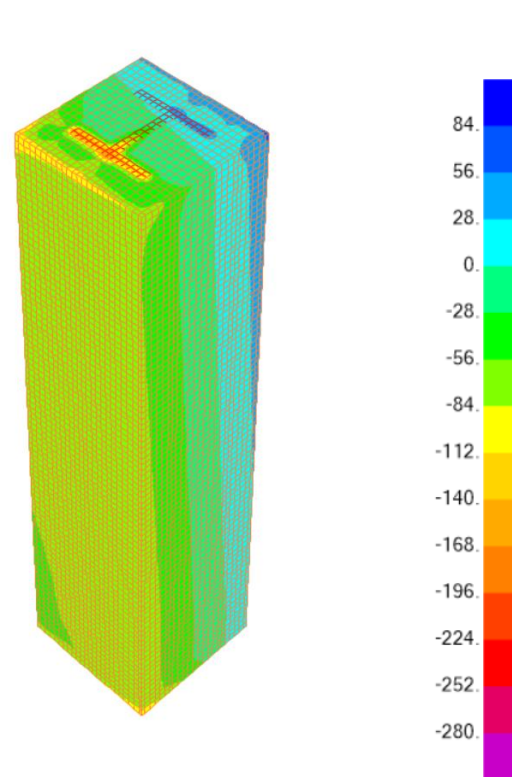
Stresses on Encased Column
Bottom View



Stresses on Encased Column
Top View



Stresses on Steel I Section



Stresses on Encased Column

Fig. (4.44) Stresses' Contours Along Encased Composite Column, C70MPa, S355MPa

4.4.5.1.5 Encased Column Analysis under Axial Compression and Bi-Axial Moments, C40MPa, S275MPa.

The following [table \[4.40\]](#) summarizes the Encased Column Sectional Capacity under Axial compression and bi-axial bending moments. The section capacity has been determined using simplified approach adopted by AISC 360-16, and Eurocode-4. In addition; it shows the stresses and strains of the concrete and steel elements extracted from the 3D -Fiber (Solid) Model.

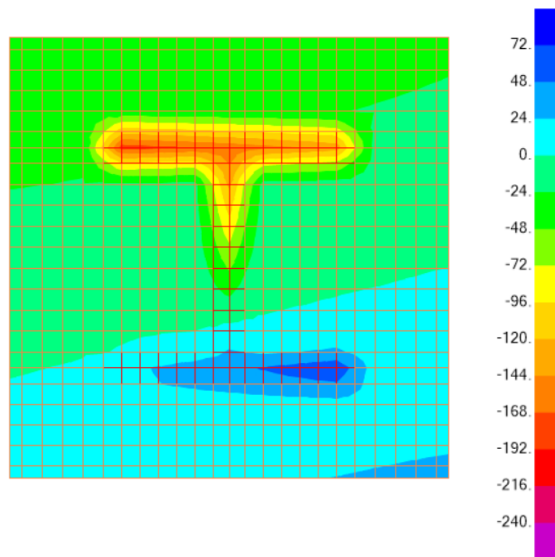
The load eccentricities were constant of 85.75mm in X-direction and 104.50mm in Y-direction.

The analysis showing in the below [table \[4.40\]](#) has been performed using Concrete Cylinder Strength of C40MPa, and Steel Grade of S275MPa.

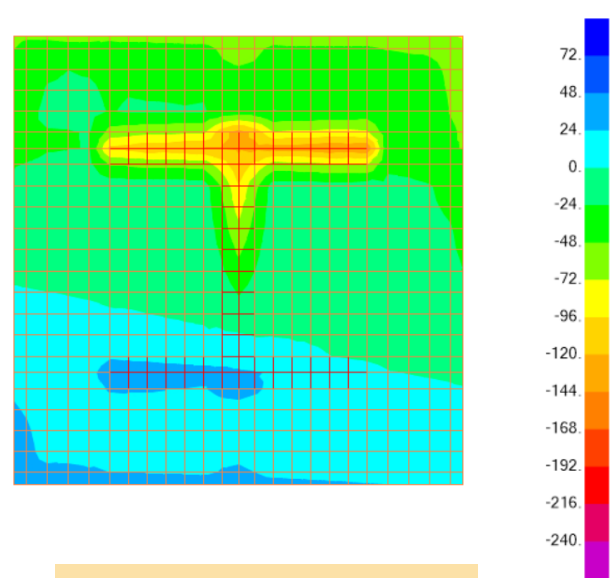
[Fig. \(4.45\)](#) presents the stress contours along the height of the encased columns as extracted from the 3D Fiber (Solid) Model.

Analysis Approach	AISC 360-16	Eurocode-4	3D-Fiber (Solid) Element Model	
Concrete Cylinder Strength (MPa)	40	40	40	
Steel Grade (MPa)	S275	S275	S275	
Axial Compression Load, P (kN)	865	805	600	
Load Eccentricity, ex (mm)	85.75	85.75	85.75	
Load Eccentricity, ey (mm)	104.50	104.50	104.50	
Bending Moments at the Top of the Column, M = P.e (kN.m)	Mx = 90.39 My = 74.17	Mx = 84.12 My = 69.03	Mx = 62.70 My = 51.45	
Section Capacity (D/C)	1.0	1.0		
Stresses on the Fiber (Solid) Model under 600 kN			Concrete Stress (MPa)	Steel Stress (MPa)
Compression Stresses on the Encased Column			(75.08 MPa) At Top & Bottom of Col (40 MPa) Average Stresses	(252.40 MPa) At the middle of the section
Tensile Stresses on the Encased Column			(42.11 MPa) At Top and Bottom	(94.29 MPa) At Bottom of Sec
Strain (ε)			Concrete Strain	Steel Strain
Compression Strain on the Encased Column			0.0025 / 0.0013	0.0013
Tensile Strain on the Encased Column			0.0014	0.0005

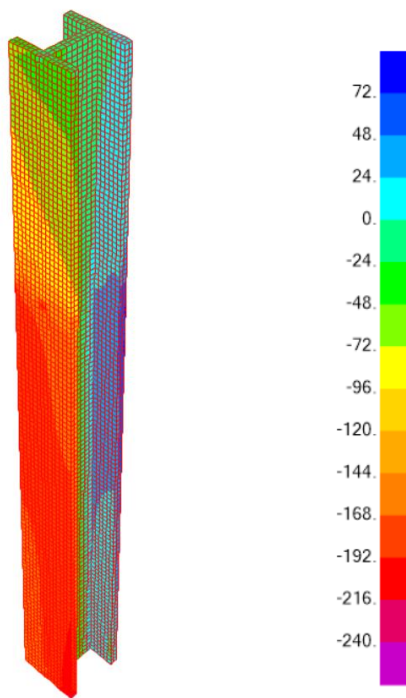
Table [4.40] Encased Column Section Capacity under Axial Compression and Bi-Axial Bending, C40MPa, S275



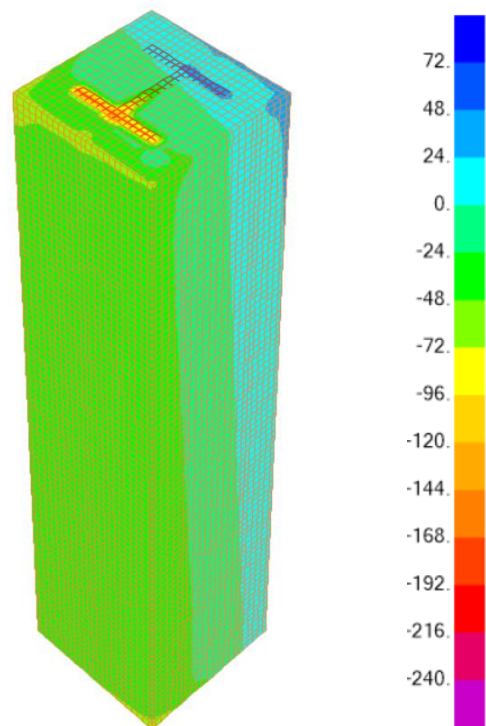
Stresses on Encased Column
Bottom View



Stresses on Encased Column
Top View



Stresses on Steel I Section



Stresses on Encased Column

Fig. (4.45) Stresses' Contours Along Encased Composite Column, C40MPa, S275MPa

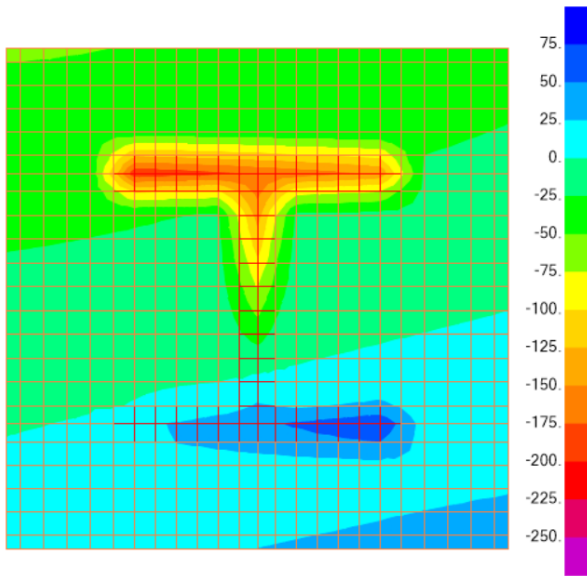
4.4.5.1.6 Encased Column Analysis under Axial Compression and Bi-Axial Moments, C50MPa, S275MPa.

The following [table \[4.41\]](#) summarizes the Encased Column Sectional Capacity under Axial compression and bi-axial bending moments. The section capacity has been determined using simplified approach adopted by AISC 360-16, and Eurocode-4. In addition; it shows the stresses and strains of the concrete and steel elements extracted from the 3D -Fiber (Solid) Model. The load eccentricities were constant of 85.75mm in X-direction and 104.50mm in Y-direction. The analysis showing in the below [table \[4.41\]](#) has been performed using Concrete Cylinder Strength of C50MPa, and Steel Grade of S275MPa.

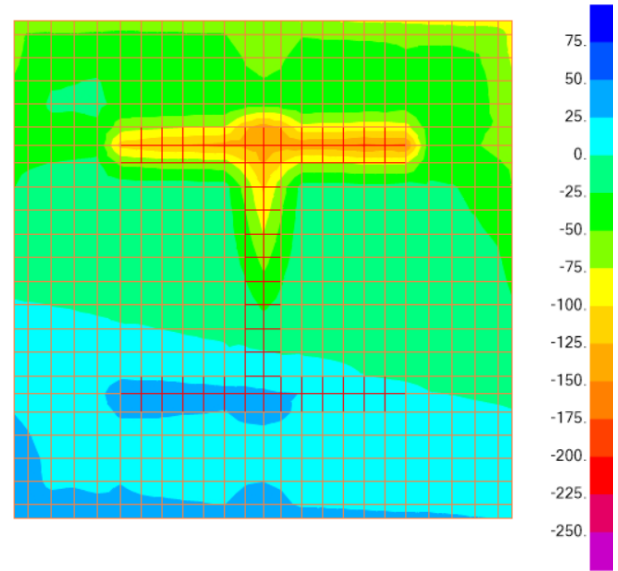
[Fig. \(4.46\)](#) presents the stress contours along the height of the encased columns as extracted from the 3D Fiber (Solid) Model.

Analysis Approach	AISC 360-16	Eurocode-4	3D-Fiber (Solid) Element Model	
Concrete Cylinder Strength (MPa)	50	50	50	
Steel Grade (MPa)	S275	S275	S275	
Axial Compression Load, P (kN)	935	870	700	
Load Eccentricity, ex (mm)	85.75	85.75	85.75	
Load Eccentricity, ey (mm)	104.50	104.50	104.50	
Bending Moments at the Top of the Column, M = P.e (kN.m)	Mx = 97.71 My = 80.18	Mx = 90.92 My = 74.60	Mx = 73.15 My = 60.03	
Section Capacity (D/C)	1.0	1.0		
Stresses on the Fiber (Solid) Model under 700 kN			Concrete Stress (MPa)	Steel Stress (MPa)
Compression Stresses on the Encased Column			(88.94 MPa) At Top & Bottom of Column (50 MPa) Average Stresses	(269.23 MPa) At the middle of the section
Tensile Stresses on the Encased Column			(49.60 MPa) At Top and Bottom	(99.90 MPa) At Bottom of Sec
Strain (ε)			Concrete Strain	Steel Strain
Compression Strain on the Encased Column			0.0027 / 0.0015	0.0013
Tensile Strain on the Encased Column			0.0015	0.0005

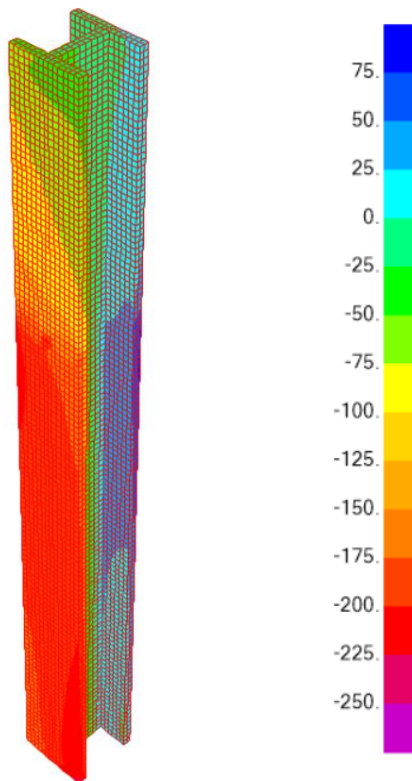
Table [4.41] Encased Column Section Capacity under Axial Compression and Bi-Axial Bending, C50MPa, S275



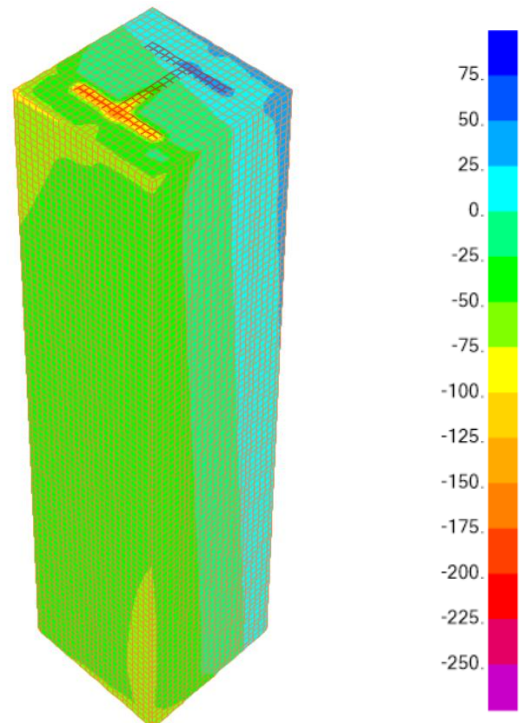
Stresses on Encased Column
Bottom View



Stresses on Encased Column
Top View



Stresses on Steel I Section



Stresses on Encased Column

Fig. (4.46) Stresses' Contours Along Encased Composite Column, C50MPa, S275MPa

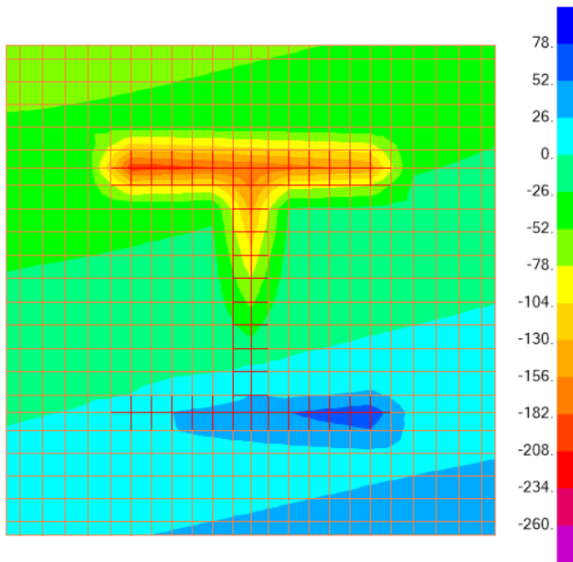
4.4.5.1.7 Encased Column Analysis under Axial Compression and Bi-Axial Moments, C60MPa, S275MPa.

The following [table \[4.42\]](#) summarizes the Encased Column Sectional Capacity under Axial compression and bi-axial bending moments. The section capacity has been determined using simplified approach adopted by AISC 360-16, and Eurocode-4. In addition; it shows the stresses and strains of the concrete and steel elements extracted from the 3D -Fiber (Solid) Model. The load eccentricities were constant of 85.75mm in X-direction and 104.50mm in Y-direction. The analysis showing in the below [table \[4.42\]](#) has been performed using Concrete Cylinder Strength of C60MPa, and Steel Grade of S275MPa.

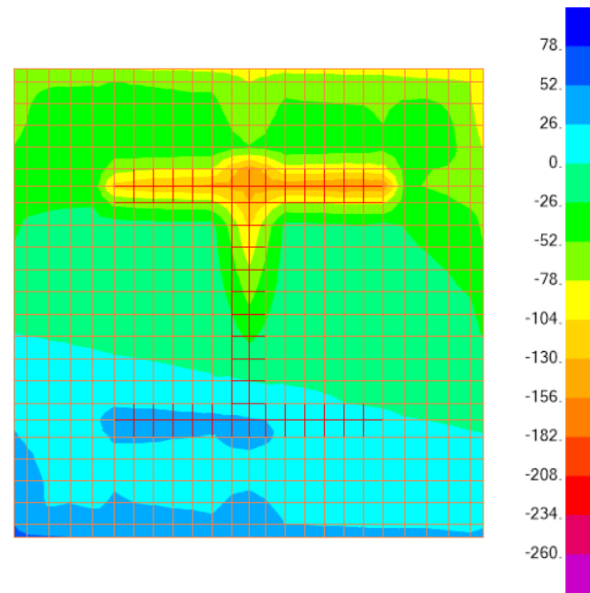
[Fig. \(4.47\)](#) presents the stress contours along the height of the encased columns as extracted from the 3D Fiber (Solid) Model.

Analysis Approach	AISC 360-16	Eurocode-4	3D-Fiber (Solid) Element Model	
Concrete Cylinder Strength (MPa)	60	60	60	
Steel Grade (MPa)	S275	S275	S275	
Axial Compression Load, P (kN)	1050	975	800	
Load Eccentricity, ex (mm)	85.75	85.75	85.75	
Load Eccentricity, ey (mm)	104.50	104.50	104.50	
Bending Moments at the Top of the Column, M = P.e (kN.m)	Mx = 109.73 My = 90.04	Mx = 101.89 My = 83.61	Mx = 83.60 My = 68.60	
Section Capacity (D/C)	1.0	1.0		
Stresses on the Fiber (Solid) Model under 800 kN			Concrete Stress (MPa)	Steel Stress (MPa)
Compression Stresses on the Encased Column			(107.21 MPa) At Top & Bottom of Column (60 MPa) Average Stresses	(263.55 MPa) At the middle of the section
Tensile Stresses on the Encased Column			(57.33 MPa) At Top and Bottom	(96.79 MPa) At Bottom of Sec
Strain (ϵ)			Concrete Strain	Steel Strain
Compression Strain on the Encased Column			0.0027 / 0.0015	0.0013
Tensile Strain on the Encased Column			0.0014	0.0005

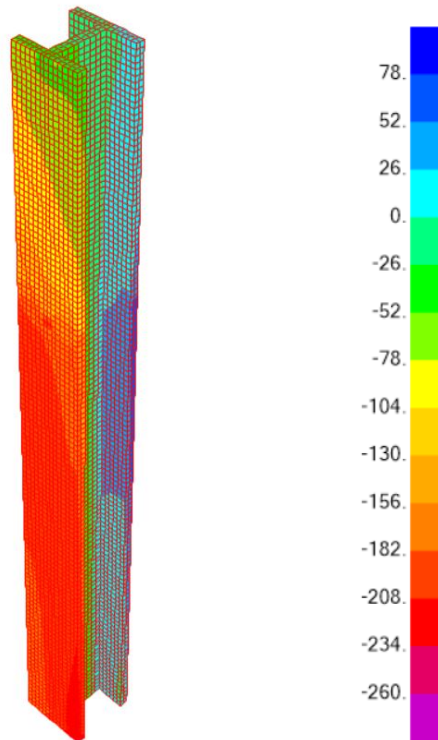
Table [4.42] Encased Column Section Capacity under Axial Compression and Bi-Axial Bending, C60MPa, S275



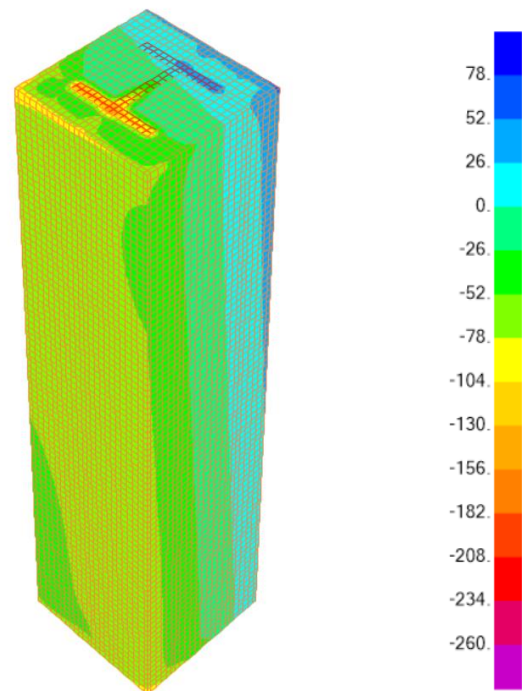
Stresses on Encased Column
Bottom View



Stresses on Encased Column
Top View



Stresses on Steel I Section



Stresses on Encased Column

Fig. (4.47) Stresses' Contours Along Encased Composite Column, C60MPa, S275MPa

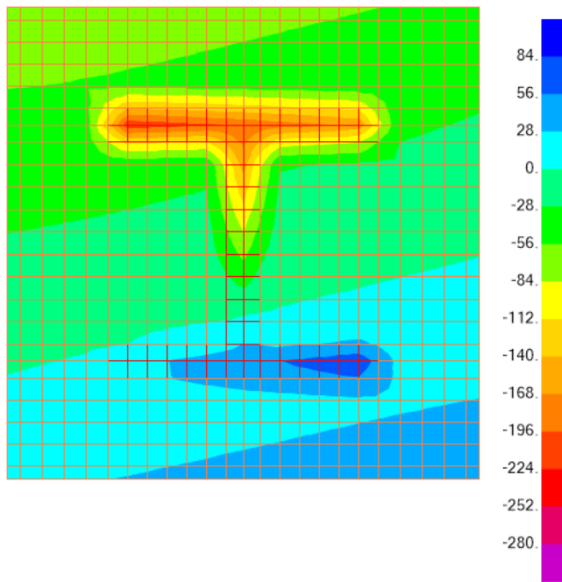
4.4.5.1.8 Encased Column Analysis under Axial Compression and Bi-Axial Moments, C70MPa, S275MPa.

The following [table \[4.43\]](#) summarizes the Encased Column Sectional Capacity under Axial compression and bi-axial bending moments. The section capacity has been determined using simplified approach adopted by AISC 360-16, and Eurocode-4. In addition; it shows the stresses and strains of the concrete and steel elements extracted from the 3D -Fiber (Solid) Model. The load eccentricities were constant of 85.75mm in X-direction and 104.50mm in Y-direction. The analysis showing in the below [table \[4.43\]](#) has been performed using Concrete Cylinder Strength of C70MPa, and Steel Grade of S275MPa.

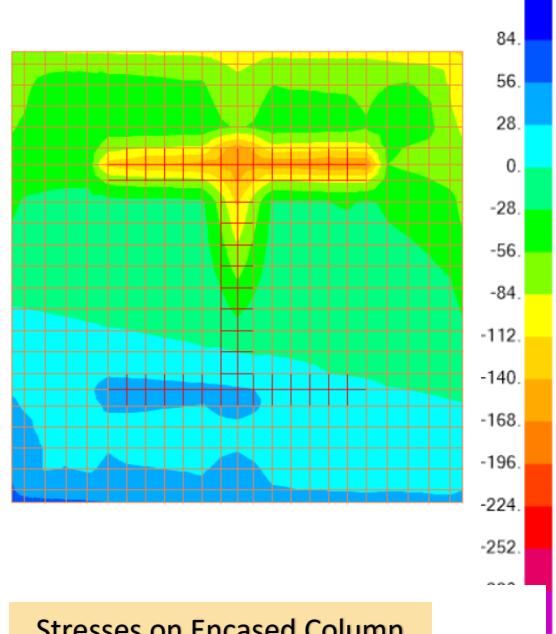
[Fig. \(4.48\)](#) presents the stress contours along the height of the encased columns as extracted from the 3D Fiber (Solid) Model.

Analysis Approach	AISC 360-16	Eurocode-4	3D-Fiber (Solid) Element Model	
Concrete Cylinder Strength (MPa)	70	70	70	
Steel Grade (MPa)	S275	S275	S275	
Axial Compression Load, P (kN)	1100	1,025	925	
Load Eccentricity, ex (mm)	85.75	85.75	85.75	
Load Eccentricity, ey (mm)	104.50	104.50	104.50	
Bending Moments at the Top of the Column, M = P.e (kN.m)	Mx = 114.95 My = 194.33	Mx = 107.11 My = 87.89	Mx = 96.66 My = 79.32	
Section Capacity (D/C)	1.0	1.0		
Stresses on the Fiber (Solid) Model under 925 kN			Concrete Stress (MPa)	Steel Stress (MPa)
Compression Stresses on the Encased Column			(125.67 MPa) At Top & Bottom of Column (70 MPa) Average Stresses	(291.88 MPa) At the middle of the section
Tensile Stresses on the Encased Column			(66.56 MPa) At Top and Bottom	(107.0 MPa) At Bottom of Sec
Strain (ε)			Concrete Strain	Steel Strain
Compression Strain on the Encased Column			0.003	0.0015
Tensile Strain on the Encased Column			0.017	0.00054

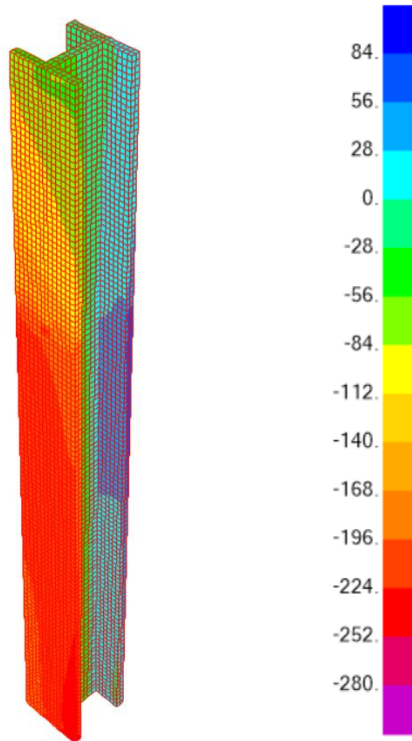
Table [4.43] Encased Column Section Capacity under Axial Compression and Bi-Axial Bending, C70MPa, S275



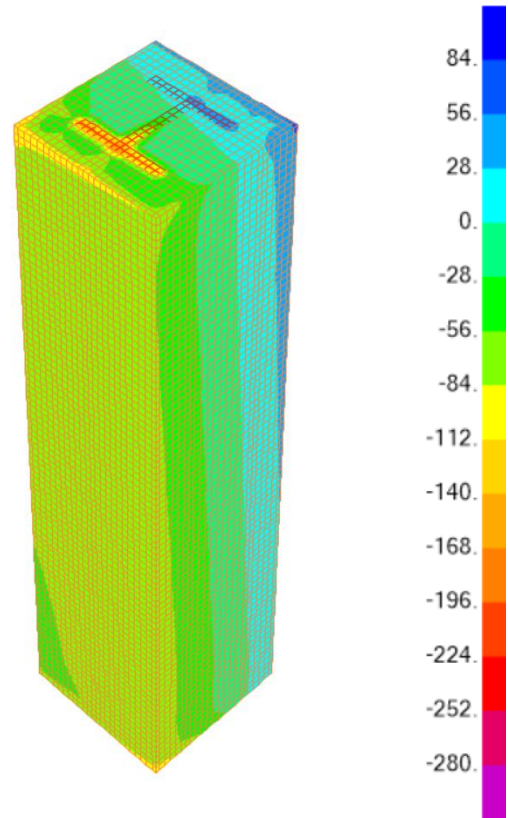
Stresses on Encased Column
Bottom View



Stresses on Encased Column
Top View



Stresses on Steel I Section



Stresses on Encased Column

Fig. (4.48) Stresses' Contours Along Encased Composite Column, C70MPa, S275MPa

4.4.5.2 Stresses on the CFST Composite Column subject to Axial Compression and Bi-Axial Bending

This clause describes the analysis of the CFST Composite Column subject to axial compression loads and bi-axial bending moments. The stresses and strains on the concrete and steel section have been evaluated and compared to the simplified methods adopted by AISC 360-16, and Eurocode-4.

It was vital to understand the sectional behavior under different concrete cylinder strengths ranging from C40MPa to C70MPa, with different Young's Modulus of Elasticity as summarized in **clause 4.4.5**.

Furthermore; the capacity of the composite section has been evaluated using two different steel grades, S275MPa and S355MPa.

4.4.5.2.1 CFST Column Analysis under Axial Compression and Bi-Axial Moments, C40MPa, S355MPa

The following [table \[4.44\]](#) summarizes the Encased Column Sectional Capacity under Axial compression and bi-axial bending moments. The section capacity has been determined using simplified approach adopted by AISC 360-16, and Eurocode-4. In addition; it shows the stresses and strains of the concrete and steel elements extracted from the 3D -Fiber (Solid) Model. The load eccentricities were constant of 85.75mm in X-direction and 104.50mm in Y-direction. The analysis showing in the below [table \[4.44\]](#) has been performed using Concrete Cylinder Strength of C40MPa, and Steel Grade of S355MPa. [Fig. \(4.49\)](#) presents the stress contours along the height of the encased columns as extracted from the 3D Fiber (Solid) Model.

Analysis Approach	AISC 360-16	Eurocode-4	3D-Fiber (Solid) Element Model	
Concrete Cylinder Strength (MPa)	40	40	40	
Steel Grade (MPa)	S355	S355	S355	
Axial Compression Load, P (kN)	1,000	935	600	
Load Eccentricity, e_x (mm)	85.75	85.75	85.75	
Load Eccentricity, e_y (mm)	104.50	104.50	104.50	
Bending Moments at the Top of the Column, M = P.e (kN.m)	M _x = 104.50 M _y = 85.75	M _x = 97.71 M _y = 80.18	M _x = 62.70 M _y = 51.45	
Section Capacity (D/C)	1.0	1.0		
Stresses on the Fiber (Solid) Model under 600 kN			Concrete Stress (MPa)	Steel Stress (MPa)
Compression Stresses on the CFST Column			(36.64) MPa	(177.45) MPa
Tensile Stresses on the CFST Column			(07.06) MPa	(85.33) MPa
Strain (ε)			Concrete Strain	Steel Strain
Compression Strain on the CFST Column			0.00123	0.00089
Tensile Strain on the CFST Column			0.00024	0.00043

Table [4.44] CFST Column Section Capacity under Axial Compression and Bi-Axial Bending, C40MPa, S355

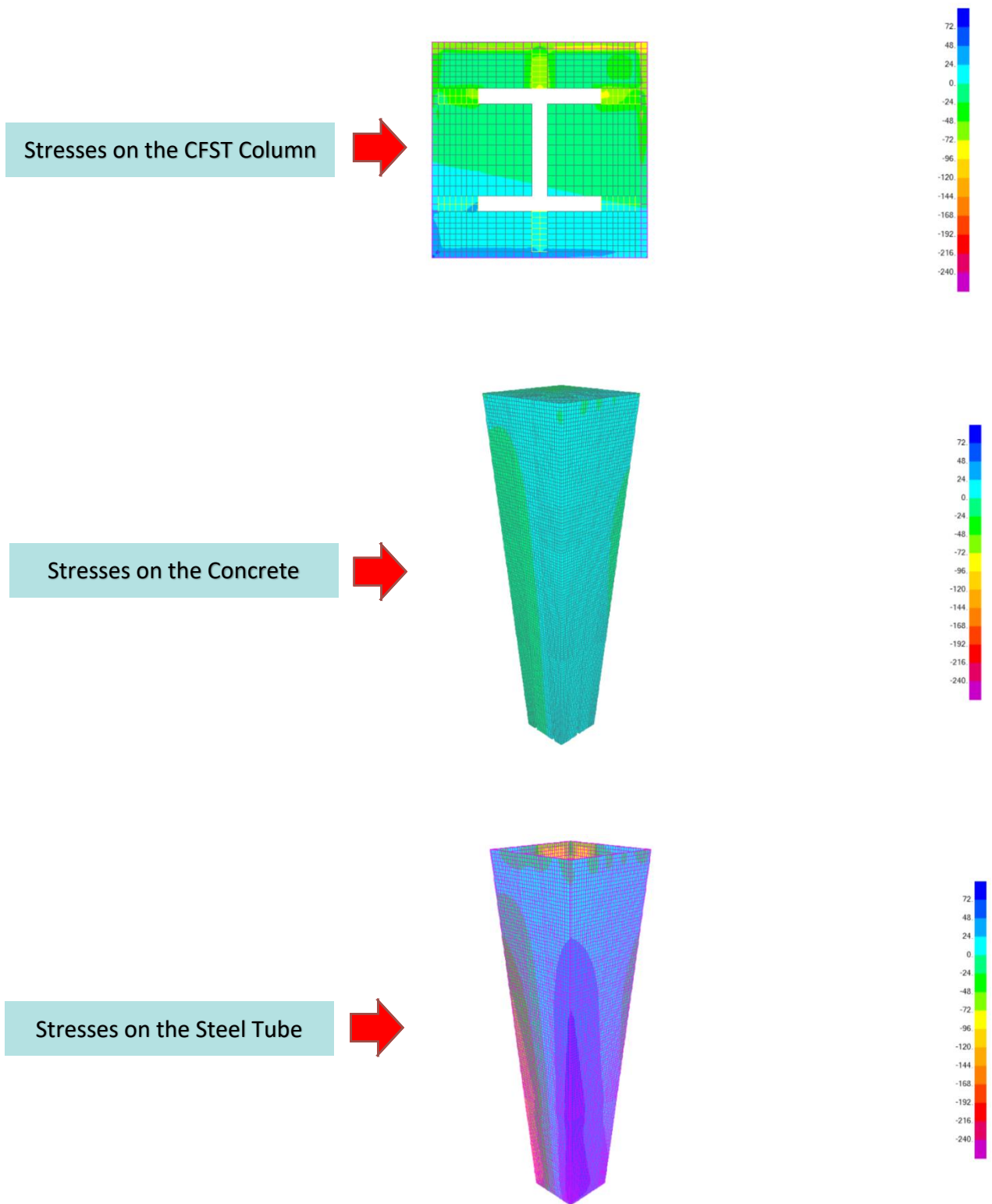


Fig. (4.49) Stresses' Contours Along CFST Composite Column, C40MPa, S355MPa

4.4.5.2.2 CFST Column Analysis under Axial Compression and Bi-Axial Moments, C50MPa, S355MPa

The following [table \[4.45\]](#) summarizes the Encased Column Sectional Capacity under Axial compression and bi-axial bending moments. The section capacity has been determined using simplified approach adopted by AISC 360-16, and Eurocode-4. In addition; it shows the stresses and strains of the concrete and steel elements extracted from the 3D -Fiber (Solid) Model. The load eccentricities were constant of 85.75mm in X-direction and 104.50mm in Y-direction. The analysis showing in the below [table \[4.45\]](#) has been performed using Concrete Cylinder Strength of C50MPa, and Steel Grade of S355MPa.

[Fig. \(4.50\)](#) presents the stress contours along the height of the encased columns as extracted from the 3D Fiber (Solid) Model.

Analysis Approach	AISC 360-16	Eurocode-4	3D-Fiber (Solid) Element Model	
Concrete Cylinder Strength (MPa)	50	50	50	
Steel Grade (MPa)	S355	S355	S355	
Axial Compression Load, P (kN)	1,065	990	700	
Load Eccentricity, e_x (mm)	85.75	85.75	85.75	
Load Eccentricity, e_y (mm)	104.50	104.50	104.50	
Bending Moments at the Top of the Column, M = P.e (kN.m)	M _x = 111.30 M _y = 91.32	M _x = 103.46 M _y = 84.89	M _x = 73.15 M _y = 60.03	
Section Capacity (D/C)	1.0	1.0		
Stresses on the Fiber (Solid) Model under 700 kN			Concrete Stress (MPa)	Steel Stress (MPa)
Compression Stresses on the CFST Column			(42.80) MPa	(192.51) MPa
Tensile Stresses on the CFST Column			(8.73) MPa	(92.50) MPa
Strain (ε)			Concrete Strain	Steel Strain
Compression Strain on the CFST Column			0.0013	0.00096
Tensile Strain on the CFST Column			0.0026	0.00046

Table [4.45] CFST Column Section Capacity under Axial Compression and Bi-Axial Bending, C50MPa, S355

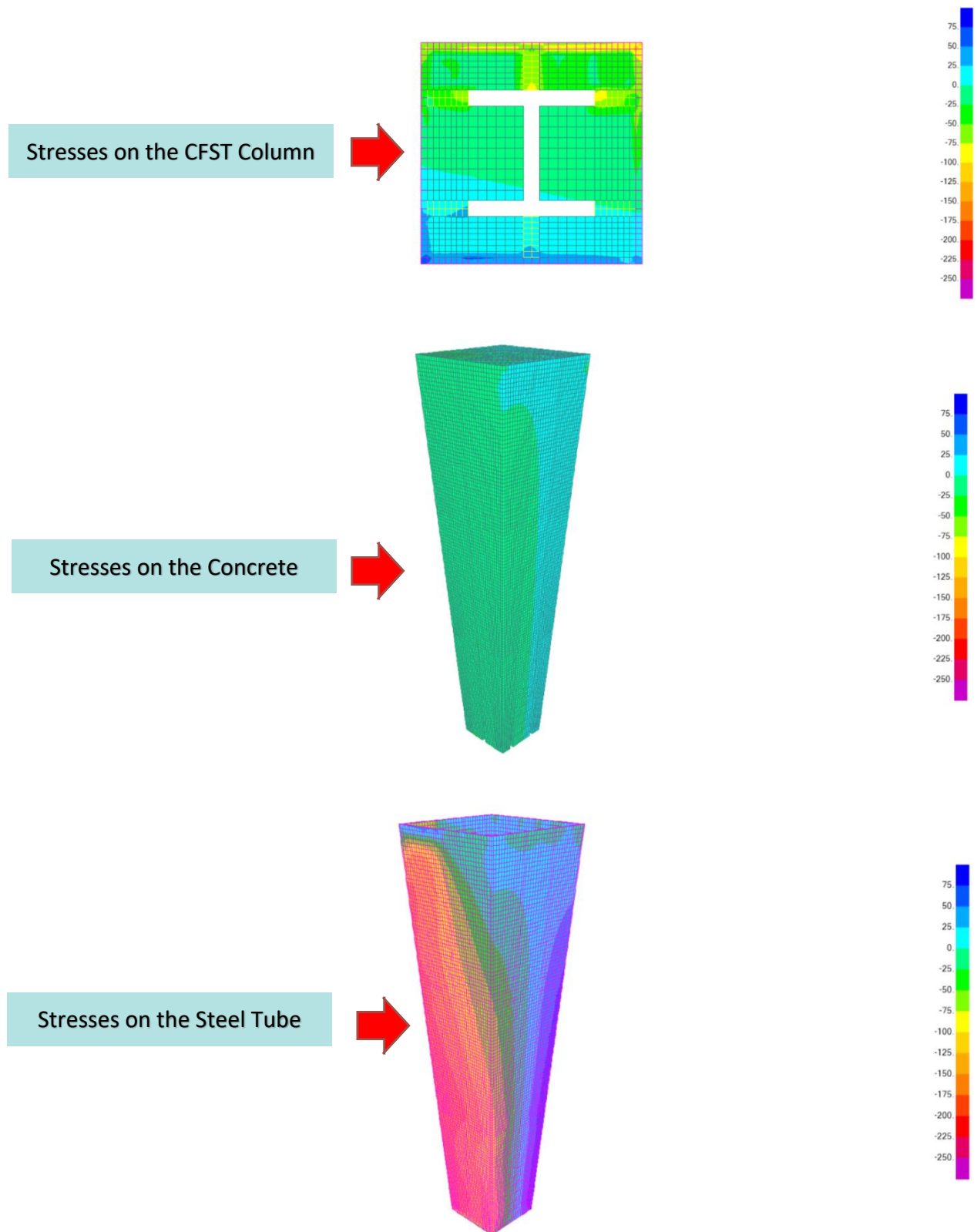


Fig. (4.50) Stresses' Contours Along CFST Composite Column, C50MPa, S355MPa

4.4.5.2.3 CFST Column Analysis under Axial Compression and Bi-Axial Moments, C60MPa, S355MPa

The following [table \[4.46\]](#) summarizes the Encased Column Sectional Capacity under Axial compression and bi-axial bending moments. The section capacity has been determined using simplified approach adopted by AISC 360-16, and Eurocode-4. In addition; it shows the stresses and strains of the concrete and steel elements extracted from the 3D -Fiber (Solid) Model. The load eccentricities were constant of 85.75mm in X-direction and 104.50mm in Y-direction. The analysis showing in the below [table \[4.46\]](#) has been performed using Concrete Cylinder Strength of C60MPa, and Steel Grade of S355MPa.

[Fig. \(4.51\)](#) presents the stress contours along the height of the encased columns as extracted from the 3D Fiber (Solid) Model.

Analysis Approach	AISC 360-16	Eurocode-4	3D-Fiber (Solid) Element Model	
Concrete Cylinder Strength (MPa)	60	60	60	
Steel Grade (MPa)	S355	S355	S355	
Axial Compression Load, P (kN)	1,150	1,070	800	
Load Eccentricity, e_x (mm)	85.75	85.75	85.75	
Load Eccentricity, e_y (mm)	104.50	104.50	104.50	
Bending Moments at the Top of the Column, M = P.e (kN.m)	M _x = 120.18 M _y = 98.61	M _x = 111.82 M _y = 91.75	M _x = 83.60 M _y = 68.60	
Section Capacity (D/C)	1.0	1.0		
Stresses on the Fiber (Solid) Model under 800 kN			Concrete Stress (MPa)	Steel Stress (MPa)
Compression Stresses on the CFST Column			(49.08) MPa	(201.38) MPa
Tensile Stresses on the CFST Column			(10.87) MPa	(101.57) MPa
Strain (ϵ)			Concrete Strain	Steel Strain
Compression Strain on the CFST Column			0.00123	0.001
Tensile Strain on the CFST Column			0.00027	0.00051

Table [4.46] CFST Column Section Capacity under Axial Compression and Bi-Axial Bending, C60MPa, S355

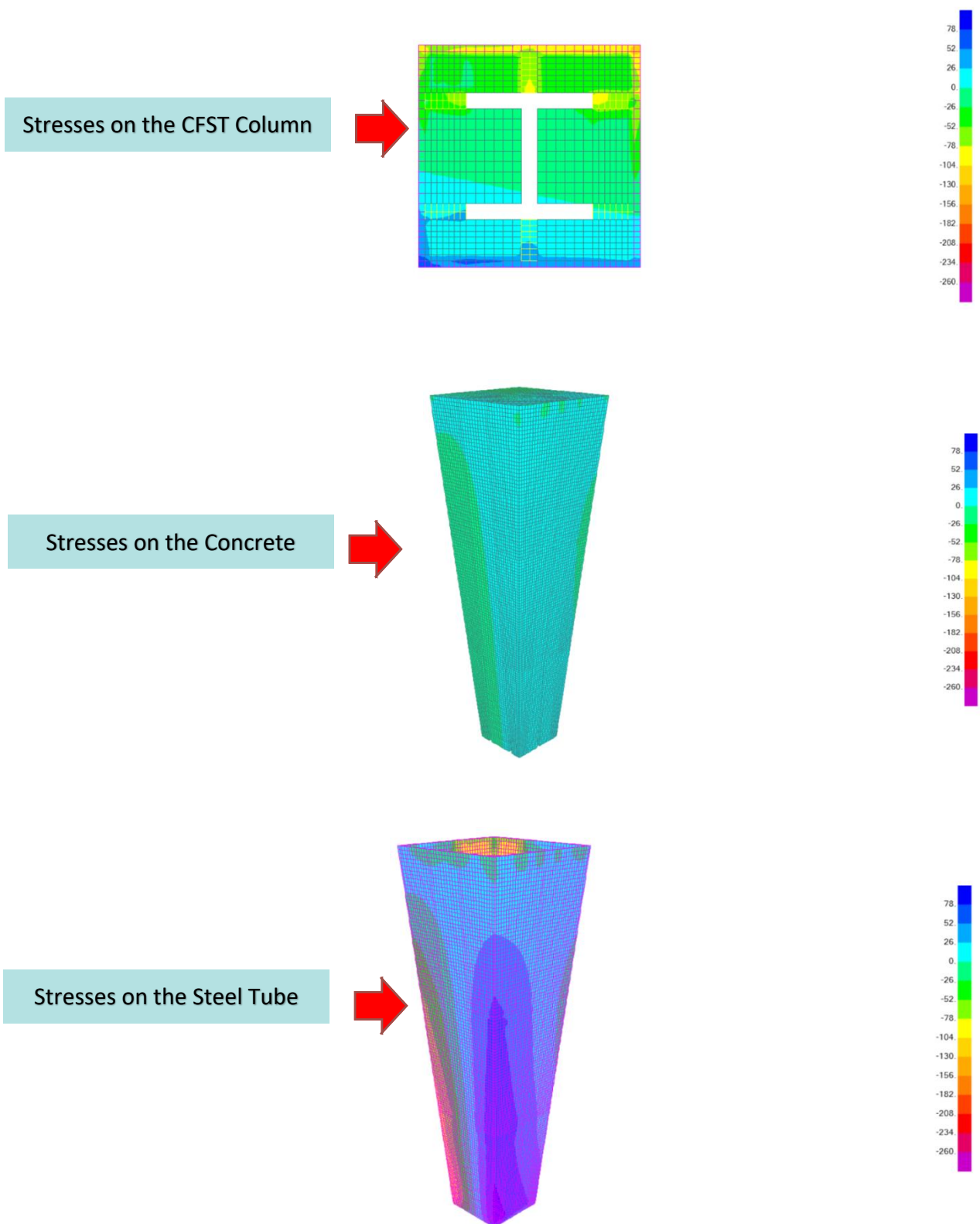


Fig. (4.51) Stresses' Contours Along CFST Composite Column, C60MPa, S355MPa

4.4.5.2.4 CFST Column Analysis under Axial Compression and Bi-Axial Moments, C70MPa, S355MPa

The following [table \[4.47\]](#) summarizes the Encased Column Sectional Capacity under Axial compression and bi-axial bending moments. The section capacity has been determined using simplified approach adopted by AISC 360-16, and Eurocode-4. In addition; it shows the stresses and strains of the concrete and steel elements extracted from the 3D -Fiber (Solid) Model. The load eccentricities were constant of 85.75mm in X-direction and 104.50mm in Y-direction. The analysis showing in the below [table \[4.47\]](#) has been performed using Concrete Cylinder Strength of C70MPa, and Steel Grade of S355MPa. [Fig. \(4.52\)](#) presents the stress contours along the height of the encased columns as extracted from the 3D Fiber (Solid) Model.

Analysis Approach	AISC 360-16	Eurocode-4	3D-Fiber (Solid) Element Model	
Concrete Cylinder Strength (MPa)	70	70	70	
Steel Grade (MPa)	S355	S355	S355	
Axial Compression Load, P (kN)	1,200	1,115	925	
Load Eccentricity, e_x (mm)	85.75	85.75	85.75	
Load Eccentricity, e_y (mm)	104.50	104.50	104.50	
Bending Moments at the Top of the Column, M = P.e (kN.m)	M _x = 125.40 M _y = 102.90	M _x = 116.52 M _y = 95.61	M _x = 96.66 M _y = 79.32	
Section Capacity (D/C)	1.0	1.0		
Stresses on the Fiber (Solid) Model under 925 kN			Concrete Stress (MPa)	Steel Stress (MPa)
Compression Stresses on the CFST Column			(56.88) MPa	(228.12) MPa
Tensile Stresses on the CFST Column			(12.84) MPa	(114.27) MPa
Strain (ϵ)			Concrete Strain	Steel Strain
Compression Strain on the CFST Column			0.00135	0.00114
Tensile Strain on the CFST Column			0.00031	0.00057

Table [4.47] CFST Column Section Capacity under Axial Compression and Bi-Axial Bending, C70MPa, S355

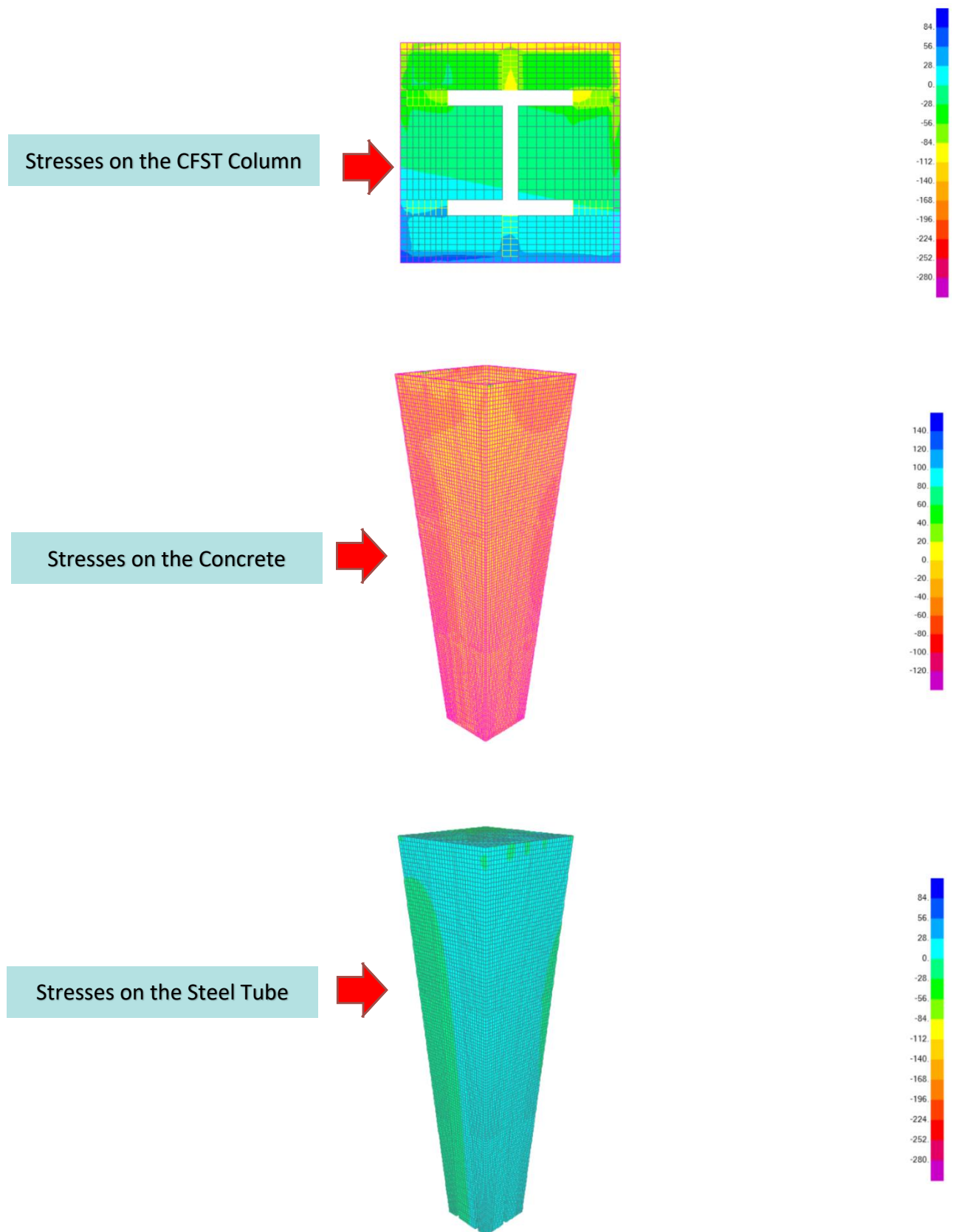


Fig. (4.52) Stresses' Contours Along CFST Composite Column, C70MPa, S355MPa

4.4.5.2.5 CFST Column Analysis under Axial Compression and Bi-Axial Moments, C40MPa, S275MPa

The following [table \[4.48\]](#) summarizes the Encased Column Sectional Capacity under Axial compression and bi-axial bending moments. The section capacity has been determined using simplified approach adopted by AISC 360-16, and Eurocode-4. In addition; it shows the stresses and strains of the concrete and steel elements extracted from the 3D -Fiber (Solid) Model. The load eccentricities were constant of 85.75mm in X-direction and 104.50mm in Y-direction. The analysis showing in the below [table \[4.48\]](#) has been performed using Concrete Cylinder Strength of C40MPa, and Steel Grade of S275MPa.

[Fig. \(4.53\)](#) presents the stress contours along the height of the encased columns as extracted from the 3D Fiber (Solid) Model.

Analysis Approach	AISC 360-16	Eurocode-4	3D-Fiber (Solid) Element Model	
Concrete Cylinder Strength (MPa)	40	40	40	
Steel Grade (MPa)	S275	S275	S275	
Axial Compression Load, P (kN)	815	760	600	
Load Eccentricity, e_x (mm)	85.75	85.75	85.75	
Load Eccentricity, e_y (mm)	104.50	104.50	104.50	
Bending Moments at the Top of the Column, M = P.e (kN.m)	M _x = 85.17 M _y = 69.89	M _x = 79.42 M _y = 65.17	M _x = 62.70 M _y = 51.45	
Section Capacity (D/C)	1.0	1.0		
Stresses on the Fiber (Solid) Model under 600kN			Concrete Stress (MPa)	Steel Stress (MPa)
Compression Stresses on the CFST Column			(36.64) MPa	(177.45) MPa
Tensile Stresses on the CFST Column			(7.06) MPa	(85.33) MPa
Strain (ϵ)			Concrete Strain	Steel Strain
Compression Strain on the CFST Column			0.00123	0.00089
Tensile Strain on the CFST Column			0.00024	0.00043

Table [4.48] CFST Column Section Capacity under Axial Compression and Bi-Axial Bending, C40MPa, S275

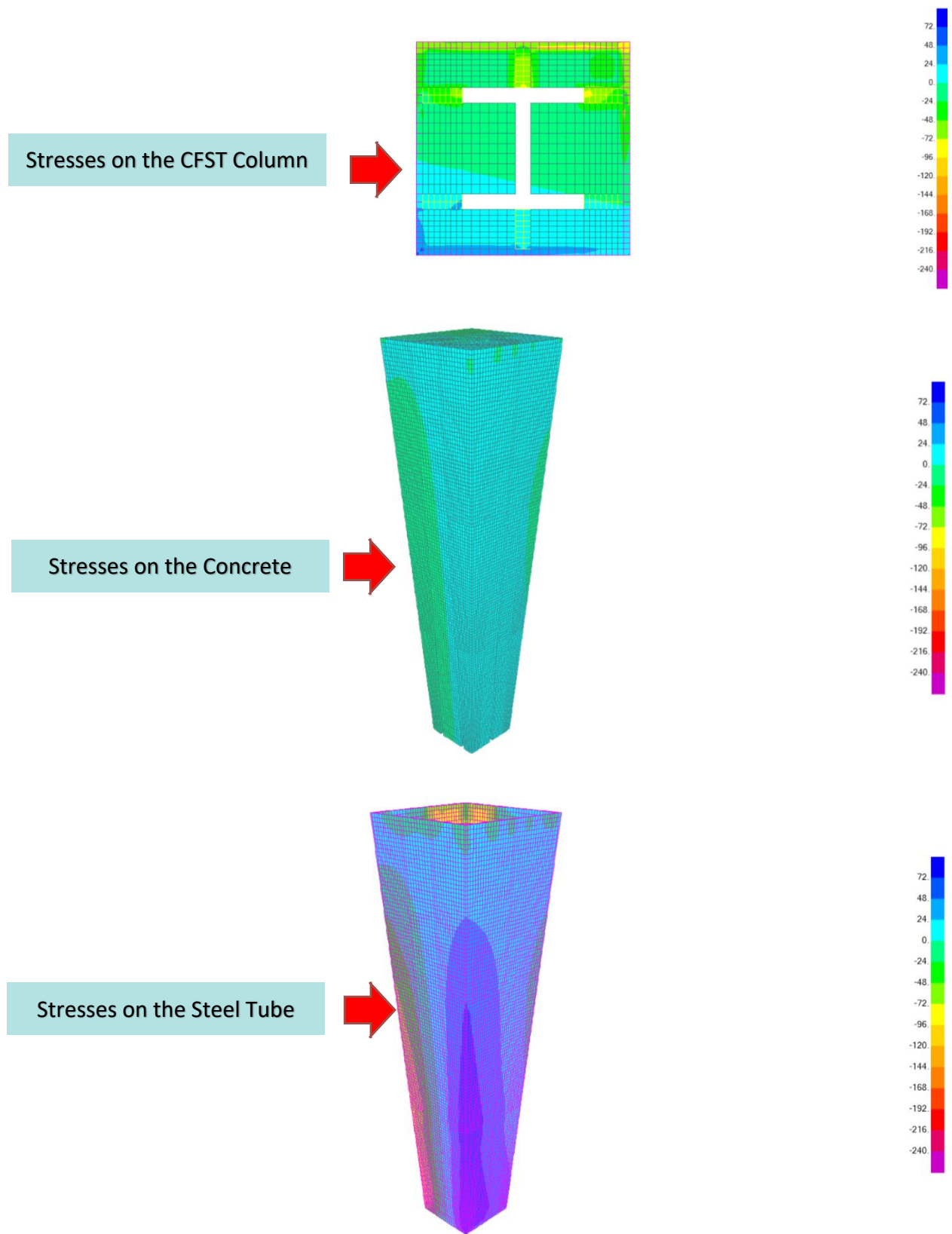


Fig. (4.53) Stresses' Contours Along CFST Composite Column, C40MPa, S275MPa

4.4.5.2.6 CFST Column Analysis under Axial Compression and Bi-Axial Moments, C50MPa, S275MPa

The following [table \[4.49\]](#) summarizes the Encased Column Sectional Capacity under Axial compression and bi-axial bending moments. The section capacity has been determined using simplified approach adopted by AISC 360-16, and Eurocode-4. In addition; it shows the stresses and strains of the concrete and steel elements extracted from the 3D -Fiber (Solid) Model. The load eccentricities were constant of 85.75mm in X-direction and 104.50mm in Y-direction. The analysis showing in the below [table \[4.49\]](#) has been performed using Concrete Cylinder Strength of C50MPa, and Steel Grade of S275MPa.

[Fig. \(4.54\)](#) presents the stress contours along the height of the encased columns as extracted from the 3D Fiber (Solid) Model.

Analysis Approach	AISC 360-16	Eurocode-4	3D-Fiber (Solid) Element Model	
Concrete Cylinder Strength (MPa)	50	50	50	
Steel Grade (MPa)	S275	S275	S275	
Axial Compression Load, P (kN)	875	815	700	
Load Eccentricity, e_x (mm)	85.75	85.75	85.75	
Load Eccentricity, e_y (mm)	104.50	104.50	104.50	
Bending Moments at the Top of the Column, M = P.e (kN.m)	M _x = 91.44 M _y = 75.03	M _x = 85.17 M _y = 69.89	M _x = 73.15 M _y = 60.03	
Section Capacity (D/C)	1.0	1.0		
Stresses on the Fiber (Solid) Model under 700 kN			Concrete Stress (MPa)	Steel Stress (MPa)
Compression Stresses on the CFST Column			(42.80) MPa	(192.51) MPa
Tensile Stresses on the CFST Column			(8.73) MPa	(95.49) MPa
Strain (ϵ)			Concrete Strain	Steel Strain
Compression Strain on the CFST Column			0.0013	0.00096
Tensile Strain on the CFST Column			0.00026	0.00048

Table [4.49] CFST Column Section Capacity under Axial Compression and Bi-Axial Bending, C50MPa, S275

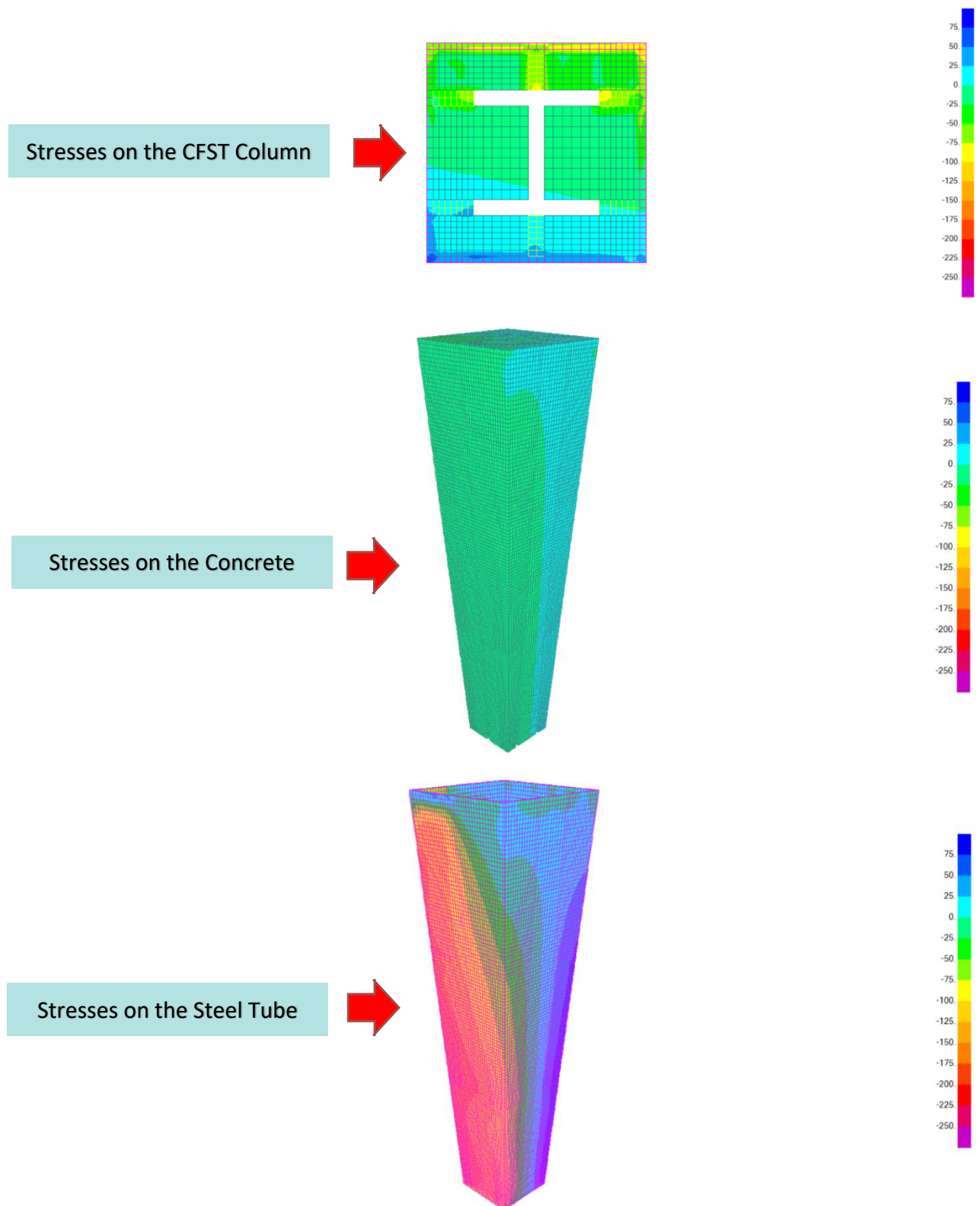


Fig. (4.54) Stresses' Contours Along CFST Composite Column, C50MPa, S275MPa

4.4.5.2.7 CFST Column Analysis under Axial Compression and Bi-Axial Moments, C60MPa, S275MPa

The following [table \[4.50\]](#) summarizes the Encased Column Sectional Capacity under Axial compression and bi-axial bending moments. The section capacity has been determined using simplified approach adopted by AISC 360-16, and Eurocode-4. In addition; it shows the stresses and strains of the concrete and steel elements extracted from the 3D -Fiber (Solid) Model. The load eccentricities were constant of 85.75mm in X-direction and 104.50mm in Y-direction. The analysis showing in the below [table \[4.50\]](#) has been performed using Concrete Cylinder Strength of C60MPa, and Steel Grade of S275MPa. [Fig. \(4.55\)](#) presents the stress contours along the height of the encased columns as extracted from the 3D Fiber (Solid) Model.

Analysis Approach	AISC 360-16	Eurocode-4	3D-Fiber (Solid) Element Model	
Concrete Cylinder Strength (MPa)	60	60	60	
Steel Grade (MPa)	S275	S275	S275	
Axial Compression Load, P (kN)	950	885	800	
Load Eccentricity, e_x (mm)	85.75	85.75	85.75	
Load Eccentricity, e_y (mm)	104.50	104.50	104.50	
Bending Moments at the Top of the Column, M = P.e (kN.m)	M _x = 99.30 M _y = 81.46	M _x = 92.48 M _y = 75.89	M _x = 83.60 M _y = 68.60	
Section Capacity (D/C)	1.0	1.0		
Stresses on the Fiber (Solid) Model under 800 kN			Concrete Stress (MPa)	Steel Stress (MPa)
Compression Stresses on the CFST Column			(49.08) MPa	(201.38) MPa
Tensile Stresses on the CFST Column			(10.87) MPa	(101.04) MPa
Strain (ϵ)			Concrete Strain	Steel Strain
Compression Strain on the CFST Column			0.00123	0.001
Tensile Strain on the CFST Column			0.00027	0.0005

Table [4.50] CFST Column Section Capacity under Axial Compression and Bi-Axial Bending, C60MPa, S275

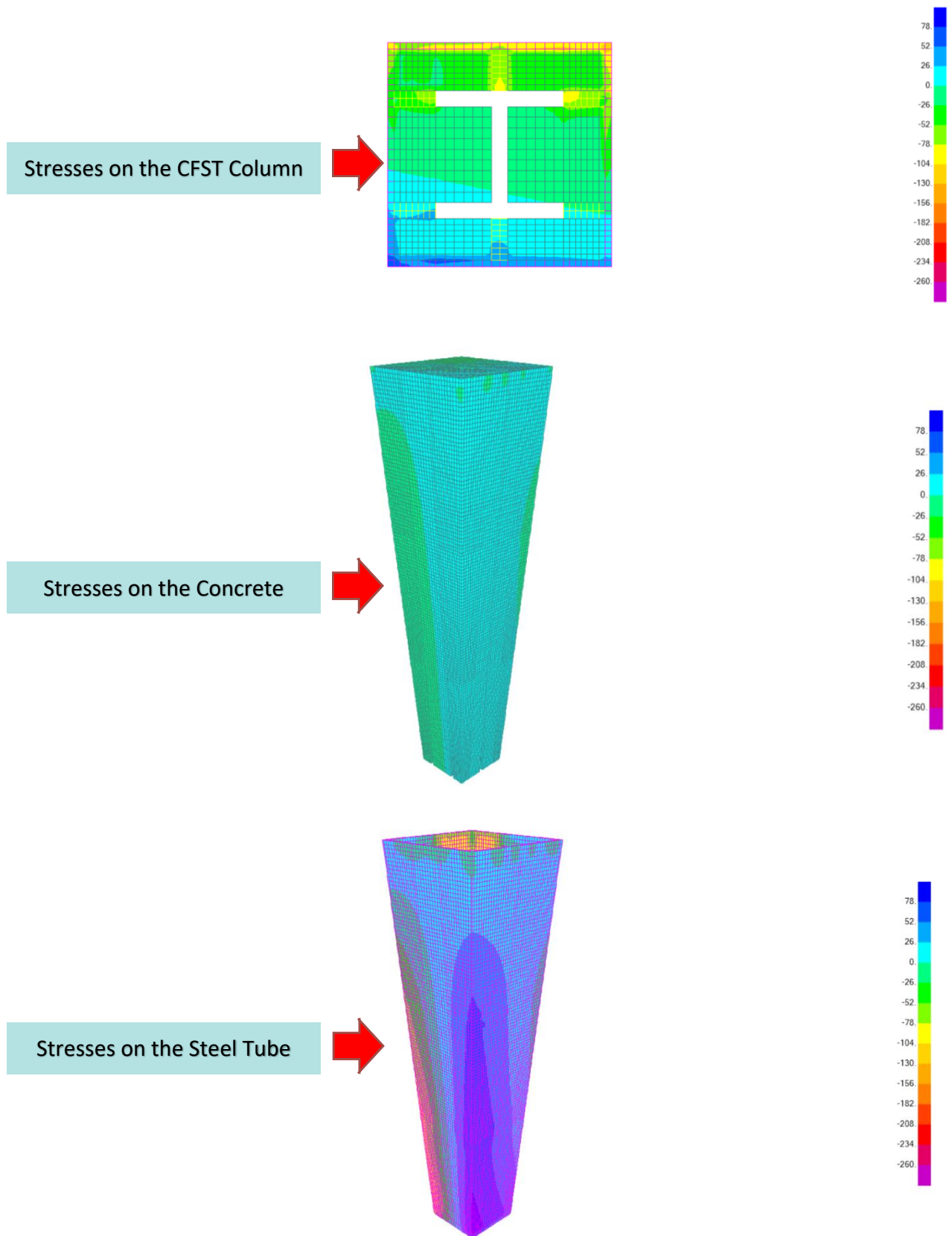


Fig. (4.55) Stresses' Contours Along CFST Composite Column, C60MPa, S275MPa

4.4.5.2.8 CFST Column Analysis under Axial Compression and Bi-Axial Moments, C70MPa, S275MPa

The following [table \[4.51\]](#) summarizes the Encased Column Sectional Capacity under Axial compression and bi-axial bending moments. The section capacity has been determined using simplified approach adopted by AISC 360-16, and Eurocode-4. In addition; it shows the stresses and strains of the concrete and steel elements extracted from the 3D -Fiber (Solid) Model. The load eccentricities were constant of 85.75mm in X-direction and 104.50mm in Y-direction. The analysis showing in the below [table \[4.51\]](#) has been performed using Concrete Cylinder Strength of C70MPa, and Steel Grade of S275MPa. [Fig. \(4.56\)](#) presents the stress contours along the height of the encased columns as extracted from the 3D Fiber (Solid) Model.

Analysis Approach	AISC 360-16	Eurocode-4	3D-Fiber (Solid) Element Model	
Concrete Cylinder Strength (MPa)	70	70	70	
Steel Grade (MPa)	S275	S275	S275	
Axial Compression Load, P (kN)	1,000	935	925	
Load Eccentricity, e_x (mm)	85.75	85.75	85.75	
Load Eccentricity, e_y (mm)	104.50	104.50	104.50	
Bending Moments at the Top of the Column, M = P.e (kN.m)	M _x = 104.50 M _y = 85.75	M _x = 97.71 M _y = 80.18	M _x = 96.66 M _y = 79.32	
Section Capacity (D/C)	1.0	1.0		
Stresses on the Fiber (Solid) Model under 925 kN			Concrete Stress (MPa)	Steel Stress (MPa)
Compression Stresses on the CFST Column			(56.89) MPa	(228.12) MPa
Tensile Stresses on the CFST Column			(12.84) MPa	(114.26) MPa
Strain (ϵ)			Concrete Strain	Steel Strain
Compression Strain on the CFST Column			0.00135	0.00114
Tensile Strain on the CFST Column			0.00031	0.00057

Table [4.51] CFST Column Section Capacity under Axial Compression and Bi-Axial Bending, C70MPa, S275

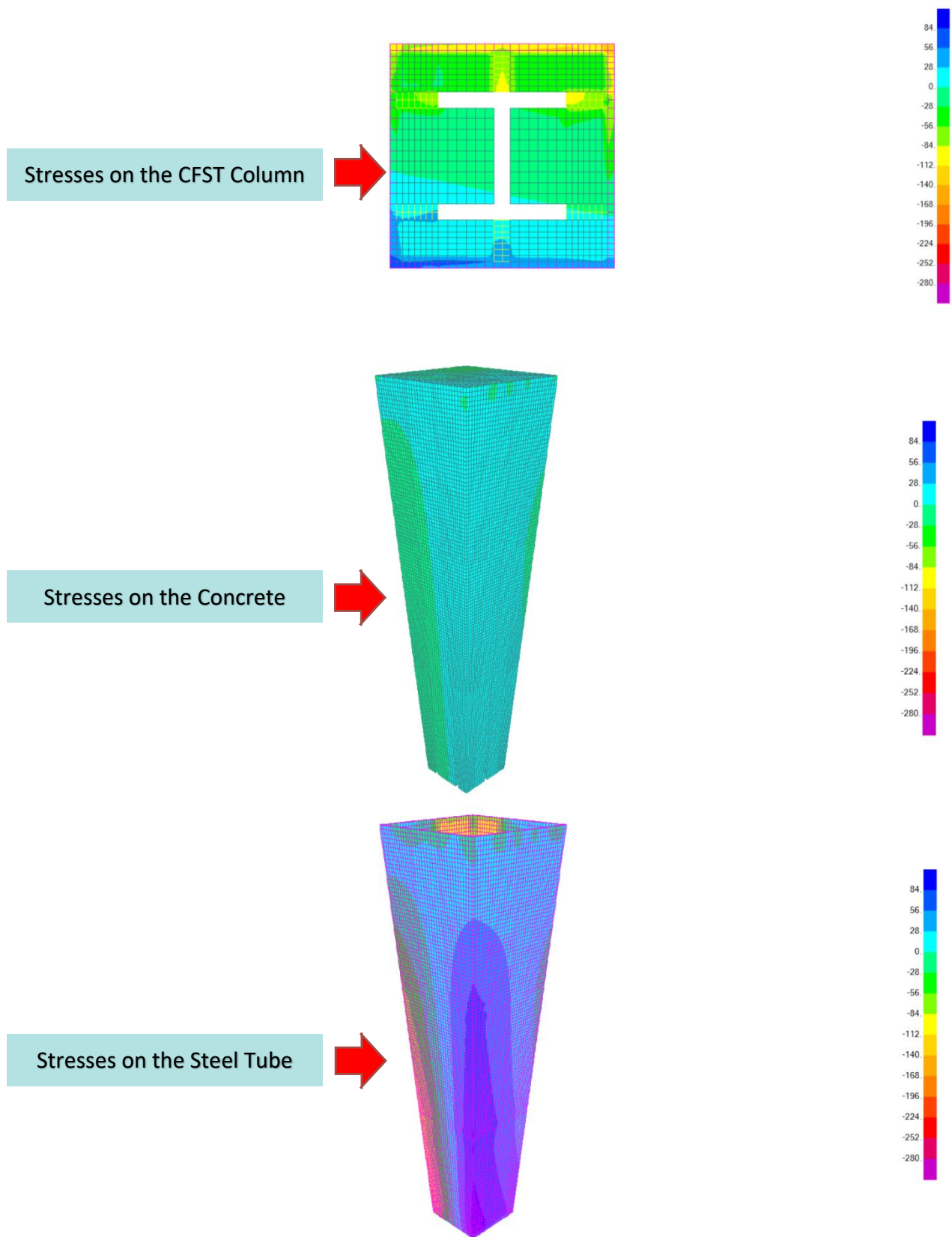


Fig. (4.56) Stresses' Contours Along CFST Composite Column, C60MPa, S275MPa

4.4.5.3 Stresses on the stiffener Plates welded to the CFST and Encased Element, under Axial Compression and Bi-Axial Bending Moments

This clause describes the analysis of stiffener plates connected to the CFST Tube and I section under axial compression loads and bi-axial bending. The stresses and strains on the steel plates have been presented in the below table.

It was vital to understand the stresses transferred through stiffener plates using different concrete cylinder strengths ranging from C40MPa to C70MPa, with different Young's Modulus of Elasticity as summarized in clause 4.4.3.

Furthermore; the stresses have been evaluated using two different steel grades, S275MPa and S355MPa.

Table [4.52] illustrates the stresses on the steel stiffener plates under different concrete strengths and using two different steel grades.

Fig. (4.57) demonstrates the stress contours along the height of the stiffener plates as extracted from the 3D Fiber (Solid) Model.

Steel Grade, (MPa)	S355	S355	S355	S355
Concrete Cylinder Strength (MPa)	C40MPa	C50MPa	C60MPa	C70MPa
Compression Steel Stresses (MPa)	134.60	148.60	154.45	173.96
Tensile Steel Stresses (MPa)	51.53	56.10	58.78	67.24
Steel Strain in Compression	0.000673	0.000743	0.000772	0.000870
Steel Strain in Tension	0.00026	0.00028	0.00029	0.00034
Steel Grade, (MPa)	S275	S275	S275	S275
Concrete Cylinder Strength (MPa)	C40MPa	C50MPa	C60MPa	C70MPa
Compression Steel Stresses (MPa)	134.60	148.60	154.45	173.96
Tensile Steel Stresses (MPa)	51.53	56.10	58.78	67.24
Steel Strain in Compression	0.000673	0.000743	0.000772	0.000870
Steel Strain in Tension	0.00026	0.00028	0.00029	0.00034

Table [4.52] Stresses on the Steel Stiffener Plates due to Axial Compression and Uni-Direction Bending

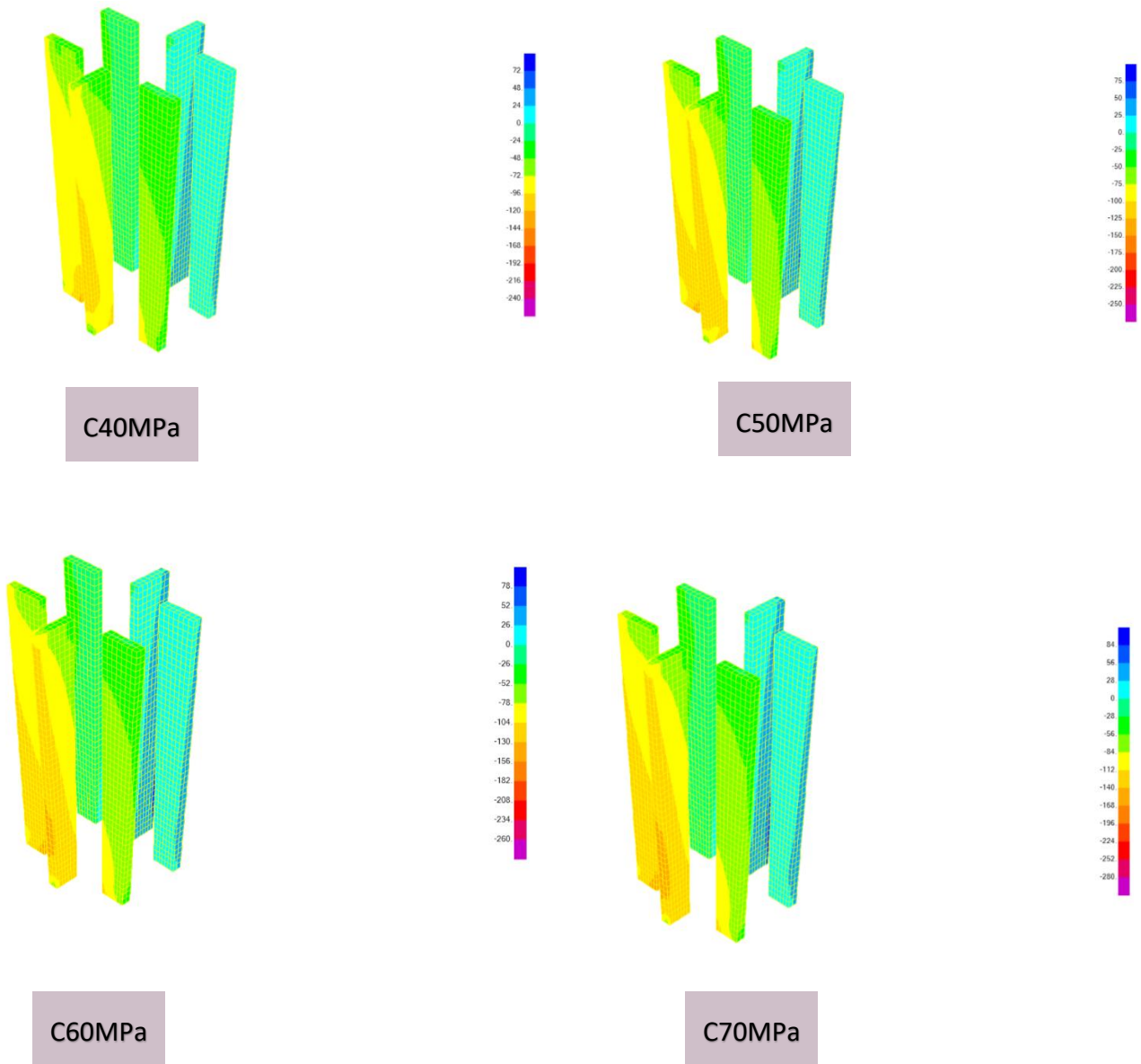


Fig. (4.57) Stresses' Contours Along Stiffener Plates, under Axial Compression and Bi-Axial Bending

CHAPTER 5

DISCUSSION OF RESULTS

5.1 INTRODUCTION

This section is a discussion of the results illustrated in section-4 of the research. The discussion is focusing on the behavior of the research finite element model of a tapered CFST column connected to Encased column under 3 different types of loading, pure axial compression load, combined axial compression & uni-direction bending moments, and combined axial compression & bi-axially bending moments.

5.2 COMPOSITE COLUMN BEHAVIOR SUBJECT TO CONCENTRIC AXIAL COMPRESSION LOAD

The behavior of the composite column has been examined by divided the model into three main parts, the first part is the encased composite column of (210 x 210) mm. The second part is the tapered CFST composite column with a sizing varying from (210x210) mm to (340x340) mm. The third part is the stiffener plates connecting steel tube to the steel I section. The composite column has been analyzed under concentric axial compression load.

5.2.1 Encased Composite Column Subject to Concentric Axial Compression Load

The Encased column resistance to Axial compression loads has been assessed using different international codes such as AISC 316-16, ACI 318-11, and Eurocode-4.

In addition; a detailed 3D fiber (Solid) element model has been created to evaluate the column behavior and to compare the results with the simplified approach adopted by the international codes mentioned above.

The column has been analyzed under pure axial compression load, taking into consideration the boundary conditions illustrated in clause 4.4.2.

The analysis has been performed using 4 different concrete cylinder strength C40MPa, C50MPa, C60MPa, and C70MPa. Each concrete grade has been evaluated with two different steel grades, S275MPa and S355MPa.

The results illustrated in section-4 indicates that the Eurocode-4 provides a very close results to the ACI318-11 with concrete strength of C40MPa and C50MPa, while ACI318-11 provides slightly higher values than Eurocode-4 with high strength concrete of C60MPa and C70MPa.

The nominal strength adopted by AISC316-16 is slightly higher than the provided by ACI318-11 and Eurocode-4.

For Encased Composite Column with steel grade of S355MPa, the nominal compressive strength illustrated in the 3D Fiber (Solid) model is less than the simplified approach by the codes with concrete strength of C40MPa, while it shows an increase in the stresses with high strength concrete of C50MPa, C60MPa and C70MPa.

The nominal compressive strength extracted from the 3D fiber model with **C40MPa**, is less than AISC316-16, ACI318-11, and Eurocode-4 by 13%, 10% , and 10% respectively.

The nominal compressive strength extracted from the 3D fiber model with **C50MPa**, is less than AISC316-16, and ACI318-11, by 6%, 1%, while it is inline with the Eurocode-4 simplified formulas.

The nominal compressive strength extracted from the 3D fiber model with **C60MPa**, is higher than AISC316-16, ACI318-11, and Eurocode-4 by 1%, 6%, and 9% respectively.

The nominal compressive strength extracted from the 3D fiber model with **C70MPa**, is higher than AISC316-16, ACI318-11, and Eurocode-4 by 7%, 11%, and 16% respectively.

Fig. (5.1) demonstrating the nominal compressive strength chart of the Encased Column using AISC316-16, ACI318-11, Eurocode-4, and 3D Fiber Model under different concrete strength and the same steel grade of S355MPa.

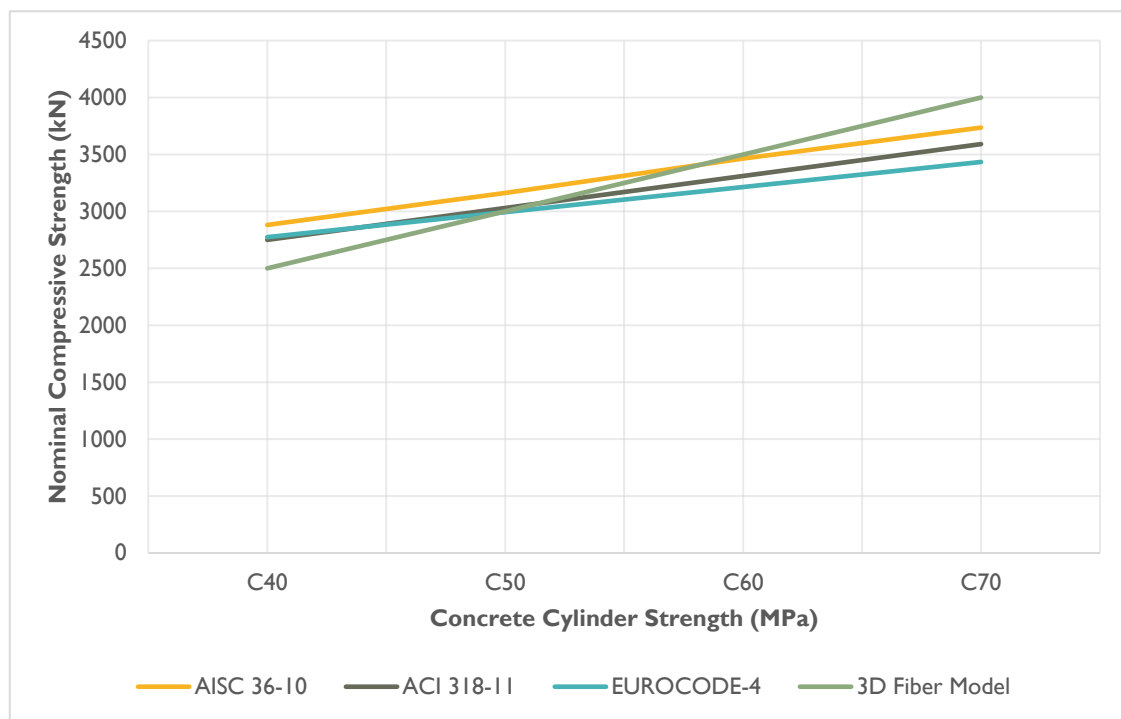


Fig. (5.1) Nominal Compressive Strength for Encased Column with Steel Grade, S355 MPa

The concrete section in the 3D Fiber models with steel grade S355MPa, showing a local concentration in the stresses at the interface with the steel tube of the CFST. The local stress concentration is anticipated as a result of connecting two materials with different mechanical properties, and it might not affect the overall behavior of the encased column section.

However; it was noticed that the interface between two different materials is leading to additional stresses on the top part of the concrete section, which cannot be predicated using the simplified analysis method.

Fig. (5.2) presenting the maximum and average concrete compressive stress of the encased column with steel grade S355MPa under nominal compressive loads specified in the 3D Fiber Model.

The steel section of the encased column with steel grade S355MPa, showing a very local concentration stresses at the transition level from CFST section to Encased section, the

remaining steel I section showing lower stress values. The local stress concentration in the steel section is not anticipated to have a significant impact on the overall behavior and capacity of the composite column.

Fig. (5.3) demonstrating the steel compressive stress of the Encased column with steel grade S355MPa, under nominal compressive loads specified in the 3D Fiber Model.

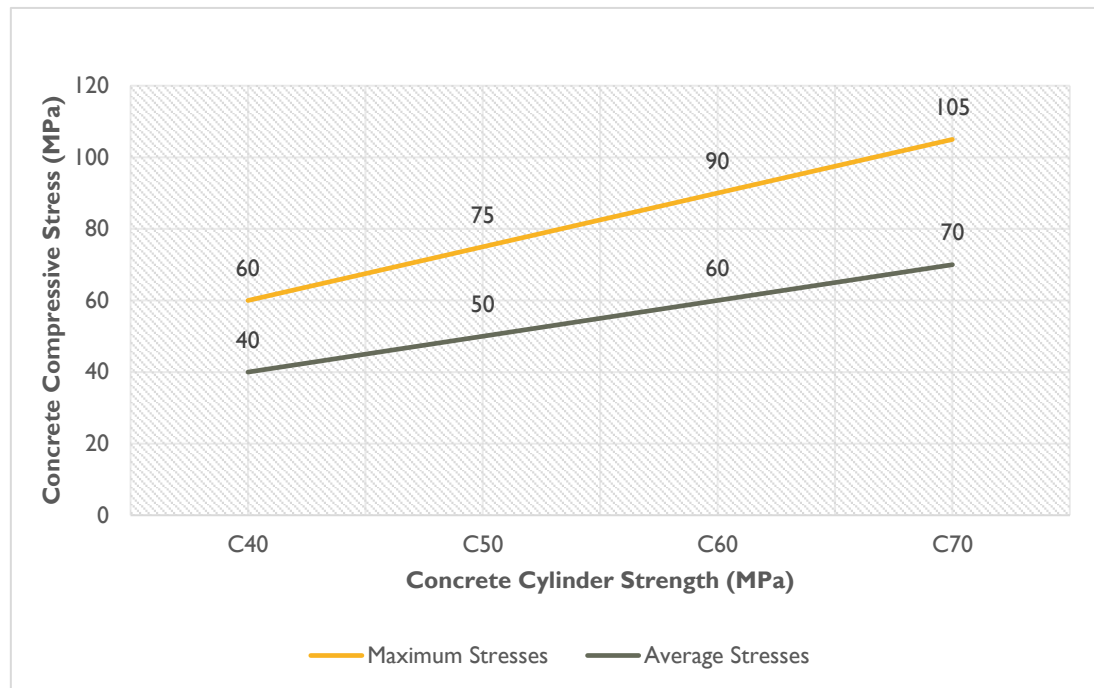


Fig. (5.2) Concrete Compressive Stress of Encased Column under Nominal Compressive Loads specified in the 3D-Fiber (Solid) Model, S355 MPa

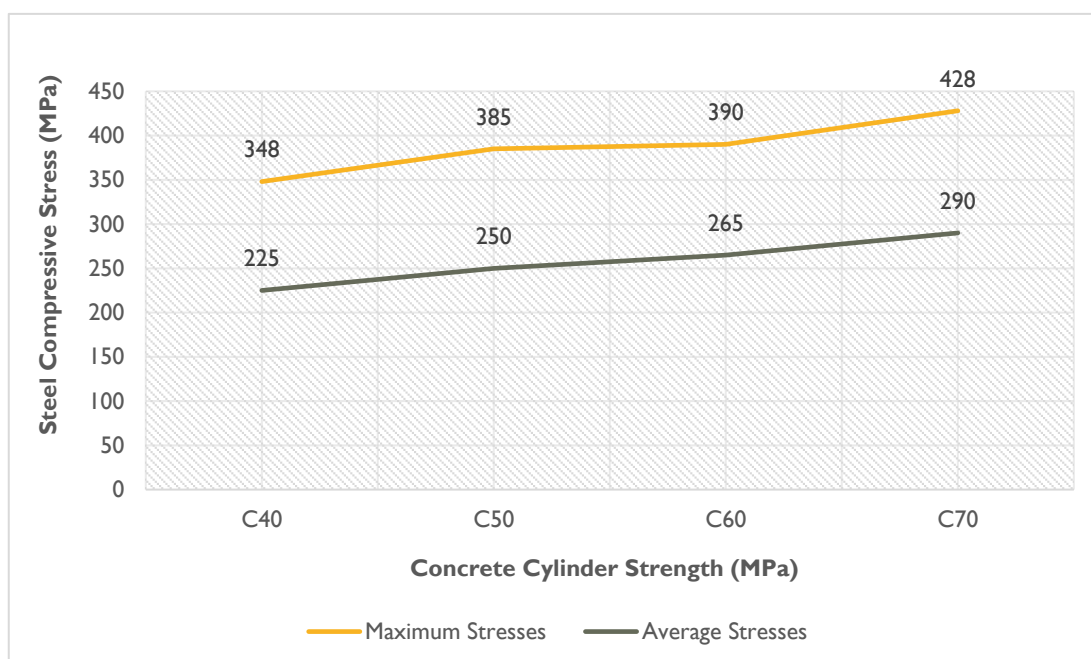


Fig. (5.3) Steel Compressive Stress of Encased Column under Nominal Compressive Loads specified in the 3D-Fiber (Solid) Model, S355 MPa

For Encased Composite Column with steel grade of S275MPa, the nominal compressive strength adopted by AISC316-16, ACI318-11, and Eurocode-4 is less than the strength determined by using steel grade S355MPa, while the 3D Fiber Model is showing almost same compressive strength for both steel grades S275MPa and S355MPa, except the encased column with C70MPa, which the nominal compressive strength reduced by 6% in order not to exceed the yield stress of 275MPa. It was observed from the stress contours that the concrete reach the ultimate compressive strength, while the steel stress still beneath the yield limit, so the influence of changing the steel grade on the nominal compressive strength can be ignored, even with high strength concrete of C70MPa, the area of the steel exceeding the yield limit is very local and not predicted to affect the overall integrity and behavior of the composite section.

Fig. (5.4) illustrating the nominal strength capacity of the Encased Column adopted by the codes and 3D-Fiber Model for both steel grades S275MPa and S355MPa.

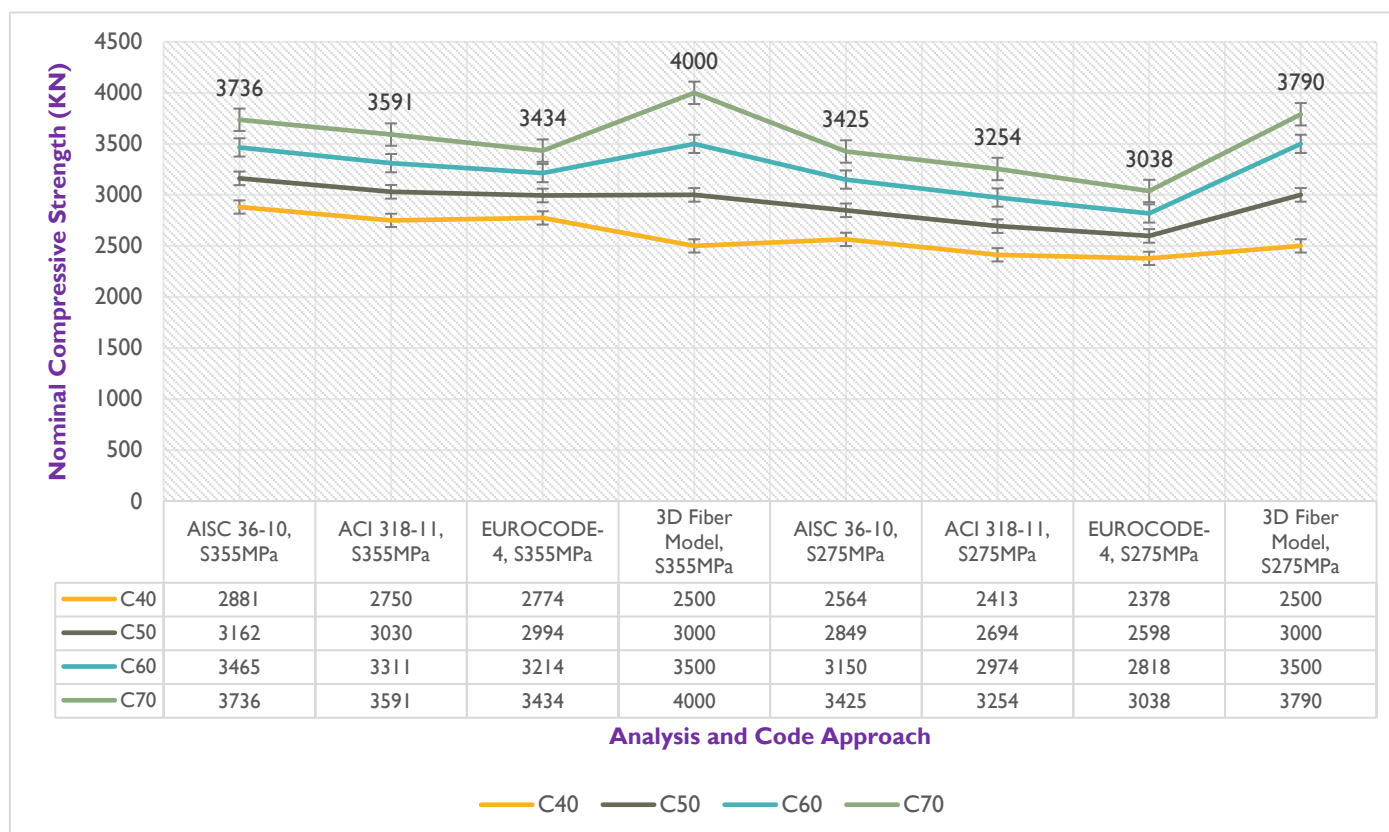


Fig. (5.4) Nominal Compressive Strength of Encased Column Adopted by Codes and 3D-Fiber Model for Both Steel Grades, S275MPa and S355MPa

The nominal compressive strength illustrated in the 3D Fiber (Solid) model is less than the simplified approach by AISC316-16 with concrete strength of C40MPa, while it shows an increase in the stresses by changing other parameters and other different codes.

The nominal compressive strength extracted from the 3D fiber model with **C40MPa**, is less than AISC316-16 by 2.5%, while it is higher than the compressive strength adopted by ACI318-11 and Eurocode-4 by 3% , and 5% respectively.

The nominal compressive strength extracted from the 3D fiber model with **C50MPa**, is higher than AISC316-16, ACI318-11, and Eurocode-4 by 5%, 11%, and 15% respectively.

The nominal compressive strength extracted from the 3D fiber model with **C60MPa**, is higher than AISC316-16, ACI318-11, and Eurocode-4 by 11%, 17% , and 24% respectively.

The nominal compressive strength extracted from the 3D fiber model with **C70MPa**, is higher than AISC316-16, ACI318-11, and Eurocode-4 by 10%, 16%, and 25% respectively.

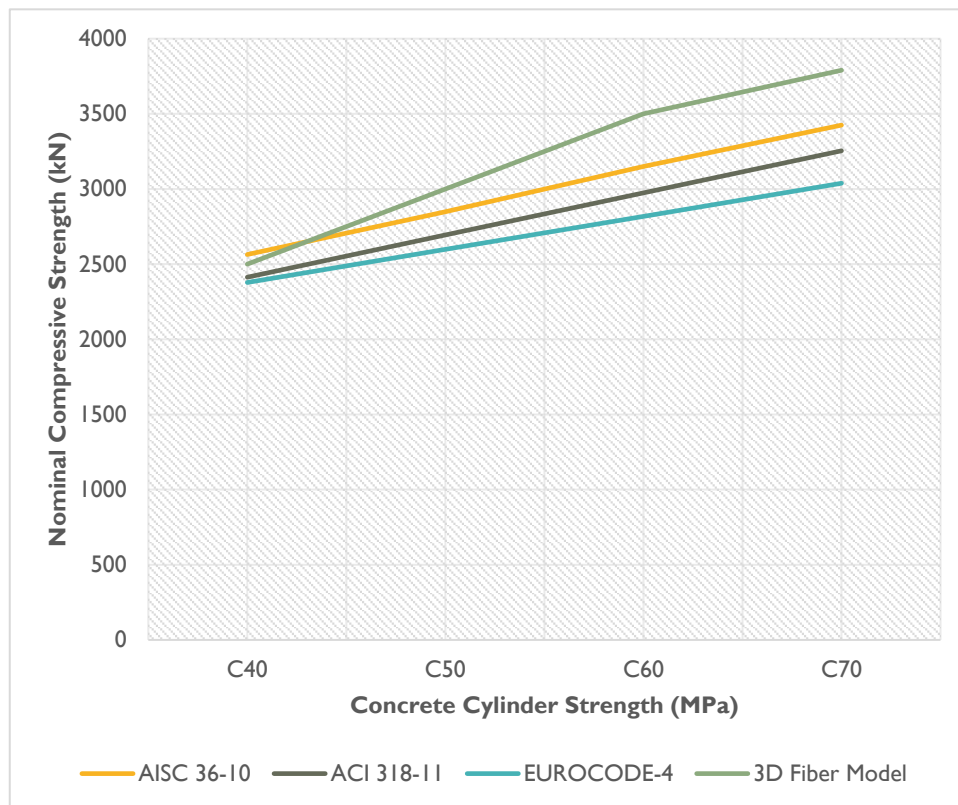


Fig. (5.5) Nominal Compressive Strength for Encased Column with Steel Grade, S275 MPa

The concrete section in the 3D Fiber models with steel grade S275MPa, showing a local concentration in the stresses at the interface with the steel tube of the CFST. The local stress concentration is anticipated as a result of connecting two materials with different mechanical properties, and it might not affect the overall behavior of the encased column section.

However; it was noticed that the interface between two different is leading to additional stresses on the top part of the concrete section, which cannot be predicated using the simplified analysis method.

Fig. (5.6) presenting the maximum and average concrete compressive stress of the encased column with steel grade S275MPa under nominal compressive loads specified in the 3D Fiber Model.

The steel section of the encased column with steel grade S275MPa, showing a very local concentration stresses at the transition level from CFST section to Encased section, the remaining steel I section showing lower stress values. The local stress concentration in the steel section is not anticipated to have a significant impact on the overall behavior and capacity of the composite column.

Fig. (5.7) demonstrating the steel compressive stress of the Encased column with steel grade S275MPa, under nominal compressive loads specified in the 3D Fiber Model.

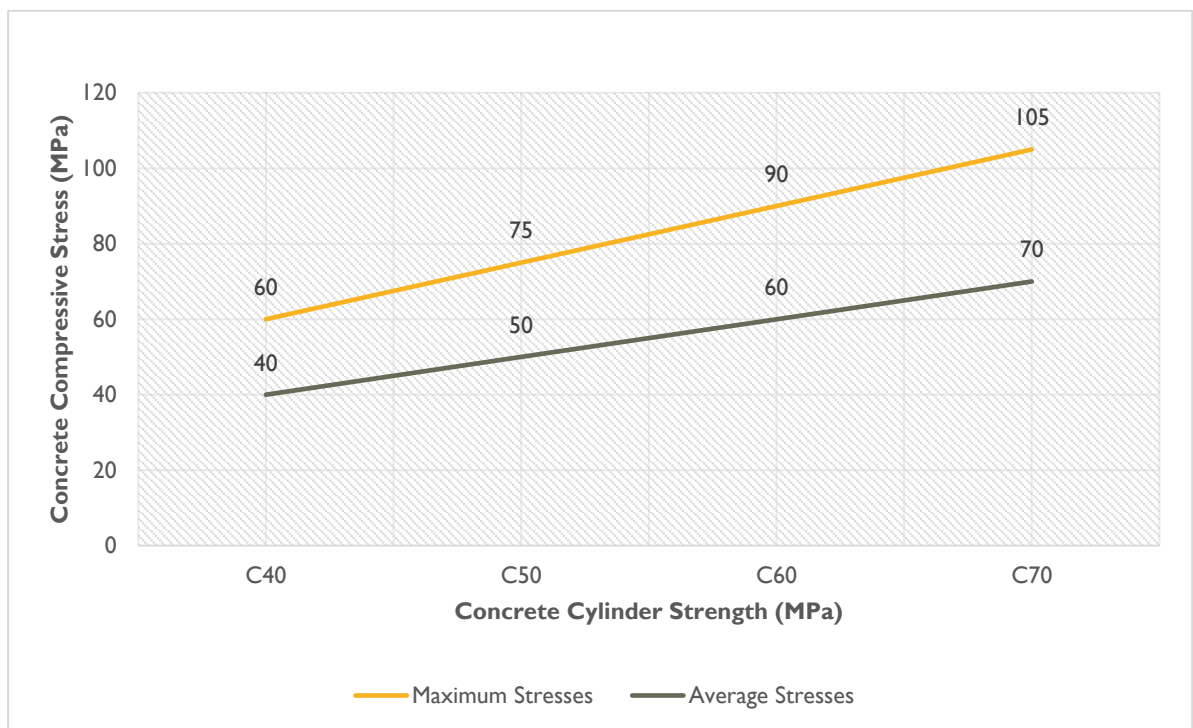


Fig. (5.6) Concrete Compressive Stress of Encased Column under Nominal Compressive Loads specified in the 3D-Fiber (Solid) Model, S275 MPa

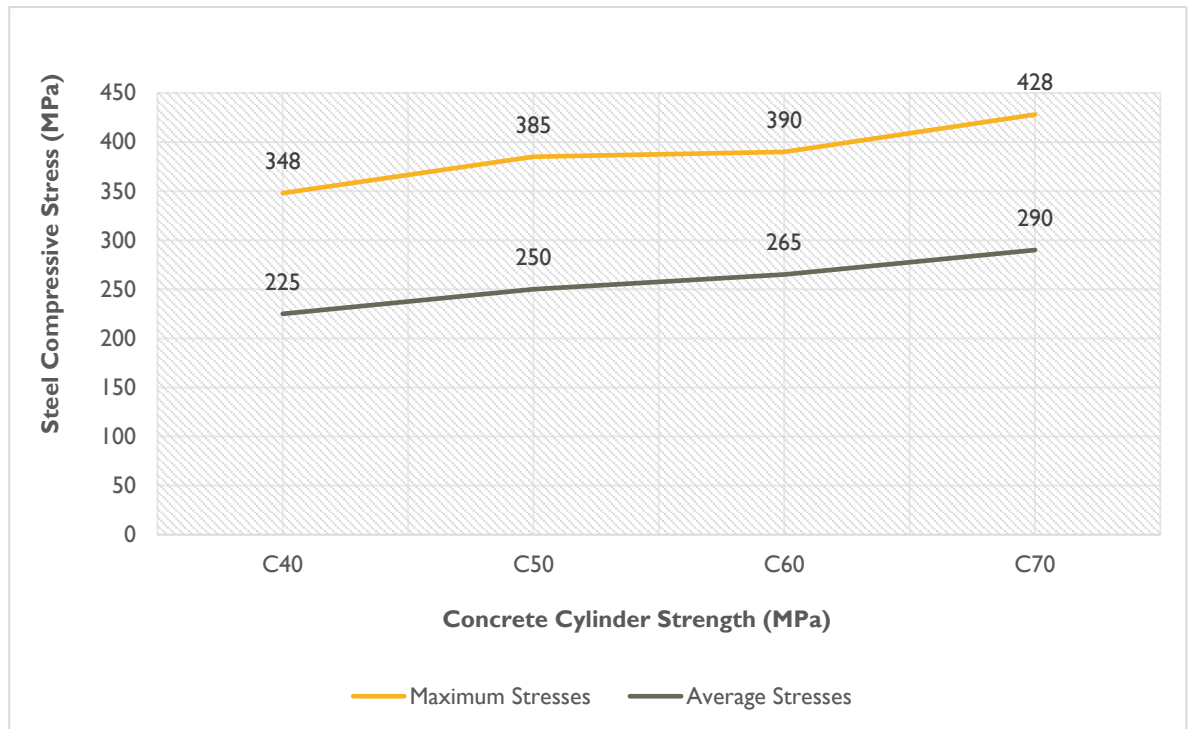


Fig. (5.7) Steel Compressive Stress of Encased Column under Nominal Compressive Loads specified in the 3D-Fiber (Solid) Model, S275 MPa

5.2.2 CFST Composite Column Subject to Concentric Axial Compression Load

The CFST column resistance to Axial compression loads has been assessed using different international codes such as AISC 316-16, ACI 318-11, and Eurocode-4.

In addition; a detailed 3D fiber (Solid) element model has been created to evaluate the column behavior and to compare the results with the simplified approach adopted by the international codes mentioned above.

The column has been analyzed under pure axial compression load, taking into consideration the boundary conditions illustrated in clause 4.4.2.

The analysis has been performed using 4 different concrete cylinder strength C40MPa, C50MPa, C60MPa, and C70MPa. Each concrete grade has been evaluated with two different steel grades, S275MPa and S355MPa.

The results are showing that the Eurocode-4 provides a very close results to the ACI318-11, while AISC316-16 provides a higher compression resistance compared to the other two codes.

For CFST Composite Column with steel grade of S355MPa, the nominal compressive strength illustrated in the 3D Fiber (Solid) model is higher than the simplified approach by the codes with different concrete strengths, C40MPa, C50MPa, C60MPa, and C70MPa. The nominal compressive strength extracted from the 3D fiber model with **C40MPa**, is higher than AISC316-16, ACI318-11, and Eurocode-4 by 14%, 34%, and 26% respectively. The nominal compressive strength extracted from the 3D fiber model with **C50MPa**, is higher than AISC316-16, ACI318-11, and Eurocode-4 by 17%, 38%, and 31% respectively. The nominal compressive strength extracted from the 3D fiber model with **60MPa**, is higher than AISC316-16, ACI318-11, and Eurocode-4 by 20%, 41%, and 36% respectively. The nominal compressive strength extracted from the 3D fiber model with **C70MPa**, is higher than AISC316-16, ACI318-11, and Eurocode-4 by 22%, 44%, and 40% respectively.

Fig. (5.8) demonstrating the nominal compressive strength chart of the CFST Column using AISC316-16, ACI318-11, Eurocode-4, and 3D Fiber Model under different concrete strength and the same steel grade of S355MPa.

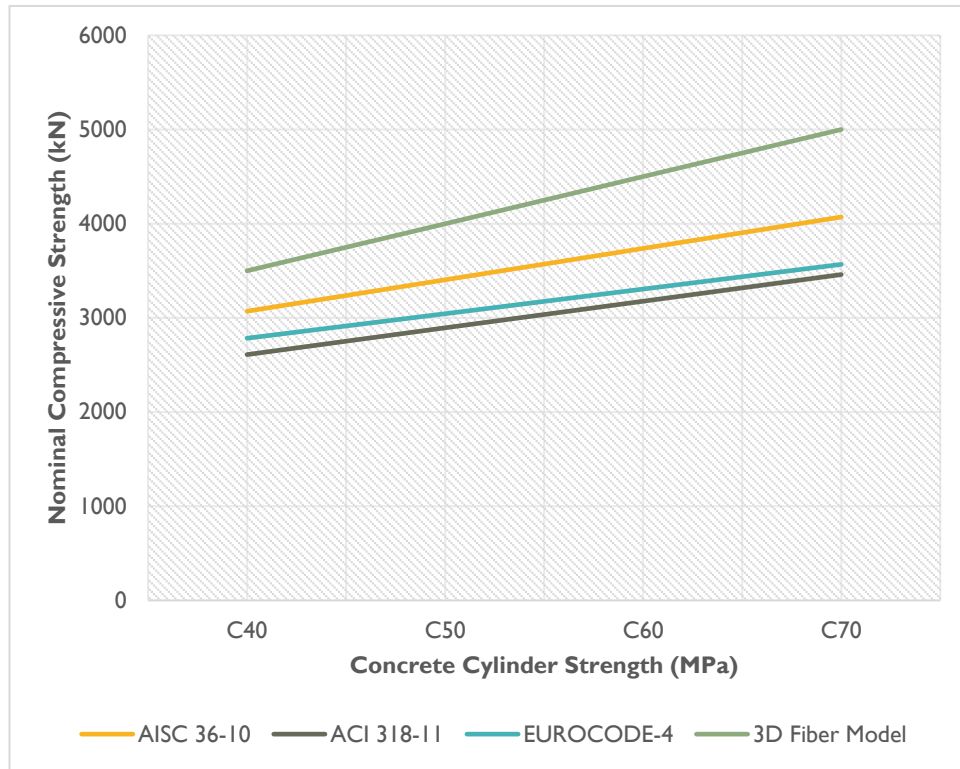


Fig. (5.8) Nominal Compressive Strength for CFST Column with Steel Grade, S355 MPa

The concrete section in the 3D Fiber models with steel grade S355MPa, showing a local concentration in the stresses at the interface with the steel stiffener plates connecting steel tube to the steel I section. The maximum stresses on the steel section has been observed at the interface level with the stiffener plates, which is located 425mm above the bottom of the CFST column, as per section (b-b) in **Fig. (4.3)**.

Accordingly; the steel stiffener plates and the overlapping between I section, and steel tube has a significant influence on the section capacity under axial compression load, which was ignored from the simplified analysis approach.

Fig. (5.9) presenting the maximum and average concrete compressive stress of the CFST column with steel grade S355MPa under nominal compressive loads specified in the 3D Fiber Model.

The steel tube section of the CFST column with steel grade S355MPa, showing a very local concentration stresses at the interface level with the steel stiffener plates and overlapping with steel I section, while the remaining section showing normal stress distribution inline with the load path applied on the composite column.

The local stress concentration in the steel section is not anticipated to have a significant impact on the overall behavior and capacity of the composite column.

Fig. (5.10) demonstrating the steel compressive stress of the Encased column with steel grade S355MPa, under nominal compressive loads specified in the 3D Fiber Model.

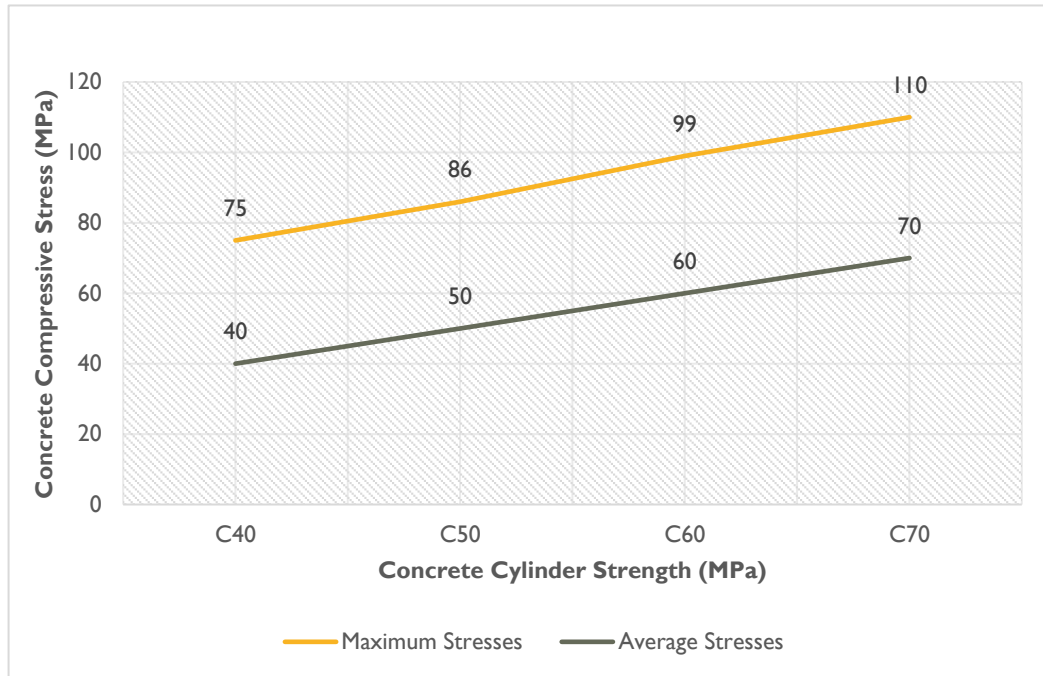


Fig. (5.9) Concrete Compressive Stress of CFST Column under Nominal Compressive Loads specified in the 3D-Fiber (Solid) Model, Steel Grade S355 MPa

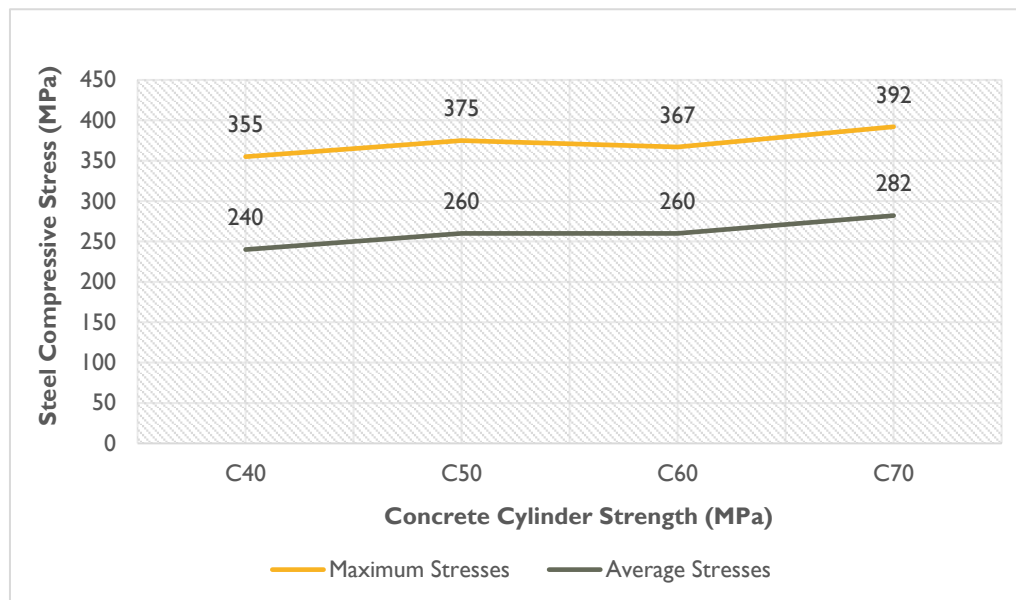


Fig. (5.10) Steel Compressive Stress of CFST Column under Nominal Compressive Loads specified in the 3D-Fiber (Solid) Model, Steel Grade 355 MPa

For CFST Composite Column with steel grade of S275MPa, the nominal compressive strength illustrated in the 3D Fiber (Solid) model is higher than the simplified approach by the codes with different concrete strengths, C40MPa, C50MPa, C60MPa, and C70MPa. The nominal compressive strength extracted from the 3D fiber model with **C40MPa**, is higher than AISC316-16, ACI318-11, and Eurocode-4 by 30%, 53%, and 46% respectively. The nominal compressive strength extracted from the 3D fiber model with **C50MPa**, is higher than AISC316-16, ACI318-11, and Eurocode-4 by 32%, 56%, and 50% respectively. The nominal compressive strength extracted from the 3D fiber model with **C60MPa**, is higher than AISC316-16, ACI318-11, and Eurocode-4 by 34%, 58%, and 54% respectively. The nominal compressive strength extracted from the 3D fiber model with **C70MPa**, is higher than AISC316-16, ACI318-11, and Eurocode-4 by 32%, 56%, and 53% respectively.

Fig. (5.11) demonstrating the nominal compressive strength chart of the CFST Column using AISC316-16, ACI318-11, Eurocode-4, and 3D Fiber Model under different concrete strength and the same steel grade of S275MPa.

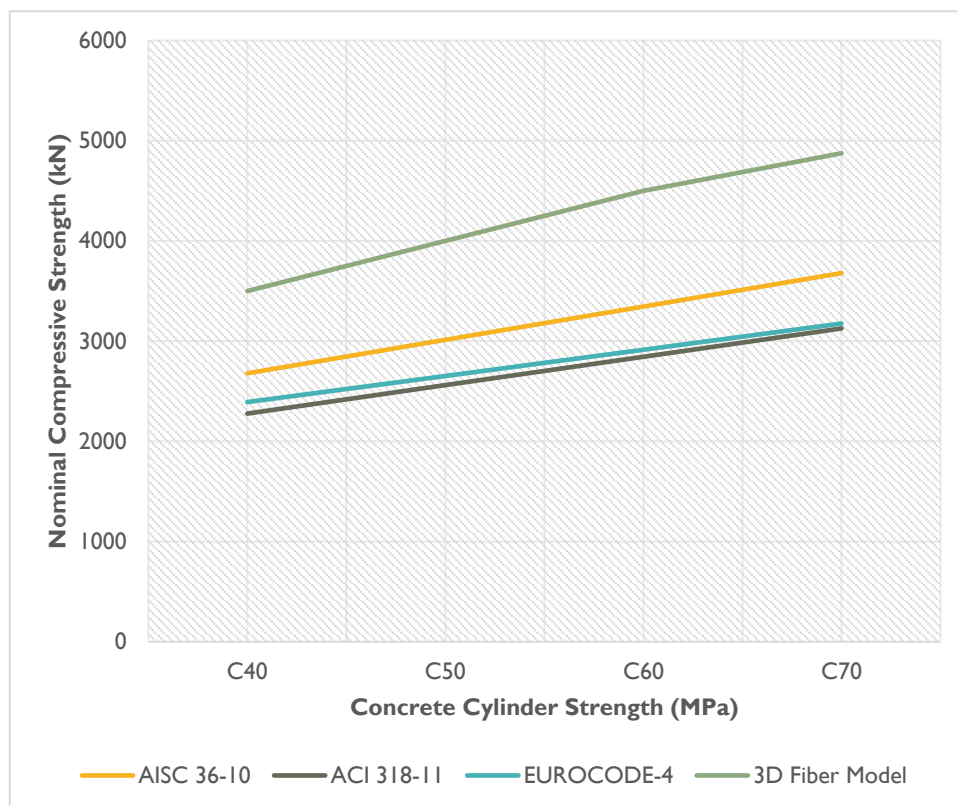


Fig. (5.11) Nominal Compressive Strength for CFST Column with Steel Grade, S275 MPa

the nominal compressive strength of the CFST adopted by AISC316-16, ACI318-11, and Eurocode-4 is less than the strength determined by using steel grade S355MPa, while the 3D Fiber Model is showing almost same compressive strength for both steel grades S275MPa and S355MPa, except the encased column with C70MPa, which the nominal compressive strength reduced by 2.5% in order not to exceed the yield stress of 275MPa. It was observed from the stress contours that the concrete reach the ultimate compressive strength, while the steel stress still beneath the yield limit, so the influence of changing the steel grade on the nominal compressive strength can be ignored, even with high strength concrete of C70MPa, the area of the steel exceeding the yield limit is very local and not predicted to affect the overall integrity and behavior of the composite section.

Fig. (5.12) illustrating the nominal strength capacity of the CFST Column adopted by the codes and 3D-Fiber Model for both steel grades S275MPa and S355MPa.

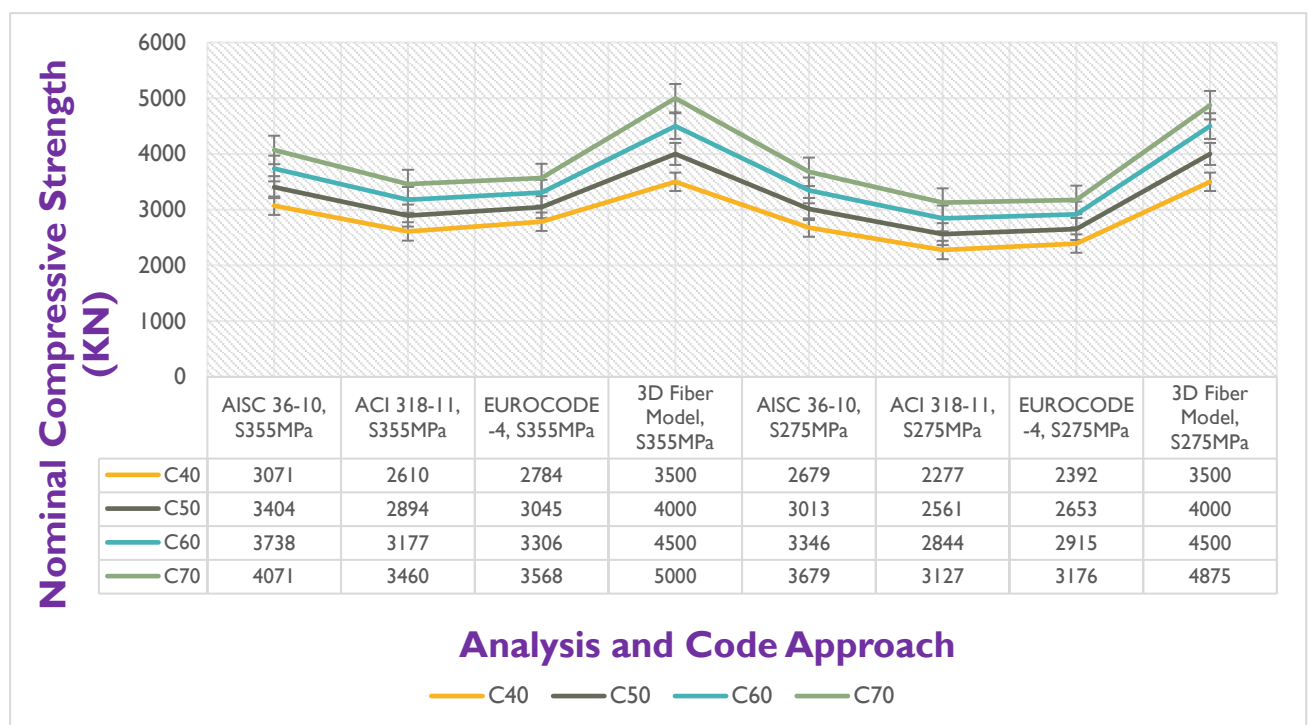


Fig. (5.12) Nominal Compressive Strength of CFST Column Adopted by Codes and 3D-Fiber Model for Both Steel Grades, S275MPa and S355MPa

5.2.3 Steel Stiffener Plates Behavior connected to CFST and Encased Column under Concentric Axial Compression Loads

The stiffener plates have been provided to connect steel tube to the steel I section. The provided stiffeners enhance the load transition from the CFST element to the Encased element.

The stresses on the steel stiffeners has been evaluated using two different steel grades, S355MPa and S275MPa. The concrete strength adopted in the analysis was varying from C40MPa to C70MPa.

The 3D Fiber Model demonstrating that the stresses on the steel stiffener plates are the same with different steel grades S275MPa and S355MPa.

The results showing that the use of steel grade S275 is quite reasonable for the composite column with concrete cylinder strength of C40MPa, C50MPa, and C60MPa, since the steel stresses not exceeding the yield limit.

For the composite column with concrete cylinder strength of C70MPa, it is recommended to use high strength steel i.e. S355MPa since the steel stresses reach 293MPa

Fig. (5.13) illustrating the stresses on the steel stiffener plates with different steel grades and different concrete strengths.

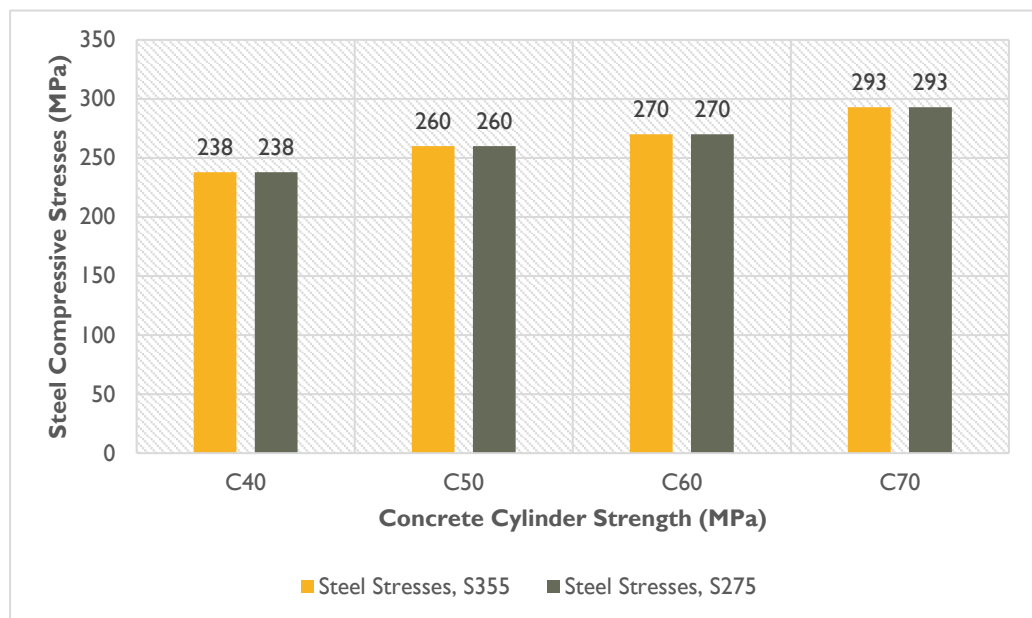


Fig. (5.13) Compression Steel Stresses in the Stiffener Plates under Axial Compression Loads

5.3 COMPOSITE COLUMN BEHAVIOR UNDER AXIAL COMPRESSION AND UNI-DIRECTION BENDING

The behavior of the composite column has been examined by divided the model into three main parts, the first part is the encased composite column of (210 x 210) mm. The second part is the tapered CFST composite column with a sizing varying from (210x210) mm to (340x340) mm. The third part is the stiffener plates connecting steel tube to the steel I section. The composite column has been analyzed under eccentric axial compression load to allow for uni-direction bending moments.

5.3.1 *Encased Composite Column Subject to Axial Compression and Uni-direction Bending*

The Encased column resistance to Axial compression and uni-direction bending has been assessed using different international codes such as AISC 316-16, and Eurocode-4. In addition; a detailed 3D fiber (Solid) element model has been created to evaluate the column behavior and to compare the results with the simplified approach adopted by the international codes mentioned above.

The column has been analyzed under axial compression load and uni-direction bending taking into consideration the boundary conditions illustrated in clause 4.4.2.

The load eccentricity (e) was constant of 85.75mm from the centroid of the composite column.

The analysis has been performed using 4 different concrete cylinder strength C40MPa, C50MPa, C60MPa, and C70MPa. Each concrete grade has been evaluated with two different steel grades, S275MPa and S355MPa.

The nominal compressive load with constant eccentricity (e) of 85.75mm has been determined using the simplified approach by AISC316-16 and Eurocode.

The results illustrated in section-4 indicates that the Eurocode-4 provides a very close result to the AISC316-16.

For Encased Composite Column with steel grade of S355MPa; the section capacity under axial and uni-direction bending moment was 1,625kN, 1,775kN, 1,975kN, and 2,075kN for concrete cylinder strength C40MPa, C50MPa, C60MPa, and C70Mpa respectively.

For Encased Composite Column with steel grade of S275MPa; the section capacity under axial and uni-direction bending moment was 1,375kN, 1,500kN, 1,650kN, and 1,750kN for concrete cylinder strength C40MPa, C50MPa, C60MPa, and C70Mpa respectively.

The results show that the Encased composite column with steel grade S275MPa, has less capacity than the composite column with steel grade S355MPa, while the 3D Fiber (Solid) model shows the same stresses for both steel grades. **Fig. (5.14)** is showing the nominal

compressive strength under constant eccentricity (e) of 85.75mm by adopting AISC316-16 and Eurocode-4 for both steel grades S275MPa, and S355MPa.

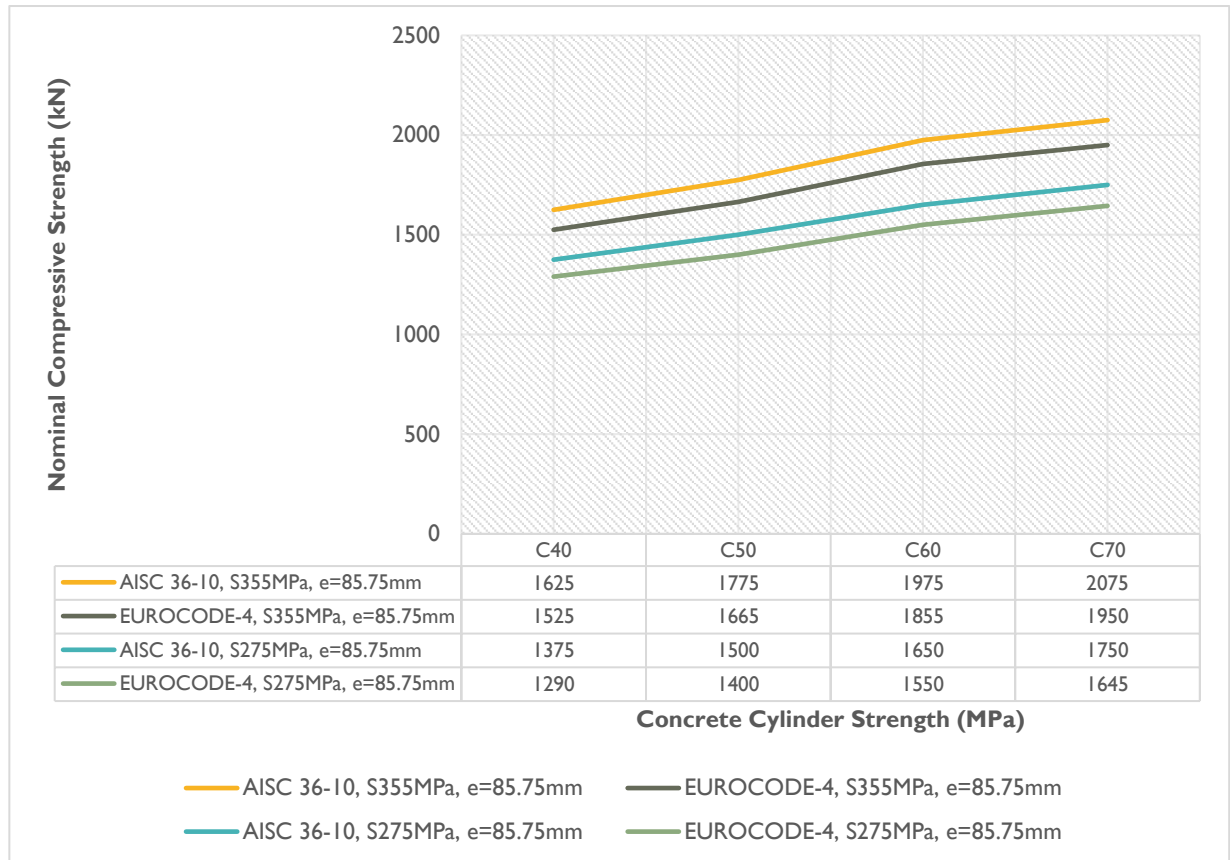


Fig. (5.14) Nominal Compressive Strength of Encased Column under Axial Compression and Uni-direction Bending Moments

The concrete section in the 3D Fiber models with both steel grades, showing a local concentration in the stresses at the interface with the steel tube of the CFST and the bottom of the concrete section close to the support. The local stress concentration at the top of the encased section is anticipated as a result of connecting two materials with different mechanical properties, and it might not affect the overall behavior of the encased column section.

However; it was noticed that the interface between two different materials connecting to each other is leading to additional stresses on the top part of the concrete section, which cannot be predicated using the simplified analysis method.

Fig. (5.15) presenting the maximum and average concrete compressive stress of the encased column with both steel grade S275MPa, S355MPa under nominal compressive loads specified in the 3D Fiber Model.

The steel section of the encased column with both steel grade, showing a very local concentration stresses at the transition level from CFST section to Encased section and at the bottom of the steel section close to the support, the remaining steel I section showing lower stress values. The local stress concentration in the steel section is not anticipated to have a significant impact on the overall behavior and capacity of the composite column.

Fig. (5.16) demonstrating the steel compressive stress of the Encased column with steel grade S355MPa, under nominal compressive loads specified in the 3D Fiber Model.

The tensile stresses on the concrete section under axial compression with uni-direction bending is negligible.

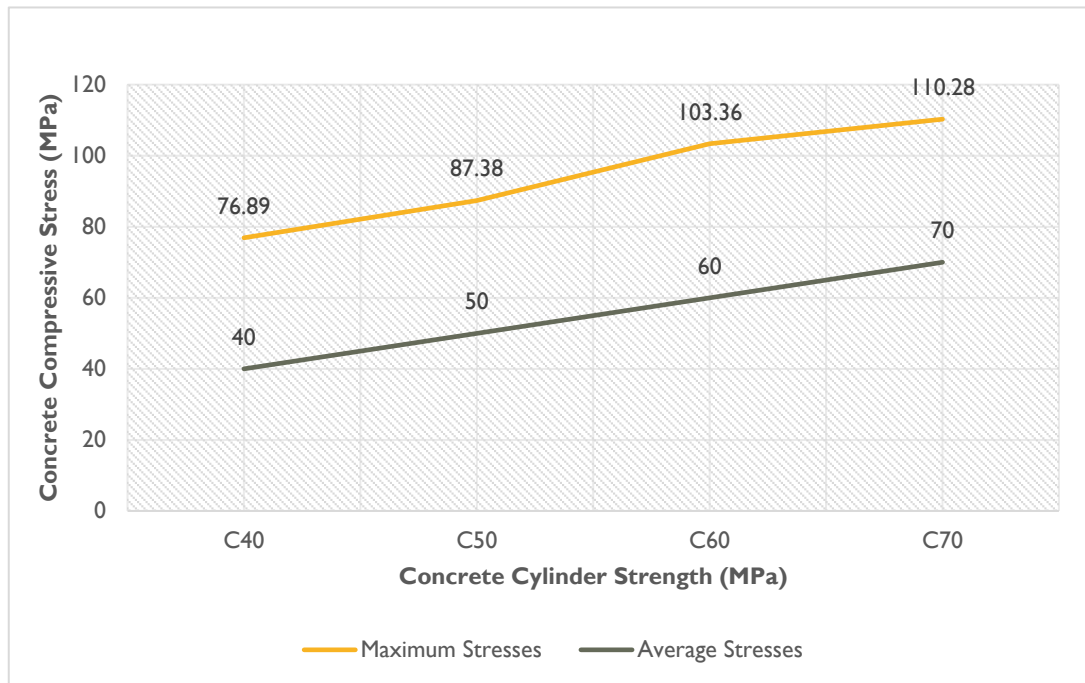


Fig. (5.15) Concrete Compressive Stress of Encased Column under Axial Compression Load and Uni-direction Bending as extracted from 3D-Fiber (Solid) Model, S275MPa, and S355 MPa

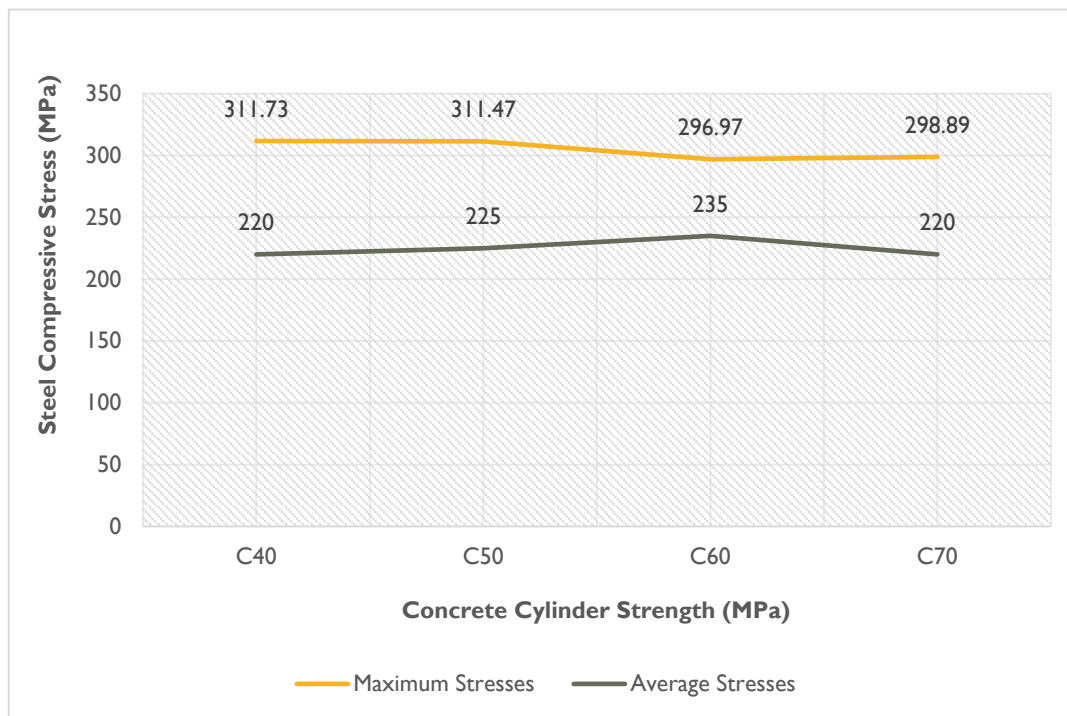


Fig. (5.16) Steel Compressive Stress of Encased Column under Axial Compression Load and Uni-direction Bending as extracted from 3D-Fiber (Solid) Model, S275MPa, and S355 MPa

5.3.2 CFST Composite column Subject to Axial Compression and Uni-direction Bending

The CFST column behavior under Axial compression and uni-direction bending moments has been assessed using AISC 316-16, and Eurocode-4.

In addition; a detailed 3D fiber (Solid) element model has been created to evaluate the column behavior and to compare the results with the simplified approach adopted by the international codes mentioned above.

The column has been analyzed under eccentric axial compression load, taking into consideration the boundary conditions illustrated in clause 4.4.2. The load eccentricity (e) is 85.75mm from one direction only. The analysis has been performed using 4 different concrete cylinder strength C40MPa, C50MPa, C60MPa, and C70MPa. Each concrete grade has been evaluated with two different steel grades, S275MPa and S355MPa.

The results presented in section (4) showing that the 3D Fiber (solid) Model provides a higher capacity than the simplified method adopted by AISC 316-16, and both methods provide higher capacity than the Encased column. The CFST has been evaluated based on the maximum eccentric load can be applied on the encased composite column which is governing the overall column capacity.

Fig. (5.17) denotes the maximum eccentric load can be applied on the column extracted from the AISC 316-16, 3D Fiber Model, and the capacity of the Encased Column considering the steel grade S355MPa.

Fig. (5.18) showing the maximum eccentric compression load for the CFST column with steel grade S275MPa. The eccentricity of the axial load in all cases was constant of 85.75mm from one direction

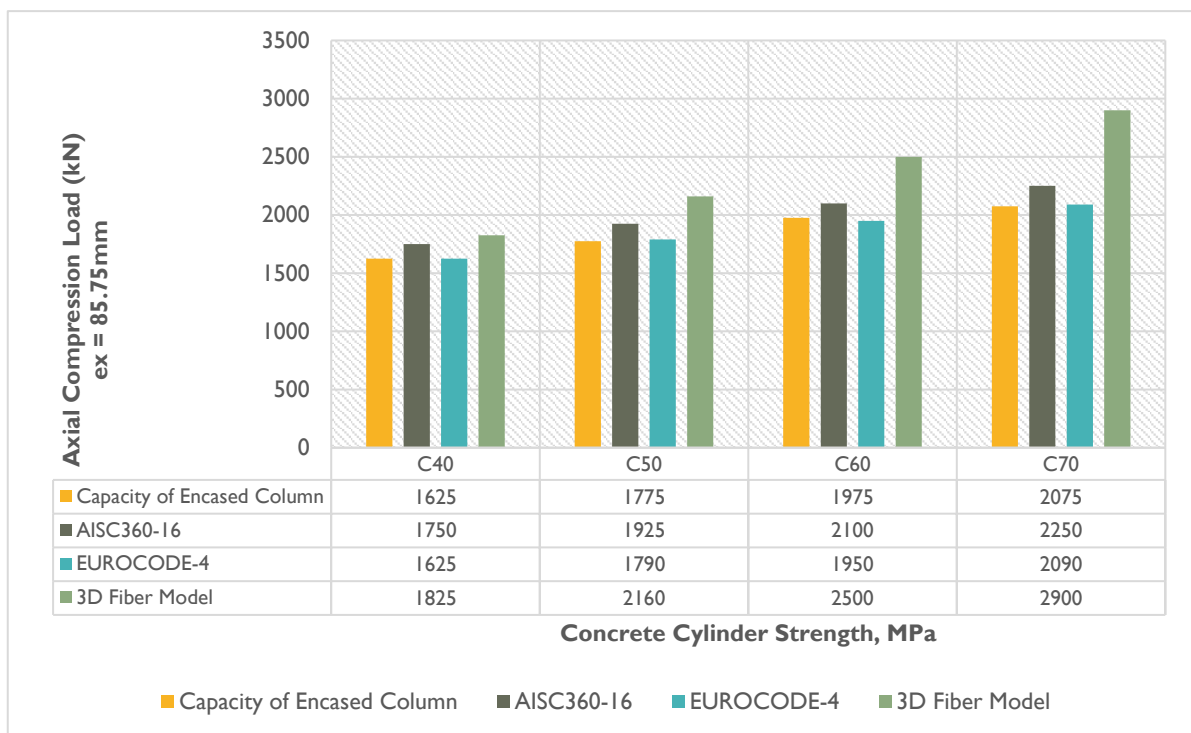


Fig. (5.17) Maximum Eccentric Compression Load on the CFST Column, $e=85.75\text{mm}$, S355MPa

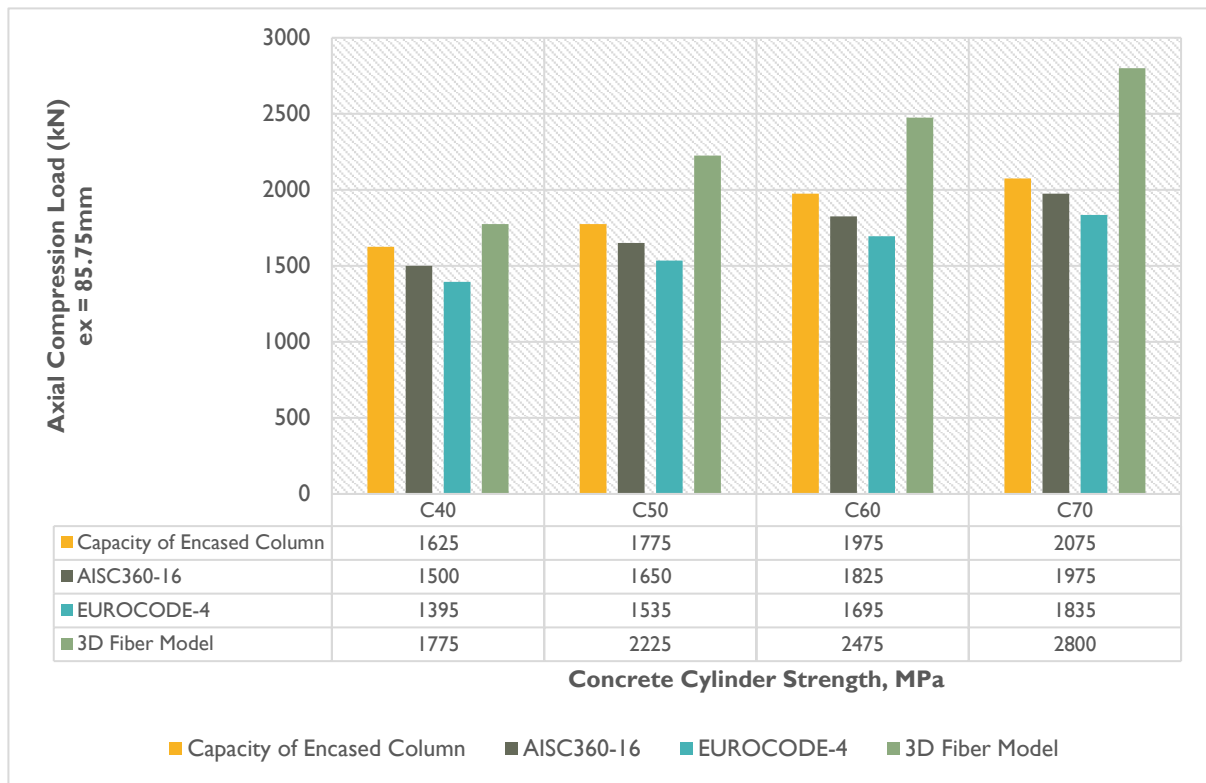


Fig. (5.18) Maximum Eccentric Compression Load on the CFST Column, $e_x=85.75\text{mm}$, S275MPa

The concrete section in the 3D Fiber models with steel grade S355MPa, showing a local concentration in the stresses at the interface with the steel stiffener plates connecting steel tube to the steel I section. The maximum stresses on the steel section has been observed at the interface level with the stiffener plates, which is located 425mm above the bottom of the CFST column, as per section (b-b) in Fig. (4.3).

Accordingly; the steel stiffener plates and the overlapping between I section, and steel tube has a significant influence on the section capacity under axial compression load, which was ignored from the simplified analysis approach.

Fig. (5.19) presenting the maximum and average concrete compressive stress of the CFST column with both steel grades S275MPa, and S355MPa under nominal compressive loads specified in the 3D Fiber Model.

The steel tube section of the CFST column with steel grade S355MPa, showing a very local concentration stresses at the interface level with the steel stiffener plates and overlapping with steel I section, while the remaining section showing normal stress distribution inline with the load path applied on the composite column.

The local stress concentration in the steel section is not anticipated to have a significant impact on the overall behavior and capacity of the composite column.

Fig. (5.20) demonstrating the steel compressive stress of the Encased column with both steel grades S275MPa, and S355MPa, under nominal compressive loads specified in the 3D Fiber Model.

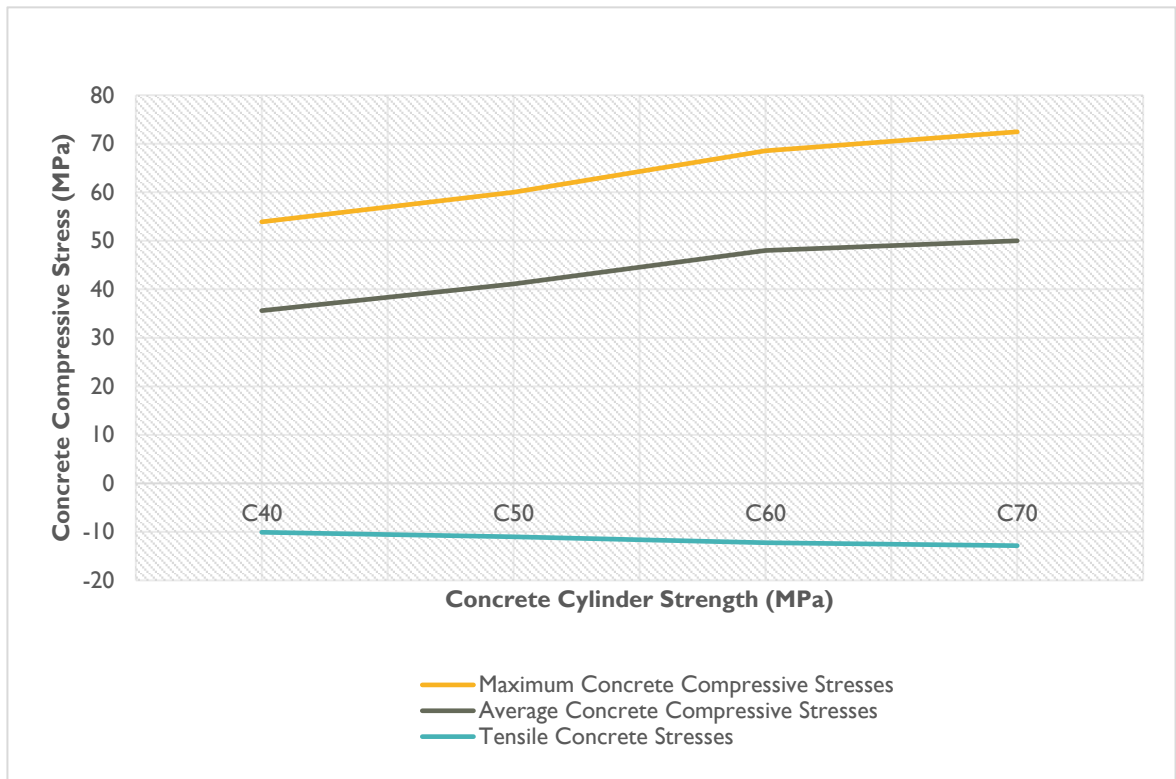


Fig. (5.19) Concrete Compressive Stress of CFST Column under Nominal Compressive Loads specified in the 3D-Fiber (Solid) Model, Steel Grade S275MPa, and S355 MPa

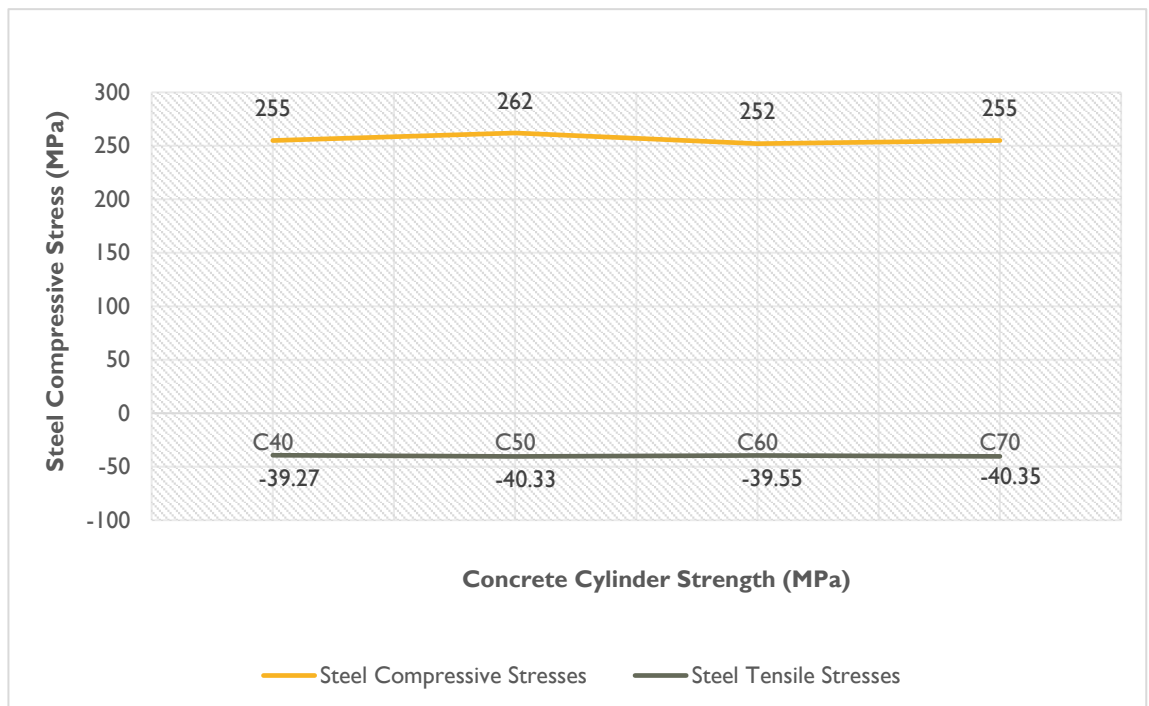


Fig. (5.20) Steel Compressive Stress of CFST Column under Nominal Compressive Loads specified in the 3D-Fiber (Solid) Model, Steel Grade S275MPa, and S355 MPa

5.3.3 Steel Stiffener Plates Behavior connected to CFST and Encased Column under Axial Compression Load and Uni-direction Bending

The stiffener plates have been provided to connect steel tube to the steel I section. The provided stiffeners enhance the load transition from the CFST element to the Encased element.

The stresses on the steel stiffeners has been evaluated using two different steel grades, S355MPa and S275MPa. The concrete strength adopted in the analysis was varying from C40MPa to C70MPa.

The 3D Fiber Model demonstrating that the stresses on the steel stiffener plates are the same with different steel grades S275MPa and S355MPa.

The results showing that the use of high strength steel has no impact on the sectional capacity, since the maximum stresses on the steel stiffeners still not exceeding 161.97MPa.

Fig. (5.21) illustrating the stresses on the steel stiffener plates with different steel grades and different concrete strengths.

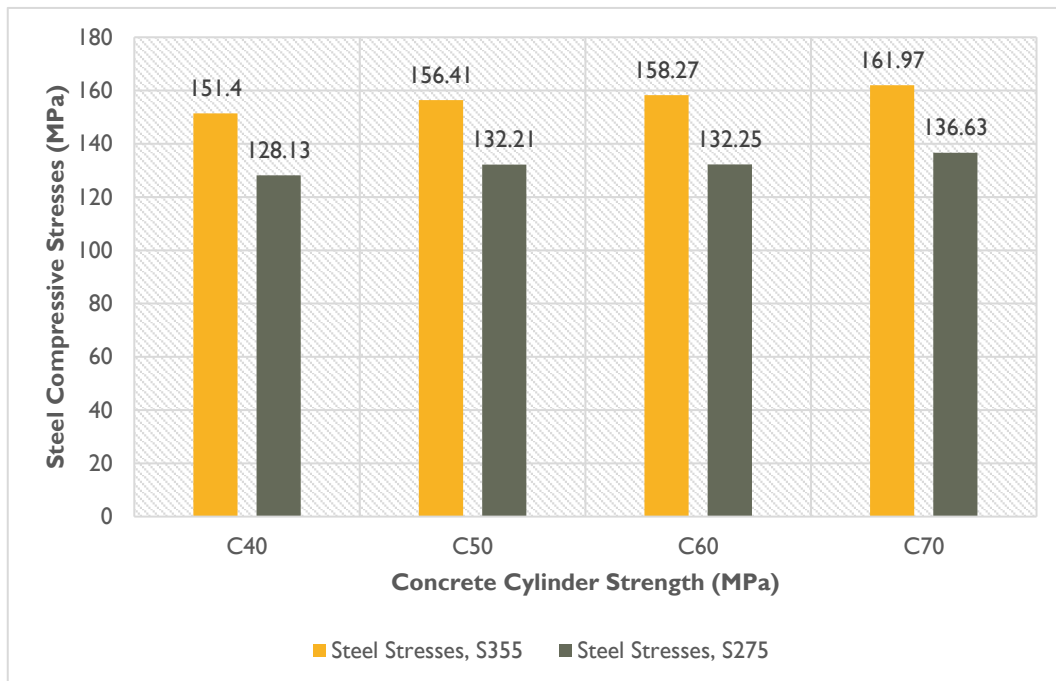


Fig. (5.21) Compression Steel Stresses on the Stiffener Plates under Axial Compression Loads and Uni-Direction Bending Moments

5.4 COMPOSITE COLUMN BEHAVIOR UNDER AXIAL COMPRESSION AND BI-AXIALLY BENDING MOMENTS

The behavior of the composite column has been examined by divided the model into three main parts, the first part is the encased composite column of (210 x 210) mm. The second part is the tapered CFST composite column with a sizing varying from (210x210) mm to (340x340) mm. The third part is the stiffener plates connecting steel tube to the steel I section. The composite column has been analyzed under axial compression load with bi-axially bending moments.

5.4.1 Encased Column Subject to Axial Compression and Bi-Axially Bending Moments

The Encased column resistance to Axial Compression and Bi-Axial Bending has been assessed using different international codes such as AISC 316-16, and Eurocode-4. In addition; a detailed 3D fiber (Solid) element model has been created to evaluate the column behavior and to compare the results with the simplified approach adopted by the international codes mentioned above.

The column has been analyzed under axial compression load and bi-axial bending taking into consideration the boundary conditions illustrated in clause 4.4.2.

The load eccentricity (e) was constant of 85.75mm, and 104.50mm in X & Y direction.

The analysis has been performed using 4 different concrete cylinder strength C40MPa, C50MPa, C60MPa, and C70MPa. Each concrete grade has been evaluated with two different steel grades, S275MPa and S355MPa.

The nominal compressive load with constant eccentricity in both direction ($e_x=85.75\text{mm}$, and $e_y=104.50\text{mm}$) has been determined using the simplified approach adopted by AISC316-16 and Eurocode-4. In addition; a 3D-Fiber Model has been created to examine the behavior of the Composite column and to compare it with the simplified approach by the specified codes in this research.

The output from the 3D Fiber Model indicates that the nominal compressive load with bi-axial bending is significant less than the values determined by the simplified methods.

The concrete section is showing a local concentration in the stresses

The difference in the section strength between 3D Fiber Model and Simplified Methods with the use of steel grade S355MPa. is ranging between 17% to 40%

The difference in the strength between 3D Fiber model and Simplified Methods with the use of steel grade S275 is ranging from 16% to 31%.

Fig. (5.22) and **Fig. (5.23)** illustrate the nominal compressive strength under bi-axial bending for both steel grades S355MPa and S275MPa.

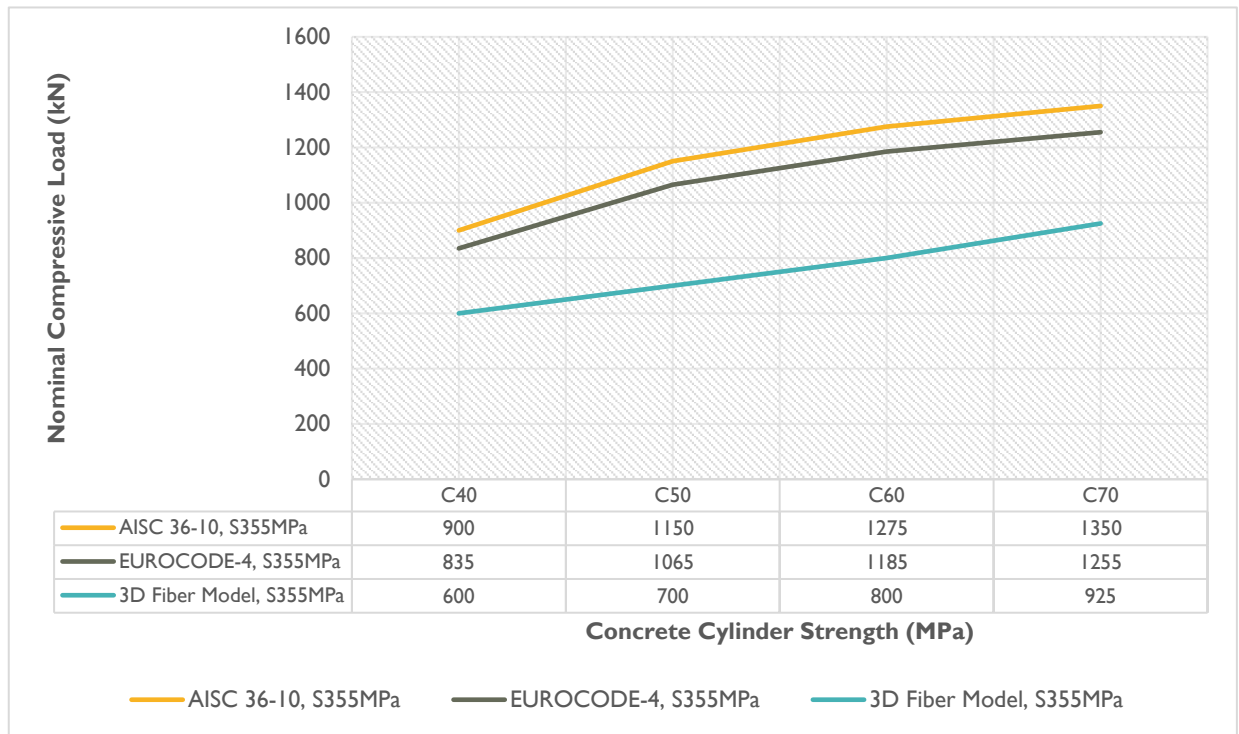


**Fig. (5.22) Nominal Compressive Strength of the Encased Section under Biaxial loading,
Steel Grade S355MPa, $e_x=85.75\text{mm}$, and $e_y=104.50\text{mm}$**

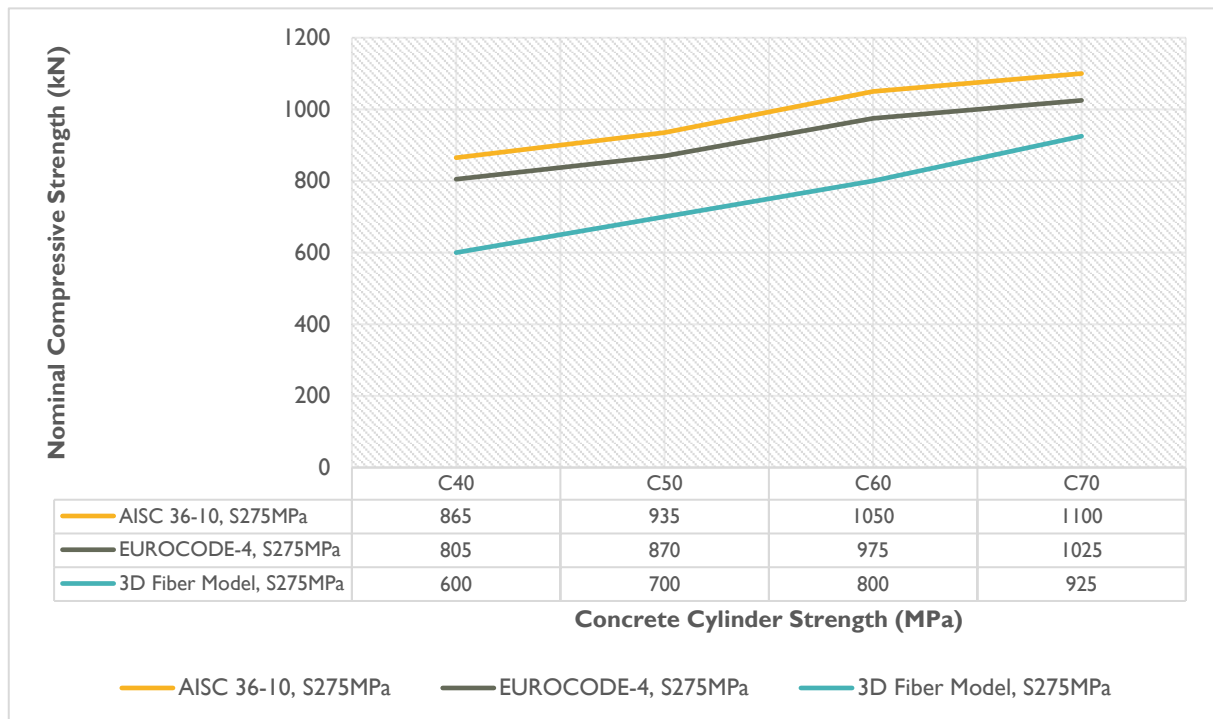


**Fig. (5.23) Nominal Compressive Strength of the Encased Section under Biaxial loading,
Steel Grade S275MPa, $e_x=85.75\text{mm}$, and $e_y=104.50\text{mm}$**

The 3D Fiber (Solid) Model is showing a local stress concentration at the extreme top and bottom edges, which is exceeding the maximum allowable stresses, however; it is not predicted to have an impact on the overall integrity and capacity of the encased section. The local stress concentration is developed at the interface between steel tube of the CFST part and Concrete surface of the encased part, which is related to the change in the mechanical properties of each material. The local stress concentration at the bottom of the encased part is also observed very close to the support fixation.

The local stress concentration is not extended along the column height, but it has an influence on the overall stresses on the encased section compared to the simplified methods adopted by AISC316-16 and Eurocode-4, so the average stresses on the concrete as a result of the 3D Fiber Model is less than the simplified methods.

In this case of bi-axially loaded composite column, Tensile Stresses have been developed locally in the concrete section, which is a very essential to be considered in the analysis and design of the encased composite column. The concrete usually has a limited strength to the tensile stresses, so the encased column under bi-axially loaded should be reinforced properly to withstand the tensile stresses developed on the extreme fiber of the column section.

The use of different steel grades has no impact on the stresses developed on the concrete section, so the results are the same with both steel grades S355MPa, and S275MPa.

The maximum steel stresses on the concrete of the Encased column is 42.11MPa, 49.60MPa, 57.33MPa, and 66.56MPa for concrete strength C40MPa, C50MPa, C60MPa, and C70MPa.

The tensile stresses can be reduced by considering the average stresses for the fiber element, so the average stresses can be estimated as 35MPa, 40MPa, 50MPa, and 60MPa for concrete strength C40MPa, C50MPa, C60MPa, and C70MPa respectively.

Fig. (5.24) demonstrates the stress distributions along concrete of the encased composite part for both steel grades S355MPa, and S275MPa

The steel section embedded in the Encased column showing the maximum compression stresses at the middle Height of the element. The compression stresses on the steel I section as extracted from the 3D Fiber Model are 252.40MPa, 269.23MPa, 263.55MPa, and 291.80MPa for concrete strength C40MPa, C50MPa, C60MPa, and C70MPa respectively.

The tensile stresses have been observed in the bottom and top of the steel I section. The maximum tensile stresses extracted from the 3D Fiber Model are 94.30MPa, 99.90MPa, 96.79MPa, and 107MPa

The tensile stresses showing that the use of steel grade S275MPa is adequate for the encased column with concrete strength ranging from C40MPa to C60MPa. For the encased column with high strength concrete of C70MPa, the maximum stresses exceed the maximum allowable limit, so the use of high strength steel of grade S355MPa is highly recommended.

Fig. (5.25) denotes the stress distributions on the Steel I section embedded in the Encased column

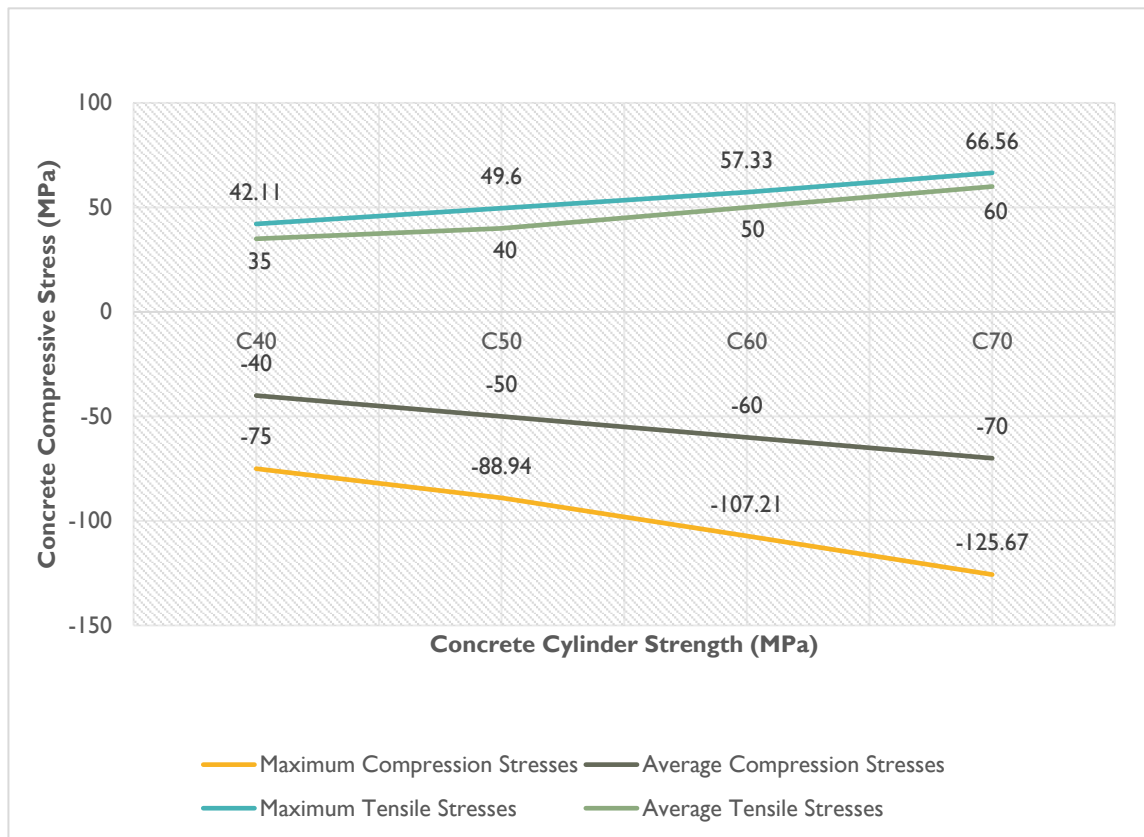


Fig. (5.24) Stress Distributions along Concrete of the Encased Composite Column

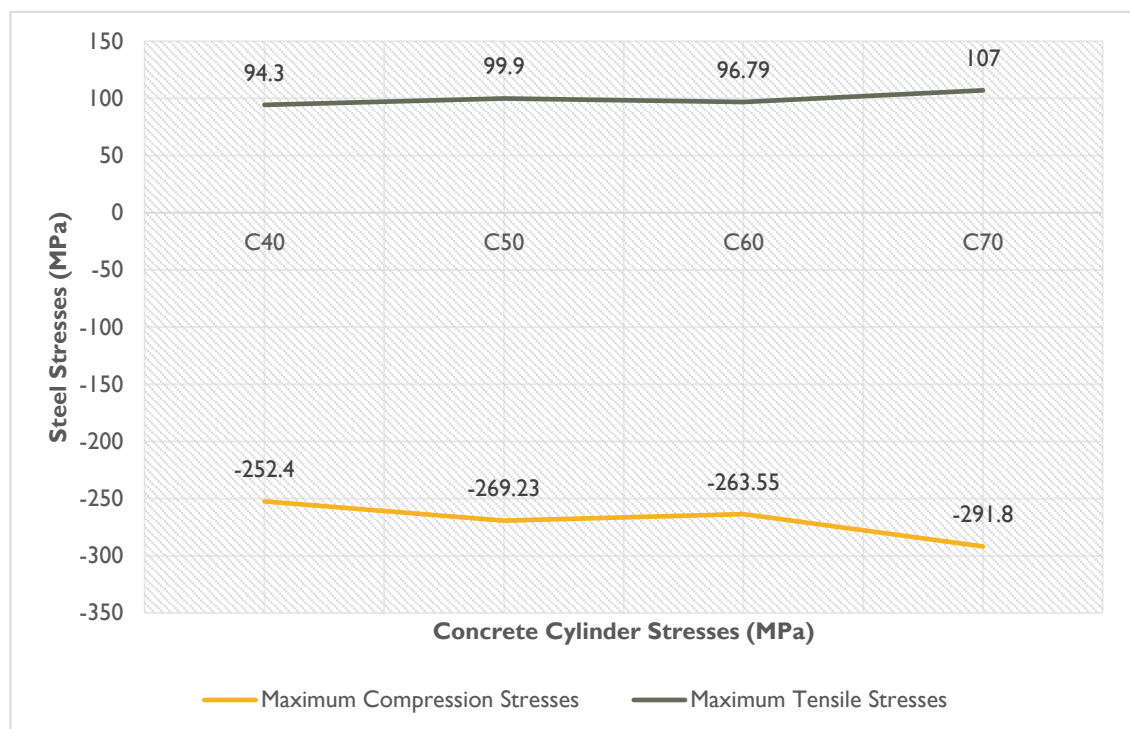


Fig. (5.25) Stress Distributions along Steel I Section Embedded in the Encased Composite Column

5.4.2 CFST Composite Column Subject to Axial Compression and Bi-Axially Bending Moments

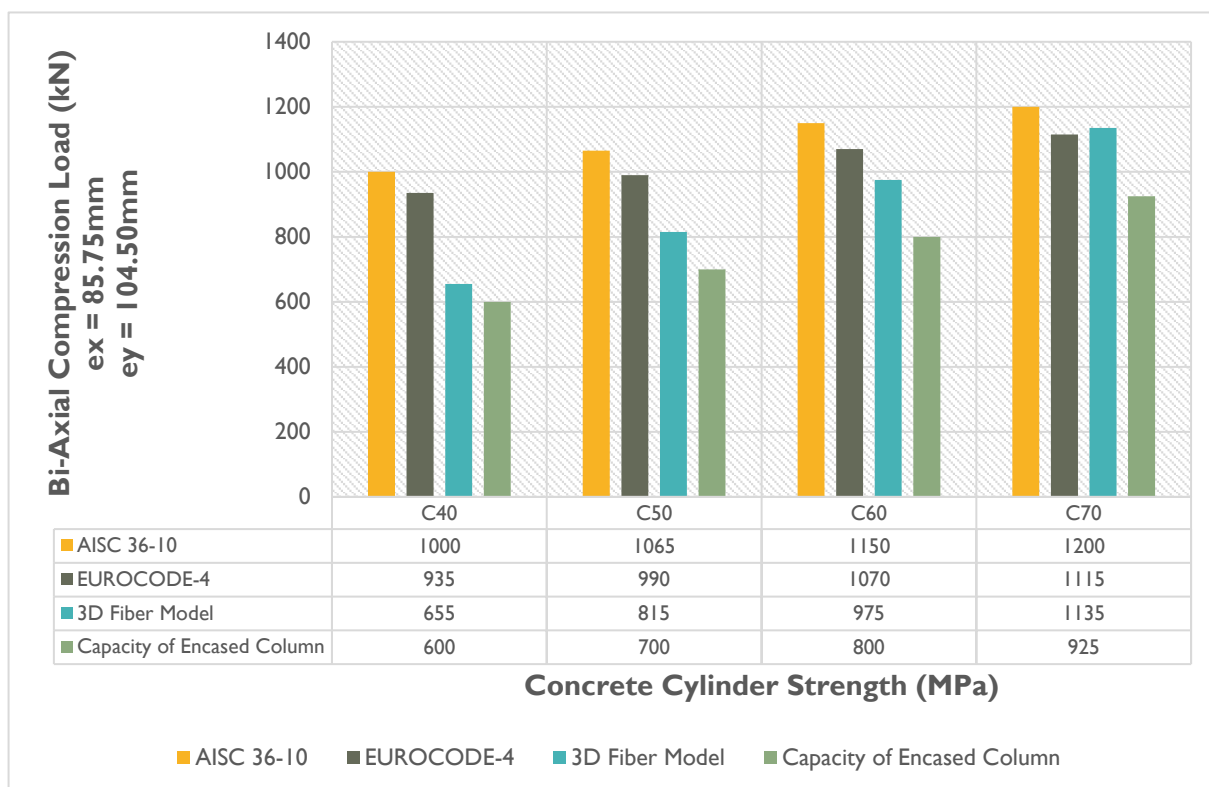
The CFST column behavior under Axial compression and bi-axial bending moments has been assessed using AISC 316-16, and Eurocode-4.

In addition; a detailed 3D fiber (Solid) element model has been created to evaluate the column behavior and to compare the results with the simplified approach adopted by the international codes mentioned above.

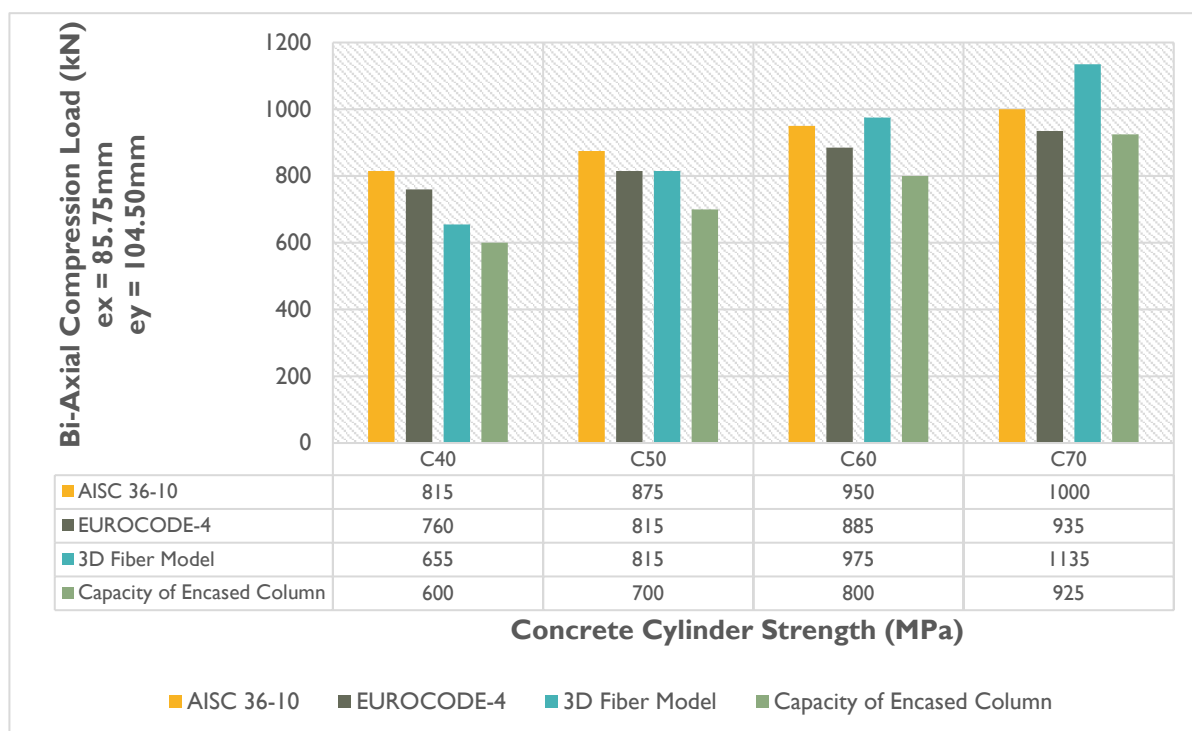
The column has been analyzed under eccentric axial compression load, taking into consideration the boundary conditions illustrated in clause 4.4.2. The load eccentricity in both directions are ($e_x=85.75\text{mm}$ and $e_y=104.50\text{mm}$). The analysis has been performed using 4 different concrete cylinder strength C40MPa, C50MPa, C60MPa, and C70MPa. Each concrete grade has been evaluated with two different steel grades, S275MPa and S355MPa. The results presented in section (4) showing that the 3D Fiber (solid) Model provides a higher capacity than the simplified method adopted by AISC 316-16, and both methods provide higher capacity than the Encased column. The CFST has been evaluated based on the maximum eccentric load can be applied on the encased composite column which is governing the overall column capacity.

Fig. (5.26) denotes the maximum eccentric load can be applied on the column extracted from the AISC 316-16, Eurocode-4, 3D Fiber Model, and the capacity of the Encased Column considering the steel grade S355MPa.

Fig. (5.27) showing the maximum eccentric compression load for the CFST column with steel grade S275MPa. The eccentricity of the axial load in all cases was constant in both directions ($e_x=85.75\text{mm}$ and $e_y=104.50\text{mm}$).



**Fig. (5.26) Maximum Eccentric Compression Load on the CFST Column,
ex=85.75mm, ey=104.50mm, S355MPa**



**Fig. (5.27) Maximum Eccentric Compression Load on the CFST Column,
ex=85.75mm, ey=104.50mm, S275MPa**

The concrete section in the 3D Fiber models with steel grade S355MPa, showing a local concentration in the stresses at the interface with the steel stiffener plates connecting steel tube to the steel I section. The maximum stresses on the steel section has been observed at the interface level with the stiffener plates, which is located 425mm above the bottom of the CFST column, as per section (b-b) in **Fig. (4.3)**.

Accordingly; the steel stiffener plates and the overlapping between I section, and steel tube has a significant influence on the section capacity under bi-axially loading, which was ignored from the simplified analysis approach.

Fig. (5.28) presenting the maximum and average stresses on the concrete of the CFST column with both steel grades S275MPa, and S355MPa under nominal compressive loads specified in the 3D Fiber Model.

The steel tube section of the CFST column with steel grade S355MPa, showing a very local concentration stresses at the interface level with the steel stiffener plates and overlapping with steel I section, while the remaining section showing normal stress distribution inline with the load path applied on the composite column.

The local stress concentration in the steel section is not anticipated to have a significant impact on the overall behavior and capacity of the composite column.

Fig. (5.29) demonstrating the steel compressive stress of the Encased column with both steel grades S275MPa, and S355MPa, under nominal compressive loads specified in the 3D Fiber Model.

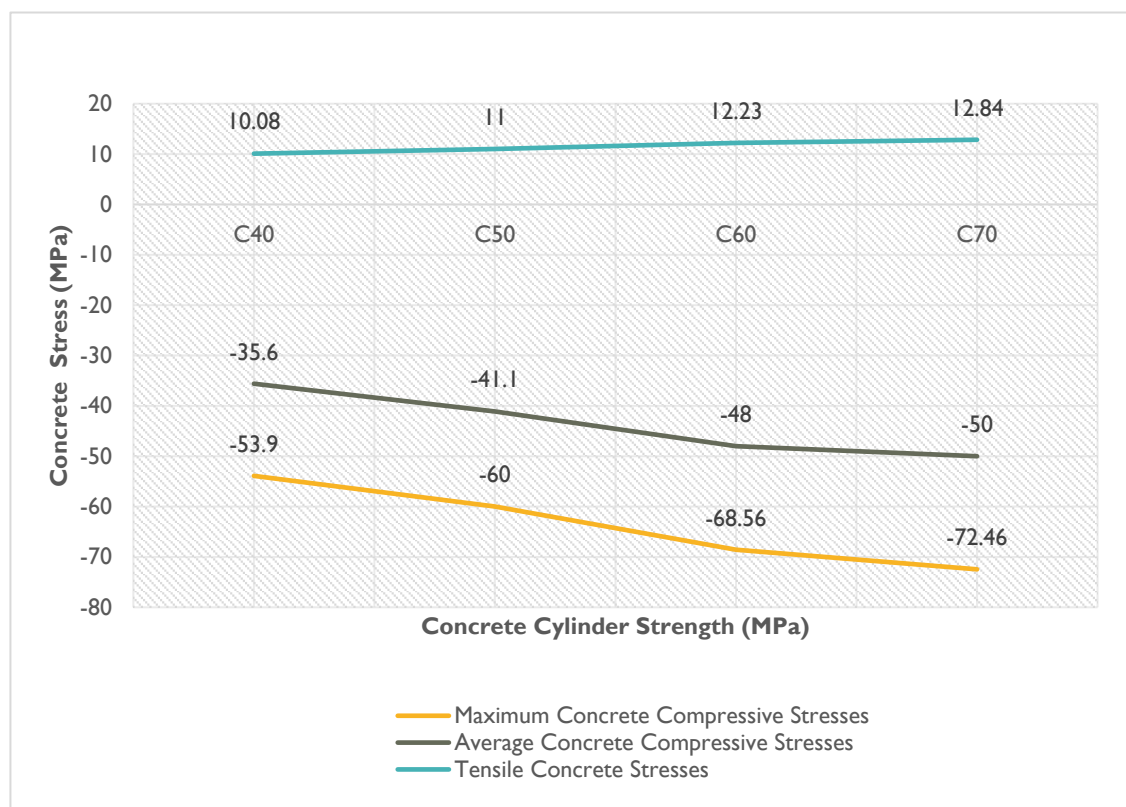


Fig. (5.28) Concrete Compressive Stress of CFST Column under Bi-Axially Loading specified in the 3D-Fiber (Solid) Model, Steel Grade S275MPa, and S355 MPa

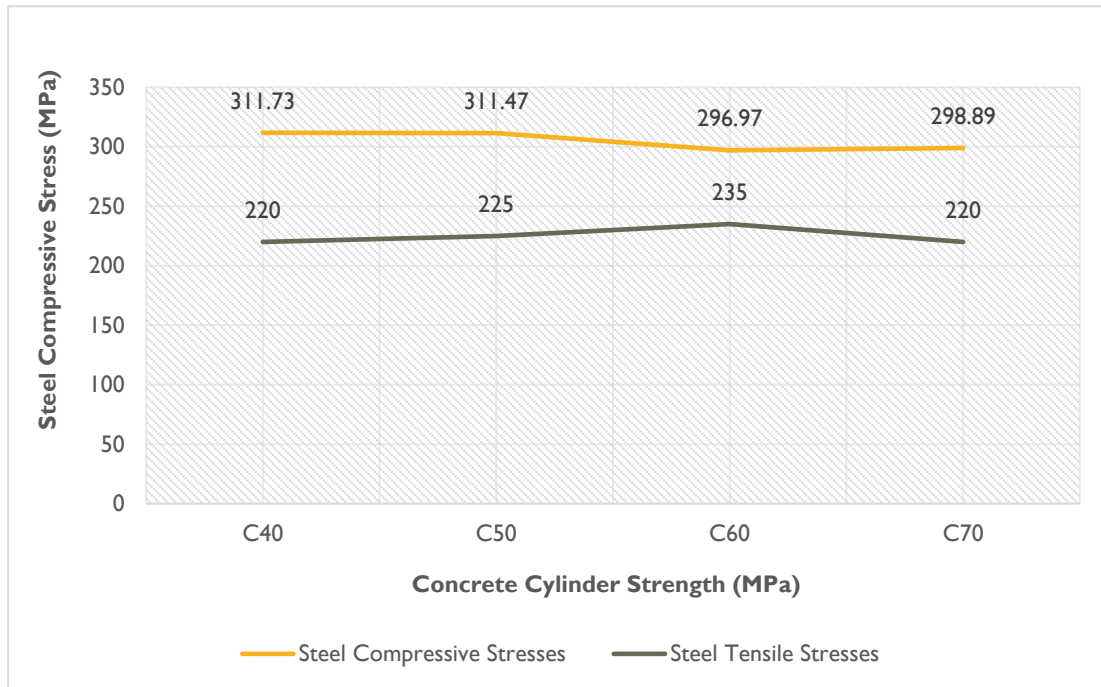


Fig. (5.29) Steel Compressive Stress of CFST Column under Bi-Axially Loading specified in the 3D-Fiber (Solid) Model, Steel Grade S275MPa, and S355 MPa

5.4.3 Steel Stiffener Plates Behavior connected to CFST and Encased Column under Axial Compression and Bi-Axial Bending Moments

The stiffener plates have been provided to connect steel tube to the steel I section. The provided stiffeners enhance the load transition from the CFST element to the Encased element.

The stresses on the steel stiffeners has been evaluated using two different steel grades, S355MPa and S275MPa. The concrete strength adopted in the analysis was varying from C40MPa to C70MPa.

The 3D Fiber Model demonstrating that the stresses on the steel stiffener plates are the same with different steel grades S275MPa and S355MPa.

The results showing that the use of high strength steel has no impact on the sectional capacity, since the maximum stresses on the steel stiffeners still not exceeding the maximum strength.

Fig. (5.30) illustrating the stresses on the steel stiffener plates with different steel grades and different concrete strengths.

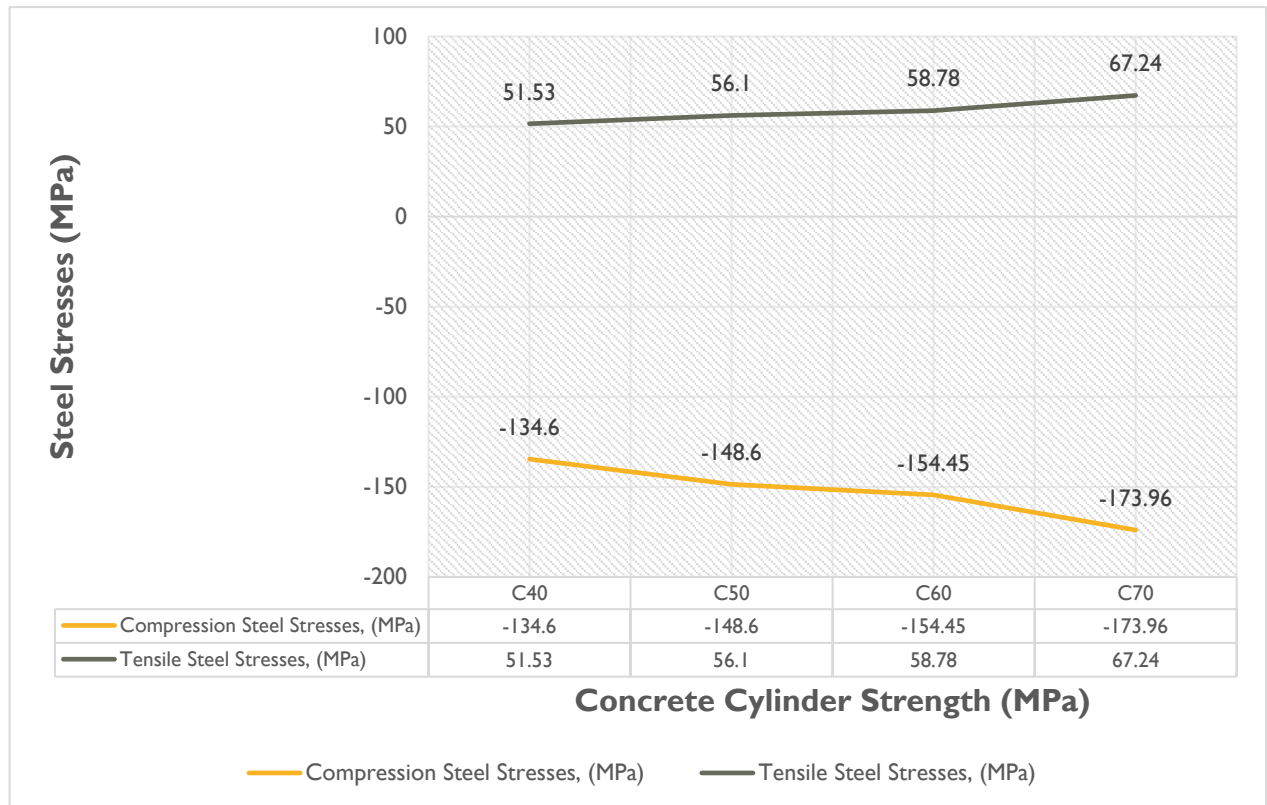


Fig. (5.30) Steel Stresses in the Stiffener Plates under Axial Compression Loads and Bi-Axial Bending Moments, Steel Grade S275MPa, and S355MPa

CHAPTER 6

SUMMARY AND CONCLUSION

The research was focusing a case study of tapered concrete filled steel tube (CFST) column connected encased composite (SRC) column designed in an existing high-rise building.

The idea of having two different columns connected to each other is to accommodate the straining actions applied on the column. The top part of the column receives a high bi-axial loading, while the bottom part of the column receive an axial compression load with significant reduction in the bending moments compared to the top part, so it was a convenient solution since the CFST column has a high resistance to the combined axial compression and bi-axial bending, while the Encased Composite Column is an efficient and more economy with uni-axial loading.

The scale of the research finite element model was 1/5 of the actual size presented in the case study.

The size of the Encased column was (210x210) mm with steel I section of (120x120x15). The area of steel section was about 11.22% of the total gross area of the concrete section. The size of the tapered CFST column is ranging from (210x210) mm at the bottom to (340x340) mm at the top. The area of steel tube section was (210x210x6) mm at the bottom and (340x340x6) mm at the top.

The area of steel tube was about 11.1% of the total gross area at the bottom and 6.90% of the total gross area at the top.

The research illustrated a comparison between simplified methods adopted by international codes, AISI316-16, ACI318-11, Eurocode-4, and a detailed numerical analysis using 3D Fiber (Solid) Finite Element Model. The 3D Fiber Model has been developed to represent in-details the steel tube, steel I section, concrete elements, overlapping between steel tube and steel I section, and stiffener plates connecting steel tube to the steel I section.

The simplified design methods have been developed using spreadsheets inline with the formulas adopted by each code.

The intended composite column has been studied using 3 different types of loading, Uni-Axial Compression Load, Combined Axial Compression with uni-axial bending, and Combined Axial compression with bi-axial bending.

The behavior of the composite column has been evaluated using different parameters such as concrete strength, and steel grades as well. The numerical analysis adopted in this research display 4 different concrete cylinder strength, C40MPa, C50MPa, C60MPa, and C70MPa. Each concrete strength studied with two different steel grades, S355MPa, and S275MPa.

6.1 COMPOSITE COLUMN SUBJECT TO UNI-AXIAL COMPRESSION LOAD

The composite column has been analyzed using 3D-Fiber (Solid) Model under concentric Axial Compression Load. The output from the 3D Model has been compared with the simplified methods adopted by AISC 316-16, ACI318-11, and Eurocode-4.

The following points can be concluded from the analysis of the composite column specified in the dissertation under concentric axial compression load:

- The simplified approach adopted by Codes, demonstrates that the AISC316-16 formula has slightly higher capacity to the axial compression compared to the ACI 318-11, and Eurocode-4.
- The simplified approach adopted by codes showing that the nominal compressive load increase by using high strength steel S355MPa compared to a lower strength steel of S275MPa, while the 3D finite element model illustrating that the nominal compressive strength is almost the same with both steel grades.
- The 3D Fiber (Solid) Finite Element Model illustrates less compressive strength for the Encased section with C40MPa compared to the simplified code, by increasing the concrete strength from C50 to C70MPa, the 3D model displays higher compressive strength than provided by the codes. The interface between CFST element and Encased Element is leading to a local stress concentration on the concrete, so the high-strength concrete is highly recommended than normal concrete in order to accommodate the local increase in the stresses observed in the 3D Finite element model, which cannot be predicted by applying the code simplified formulas, or using simplified frame element analysis.
- The 3D Fiber Model showing that the CFST element has a significant increase in the compressive resistance compared to the simplified code formulas. In addition; the maximum stresses on the CFST is located at the interface level between steel I section, stiffener plates, and steel tube as highlighted in sec. (B-B), **Fig. (4.3)**, so it is proofing that part of the load transferred to the Steel I section and stiffener plates at the overlapping zone. The simplified approach by codes ignores the contribution of the steel section and stiffeners at the overlapping zone, while the 3D Fiber Model provides more accurate results.

- The 3D Model presents high local concentration stresses on the concrete at 2 levels, the first level is the interface between steel I section, and steel tube at overlapping zone, and the second level is the transition level from CFST section to Encased section. These local stresses developed as a result of connecting two materials with two different mechanical properties, so it is not predicted to affect the overall integrity of the composite column, In addition; the concrete at the overlapping zone is highly confined by the steel tubes, so the concrete strength allowed to be increased as stated by [Chen and Lin, 2006]
- The overlapping between Steel I section, and Steel Tube is a conservative approach, and can be optimized.
- The 3D Fiber Model showing a local stress concentration on the Steel section of the Encased Part, however the local concentration stresses is developed in a very local area at the transition level from CFST element to Encased element and it is not anticipated to affect the overall behavior of column under axial compression load.
- The stresses on steel elements of the CFST element have a linear relation with the concrete strength, so the use of high strength concrete increase nominal compressive strength of the composite section and consequently increase the stresses on the steel section.
- The concrete reach the maximum compressive strength under nominal compressive load, while the steel stresses still beyond the yield limit, so using high strength steel of S355MPa, has no influence on the encased column capacity, except the encased column with concrete strength C70MPa, which noticed that the stresses exceeding the yield strength by 5%. Accordingly; the use of steel grade S275MPa, is recommended with concrete strength up to C60MPa. For the encased column with high strength concrete C70MPa, it is recommended to use high strength steel of grade S355MPa.
- The 3D Fiber Model showing also a local concentration stress in the steel tube at the interface with the Steel I section and stiffener plates (overlapping zone), located 850mm from the top of the column as per section (B-B), **Fig. (4.3)**. The average stresses on the steel tube is still beyond the yield limit under nominal compressive strength load with concrete strength up to C60MPa. For the CFST with high strength concrete of C70Mpa, the stresses on the steel is exceeding yield limit by 2.50%, so it is recommended to use normal steel grade of S275Mpa with concrete strength up C60MPa. For the encased

column with high strength concrete C70MPa, it is recommended to use high strength steel of grade S355MPa.

- The behavior of the stiffener plates is similar to the steel tube of the CFST part and Steel I section of the Encased part, so the use of steel grade S275MPa is recommended with concrete strength up to C60MPa, while it is recommended to use high strength steel of S355Mpa with high strength concrete of C70MPa.

6.2 COMPOSITE COLUMN SUBJECT TO COMBINED AXIAL COMPRESSION AND UNI-DIRECTION BENDING

The composite column has been analyzed using 3D-Fiber (Solid) Model under Axial Compression and Uni-Direction Bending. The output from the 3D Model has been compared with the simplified methods adopted by AISC 316-16, and Eurocode-4.

The following points can be concluded from the analysis of the composite column specified in the dissertation under combined axial compression and uni-direction bending ($e=85.75\text{mm}$)

- The simplified approach adopted by Codes, demonstrates that the AISC316-16 formula has slightly higher capacity to the axial compression compared to Eurocode-4.
- The simplified approach adopted by codes showing that the nominal compressive load of the encased element increased by using high strength steel S355MPa compared to a lower strength steel of S275MPa, while the 3D finite element model illustrating that the nominal compressive strength is almost the same with both steel grades. As per the stress contours, the concrete reach the maximum compressive strength under nominal compressive load, while the steel stresses still beyond the ultimate strength limit, so using high strength steel of S355MPa, has no influence on the composite column capacity.
- The 3D Fiber (Solid) Finite Element Model illustrates a very close results compared to AISC under Combined Axial Compression Load and Uni-Direction Bending Moment.
- The 3D Fiber Model showing local stresses' concentration on the Steel section of the Encased Part, however the local concentration stresses is developed in a very local area at the transition level from CFST element to Encased element and it is not anticipated to

affect the overall behavior of column under axial compression load with uni-direction bending.

- The fiber elements close to the fixed support showing a local increase in the concrete stresses which can be ignored since it is developed in a very local area, while the remaining entire fiber elements have less stresses, so the average stresses has been considered in the analysis of the composite column specifically in the local areas with high stresses.
- The steel stresses on the I section of the Encased element showing a low stress ranging from 220MPa up to 235MPa, so the use of high strength steel has no impact on the overall section capacity.
- The 3D Fiber Model showing that the CFST element illustrated a higher resistance compared to the simplified code formulas. In addition; the maximum stresses on the CFST is located at the interface level between steel I section, stiffener plates, and steel tube as highlighted in sec. (B-B), **Fig. (4.3)**, so it is proofing that part of the load transferred to the Steel I section and stiffener plates at the overlapping zone. The simplified approach by codes ignores the contribution of the steel section and stiffeners at the overlapping zone, while the 3D Fiber Model provides more accurate results.
- The 3D Model presents a high local concentration stresses on the concrete at 2 levels, the first level is the interface between steel I section, and steel tube at overlapping zone, and the second level is the transition level from CFST section to Encased section. These local stresses developed as a result of connecting two materials with two different mechanical properties, so it is not predicted to affect the overall integrity of the composite column, In addition; the concrete at the overlapping zone is highly confined by the steel tubes, so the concrete strength allowed to be increased as stated by [Chen and Lin, 2006].
- The overlapping between Steel I section, and Steel Tube is a conservative approach, and can be optimized.
- The behavior of the stiffener plates showing about 19% difference in the stresses between two steel grades S355MPa, and S275MPa, however; the maximum stresses sill below the maximum strength limit, so the use of high strength steel has no influence on the overall capacity of the composite column.

6.3 COMPOSITE COLUMN SUBJECT TO COMBINED AXIAL COMPRESSION AND BI-DIRECTION BENDING

The composite column has been analyzed using 3D-Fiber (Solid) Model under Axial Compression and Bi-Direction Bending. The output from the 3D Model has been compared with the simplified methods adopted by AISC 316-16, and Eurocode-4.

The following points can be concluded from the analysis of the composite column specified in the dissertation under combined axial compression and bi-direction bending ($e_x=85.75\text{mm}$ & $e_y=104.50\text{mm}$)

- The simplified approach adopted by Codes, demonstrates that the AISC316-16 formula has slightly higher capacity to the axial compression compared to Eurocode-4.
- The simplified approach adopted by codes showing that the nominal compressive load of the encased element increased by using high strength steel S355MPa compared to a lower strength steel of S275MPa, while the 3D finite element model illustrating that the nominal compressive strength is almost the same with both steel grades. As per the stress contours, the concrete reach the maximum compressive strength under nominal compressive load, while the steel stresses still beyond the ultimate strength limit, so using high strength steel of S355MPa, has no influence on the composite column capacity.
- The 3D Fiber (Solid) Finite Element Model illustrates a significant reduction in the section capacity under bi-axially loading by more than 30%, compared to the simplified code formulas adopted by AISC316-16 and Eurocode-4.
- The 3D Fiber Model showing local stresses' concentration on the Steel section of the Encased Part, however the local concentration stresses is developed in a very local area at the transition level from CFST element to Encased element and it is not anticipated to affect the overall behavior of column under bi-axially loading.
- The fiber elements close to the fixed support showing a local increase in the concrete stresses which can be ignored since it is developed in a very local area, while the remaining entire fiber elements have less stresses, so the average stresses has been considered in the analysis of the composite column specifically in the local areas with high stresses.

- The compression stresses on the steel I section of the Encased element showing the same stress with two different steel grades. The compression stresses on the I section are ranging from 252.40MPa up to 291.80MPa, so the use of high strength steel, S355MPa, is recommended with high strength concrete of C70MPa.
- The tensile stresses on the steel I section is ranging from 94.30MPa up to 107MPa with both steel grades, which is lower than the yield limit.
- The Encased Column is showing high tensile stresses on the concrete section, as a result of the bi-axially loading. The tension zone of the encased column should be adequality reinforced to accommodate the tensile stresses, since the concrete has a less resistance to the tension compared to compression.
- The 3D Fiber model showing that the CFST has less capacity against bi-axial loading compared to the simplified approach by codes. The difference between 3D Fiber Model and Simplified code formulas is 35%, 24%, 15%, and 6% for CFST with concrete strength C40MPa, C50MPa, C60MPa, and C70MPa. Accordingly, the high strength concrete provides more convince results and very close the code formulas.
- The 3D Model presents a high local concentration stresses on the concrete at 2 levels, the first level is the interface between steel I section, and steel tube at overlapping zone, and the second level is the transition level from CFST section to Encased section. These local stresses developed as a result of connecting two materials with two different mechanical properties, so it is not predicted to affect the overall integrity of the composite column, In addition; the concrete at the overlapping zone is highly confined by the steel tubes, so the concrete strength allowed to be increased as stated by [Chen and Lin, 2006].
- The overlapping between Steel I section, and Steel Tube is a conservative approach, and can be optimized.
- The behavior of the stiffener plates showing the stress results with both steel grades. The compression / tensile stresses on the stiffener is quite below the maximum allowable strength.

6.4 RECOMMENDATIONS FOR DESIGN AND FUTURE RESEARCHES

The research detects the necessity of studying the load path and stresses distribution for the case of having CFST Column connected to Encased Column as per the case study presented in this research.

It very crucial to evaluate both members under different type of loading, with different design parameters such as concrete strength and steel grade as well.

The detailed study and analysis of this sophisticated element expose more accurate results and provides appropriate comparison with the simplified analysis methods usually adopted by the Engineer. In addition; it shows all uncertainties not predicted by the simplified analysis approach.

The subsequent clauses demonstrating the design recommendations and future researches for similar cases.

6.4.1 Design Recommendations

The following points outline the design recommendation for the CFST column connected to Encased column

- The use of high strength concrete is highly recommended for the column under bi-axial loading.
- The connection between CFST column and Encased column is leading to additional stresses on the concrete, which cannot be anticipated from the simplified analysis approach, so it is highly recommended to perform advance three dimensional finite element model for such kind elements in order to identify the actual stresses on each element along the column height.
- The use of normal steel grade S275MPa is recommended with normal concrete strength, while it is recommended to use high tensile steel such as S355MPa with high strength concrete.
- The stiffener plates connecting steel tube to the steel I section not required to have strength steel. The stresses are the same with different steel grades and quite below the allowable strength limit (275MPa).
- The maximum stresses on the tapered CFST column is located at the interface between steel I section and steel tube which can not be predicted by the simplified analysis approach.
- The Encased column under bi-axially loading required appropriate reinforcement to accommodate the tensile stresses developed on the concrete element.
- The overlapping between CFST column and Encased column is a conservative approach and not required to have long overlapping zone.
- It is highly recommended to ensure that the concrete is confined at the interface between CFST member and Encased member. The confinement of

concrete is significantly increasing the concrete resistance compared to the un-confined concrete.

- Full horizontal stiffener plate is recommended to be provided between steel tube and steel I section at the interface between two members in order to mitigate the stress concentration at this level.
- The use of rigid shear connectors (steel Plates) is recommended at the interface between CFST member and Encased member.

6.4.2 Research Recommendations

There are many factors affecting the behavior of the CFST column connected to Encased Column, which cannot be included in the simplified analysis approach or by adopting the international code formulas.

The following points need to be studied in the future researches:

- The behavior of the CFST column connected to Encased Column should be experimentally investigated.
- The bond between concrete and steel need to experimentally investigated
- The effect of shear connectors on the column's resistance need to be investigated.
- The need of overlapping between CFST member and Encased member should be experimentally investigated.
- The use of different steel grades should be experimentally investigated.
- The results of the experiments should be mutual with monotonic and cyclic loading in order to perform seismic design guidelines for the CFST column connected to Encased Column.

Word count 46,530

CHAPTER 7

REFERENCES

ACI 318-11 Building Code requirements for Structural Concrete and Commentary

ANSI / AISC 360-16 American Standard Specifications for Steel Buildings

Eurocode 4: Design of Composite Steel and Concrete Structures

Popovics, "A Numerical Approach to the Complete Stress-Strain Curve of Concrete," Cement and Concrete Research, Vol.3, No.5, May 1973.

Collins, M.P., Mitchell, D., "Prestressed Concrete Structures," Prentice-Hall Inc., Englewood Cliffs, New Jersey, 1991.

Ahmad, S.H., and Shah, S.P., 1985, "Structural Properties of High Strength Concrete and Its Implications on Precast and Prestressed Concrete, "PCI Journal, Nov.-Dec., pp.91-119.

Sooi, T.K., Green P.S., Sause, R., Rides, J.M., "Stress-Strain Properties of High-Performance Steel and the Implications for Civil-Structure Design," Proceedings of the International Symposium on High-performance Steels for Structural Applications, Cleveland, OH, 1995.

Mander, J.B., Priestley, M.J.N., Park, R., "Theoretical Stress-Strain Model for Confined Concrete," Journal of Structural Engineering, ASCE, Vol. 114, No. 8, 1988.

Chen C. & Lin N., "Analytical model for predicting axial capacity and behavior of concrete encased steel composite stub columns", Journal of constructional steel research, 62, pp. 424 -433, 2006.

Chen J.& Young B., "Stress-strain curves for stainless steel at elevated temperatures", 28, pp. 229-239, 2006.

Nilson, A.H., (1987), Design of Prestressed Concrete, 2nd Edition, U.S.

Roeder, C.W., Cameron, B., Brown, C.B., (1999), "Composite Action in Concrete Filled Tubes," Journal of Structural Engineering, May.

Salmon, G., and Jolinson, J.E., (1996), Steel Structures Design and Behavior, 4th Edition, New York, NY.

Performance and Capacity of Isolated Steel Reinforced Concrete Columns and Design Approaches, (China Academy of Building Research (CABR) Technology CO., LTD

Furlong, R.W., "Strength of Steel Encased Concrete Beam-Columns," Journal of Structural Engineering, ASCE, Vol. 93, No. ST5, 1967.

Tomii, M., Yoshimura, K., Morishita, Y., "Experimental Studies on Concrete Filled Steel Tubular Columns Under Concentric Loading," Proceedings of the Second Joint. Technical Coordinating Committee Meeting, U.S.-Japan Cooperative Earthquake Research Program Composite and Hybrid Structures, Honolulu, Hawaii, 1995.

Baba, T., Nishiyama, I., Mukai, A., Fujimoto, T., "Compressive Tests on CPT Short Columns- Part 2: Square CPT Columns," Proceedings of the Second Joint Technical Coordinating Committee Meeting, Honolulu, Hawaii, 1995.

Sakino, K., "Elasto.; Plastic Behavior of Concrete Filled Circular Steel Tubular Beam Columns," Proceedings of the Second Joint Technical Coordinating Committee. Meeting U.S.-Japan Cooperative Earthquake Research Program Composite and Hybrid Structures, Honolulu, Hawaii, 1995.

Fujimoto, T., Nishiyama, I., Mukai, A., Baba, T., "Test Results of Eccentrically Loaded Short Columns - Square CFT Columns," Proceedings of the Second Joint Technical Coordinating Committee Meeting, U.S.-Japan Cooperative Earthquake Research Program Composite and Hybrid Structures, Honolulu, Hawaii, 1995.

Sakino, K., "Confining Effect on the Ultimate Strength of CFT Columns," Proceedings of the Third Joint Technical Coordinating Committee Meeting, U.S. Japan Cooperative Earthquake Research Program Composite and Hybrid Structures, Hong Kong, China, 1996.

Inai, E., Sakino, K., "Simulation of Flexural Behavior of Square Concrete Filled Steel Tubular Columns," Proceedings of the Third Joint Technical Coordinating Committee Meeting, U.S.-Japan Cooperative Earthquake Research Program Composite and Hybrid Structures, Hong Kong, 1996.

Toshiyuki, F., Naguchi, T., Mori, O., "Evaluation for Deformation Capacity of (CFT) Beam Columns," Proceedings of the Third Joint Technical Coordinating Committee Meeting U.S.-Japan Cooperative Earthquake Research Program Composite and Hybrid Structures, Hong Kong, 1996.

Zhang, W., and Shahrooz, B.M., "Analytical and Experimental Studies into the Behavior of CFT Columns," Report No. UC-CII 97101, Department of Civil Engineering, University of Cincinnati, 1997.

Hull, B.K., (1998), "Experimental Behavior of High Strength Concrete Filled Tube Columns," Master of Science Thesis, Department of Civil Engineering, Lehigh University.

Nakahara, H., and Sakino, K., (1998), "Axial Compressive and Uniform Bending Tests of High Strength Concrete Filled Square Steel Tubular Columns," Proceedings of the Fifth Pacific Structural Steel Conference, Seoul, Korea, October.

Kawaguchi, J., Morino, S., Shirai, J., Tatsuta, E., (1998), "Database and Structural Characteristics of CFT Beam-Columns," Proceedings of the Fifth Pacific Structural Steel Conference, Seoul, Korea, October.

Sakino, K., and Nakahara, H., (2000), "Flexural Capacities of Concrete Filled Square Steel Tubular Beam-Columns with High Strength Concrete," Proceedings of 6th ASCCS Conference, Los Angeles, CA.

Inai, E., Noguchi, T., Mori, O., Fugimoto, T., (2000), "Deformation Capacity and Hysteretic Model of Concrete-Filled Steel Tubular Beam-Columns," Proceedings of 6th ASCCS Conference, Los Angeles, CA.

Skino Kenji, Hiroyuki Nakahara, Shosuke Morino, and Isao Nishiyama, (2004) "Behavior of Centrally Loaded Concrete Filled Steel Tube Short Column, U.S.-Japan Cooperative Earthquake Research Program.

Hull, Bradford K. (1999), Experimental Behavior of High Strength concrete Filled Tube Columns, Lehigh University

Ream, Anthony P. (2000), Behavior of Square CFT Beam-columns with High Strength Concrete Under Seismic Loading, Lehigh University

Serkan Tokgoz., Cengiz Dunder., (2010) "Experimental study on steel tubular columns in-filled with plain and steel fiber reinforced concrete".

Jang-Woon Baek., Hyeon-Jong Hwang., (2012)., "Performance of Shear Connectors in Concrete Mega Column-to-Steel Beam Connection".

Qing Quan Liang., Vipulkumar Ishvarbhai., Muhammad N.S. Hadi., (2014)., "Behavior of biaxially-loaded rectangular concrete -filled steel tubular slender beam-columns with preload effects".

Jin won Kim., Cheol-Ho Lee., " Shearhead Reinforcement for Concrete Slab to Concrete-Filled Tube Column Connections, ACI Structural Journal-May 2014

Jing-ming Cai., Jin-long Pan., and Yu-fei Wu., "Performance of Steel-Reinforced Square Concrete-Filled Steel Hollow Section (SRSCFSHS) Columns under Uniaxial Compression"., Advanced Steel Construction Vol. 12, No. 4, pp. 410-427 (2016).

Fa-xing Ding., Jiang Zhu., ShanShan Cheng., Xuemei Liu., (2017)., "Comparative study of stirrup-confined circular concrete-filled steel tubular stub columns under axial loading

T.Kibriya., " Performance of concrete Filled Steel Tubular Columns"., American Journal of Civil Engineering and Architecture, 2017, Vol. 5, No. 2.

Jizhong Wang., Lu Cheng., "Compressive behavior of SFRP-steel composite tubed steel-reinforced column with high-strength concrete"., Journal of Constructional Steel Research, November 2018.

Morino, S., Matsui, C., and Watanabe, H. (1984). "Strength of biaxially loaded SRC column." Proc., US/Joint Seminar

Sherif El-Tawil., Gregory G. Deierlein., "Strength and Ductility of Concrete Encased Composite Column.", Journal of Structural Engineering, September 1999.

Cengiz Dunder., Serkan Tokgoz., A. Kamil Tanrikulu., Tarik Baran., “ Behavior of Reinforced Concrete-encased composite columns subjected to biaxial bending and axial load

Z. Huang., X. Huang., W.Li., Y. Zhou., L.Sui., and J. Y. Richard Liew., “ Experimental behavior of very high-strength concrete-encased steel composite column subjected to axial compression and end moments.”. (ASCCS 2018).

Ricles, J.M., Sause, R., Green., P.S., Lu, L., “Advanced Materials Research at Lehigh: Applications for Civil Infrastructure,” Proceedings of the 2nd International Symposium on Civil Infrastructure System, Hong Kong, China, December, 1996.

Zhang, H., and Ricles, J.M., “An Analytical Study of Seismic Resistant CFT MRFs” Fritz Laboratory Research Report, Department of Civil Engineering, Lehigh University, 1996.

CHAPTER 8

APPENDICES

Appendix (A); Unit Conversions (Imperial Units to SI Units)

General

1 ft	=	0.3048	m
1 in	=	25.40	mm
1 ft ²	=	0.0929	m ²
1 in ²	=	645.20	mm ²
1 ft ³	=	0.0283	m ³
1 in ³	=	16.39 x 10 ³	mm ³
1 in ⁴	=	0.4162 x 10 ⁶	mm ⁴

Structural Material Characteristics

Density	1 lb/ft ³	=	16.03	kg/m ³
Young's Modulus / Stresses	1 lb/in ²	=	0.006895	MPa
	1 kip / in ²	=	6.895	MPa

Loading

1 lb	=	4.448	N
1 Kip	=	4.448	kN
1 lb / ft ³	=	0.1571	kN/m ³
1 Kip/ft	=	14.59	kN/m
1 lb/ft ²	=	0.0479	kN/m ²
1 Kip/ft ²	=	47.90	kN/m ²

Moments and Torsional Moments

1 ft-Kip	=	1.356	N.m
1 ft-Kip	=	1.356	kN.m